DESIGN AND DEVELOPMENT OF A LAYER-BASED ADDITIVE MANUFACTURING PROCESS FOR THE REALIZATION OF METAL PARTS OF DESIGNED MESOSTRUCTURE

A Dissertation
Presented to
The Academic Faculty

by

Christopher Bryant Williams

In Partial Fulfillment
of the Requirements for the Degree
Doctor of Philosophy in Mechanical Engineering

Georgia Institute of Technology
April 2008

DESIGN AND DEVELOPMENT OF A LAYER-BASED ADDITIVE MANUFACTURING PROCESS FOR THE REALIZATION OF METAL PARTS OF DESIGNED MESOSTRUCTURE

Approved by:

David Rosen, Co-Chair
Associate Chair for Graduate Studies
Professor, Mechanical Engineering

Farrokh Mistree, Co-Chair
Associate Chair for GT Savannah
Professor, Mechanical Engineering

Joe Cochran
Professor Emeritus,
Materials Science and Engineering

Hamid Garmestani
Professor,
Materials Science and Engineering

David McDowell
Distinguished Chair in Metals Processing
Regents' Professor,
Mechanical Engineering

Shreyes Melkote
Professor, Mechanical Engineering

Date Approved:
December 3, 2007

I dedicate this dissertation to my grandparents, John & Lena Belcher and Ernest & Bessie Williams, as well as to my parents, Charles & Linda Williams, all of whom taught me to leave a legacy of service to others.

ACKNOWLEDGEMENTS

I consider myself extremely fortunate to have found the Systems Realization Laboratory (SRL) at Georgia Tech. When people asked me what I wanted in an advisor and/or graduate school experience, my answer was simple; I wanted to work in an environment where students and professors got together for dinner. The specific research topic wasn't at the top of my priorities, having an advisor with a "big name" wasn't a concern; instead, I wanted to find a place where I felt at home. Lucky for me, the SRL not only met this primary requirement, but it also fulfilled the other, more traditional, selection criteria as well. The working environment of the SRL made such an impression on me during my initial visit that I chose the lab before I chose an advisor with whom to work.

Fortunately, the selection of an advisor within the SRL was not difficult, as I was given the opportunity to work with both Dr. Farrokh Mistree and Dr. David Rosen who both displayed characteristics that I was searching for in a mentor. As my co-advisors, I must first acknowledge their efforts as a team – I would like to thank them for broadening my engineering knowledge, for assisting me in surpassing my own expectations, for stressing scholarship in all that I do, for taking a "risk" in hiring one additional student in the fall of 2000, for showing me a proper balance between teaching and research as a professor, and of course, for establishing the SRL and its environment.

I thank Farrokh Mistree for his constant encouragement, for sharing his wisdom and insight, and for fueling my passion of becoming a professor. I hope I can provide my

future students a warm home, a bright smile, a strong sense of scholarship, academic insight, and maybe an occasional hug just as he provided for me over these past years.

I thank David Rosen for his research insight, his encouragement, for pushing me to be a better engineer, for providing me with challenging and rewarding research questions, for adapting to my work habits (read: procrastination), and for encouraging me to better them. I hope that I can provide my future students with the strong sense of curiosity, insight, professionalism, and scholarship that he has instilled in me.

I also acknowledge the other professors of the SRL, Janet K. Allen, Bert Bras, and Chris Paredis, who all contributed to my growth despite not being an official advisor. Dr. Jack Lackey is yet another professor of the Woodruff School that mentored me (through providing me with a basic understanding of ceramics processing) during my career here.

I also acknowledge the guidance and insight provided to me by the reading committee of this dissertation: Dr. Joe Cochran, Dr. Hamid Garmestani, Dr. David McDowell, and Dr. Shreyes Melkote. Special thanks are offered to Dr. Cochran for being a tertiary research advisor to me during the completion of this dissertation. His limitless knowledge of ceramics, reduction, and material science was invaluable in the development of the secondary hypothesis of this work. Despite being officially retired, Dr. Cochran met with me on several occasions to discuss this topic of research; and more often than not, to review the fundamentals of materials science. I am grateful that he always did so with patience, understanding, and enthusiasm. There is no doubt that this research could not have been completed without the donation of his time, intellect, and lab resources.

In the same vein, Michael Middlemas, Tammy McCoy, and Laura Cerully (graduate students in the School of Materials Science and Engineering) were all instrumental in the completion of this research. Their constant support and assistance in the reduction and sintering of the green ceramic parts that I created were invaluable. Special thanks is offered to Michael Middlemas for spending countless hours tutoring me in operating various pieces of equipment related to the materials science discipline. His generous donation of time, knowledge, and lab resources will not be forgotten. I thank Dr. Jin Lee, a research scientist of the GT Lightweight Structures Group for guiding and assisting me at the beginning of this research – his suggestion to abandon the stereolithography working principle early in the research was invaluable.

I acknowledge Mike Stewart and Sterling Skinner of the Woodruff school for assisting me in obtaining the three-dimensional printing machine. I acknowledge Dr. Scott Johnston for training me on the 3DP machine and for assisting me with the creation of the mini-build bins. I also acknowledge the generosity of Joe Pechin, President of Aero-Instant Spray Drying Services, for donating the spray-dried material used in this research.

I acknowledge all of the members of the SRL, both present and past, for providing an environment in which I enjoyed working. Special thanks are offered to Dr. Carolyn Seepersad for bringing the research topic of this dissertation to my attention and for being yet another co-advisor. I thank Dr. Marco Fernandez, Dr. Benay Sager, Dr. Jitesh Panchal, Dr. Greg Mocko, Dr. Ameya Limaye, Andrew Schnell, and Nathan Rolander for their continuing encouragement and support. I acknowledge current lab members Jamal Wilson, Stephanie Thompson, Nathan Young, and Greg Graf for lending their ears and

advice during the final trying months of completing this research. Jamal Wilson is further acknowledged for assisting in the completion of Appendix A.

A special acknowledgement is offered to Dr. Matthew Chamberlain and Dr. Scott Duncan for their friendship and support during my stay at Georgia Tech. The friendship and memories that we established are some of the most important and enjoyable parts of my stay in Atlanta. My graduate school experience would not have been as meaningful as it was without them.

I gratefully acknowledge the support of a G. W. Woodruff Presidential Fellowship and NSF Grants DMI-0522382 and IGERT-0221600. The latter grant represents the funding offered by the Georgia Tech TI:GER program which deserves special recognition for providing sufficient financial support for initiating this research.

Finally, I must attempt to express the amount of gratitude that I have for the constant support and encouragement of my entire family. Specifically I thank my mom, Linda Williams, and dad, Dr. Charles Williams, for instilling in me the importance of education at a young age, and for constantly encouraging me throughout these many years at Georgia Tech. I thank my sister, Dr. Lunetta Williams, for her support and friendship, and for leading the way towards a PhD and assistant professorship position – yet another example of her bravely forging a path in life in which I can follow. I also offer gratitude to Dr. Richard Brantley, Diana Brantley, Dr. Jessica Brantley, Dr. Thomas Fulton, and Gabriel Fulton for providing an additional warm, supportive, and caring family for me to be a part of. I am extremely fortunate to have such a wonderful family.

Of course, no amount of words can express the gratitude that I owe my wife, Justine Brantley, for her constant love and support during the completion of my PhD degree.

Justine stood beside me and comforted me during the trying times; she stood in front of me to lead the way forward as she completed her Master's degree; and at times, she was forced to stand behind me in order to push me and cheer me towards completion. Most of all, I thank her for not losing faith in me during these many years at Georgia Tech, and for supporting my dream to become a professor. I am truly lucky to be partnered with her in our journey through life together.

TABLE OF CONTENTS

LIST OF TABLES

LIST OF FIGURES

NOMENCLATURE

a	Major radius of ellipse
α	Angle of incidence of truss with build surface
AM	Additive manufacturing
$A_{overhang}$	Area of overhanging material between two sequential layers
$A_{overlap}$	Area of overlapping material between two sequential layers
b	Minor radius of ellipse
C_{3DP}	Cost of 3DP machine
C_{batch}	Cost per production batch
C_{binder}	Cost of binder material
C_d	Depth of cure (stereolithography)
C_{fixed}	Fixed costs of production
$C_{furnace}$	Cost of purchasing sintering furnace
C_{maint}	Maintenance cost of 3DP
COMPGEO	Complex geometry (selection criterion)
$C_{operation}$	Operating cost of 3DP machine
C_{oxide}	Cost of oxide material
C_{part}	Cost per part
$C_{reduction}$	Cost of reducing parts
$C_{solvent}$	Cost of solvent material
$C_{spraydry}$	Cost of spray-drier equipment
C_{tot}	Total annual cost of producing parts

d	Particle diameter
d_b	Depth of build bed
DEPRATE	Rate of deposition (selection criterion)
d_{green}	dimension of feature in green state
dn	Diameter of nozzles
d_p	Depth of part
D_p	Penetration depth of energy into resin (stereolithography)
$d_{sintered}$	Dimension of feature after sintering
E_c	Critical energy density below which polymeriszation will not occur (stereolithogrpaphy)
E_{max}	Peak value of exposure of laser beam (stereolithography)
ϕ	Fraction of particles in suspension
GREENLOD	Solids loading of green part (selection criterion)
γ_{LV}	Surface tension of liquid-vapor interface
γ_{SL}	Surface tension of solid-liquid interface
γ_{SV}	Surface tension of solid-vapor interface
η	Viscosity of suspension
h_b	Height of build bed
h_p	Height of part
i	Degree of roughness of powder
φ	Length of overhang between two sequential layers
k	Permeability of powder bed
l	Infiltration length

λ	Length of overlap between two sequential layers
LT	Layer thickness
MATPREP	Material preparation effort (selection criterion)
MATSEL	Material selection (selection criterion)
MINFEAT	Minimum feature size (selection criterion)
N_{3DP}	Number of 3dp machines
N_{bands}	Number of passes/bands required of printhead to deposit a build layer
N_{heads}	Number of printheads
N_l	Number of layers required to build a part
$N_{nozzles}$	Number of nozzles
Np	Number of parts in a part layer
Npl	Number of part layers in a build
$Nppy$	Number of parts per year to be fabricated
P_{binder}	Wt % of binder in granules
POWSIZ	Powder size (selection criterion)
PVA	Poly-vinyl alcohol (spray-dried binder coating)
Q	Scattering efficiency term for suspended particles
θ	Contact of angle in wetting
RESTRESS	Residual stress in final part (selection criterion)
Re	Reynolds number
ρ_{oxide}	Density of oxide powder in granules
SURFIN	Surface finish (selection criterion)
t	Truss thickness

t_{infil}	Time of infiltration
T_{clean}	Time to clean each part
t_{dry}	Drying time of batch
TECHCOST	Cost of technology (selection criterion)
t_l	Time required to print a single build layer
t_{pl}	Time to build a layer of several parts
t_{prime}	Time to prime the nozzles
$t_{prime,tot}$	Total time spent priming the print cartridge during the build
T_{recoat}	Time to recoat the build
T_{setup}	Time to set up the build
t_{sinter}	Sintering time of batch
V	Droplet volume
v_{fast}	Velocity of fast axis
$V_{overhang}$	Volume of overhanging material between two sequential layers
V_{part}	Volume of part
v_{pist}	Velocity of piston lowering/raising
v_{recoat}	Velocity of recoat
v_{slow}	Velocity of slow axis
W_a	Work of adhesion
We	Weber number
Wf	Width of feed build
W_p	Work of penetration
w_p	Width of part

W_S	Work of spreading
x_{space}	Horizontal spacing between parts
y_{space}	Vertical spacing between parts

SUMMARY

Low-density cellular materials, metallic bodies with gaseous voids, are a unique class of materials that are characterized by their high strength, low mass, good energy absorption characteristics, and good thermal and acoustic insulation properties. In an effort to take advantage of this entire suite of positive mechanical traits, designers are tailoring the cellular mesostructure for multiple design objectives. Unfortunately, existing cellular material manufacturing technologies limit the design space as they are limited to certain part mesostructure, material type, and macrostructure.

The opportunity that exists to improve the design of existing products, and the ability to reap the benefits of cellular materials in new applications is the driving force behind this research. As such, the primary research goal of this work is to design, embody, and analyze a manufacturing process that provides a designer the ability to specify the material type, material composition, void morphology, and mesostructure topology for any conceivable part geometry.

The accomplishment of this goal is achieved in three phases of research:

- *Design* – Following a systematic design process and a rigorous selection exercise, a layer-based additive manufacturing process is designed that is capable of meeting the unique requirements of fabricating cellular material geometry. Specifically, metal parts of designed mesostructure are fabricated via three-dimensional printing of metal oxide ceramic powder followed by post-processing in a reducing atmosphere.

- *Embodiment* – The primary research hypothesis is verified through the use of the designed manufacturing process chain to successfully realize metal parts of designed mesostructure.
- *Modeling & Evaluation* – The designed manufacturing process is modeled in this final research phase so as to increase understanding of experimental results and to establish a foundation for future analytical modeling research. In addition to an analysis of the physics of primitive creation and an investigation of failure modes during the layered fabrication of thin trusses, build time and cost models are presented in order to verify claims of the process's economic benefits.

The main contribution of this research is the embodiment of a novel manner for realizing metal parts of designed mesostructure.

CHAPTER 1

LOW-DENSITY CELLULAR MATERIALS

Low-density cellular materials are a special classification of metallic structures which have gaseous voids dispersed throughout the material. These voids reduce the part density while improving the part strength, impact-absorption, and acoustic insulation. Whether used for lightweight, high-strength skins for the aerospace or automotive industry, or for simple structural members, there are many applications that would benefit from the use of cellular materials.

Unfortunately, existing cellular material manufacturing technologies are extremely limited. Current cellular material production techniques are limited by poor material selection, pre-determined part geometry and mesostructure, and non-repeatable results. An ideal cellular material manufacturing process would provide a designer the ability to prescribe the material type and the specific material location throughout a part based upon the artifact's intended purpose.

The principal goal in this dissertation is to design, embody, and analyze a manufacturing process that provides a designer with the ability to specify the material type, material composition, void morphology, and mesostructure topology for any conceivable part geometry.

In this introductory chapter, the motivation for the above stated goal is presented. In the first subsection of this chapter, the existing types of low-density cellular materials are introduced and classified. In Section 1.2, the different cellular material manufacturing processes are critically evaluated. The primary research question that

drives this research is presented in Section 1.3. Finally, the organization of the dissertation is presented in Section 1.4.

1.1 LOW-DENSITY CELLULAR MATERIALS

"When modern man builds large load-bearing structures, he uses dense solids; steel, concrete, glass. When nature does the same, she generally uses cellular materials; wood, bone, coral. There must be a reason for it" (Ashby et al., 2000).

The observations of cellular materials found in the natural world have directed more than 50 years of research towards manufacturing processes capable of producing high-strength, light-weight artifacts with cellular mesostructure. Low-density cellular materials are metallic bodies in which any kind of gaseous voids are dispersed (Figure 1.1). This special class of materials features a metallic phase that divides space into closed cells which contain a gaseous phase. The key advantage offered by cellular materials is high strength accompanied by a relatively low mass. Cellular materials can also offer large stiffness, improved impact-absorption, and thermal and acoustic insulation to their applications (Banhart, 2000).

Figure 1.1 – Low Density Cellular Materials

1.1.1 Cellular Material Applications

The ability to create components with cellular materials would be extremely valuable to the aerospace, automotive, and defense industries. The high-strength, low-weight characteristics of these materials could be successfully applied for any type of structural component. The low mass of these materials would benefit applications that require low moments of inertia, such as arms for industrial robots. The material's ability to absorb impact could be used for lightweight armored plating on military vehicles, or as effective bumpers on automobiles. Fluid can be passed through the internal geometry of these materials as a means of actively cooling the structure; as such, support structures for satellites could be actively cooled to provide thermal management associated with solar radiation.

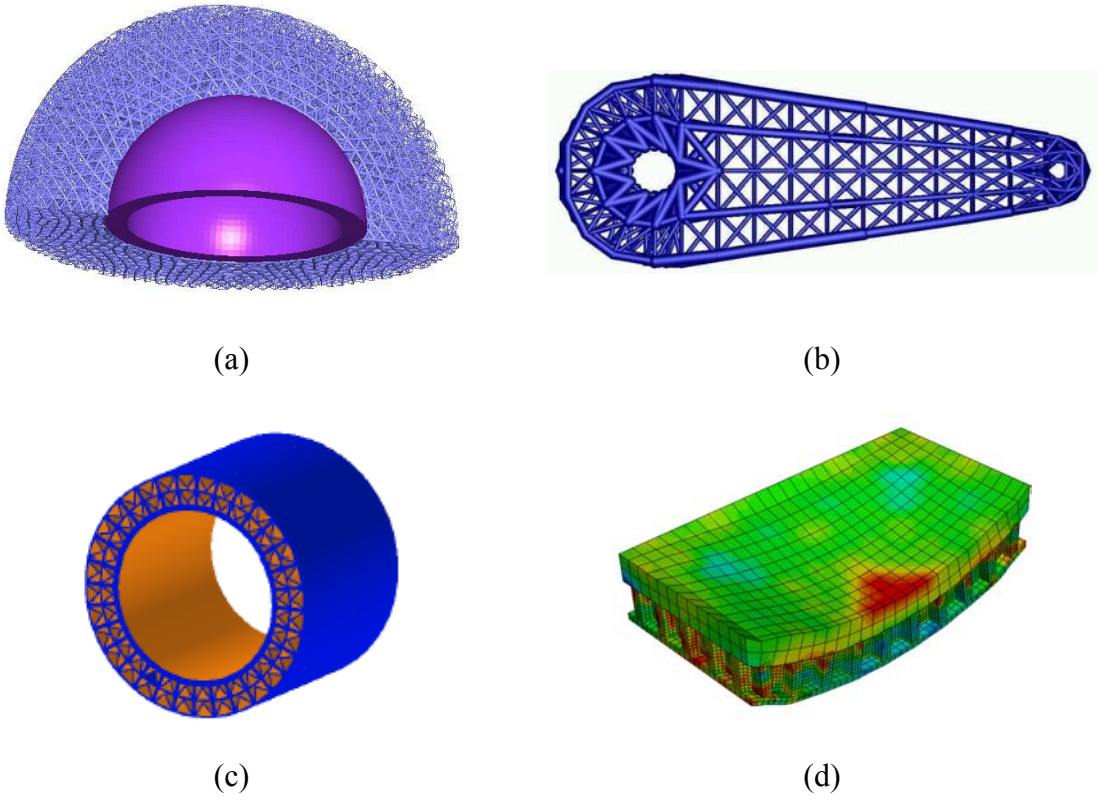

(a) (b)

(c) (d)

Figure 1.2 – Example Applications of Cellular Materials with Designed Mesostructure

Recent research of the Georgia Tech Systems Realization Laboratory has focused in designing the mesoscopic topology (the geometric arrangement of the solid phases and voids within a material or product on the size range of 0.1 to 10 mm) of cellular materials in order to effectively support and improve multiple design objectives of the artifact. For example, Wang and coauthors designed an acetabular cup (Figure 1.2a) in which the porosity of the truss structure has been configured to match the porosity of the recipient's bone so as to encourage bone growth upon implantation (Wang et al., 2006). Wang and coauthors have also created a trussed robot arm (Figure 1.2b) that has been optimized to minimize mass while meeting strength and deflection constraints (Wang and Rosen, 2002a). Seepersad and coauthors use a robust topology design methodology to design a jet engine combustor liner with cellular material (Figure 1.2c) that has sufficient strength to withstand the combustion chamber's extreme pressures and stresses associated with thermal expansion while still maintaining open cells that allow for active cooling via forced convection (Seepersad et al., 2004; Seepersad et al., 2006). Finally, Thompson and coauthors designed blast resistant panels to efficiently absorb impact from large impulse forces (Figure 1.2d) (Thompson et al., 2006).

1.1.2 Classification of Cellular Materials

Several different types of cellular materials have resulted from the multiple decades of research dedicated to creating manufacturing processes capable of producing man-made cellular materials. Cellular materials are classified by the nature of placement of the internal voids – either stochastic or ordered (Figure 1.3).

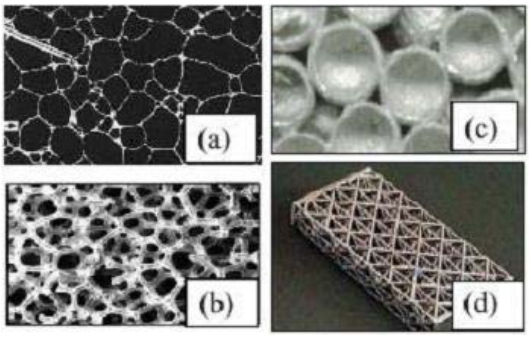

LOW-DENSITY CELLULAR MATERIALS

Stochastic	*Ordered*
• (Solid) metal foams **(a)**	• Honeycomb (via crimping & stamping)
• Metal sponges **(b)**	• Lattice Block Materials **(d)**
• Porous metals	
• Hollow sphere foams **(c)**	

Figure 1.3 – Low Density Cellular Material Mesostructure (Banhart, 2000) and Classification

Stochastic Cellular Materials

Stochastic cellular materials are composed of cells of random shape, morphology, and distribution. Stochastic materials have excellent thermal and acoustic insulation properties (Hayes et al., 2001). Bahnhart distinguishes three types of stochastic cellular metals: (i) porous metals, (ii) solid metal foams, and (iii) metal sponges (Banhart, 2000). Porous metals are a special class of cellular metals in which the pores are usually round and are isolated from each other. Solid metal foams originate from liquid-metal foams and have closed, round, or polyhedral cells that are separated by thin films (Figure 1.3a). Metal sponges, alternatively, have interconnected voids throughout the structure (Figure 1.3b). Research effort has been put towards generating some order into stochastic cellular structures. Hollow sphere foams (Figure 1.3c) are composed of miniature hollow spheres. Although still arranged stochastically, they have the advantage of having uniform cell size distribution and regular cell shape.

Ordered Cellular Materials

Ordered cellular structures are much more difficult and expensive to make than stochastic structures. These structures are characterized by a periodic unit cell or by a repeating structure topology throughout the part. Unlike stochastic cellular materials, this

class of structures offers repeatable part quality. Ordered cellular materials have superior mechanical properties, including energy absorption, strength, and stiffness (Gibson and Ashby, 1997), as well as lower pressure drop and high surface area densities than stochastic metal cellular structures – two important properties for heat transfer performance (Hayes et al., 2001).

Interest in these structures has been driven by both structural and thermal management applications of cellular metals. Honeycomb sandwich panels, for example, are extremely mechanically efficient structures: very effective cross flow heat exchangers can be created by flowing a coolant along the channels of honeycomb structures; stiffness can be created by placing the channels perpendicular to the face plates (Wadley, 2002). Furthermore, honeycomb geometry has proven to have better strength and stiffness than its stochastic counterparts (Cochran et al., 2000).

To date, two different types of ordered metallic cellular structures have been successfully manufactured:

i. *honeycomb materials* – Honeycomb materials are characterized by periodically repeating unit cells with wall thicknesses typically no greater than 500 microns. They are made by stamping or crimping thin sheets of metal into a corrugated shape and then joining them to create ordered cellular structures (Wadley et al., 2003). These materials have periodic cells and are excellent for lightweight structural support.

ii. *lattice block panels* – Developed by Jamcorp, these materials are classified by thick trusses with many trusses (four or more) per node (Figure 2d), which form cells with sizes typical of cellular metals (Jamcorp, 2004). The truss structures

are typically tetrahedral in shape, and are repeated periodically throughout the structure.

With a classification schema for low-density cellular materials established, focus is shifted to an investigation of their manufacturing processes in order to analyze possibilities for improvement through further research.

1.2 MANUFACTURING CELLULAR MATERIALS

As outlined in the previous section, there are many different classifications of cellular materials. For each classification, there are several types of manufacturing processes capable of creating these structures. In this section, these processes are reviewed and critically analyzed.

Due to the required intricate internal geometry, manufacturing a component with cellular mesostructure is nearly impossible with traditional subtractive machining. As such, researchers have looked to other technologies such as additive manufacturing, molding, forming, and joining as a means of producing this unique class of material.

1.2.1 Stochastic Cellular Materials

Having a random distribution of pores throughout, stochastic cellular materials are typically produced by introducing a bubbling agent to the metal during a solidification transition.

Metal Sponges

Metal sponges are typically manufactured by sintering metal powders that are either loosely compacted or have a filler material that disintegrate during sintering. They can also be made by investment casting using a polymer preform. These processed sponges can be net-shape, and can be made from a wide variety of materials.

Metal Foams

Of the cellular materials currently manufactured, metal foams are the most commonly produced. Metal foam manufacturing methods are classified into two groups: direct foaming and indirect foaming via a precursor (see Figure 1.4).

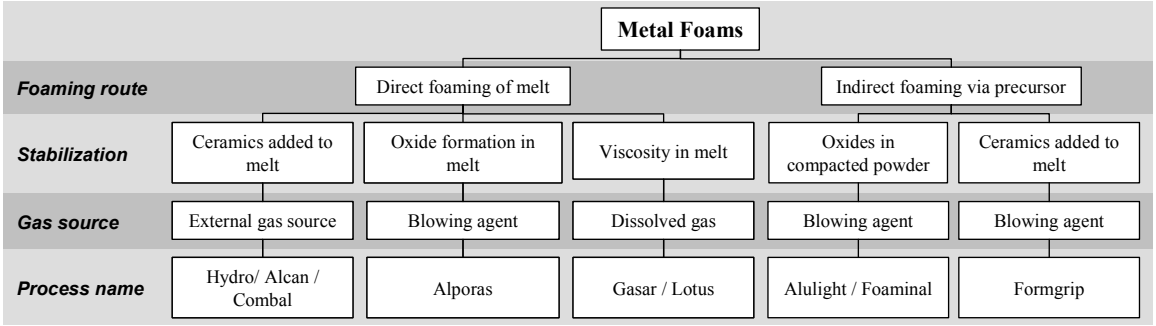

Figure 1.4 – Industrial Processes for Metal Foam Production (Banhart and Weaire, 2002)

Direct foaming of metallic melts can be accomplished in one of three ways: by injecting gas into the liquid metal from an external source (Hydro/Alcan/Combal), by causing an in-situ gas formation in the liquid by admixing gas-releasing blowing agents to the molten metal (Alporas), or by preparing supersaturated metal-gas systems under high-pressure and initiating bubble formation by pressure and temperature control (Gasar/Lotus) (Banhart, 2000).

The Hydro/Alcan/Combal processes of injecting gas directly in metallic melts are very economically efficient at producing large, continuous volume metal foams because of the way in which the foam is pulled off of the top of the liquid surface (Figure 1.5).

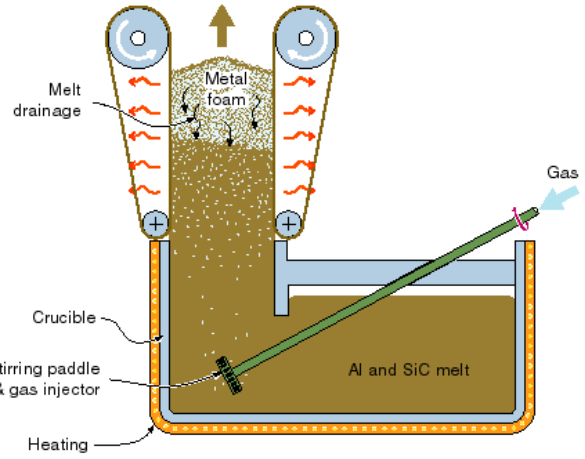

Figure 1.5 – Schematic of Melt Gas Injection (Wadley, 2002)

Unfortunately, this feature of the process is accompanied by significant drawbacks. "A natural consequence of gravitationally induced drainage is evident in foamed slabs which usually have a gradient in density, pores size, and elongation. Moreover, the shearing forces of the conveyor belt lead to diagonally distorted cells in the final product, causing a pronounced effect on the mechanical properties, which become anisotropic" (Banhart, 2000). Furthermore these techniques cannot produce net-shape parts; therefore, after processing, the foam will need to be cut to achieve the desired geometry, which will thereby open the structure's cells. The presence of a high content of ceramic particles can make machining very difficult.

The Alporas process of using blowing agents (titanium hydride, TiH_2) in melts to create foams seems to make the most homogeneous aluminum foams available (Banhart, 2000). Unfortunately, only aluminum alloys can be made with this technique because the hydrogen released in the process embrittles many metals, and the decomposition of the foaming agent occurs too quickly in higher melting point alloys (Ashby et al., 2000). Similar to the gas-injection process, this process produces bulk volumes of metal foams.

As such, machining of the bulk material is needed to achieve the desired geometry. Furthermore, it can be assumed that this process is more expensive than its counterparts because it is a batch process.

The Gasar process (a Russian word for gas-reinforced) produces foams in shaped containers, offering an ability to slightly shape the external geometry of the material. The foams have largely elongated pores oriented in the direction of solidification. The pore size distribution is non-uniform because of concurrent growth of small and large pores and coalescence (Banhart, 2000). Ashby et al., note that "with so many process variables, control and optimization of the pore structure are difficult" (Ashby et al., 2000). The authors also note that the method has "certain safety issues," and that as a batch process, the process is considered expensive.

While direct foaming techniques can only create foams in bulk, net shape parts can be molded using indirect techniques (Banhart and Weaire, 2002). Indirect foaming of metals is accomplished by mixing metal powders with a blowing agent, compacting the mix, and then foaming the compact by melting (Alulight / Foaminal techniques). "With this process, closed molds can be filled with foam, and structural foam parts of complex shape can be manufactured. Shaped sandwich panels with two dense face sheets and a cellular core can also be made" (Banhart and Weaire, 2002). The Formgrip (an acronym for "foaming of reinforced metals by gas release in precursors") process starts from a melt (instead of with powders) in which blowing-agent powder is dispersed. The melt is then solidified to form a solid precursor that can later be foamed by remelting. These two techniques are preferable foaming methods because they provide a designer the freedom to choose the part's external geometry and material composition.

Hollow Sphere Foams

Hollow sphere foams (Figure 1.3c) have been developed as an effort to place some order into the manufacturing of this class of material (Sanders and Gibson, 2003). This special material is created through joining hollow metal sphere particles through sintering or through diffusion bonding via pressure and heat (Sanders and Gibson, 2003). The use of hollow spheres provides porosity in the overall structure by both the voids within each sphere and the voids present between the outer shells of each sphere; therefore, they are of mixed open/closed-cell character (Lim et al., 2002).

1.2.2 Ordered Cellular Materials

While ordered cellular structures are more difficult and expensive to make than stochastic structures, this class of structures offers repeatable part quality though careful (and often tedious) construction of the cellular mesostructure.

Honeycombs via Metal Crimping and Stamping

This process involves stamping or crimping thin sheets of metal into a corrugated shape and then joining them to create ordered cellular structures (Figure 1.6).

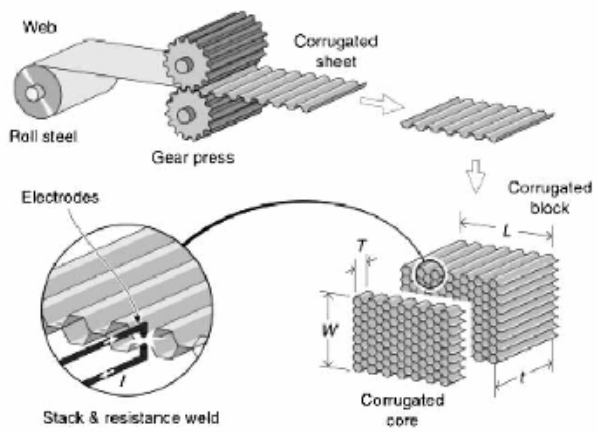

Figure 1.6 – Metal Honeycomb via Sheet Crimping (Wadley et al., 2003)

These structures consist of periodically repeating hexagonal cells. These hexagonal honeycomb materials are used in aerospace applications as heat resistant, low-density, structural elements (Cochran et al., 2000). Typically, thin strong skins are bonded to the lightweight honeycomb core to create sandwiches for structural applications.

Although this process cost-effectively creates strong, lightweight, ordered cellular structures, its major limitation is a designer's inability to design either the macro- or mesostructure. For example, the stamping/joining process is limited to only uniform, hexagonal, cellular structures. Not only do other cell shapes offer superior strength and stiffness, but it may be desirable to manufacture functionally graded cellular structures with variable cell sizes and topologies for specific applications. Furthermore, there are difficulties with forming the cellular sandwiches into complex, non-planar shapes due to induced anticlastic curvature (Sypeck and Wadley, 2002).

Lattice Block Materials

These truss structures are created by specialized casting techniques. Jamcorp creates their lattice block materials using sand casting techniques (Jamcorp, 2004). Chiras and coauthors use rapid prototyping to create truss structure patterns for an investment casting process with a high fluidity Be-Cu alloy (Figure 1.7) (Chiras et al., 2002).

Wadley notes that, "This is an expensive process and results in structures that contain significant casting porosity (a consequence in part of the complex topology which makes continuous fluid access to the solidification interface difficult). The use of a ductile Be-Cu casting alloy compensates for defects but not for the high cost and weight" (Wadley, 2002).

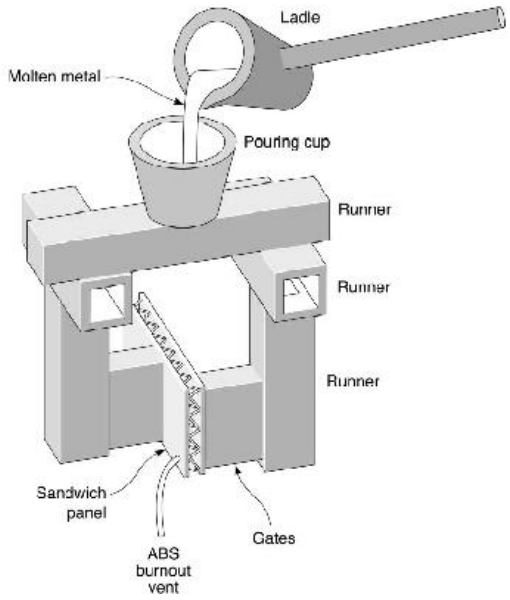

Figure 1.7 – Investment Casting of Lattice Block Material from ABS Pattern (Chiras et al., 2002)

In (Wadley et al., 2003), it is noted that, in general, cast lattice materials lack the mechanical robustness required in structural applications. Furthermore, these techniques are only capable of making truss structures with a prismatic macrostructure. Most importantly, these techniques limit a designer's freedom to specify topology due to the constraint on possible cell and truss size imposed by the use of casting techniques.

1.2.3 Critical Analysis of Cellular Material Manufacturing

From a high level of abstraction, four severe limitations are prevalent throughout cellular material manufacturing processes:

i. *non-repeatable results* – some processes create cellular structures where voids are distributed randomly; as a result, part quality is not consistent

ii. *limited materials* – existing techniques have a limited selection of working materials

iii. *limited mesostructure topology* – most cellular manufacturing techniques either cannot predict the morphology of the pores, or can only consistently produce one certain pore size or shape

iv. *limited part geometry* – existing techniques are unable to produce cellular structures for any conceivable three-dimensional geometry

The capabilities of the individual processes are presented in Table 1.1. As can be observed in the table, no single process satisfies all of the core requirements of a cellular material manufacturing process. From a high level of abstraction, these limitations are representative of the overall lack of designer freedom offered by these different manufacturing techniques.

Table 1.1 – Designer Freedom Offered by Various Cellular Material Production Techniques

		Processes	*Repeatable*	*Material Freedom*	*Mesostructure Freedom*	*Macrostructure Freedom*
Stochastic	Metal Foams	Hydro / Alcam / Combal		✓		
		Alporas				
		Gasar / Lotus				
		Alulight / Foaminal				✓
		Formgrip				✓
		Metal Sponges		✓		✓
		Hollow Sphere foams	✓			
Ordered		Honeycombs (via crimping & stamping)	✓	✓		
		Lattice Block Materials	✓			

The largest limitation of stochastic cellular structures is the complete lack of control that a designer has over the topology of the mesostructure. While these techniques provide a cost-effective means of lowering part density, the techniques do not provide repeatable, or even predictable, results. Barnhart notes that these processes are extremely difficult to control and therefore cannot be improved through process optimization (Banhart, 2000). Furthermore, these techniques limit a designer in the types of

macrostructure that can be made – only three stochastic processes can make near net-shape geometry. The majority of the techniques listed are also only capable of producing aluminum and aluminum alloys due to processing constraints (see Section 1.2.1.), thus limiting a designer's choice of material.

Comparing the two classes of cellular materials, Evans and coauthors note, "Stochastic materials are inexpensive but place material in locations where it contributes little to material properties (other than density). Periodic materials (on the other hand) can be made by several (for the most part) expensive techniques. They can be designed to optimize multifunctionality by placing material at locations where mechanical and other performance indices are simultaneously maximized" (Evans et al., 2001). While it is true that ordered cellular materials offer a designer more control over material placement, the existing manufacturing techniques constrain a designer to a predetermined part mesostructure, material type, and macrostructure. Such limitations prevent a designer from creating an ideal mesostructure for the (multiple) design goal(s) of the part's intent. Furthermore, as stated in Section 1.2.2, the processes are only capable of producing planar geometries, thus limiting a designer's choice in macrostructure.

Of the four limitations listed, the inability to create unlimited mesostructure topologies is perhaps the most debilitating. If the key benefit of using cellular materials is increased part strength while maintaining a low mass (or another performance parameter), a designer will desire to have complete control over the placement of material, and/or the determination of proper mesostructure topology for the specific product intent. *An ideal cellular material manufacturing method would provide a*

designer the freedom to dictate the morphology of the voids, the geometry of the part, and the type of material to be used.

1.3 PRIMARY RESEARCH QUESTION: MANUFACTURING CELLULAR MATERIALS WITH DESIGNED MESOSTRUCTURE

1.3.1 Parts of Designed Mesostructure

To place emphasis on the desire for designer freedom in the manufacture of cellular materials, a new classification of metallic cellular structures is introduced: *designed mesostructure*. Materials with designed mesostructure are a class of cellular structures wherein material is strategically placed in order to achieve the part's (multiple) design objective(s) (i.e., low mass, high strength, high stiffness, etc.). This classification is attributed to manufacturing processes that provide a designer the freedom to prescribe material composition and mesostructure topology for the material.

1.3.2 Applications of Parts of Designed Mesostructure

The ability to selectively place material in the mesostructure of the part would revolutionize the way in which products are manufactured; moreover, such ability would also change the way in which products are designed. The determination of an artifact's material would no longer be a selection process; instead, a designer would have the ability to design the product's macro-, meso-, and microstructure.

The industrial potential for such manufacturing freedom is unlimited. Products that require the satisfaction of multiple design objectives would greatly benefit from such a manufacturing process where material could be selectively placed. The thermal efficiency of structural heat exchangers could be improved while simultaneously maximizing their strength by appropriate design and manufacture of their mesostructure.

With the ability to design and manufacture unique mesostructure topology, support structures could have a designed mesostructure that maximizes stiffness and improves impact absorption characteristics. In addition, those products that are currently designed within existing manufacturing constraints can be re-designed for improvement. With the ability to design the material composition, the mesostructure, and the material placement, the cooling microchannels of gas turbine blades, for example, could be redesigned in order to greatly improve engine efficiency.

More concrete examples of artifacts that benefit from designed mesostructure are offered in Section 1.1.1. It is important to note that none of the existing stochastic or ordered cellular material manufacturing techniques are capable of realizing any of those applications presented (e.g., acetabular cup, blast resistant panel, robot arm, etc.).

1.3.3 Manufacturing Materials with Designed Mesostructure

There currently exist two manufacturing approaches that are classified in the "designed mesostructure" category of cellular materials: linear cellular alloys and additive manufacturing.

Linear Cellular Alloys

In order to alleviate the existing limitations and processing difficulties of creating ordered cellular structures through forming and casting, the Georgia Tech Lightweight Structure's group has looked toward the extrusion of specialized ceramic pastes to create linear cellular alloys. Displayed on the right-hand side of Figure 1.1, linear cellular alloys (LCA) are characterized by their thin cell walls. As such LCAs are similar in mesostructure to honeycomb materials; however since LCAs are manufactured via an extrusion process with an interchangeable die, the cellular mesostructure of LCAs need

not have a common topology across the cross-section. The process begins with a metal oxide-based ceramic paste (containing lubricants, binders, and other additives) that is extruded through an interchangeable die. The ceramic body is then dried and processed in a reducing atmosphere to chemically convert the precursor into a metallic artifact (Cochran et al., 2003).

Of the existing methods devoted to the creation of cellular materials, this manufacturing process offers the most design flexibility. The key to this process's superiority lies in its (possibly inadvertent) following of Suh's Independence Axiom, which states that in a good design, independence of the functional requirements is maintained (Suh, 1990). "Unlike other processing techniques for cellular materials (e.g., foaming and melt casting), Linear Cellular Alloy (LCA) technology decouples cell geometry and metal/alloy composition. Composition is controlled only by formulation of the oxide powder mixture according to the chemical specification of the intended product" (Cochran et al., 2002). With this technique, Cochran et al. have successfully processed a number of transition metal oxides, as well as many engineering alloys including stainless steel, maraging steel, Inconel and Super Invar (Cochran et al., 2000).

Cell geometry is controlled by interchangeable extrusion dies; thus, the extrusion process can create an infinite variety of honeycomb shapes with repeatable and predictable results. Complexity of cell geometry is limited only by extrusion die manufacturability and powder paste rheology (Hayes et al., 2001). Compared to the more conventional stamped and crimped sheet metal honeycomb process, this process allows for significantly more complex distributions of cell shapes and sizes, as well as precise cell alignment and wall thicknesses. Furthermore, the cellular structure is not restricted

to a periodic nature – cell morphologies can differ across the cross-section of the material.

While the extrusion process offers freedom in the design of the cellular topology, the overall geometry is limited to linear extrusions. This also forces the cross-section to be constant along the entire extruded piece. This is a significant limitation, as a designer has no control over the external geometry of the final part. Thus, in the context of Table 1.1, the LCA manufacturing process is a repeatable process that offers design freedom in material selection and in mesostructure geometry, but not in the macrostructure geometry.

Additive Manufacturing

Contrary to traditional manufacturing technologies that create artifacts through the subtraction of material from a workpiece, additive manufacturing (AM) create parts through the successive addition of material layer-by-layer. Due to this approach, AM processes offer the utmost geometrical freedom in the design and manufacture of an artifact. As such, some researchers have looked into using AM techniques for the production of cellular materials.

There are many commercial AM technologies, each having their own principal solution (from using UV laser and photopolymer resin, to precisely extruding a heated plastic filament), but each has the same end goal in common: the manufacturing of a part through successive deposition of material one cross-sectional layer at a time. AM processes begin with a three-dimensional computer model of the part to be made. This digital representation of the part is virtually sliced into layers by computer software. Each layer, representing a cross-section of the desired part, is sent to the AM machine

where it is built upon the previously built layer. This process, building the part layer-by-layer from the bottom-up, is repeated until the part is completed. This additive fabrication process is capable of building complex geometry that cannot be fabricated by any other means.

As mentioned in Section 1.2.2, AM techniques are used for the creation of truss structure patterns for the investment casting process used to make lattice block materials. Hattiangadi and Bandyopadhyay use Fused Deposition Modeling (FDM) to indirectly create porous structures through a lost mold technique (Hattiangadi and Bandyopadhyay, 1999). Chiras and coauthors use AM to create truss structure patterns for investment casting process with a high fluidity Be-Cu alloy to indirectly create cellular materials (Chiras et al., 2002).

These techniques' indirect processing routes are not only expensive, but also limit the sizes of cells and trusses that can be created. The resulting structures are typically plagued by porosity due to the inability of the fluid to access all parts of the truss structure (Wadley, 2002). Furthermore, indirect processing places a constraint on the cell topologies that can be made – only materials with interconnected cells are feasible.

Wang and Rosen have investigated using AM techniques to directly manufacture cellular materials. They use stereolithography (SL) to realize objects that feature an internal truss structure that is conformal to any given external geometry (Wang and Rosen, 2002b). Their structures differ from lattice block materials (and other constructed truss approaches) since the trusses are not constrained to periodic repetition through the structure (Wang and Rosen, 2002a). Free from this limitation, truss structures can be designed to be optimized for a product's specific design goal(s). Researchers at the

University of Leuven have created lightweight sandwich panels from glass filled nylon with the Selective Laser Sintering process (Kruth et al., 2004b).

Unfortunately, these processes are severely constrained by the limited working materials available to conventional AM techniques. In the context of Table 1.1, additive manufacturing of cellular materials is a repeatable process that offers design freedom in macrostructure and mesostructure geometry, but not in material selection.

1.3.4 Primary Research Question

A summary of the design freedom offered by of all classifications of cellular manufacturing technologies is presented in Table 1.2.

Table 1.2 – Summary of Design Freedom Offered by Cellular Material Manufacturing Techniques

		Processes	*Repeatable*	*Material Freedom*	*Mesostructure Freedom*	*Macrostructure Freedom*
Stochastic	Metal Foams	Hydro / Alcam / Combal		✓		
		Alporas				
		Gasar / Lotus				
		Alulight / Foaminal				✓
		Formgrip				✓
		Metal Sponges		✓		✓
		Hollow Sphere foams	✓			
Ordered		Honeycombs (via crimping & stamping)	✓	✓		
		Lattice Block Materials	✓			
Designed		Linear Cellular Alloys	✓	✓	✓	
		Additive Manufacturing	✓		✓	✓

The opportunity to improve the design of existing products, and the ability to reap the benefits of cellular materials in new applications, drives this research. The focus in this work is to design, develop, and analyze a manufacturing process that is capable of producing materials of designed mesostructure without constraining a designer's decisions with respect to material, mesostructure topology, or macrostructure geometry.

The primary research question of this dissertation is:

Primary Research Question:

How to manufacture three-dimensional, low-density cellular metal structures while maintaining designer freedom in the selection of the material and the design of the part mesostructure and macrostructure?

1.4 ORGANIZATION OF THIS DISSERTATION

In an effort to verify the primary research question, the focus in this dissertation is the design, embodiment, and analysis of a metallic cellular manufacturing process that does not limit a designer in his/her choice of part geometry, mesostructure topology, or material. These three phases provide a framework for the presentation of research findings and contributions in this dissertation, as shown in Figure 1.8.

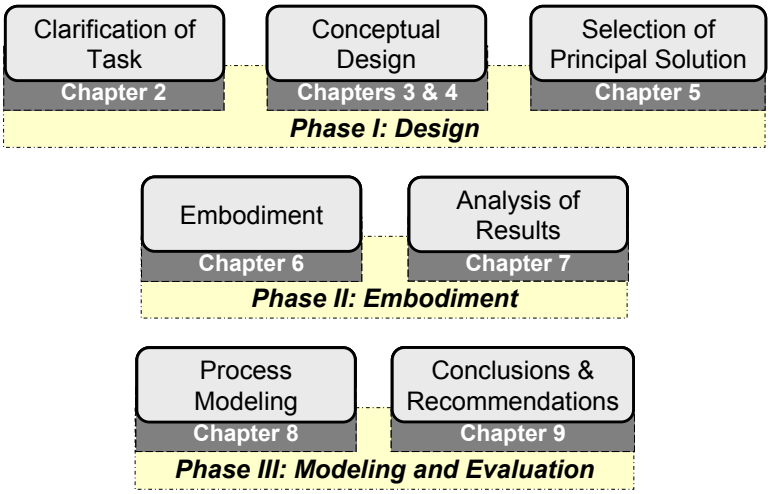

Figure 1.8 – The Three Phases of the Research

1.4.1 Phase One: Design

This first phase of this research involves the design of a manufacturing process for the realization of parts with designed mesostructure. This process is centered on a

rigorous, methodical design method, such as the one posed by Pahl & Beitz (Pahl and Beitz, 1996) (summarized in Appendix A).

The first step of the design process is the clarification of the design task. Presented in Chapter 2, this initial step begins with a preliminary list of requirements that any manufacturing process must fulfill in order to satisfactorily realize parts of designed mesostructure; this list is derived from the research foundation presented in Chapter 1. A critical analysis of two existing manufacturing processes which are capable of producing parts of designed mesostructure (direct-metal additive fabrication and linear cellular alloy extrusion and reduction) leads to the development of the primary research hypothesis:

Primary Research Hypothesis:

Three-dimensional, low-density cellular metal structures of any macrostructure, mesostructure, or material can be manufactured via layer-based additive manufacturing of metal-oxide ceramic material followed by post-processing in a reducing atmosphere.

From this hypothesis, the requirements list for the design task is refined so as to reflect the desire to create cellular green parts from metal-oxide ceramic material via a layer-based additive manufacturing that are appropriate for a thermal-chemical conversion post-processing step.

With a requirements list identified, the design portion of the research enters the conceptual design phase, which is presented in Chapters 3, 4, and 5. Following the approach suggested by Pahl and Beitz, conceptual design begins with the abstraction of the design requirements in order to formulate a solution neutral problem statement. From this, a list of sub-functions that any embodiment of the process must complete is

generated. Working principles that are a feasible means of embodying each sub-function are then ideated. These principles are then entered into a morphological matrix so that concepts ("working structures") can be systematically generated. These structures are generated and critically analyzed in Chapter 4.

The conceptual design phase closes with the completion of a selection decision in Chapter 5 wherein the principal solution of the design task is identified. This selection decision is separated into two processes: (i) a preliminary selection decision is first made in order to identify those working structures that are most-likely-to-succeed; (ii) the principal solution is then identified from the ranking of the solution principles through the use of a systematic selection decision methodology. With the principal solution identified, the design phase of the research comes to a close, and the primary research hypothesis is updated to reflect the selection decision:

Updated Primary Research Hypothesis:

Three-dimensional, low-density cellular metal structures of any macrostructure, mesostructure, or material can be manufactured via three-dimensional printing of metal-oxide ceramic powder followed by post-processing in a reducing atmosphere.

Specifically, the updated hypothesis reflects the selection of the three-dimensional printing AM process as the principal means of creating metal oxide ceramic green parts that are suitable for transition to metal via post-processing in a reducing atmosphere.

1.4.2 Phase Two: Embodiment

The embodiment phase of this research features the physical realization of the principal solution identified at the closure of conceptual design (Chapter 6). In addition

to the description of the embodiment process, this embodiment phase also features the generation and verification of a secondary research question and hypothesis:

Secondary Research Question:

How can the density of metal parts created by the thermal-chemical conversion of ceramic green parts fabricated by three-dimensional printing be improved?

Secondary Research Hypothesis:

The density of metal parts which result from the thermal-chemical conversion of ceramic green parts can be improved by creating primitives via printing a solvent into a bed of binder-coated powder particles.

The resulting parts of designed mesostructure that are created by the embodied manufacturing process chain are characterized and analyzed in an effort to verify the primary and secondary research hypotheses (Chapter 7).

1.4.3 Phase Three: Modeling & Evaluation

In an effort to better understand the underlying physical principles featured in the selected technology, three different aspects of the system are analyzed and/or modeled in Chapter 8:

- The physical principles underlying the creation of solid primitives in the three-dimensional printing process are explored. Specifically a review of existing physics-based models is provided in order to provide a foundation for future research in developing models for the specific embodiment of this research.

- A model of fabricating thin trusses via layer-based AM processes is developed in order to gain a better understanding as to why they frequently fail during fabrication.
- Due to the desire to create a process that can be easily scaled to the rate and cost of traditional manufacturing techniques, models of the process build time and technology cost are presented.

1.4.4 Dissertation Roadmap

A graphical representation of the organization of this dissertation is provided in Figure 1.9. This figure serves as a "roadmap" for the dissertation; it is presented at the closure of each chapter as a means for assisting the reader in becoming aware of the progression of the research tasks as well as the approach employed for verifying the posed research hypotheses.

As can be seen in the figure, the three research phases presented in Figure 1.8 coincide with specific chapters of the dissertation: the design phase is described in Chapters 2-5, the embodiment phase is presented in Chapters 6 and 7, and the results of the modeling and evaluation phase are presented in Chapters 8 and 9.

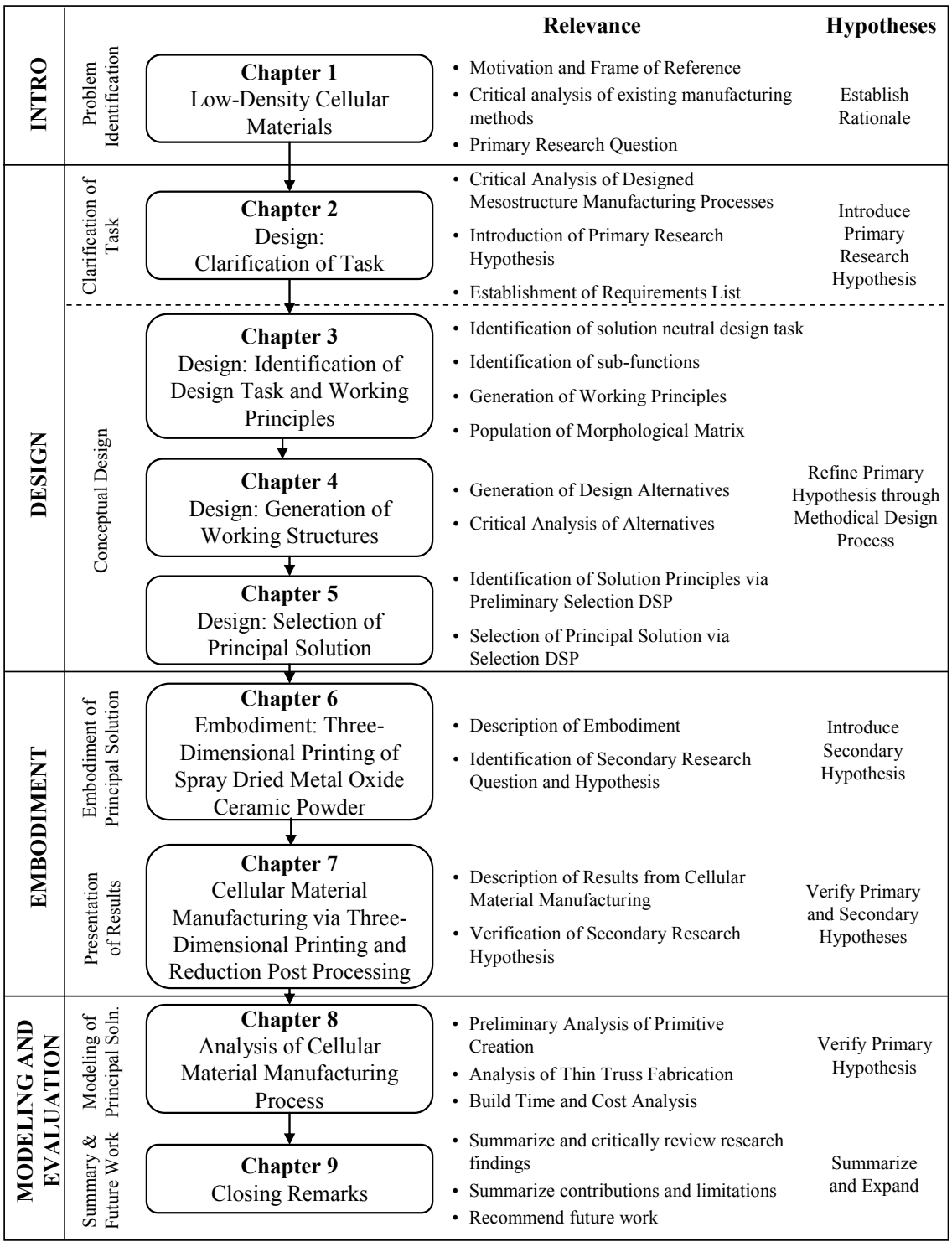

Figure 1.9 – Dissertation Roadmap

CHAPTER 2

DESIGN: CLARIFICATION OF TASK

Introduced in Section 1.3, materials of designed mesostructure are a class of cellular structures wherein material is strategically placed in order to achieve the part's (multiple) design objective(s) (i.e., low mass, high strength, high stiffness, etc.). This classification is attributed to manufacturing processes that provide a designer the freedom to prescribe material composition and mesostructure topology for the material.

This chapter marks the beginning of the design phase of this research. Before conceptualization and product development can begin, one must first clarify the given design task. In this chapter, the design information and existing constraints are specified. This task begins with the identification of a preliminary requirements list for a manufacturing process suitable for the realization of parts of designed mesostructure in Section 2.1. In an effort to further clarify the task, two existing methods for realizing parts of designed mesostructure are critically analyzed in Section 2.2. A hypothesis for the primary research question (presented in Section 1.3.4) is formulated as a result of this investigation. A finalized list of requirements is offered at the closure of the chapter (Section 2.5).

2.1 MANUFACTURING MATERIALS OF DESIGNED MESOTRUCTURE: PRELIMINARY REQUIREMENTS

Following the design methodology as outlined by Pahl and Betiz (Appendix A) (Pahl and Beitz, 1996), the design process begins with clarifying the design task through the creation of a requirements list. Within the requirements list, all requirements are

listed under their respective heading and are labeled as either a demand (D) or a wish (W). Demands are requirements that must be met before a given design may be accepted. Requirements that are wishes need to be considered whenever possible, unless their satisfaction compromises demands or more important requirements. The manner in which various design concepts fulfill the requirements will influence the evaluation and selection process.

Requirements are generated by progressing through the main headings suggested by Pahl and Beitz in an effort to make sure that nothing is forgotten. These main headings include geometry, kinematics, forces, energy, material, signals, safety, ergonomics, production, quality control, assembly, transport, operation, maintenance, recycling, costs, and schedules. It is crucial that the requirements generated in this early stage of design be solution neutral. Because the manufacturing process has yet to be determined, there are no constraints are listed for the kinematics, forces, or energy of the potential design solution. As the design effort progresses, more specific requirements will be added as design decisions are made and the design space becomes more constrained.

The preliminary requirements presented in Table 2.1 are primarily focused in the types of geometry (and associated dimensions, where appropriate) that must be created by the to-be-designed manufacturing process. These requirements are generated by exploring the prior-art of existing cellular material manufacturing techniques. Additional requirements are generated by extracting needed features from potential cellular material applications such as those presented in Sections 1.1.1 and 1.3.2.

Table 2.1 – Preliminary Requirements List for a Process for the Manufacture of Parts of Designed Mesostructure

D/W	*Requirement*
	Geometry
D	Able to process any macrostructure geometry
D	Able to process complex geometry (e.g., internal voids)
D	Able to process small cell sizes (0.5 – 2 mm)
D	Build small wall thicknesses (100 – 300 μm)
D	Build trusses from 0.5 mm – 10 mm in diameter
	Material
D	Able to process multiple materials
W	Minimize amount of effort required to adapt to a new material
W	Able to process standard working material (i.e., material is not proprietary or require specialized formulation)
	Production
D	Able to produce parts 250 x 250 x 250 mm or larger
W	Does not require additional post-processing
	Quality Control
D	Parts have ≥ 95% relative density
D	Material properties are comparable to standard
D	Minimize surface roughness before finishing (≤ 0.02 mm Ra)
	Operation
W	Does not require special operating environment
W	Minimize operator interaction
	Recycling
W	Minimize environmental impact by minimizing wasted material
W	Reusable wasted material
	Costs
D	Minimize cost of technology
D	Minimize cost of maintenance
D	Minimize cost of material
W	Easily scaled for large applications

In an effort to further clarify the task, two methods for realizing parts of designed mesostructure are explored: direct metal additive manufacturing (Section 2.2), and linear cellular alloy manufacturing (Section 2.3).

2.2 DIRECT METAL ADDITIVE MANUFACTURING

Introduced in Section 1.3.3, additive manufacturing technologies are a class of fabrication processes that create artifacts through the layer-by-layer production of cross-sectional slices. This bottom-up approach to the production of parts enables AM processes to create complex geometries that cannot be fabricated by traditional

manufacturing techniques. Relevant to this research, AM technologies are capable of producing parts with intricate internal features, which are common in parts with designed mesostructure.

Unfortunately, these processes are severely limited by the working materials available to conventional AM techniques which are typically constrained to polymers that are specialized for each process. In an effort to alleviate this limitation, recent research has focused in directly creating metal parts with AM (as opposed to previous indirect approaches which focused on using AM for tooling and mold creation).

In this sub-section, current research regarding the use of AM processes to build cellular materials is critically analyzed. A classification scheme for commercially available direct metal AM processes is offered in Section 2.2.1. These processes are detailed in Sections 2.2.2 – 2.2.6. Finally, the processes' abilities to produce parts of designed mesostructure are critically evaluated in Section 2.2.7.

2.2.1 Classification of Direct Metal Additive Manufacturing Processes

From a high-level of abstraction, all AM technologies can be described by six primary sub-functions:

i. *store material* – each AM technology relies on a starting material that will be consolidated to form the final part (e.g., powder, tape, resin, slurry, etc.)

ii. *pattern material* & *pattern energy* – these sub-functions are the heart of an AM technology as they correspond to the way in which the part is developed. The process can involve creating primitives by directly depositing and patterning material onto a substrate. Alternatively, the process can selectively pattern energy in order to transform the raw material into finished primitives. Finally,

the process can pattern both the material and energy simultaneously in order to create solid primitives.

iii. *create primitive* – each AM technology features the initiation of a phase change in order to transform/shape the raw material into the desired part. This energy is typically used to change the phase of the stored material in order to create each cross-section (e.g., liquid to solid, gas to solid, etc.). This sub-function entails such working structures as polymerization, sintering, melting, and freezing.

iv. *provide material for next layer* – as an additive fabrication process, each AM technology must have a method of supplying material for the manufacture of each layer. While some technologies directly deposit material, most use a recoating process to prepare for additional layers.

v. *support previously deposited layer* – many AM technologies have a method of supporting deposited material to ensure stability, and to be able to build complex geometry such as overhangs.

These sub-functions are combined in Figure 2.1 to form a function structure (explained in more detail in Section 3.2) that is applicable for all AM technologies.

Using the pair of "pattern" sub-functions as a foundation, a classification of direct metal AM technologies is offered in Figure 2.2. The primary differentiation is made by the technology's main patterning medium: material, energy, or the combination of the two. The technologies are further classified by the dimension in which the material and/or energy is patterned. One dimensional scanning refers to those technologies that pattern single lines. Those technologies that are classified in the two-dimensional area patterning category are capable of processing entire areas of material at a time.

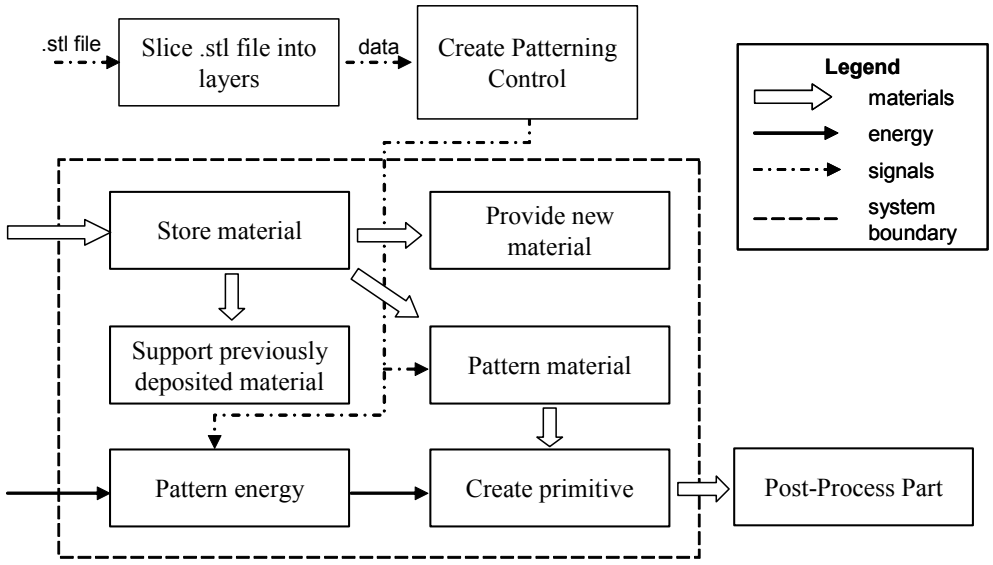

Figure 2.1 – Function Structure for Additive Manufacturing Processes

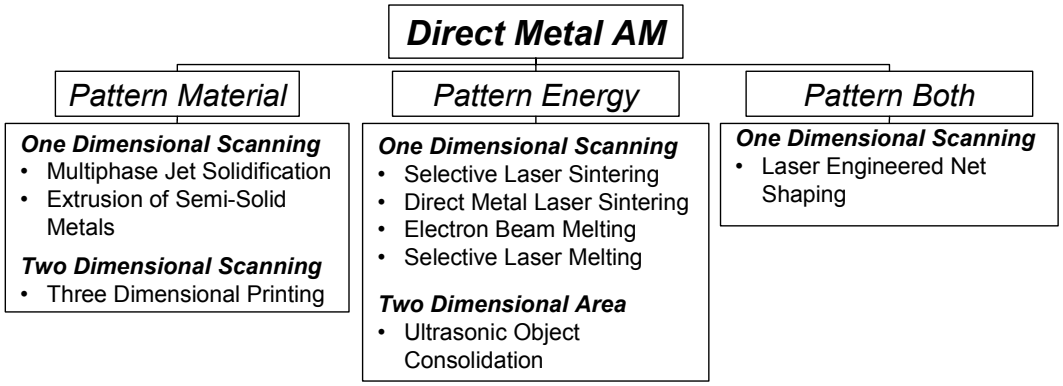

Figure 2.2 – Classification of Direct Metal Additive Manufacturing Technologies

The technologies reviewed in this section can be further classified by the solution principles they employ in their embodiment of the primary sub-functions listed above. Each technology is presented in the context of a morphological matrix (described in detail in Section 3.4) (Zwicky, 1967) in an attempt to gain understanding of the fundamental physical principles employed by each technology.

2.2.2 One-Dimensional Energy Patterning of Powder Bed

This classification of AM technology encompasses four distinct processes, Indirect Laser Sintering (LS), Direct Metal Laser Sintering (DMLS), Electron Beam Melting (EBM), and Selective Laser Melting (SLM). Observing Table 2.2, it can be observed that the solution principle of these technologies is to selectively join powder particles by scanning an energy source across a powder bed. The energy source raises the temperature of the powder above its softening or melting temperature, thus joining the particles together. Once one layer is scanned, the bed is lowered and recoated by spreading fresh powder via a roller or blade.

Table 2.2 – Solution Principles of LS, DMLS, SLM, and EBM

		Sub-Function					
		Store Material	**Pattern Material**	**Pattern Energy**	**Create Primitive**	**Provide Material for Next Layer**	**Support Previously Deposited Layer**
Solution Principle	**LS**	Binder coated powder	No material patterning	1D heat source (laser)	Liquid-phase sintering	Recoat by spreading	Bed of build material
	DMLS	Two-phase powder					
	SLM	Single phase powder		1D heat source (electron beam)	Melting		
	EBM						

Although very similar in general concept, each of these concepts differs in the type and power of energy source used to join the powder particles. This difference is conveyed in the different working principles listed in the "pattern energy" and "create primitive" sub-functions. "Liquid-phase sintering" is when necking of the particles occurs due to liquefaction of a secondary binder material so as to hold the structural material together (Kruth et al., 2003). A different form of sintering, solid-state sintering is when necking solely occurs due to diffusion of atoms along the particle surface at

elevated temperature. Liquid phase sintering requires a lower temperature, and is faster than solid state sintering since mass transport can occur much more rapidly due to liquid flow and particle rearrangement; for these reasons, liquid phase sintering is much more frequently used than solid state sintering in AM applications (Agarwala et al., 1995). "Melting" involves the use of a heat source to fully melt the powder. Melting differs from liquid phase sintering and partial melting in that melting involves full melting of the primary metal powder; liquid phase sintering involves partial melting of a secondary material with a lower melting temperature, and partial melting involves the partial melting of the grain skin but not the grain core.

Detailed machine specifications regarding cost, deposition rate, minimum feature size, z-resolution (layer thickness), and surface roughness are presented (where available) in Table 2.3. All pricing data shown in Tables 2.3, 2.5, 2.7, 2.9, and 2.11 are derived from the 2004 Wohlers Report (Wohlers, 2004).

Table 2.3 – Machine Specifications for LS, DMLS, EBM, and SLM

	Attributes						
Alternatives	Production Cost ($)	Maintenance Cost ($/year)	Deposition Rate (cm^3/hr)	Minimum Feature Size (mm)	Z-Resolution (mm)	Surface Roughness (μm, R_z)	References
LS	320,500	~ 30,000	-	0.6	-	-	(Pham et al., 2003)
DMLS	441,000	-	45	0.3	0.1	30	(Khiang et al., 2001; Feenstra et al., 2003; EOS, 2004)
EBM	479,000	-	60	1.2	0.1	-	(Cormier et al., 2004b)
SLM	380,000	-	5	0.1	0.05	20	(Fockele, 2004)

Indirect Laser Sintering (LS)

The unique material processing principle of LS is its use of polymer-coated metal powder particles. Relatively low laser power can be used to selectively melt the powders' 5 μm polymer coating in order to effectively bond the metal particles together and create a "green" part. A thermal burnout cycle is necessary to remove the polymer binder. Finally, an additional thermal cycle is necessary to sinter the part and to infiltrate it with a material (typically bronze) to fill in the voids left from binder burnout, and thus making the part fully dense. Although the process has accurate deposition both in-plane and in-growth directions, the debinding and infiltration steps can cause a loss of accuracy due to shrinkage (4.5% in horizontal, 5% in vertical) (Greulich, 1997). Another disadvantage of LS is its limited materials selection; currently only three proprietary steel alloys are available. These materials are primarily used for tooling applications.

It should be noted that indirect LS can also be accomplished by mixing a polymer powder in with a metal powder (instead of coating), thus creating a two-phase powder system. However, Beaman and coauthors note that working with binder-coated particles is preferred over simply mixing the two materials since mixed materials can segregate by density and could potentially lead to highly variable powder and part properties (Beaman et al., 1997). Coated powders also ensure that the binder is mixed homogenously in the material system. Furthermore, in LS, the strength of green parts made from coated particles are usually higher than that of parts made using a powder mixture at the same polymer content (Badrinarayan and Barlow, 1991).

Oddly, no data for the rate of material deposition for the LS process is available. The scan speed for the laser has been cited at 380 cm/s (3D, 2004), which is roughly

equivalent to the speed of the DMLS machine. Despite the lack of an exact deposition measurement, it is assumed that the overall process is rather long, since the sintering and infiltration oven cycle is 22 hours (Wohlers, 2001).

Direct Metal Laser Sintering (DMLS)

DMLS takes a more direct approach than LS in its material processing. The process is centered on the addition of a second metallic powder that has a lower melting temperature than the primary, structural phase. Upon the selective addition of laser energy, this secondary material melts first, and serves as a binder material, thus effectively sintering (liquid phase) the powder mixture (Greulich, 1997). The addition of a second phase to the material system is used to overcome balling effects that were observed when sintering was attempted with a single metal powder (Agarwala et al., 1995).

While the process doesn't require a debinding stage, infiltration is necessary to achieve full density since parts have a porosity of 70% after the build. DMLS fabrication suffers from shrinkage and induction of thermal stresses because of the direct sintering process, which can result in distorted and curled parts. Since heat is applied to the top surface of the powder bed, the top densifies to a greater extent than does the bottom surface of each layer. Additionally, the upper surface cools from a high temperature than the material below, causing additional thermal contraction on the upper surface. Together, these effects cause the deposited material to warp upward (Carter and Jones, 1993). In order to compensate for this warping, "anchors" (thin, sintered layers onto which the structure is constructed) are added to the artifact, much like the support structures featured in stereolithography. This thin frame gives stiffness to the overall

structure and thus avoids warping. Unfortunately, these thin support structures must be removed in post-processing, and can be difficult (or impossible) to remove from truss structures due to their internal geometry.

At the onset of this dissertation, the commercially available DMLS process could only produce steel-alloy proprietary materials. However, during the completion of this dissertation, titanium alloys have been developed. Furthermore, fully dense parts directly out of the powder bed are now being reported by EOS. Their approach has changed and involves the use of laser energy to partially melt a single phase metal powder.

Electron Beam Melting (EBM)

While the EBM process has a similar working structure to the other technologies of this category, its principal solution for patterning energy is very different. Instead of using a CO_2 laser to join powder particles, the EBM process uses a 4.8kW electron beam (Arcam, 2004). Parts created by this process require no additional thermal treatments and have virtually no porosity. Rather than melting the layers in a left-to-right or spiral scanning pattern, layer portions are melted in random order to evenly distribute heat and prevent thermal distortions. Another interesting feature of this process is that building takes place in a vacuum to provide the electrons a clear path to the powder bed. While this does increase the cost of the process, parts do not suffer from impurities and typically have high strength properties.

Arcam, the company that commercializes the EBM technology, states that a wide variety of metal powders can be processed with the process, although they "initially chose to concentrate on the use of H13 tool steel alloys for tooling applications." A titanium alloy has also been developed by the company. Cormier and coauthors note that

"e-beam freeform fabrication is well suited for a wide variety of metal and metal composite materials" (Cormier et al., 2004a), and have recently shown limited success with using the technology to process aluminum.

Process parameters such as beam power, operating atmosphere, environmental temperature, pre-sintering and melting patterning must be carefully controlled in order to achieve quality parts. Recent research seems to have made progress on correcting the "icicles" (sharp stalactite-like features) that appeared on the bottom-facing surfaces of early parts. Researchers have also found that pre-sintering the powder before exposing it to the full power of the electron beam has significantly improved part quality and reduced residual stresses. It should be noted, however, that this pre-sintered powder is difficult to remove from the finished part due to its increased strength. This also reduces the surface finish of the created part; bead blasting is required to remove any powder clinging to the part surface. The as-processed part of the EBM process has a "textured surface that resembles a sand casting" (Cormier et al., 2004a).

Selective Laser Melting (SLM)

The SLM process is capable of making 100% dense metal parts by selectively melting metal powder without the need for binder material, proprietary powders, or post-processing. SLM uses an intense infrared laser that is carried through an optical fiber which allows the beam diameter to be reduced down to 30 μm. This small beam diameter is very important for achieving high tolerances and better surface definition (Pham et al., 2003). While complex trussed structures have been created as a result of the small laser spot size, its use severely limits the process's deposition rate.

Processing difficulties such as balling, residual stresses, porosity, and warping plagued early research with this technology (Kruth et al., 2004a). Balling occurs when the molten material does not wet the underlying substrate due to the surface tension (Abe et al., 2001). Similar to LS, warping occurred due to large temperature gradients during part construction. Furthermore, process parameters had to be constantly reconfigured each time the material system changed, since powder behavior radically altered depending on the material and the shape and size of the power particles (Abe et al., 2003).

Fockele & Schwarze, a German manufacturing company, has commercialized the SLM technology and has seemed to overcome these processing difficulties that plagued early research with full melting of metallic powder. This unique success with laser melting seems to stem from two technological advantages, (i) the small laser spot that "melts the powder base material completely in a small area without overheating and distorting the surrounding material," and (ii) "patented curing solutions" (Mining, 2004). The process has been used to successfully process zinc, bronze, stainless steel, tool steel, titanium, chromium-cobalt, silicone carbide, and aluminum oxide with mechanical properties that are comparable to bulk material (apart from a severely reduced ductility) (Jandin et al., 2005). Due to its smaller layer thickness and laser spot size, SLM parts tend to have better mechanical properties as compared to their DMLS counterparts. However, the parts suffer from large residual stresses (Mercelis and Kruth, 2006).

2.2.3 One-Dimensional Material Patterning

Table 2.4 – MJS Solution Principle

		Sub-Function					
		Store Material	**Pattern Material**	**Pattern Energy**	**Create Primitive**	**Provide Material for Next Layer**	**Support Previously Deposited Layer**
Solution Principle	**MJS**	Binder / structural material suspension	1D extrusion	No energy patterning	Thermal polymerization	Direct material addition	-

Multi-Phase Jet Solidification (MJS)

MJS selectively deposits a powder-binder mixture through an extrusion nozzle. The mixture is passed through the machine as feedstock, where it is first heated above its solidification point to achieve a suitable viscosity. It is then squeezed out of the nozzle by a pumping system and is deposited layer by layer. The molten material solidifies once in contact with the platform or the previous layer due to the decrease in temperature and pressure (Greul et al., 1997). The contact of the liquefied material leads to a partial remelting of the previous layer and a good bonding between the layers. In order to make a functional metal part, the green part made via the deposition (typically 50-70% volume solid material) must then undergo a debinding step and a sintering step. After the sintering step, the part undergoes 10-16% linear shrinkage and the resultant part density is 95-98% (Greul et al., 1996).

The MJS process benefits from being able to process a wide variety of materials due to its similarities with metal injection molding (MIM), the only limitations being that the materials must have a suitable viscosity (10 to 200 Pa·s), and a binder melting temperature of less than 200 C. The similarity to MIM also enables the MJS process to create parts of comparable material properties. Unfortunately, the process's use of an

extrusion nozzle limits its minimum feature size, layer thickness, and planar accuracy (+/- 0.2 mm); as such, MJS is unable to make extremely small features and is "suitable for producing medium sized parts" (Greul et al., 1996). Furthermore, only overhangs under 45^{o} are feasible (the process does not currently have a separate support material deposition nozzle, although this is not without a solution). Finally, sharp edges are filleted because the molten material is yielded behind the extrusion nozzle.

The MJS machine was commercialized as the RP-Jet 200 in 1996. There are no available estimates for process cost; however, one can assume that the cost is relatively low since a high-powered energy source is not required for its operation.

Table 2.5 – Machine Specifications for MJS

	Attributes						
Alternatives	Production Cost ($)	Maintenance Cost ($/year)	Deposition Rate (cm^3/hr)	Minimum Feature Size (mm)	Z-Resolution (mm)	Surface Roughness (μm, R_z)	References
MJS	-	-	90	0.5	0.1	-	(Greul et al., 1996; Greul et al., 1997)

2.2.4 One-Dimensional Patterning of Energy and Material

Table 2.6 – LENS Solution Principle

		Sub-Function					
		Store Material	**Pattern Material**	**Pattern Energy**	**Create Primitive**	**Provide Material for Next Layer**	**Support Previously Deposited Layer**
Solution Principle	**LENS**	Single phase powder	1D powder deposition	1D energy patterning	Melt	Direct material addition	5-axis deposition

Laser Engineered Net Shaping (LENS)

The LENS process uses a high-powered laser beam to selectively clad metallic powder. "Cladding" is analogous to welding. The beam is focused on a metal substrate

to create a molten weld pool. Metallic powder is injected directly into the pool and melted; as the laser passes by the deposit it is quickly cooled, leaving behind a thin line of metal (Keicher, 1998). This technology is categorized as a process that patterns both material and energy. Other variations of this same principal solution (but with a slightly different embodiment) are Shape Deposition Manufacturing (Merz et al., 1994), Direct Metal Deposition (Mazumder et al., 1999), and Selective Laser Cladding (Laeng et al., 2000).

The major strength of the LENS process is its ability to deposit a multitude of materials. Since the material deposition relies only on the feeding of a powder or wire, it is relatively simple to use multiple kinds of materials. Currently titanium, nickel, cobalt, steel, and aluminum can be deposited with LENS. In fact, recent research has shown that LENS is capable of manufacturing binary functionally graded materials (Hedges and Keicher, 2002). Furthermore, parts made from the LENS process have superior mechanical properties to their cast counterparts. Parts created by the LENS process are 100% fully dense and require no extra processing to improve material properties (Keicher, 1998). It should be noted, however, that if the deposition is not properly controlled, pores can be generated between deposition layers, thus making the parts anisotropic.

The LENS process has its weaknesses, however. While LENS is lauded for its planar accuracy (+/- 0.127 mm), it suffers from poor accuracy in the build direction (+/- 0.508 mm) (Griffith et al., 1996). Also, unlike standard RP technologies, LENS does not have the ability to generate support structures, and thus cannot produce complex geometries featuring overhangs. As such, the geometry able to be created with the LENS

process is limited; the maximum angle achieved in a single width deposition is 30° (Laeng et al., 2000). This limitation has been recently addressed through research on the development of a five-axis LENS machine (Hedges and Keicher, 2002).

Table 2.7 – Machine Specifications for LENS

	Attributes						
Alternatives	Production Cost ($)	Maintenance Cost ($/year)	Deposition Rate (cm^3/hr)	Minimum Feature Size (mm)	Z-Resolution (mm)	Surface Roughness (μm, R_z)	References
LENS	1,000,000	~50,000	8.19	0.76	-	1095	(Griffith et al., 1996; Keicher, 1998; Optomec, 2004)

2.2.5 Two-Dimensional Material Patterning

Table 2.8 – 3DP Solution Principle

		Sub-Function					
		Store Material	**Pattern Material**	**Pattern Energy**	**Create Primitive**	**Provide Material for Next Layer**	**Support Previously Deposited Layer**
Solution Principle	**3DP**	Single-phase powder	2D drop ejection	No energy patterning	Introduce polymer to bind	Recoat by spreading	Bed of build material

Three-Dimensional Printing (3DP)

3DP involves the use of a printer head that selectively deposits a melted polymer binder material over a bed of metal powder. Binder droplets (80 μm in diameter) form spherical conglomerates of binder liquid and powder particles as well as provide bonding to the previously printed layer. Because the printer head contains several ejection nozzles, 3DP features several parallel one-dimensional avenues for patterning. Since the process can be economically scaled by simply increasing the number of printer nozzles, the process is considered a two-dimensional patterning process. Such an embodiment

would have a high deposition speed at a relatively low cost (due to the lack of a high-powered energy source) (Michaels et al., 1992).

The selectively bound part, when removed from the bed, is a relatively low-density (50%) green part. The green part is subsequently fired and infiltrated to make a dense metal part. Stainless steel-bronze parts have been made with this technology (Extrude, 2004). The process is typically accurate to +/- 0.125 mm (Feenstra et al., 2003).

Table 2.9 – Machine Specifications for 3DP

	Attributes						
Alternatives	Production Cost ($)	Maintenance Cost ($/year)	Deposition Rate (cm^3/hr)	Minimum Feature Size (mm)	Z-Resolution (mm)	Surface Roughness (μm, R_z)	References
3DP	500,000	~50,000	1605	0.1	0.15	70	(Feenstra et al., 2003; Wohlers, 2004)

2.2.6 Two-Dimensional Patterning of Energy and Material

Table 2.10 – UOC Solution Principle

		Sub-Function					
		Store Material	**Pattern Material**	**Pattern Energy**	**Create Primitive**	**Provide Material for Next Layer**	**Support Previously Deposited Layer**
Solution Principle	**UOC**	Tape / sheet	2D tape / sheet	2D ultrasonic welding	Cutting and joining	Directly place layer	Bed of build material

Ultrasonic Object Consolidation (UOC)

UOC is the one commercially available metal AM technique that joins 2D areas of material. This is accomplished in UOC by using solid-state joining techniques to bind layers of aluminum tape to form solid parts with 98-99% density without post-processing (Solidica, 2004). Once deposited, the metallic tape is then trimmed with a subtractive

milling process. The machine achieves accuracy within +/- 0.051 mm – 0.127 mm across the build envelope. The process is currently limited to producing only aluminum.

UOC has been used to create closed honeycombs with walls with an aspect ratio of 100:1. However, because the sonotrode must have a sufficient area on which to operate, free-standing, unsupported, and/or angled ribs and trusses cannot be built with this process, thus placing a limit on its ability to create complex geometries (Robinson et al., 2007).

Table 2.11 – Machine Specifications for UOC

	Attributes						
Alternatives	Production Cost ($)	Maintenance Cost ($/year)	Deposition Rate (cm^3/hr)	Minimum Feature Size (mm)	Z-Resolution (mm)	Surface Roughness (μm, R_z)	References
UOC	350,000	~25,000	369	-	0.15	70	(Solidica, 2004)

2.2.7 Critical Analysis of Direct Metal Additive Manufacturing of Cellular Materials

It should be noted that the list of direct metal AM technologies critically analyzed in this section is not completely comprehensive. There exist a handful of technologies that have yet to be commercialized, and have yet to realize metal parts of substantial size, quality, or complexity. These technologies include Laser Chemical Vapor Deposition (LCVD) (Johnson et al., 2003), Layered Object Manufacturing (LOM) (Nakagawa, 1985; Liu et al., 1997; Klosterman et al., 1999), and Electrophotographic Printing (EP) (Karlsen and Reitan, 2003) (see Table 2.12 for a list of their solution principles). These technologies are not considered in this analysis due to their current inability to produce parts of designed mesostructure.

Table 2.12 –Solution Principles of LCVD, LOM, and EP

		Sub-Function					
		Store Material	**Pattern Material**	**Pattern Energy**	**Create Primitive**	**Provide Material for Next Layer**	**Support Previously Deposited Layer**
Solution Principle	**LCVD**	Gas	No material patterning	1D heat source	Chemical reaction via heat	Direct material addition	5-axis deposition
	LOM	Tape / sheet	2D tape / sheet	1D heat source	Cutting and joining	Directly place layer	Bed of build material
	EP	Single-phase powder	2D powder deposition	2D heat	Liquid-phase sintering		

In an effort to systematically evaluate the ability of the direct metal AM technologies to produce parts of designed mesostructure (as dictated by the requirements outlined in Section 2.1), a methodical preliminary selection process was implemented. Proposed by Mistree and coauthors, the Preliminary Selection Decision Support Problem (DSP) is a technique for making selections in a complex, multi-faceted design environment (Mistree et al., 1994). The Preliminary Selection DSP provides a designer a framework in which the most-likely-to-succeed concepts can be identified through the systematic comparison of alternatives based upon "soft" (i.e., predominately qualitative) engineering data. Because the details of the preliminary selection process are not integral to this argument, the discussion of the process's implementation has been relegated to Appendix B.

From the selection exercise it was determined that Three-Dimensional Printing (3DP), Selective Laser Melting (SLM), and Electron Beam Melting (EBM) are the technologies "most likely to succeed" in the creation of parts of designed mesostructure. These technologies were consistently preferred because of their ability to create complex geometries with multiple materials and with good material properties. 3DP was often

preferred over SLM and EBM because of its high deposition rate and its ability to be economically scaled. Technologies such as SLS and DMLS were often scored low because of their poor selection of materials, poor material properties (due to the necessary infiltration), and poor surface finish. UOC was often scored low despite of its high deposition rate, because of its ability to only process aluminum, its anisotropic material properties, and inability to create complex geometry.

The most important learning point taken away from the preliminary selection exercise (presented in Appendix B) is the uncovering of the limitations of existing metal AM technologies. Materials of designed mesostructure are a unique class of geometry that require a manufacturing process that can selectively deposit a wide variety of materials with good surface finish, material properties, resolution, and shape complexity. From this investigation of metal AM technologies it is observed that no current technology is capable of satisfying all of the requirements listed in Section 2.1. Even those technologies identified as most likely to succeed are not completely sufficient for the creation of materials of designed mesostructure.

After further investigation it was determined that the available metal-based AM techniques do not offer an ideal means of producing cellular materials since they suffer from several technical limitations (Williams et al., 2005a). This conclusion stems from the identification of four specific, technology-level limitations:

1. *Poor Resolution* – many of the technologies' depositions are too large to make the thin walls necessary to create cellular materials.

2. *Limited Material Selection* – many of the techniques can only deposit only certain types of metals (e.g., steel alloys); furthermore, most of the techniques are only capable of making parts of a proprietary material.
3. *Poor Surface Finish*: due to the layer-by-layer deposition process, surface finishes of parts created by AM suffer from rough external features ("stair-stepping"); furthermore, poor surface finish results from the use of powders, laser cladding, and warping effects from use of high-powered lasers. Poor surface finish limits a process's ability to create small features for cellular materials. It also worsens its ability to efficiently pass fluids, thus increasing the pressure drop across the structure - important considerations for heat exchanger applications.
4. *Poor Material Properties*: metallic parts created by direct metal AM typically feature material properties that do not closely match their traditionally manufactured counterparts. Layered manufacturing also usually results in parts with anisotropic properties.

Further limitations of direct metal AM technologies were observed by investigating the processes at a functional level. Further investigation leads to specific working principles implemented for the primary sub-functions of an AM technologies that are not suited for the realization of parts of designed mesostructure:

5. *Provide Support* – While the use of a powder bed eliminates the need for support structures and allows for the creation of complex geometry, un-patterned material can be trapped or be extremely difficult to remove in extremely complex internal geometry (i.e., microchannels found in cellular honeycombs). This un-patterned material is even more difficult to remove if the entire powder bed is pre-sintered

before patterning, as is the case in DMLS and EBM. Thus, as a manufacturing process of cellular materials, this characteristic advantage may be more of a nuisance for this specific class of geometry. Furthermore, processes that use powder beds typically create porous parts with poor surface finishes. Finally, those processes that implement dedicated support material (that must be manually removed) can be impossible to remove from parts of designed mesostructure.

6. *Provide New Material* – An important component of manufacturing parts of designed mesostructure is providing a designer the ability to prescribe the composition of a part. While many of the existing AM technologies are capable of producing a range of materials, many are not capable of producing functionally graded materials. For most AM technologies, this limitation stems from the "provide new material" function. While it is technically possible for most AM technologies to make graded materials by recoating a powder bed with different material layers, it is very inefficient. Furthermore, this solution principle would only enable grading across the part's build direction.
7. *Pattern* – The application potential of the AM technologies that rely on patterning in one dimension is significantly limited. Even when ignoring all material processing constraints, there exists a fundamental limit on the scanning speed of an AM machine. It is not possible to scan a single deposition spot fast enough to be economically competitive with traditional manufacturing technologies. Furthermore, when a requirement for small features exists, as it does with cellular material manufacturing, the act of patterning with small-width one-dimensional scans becomes even more limiting.

A summary of the working principles of metal-based AM techniques, and their corresponding limitations (out of the seven listed above) is offered in Table 2.13.

Table 2.13 – Limitations of Metal Solid Layer-Based Additive Manufacturing Techniques

Name	*Working Principle*	*Limitations*	*References*
Selective Laser Sintering (LS)	Uses a CO_2 laser to selectively fuse polymer-coated metallic powder (stored in a bed) one layer at a time. Requires debinding, sintering, and infiltration	# 2 - 7	(Greulich, 1997), (Kruth et al., 2003), (Pham et al., 2003)
Direct Metal Laser Sintering (DMLS)	Similar to LS, DMLS patterns energy in a powder bed. DMLS directly sinters a two-phase metallic powder system. Requires infiltration.	# 2 - 7	(Carter and Jones, 1993), (Agarwala et al., 1995), (Khiang et al., 2001), (Feenstra et al., 2003), (EOS, 2004)
Selective Laser Melting (SLM)	Selectively melts metallic powder with an infrared laser. Does not require additional post-processing. Can make extremely small features.	# 3, 5-7	(Kruth et al., 2004a), (Mining, 2004)
Electron Beam Melting (EBM)	Uses a 4.8 kW electron beam to selectively scan and melt layers of metal powder	# 2, 3, 5-7	(Cormier et al., 2004b), (Cormier et al., 2004a)
3D Printing (3DP)	Use of a printer head to print binder polymer over a metal powder bed. Requires sintering and infiltration.	# 3 - 6	(Feenstra et al., 2003)
Multiphase Jet Solidification (MJS)	A metal powder-binder mixture is extruded through a heated nozzle to create layers (similar to Fused Deposition Modeling). Requires debinding, sintering, and infiltration	# 1, 3 - 7	(Greul et al., 1997), (Greul et al., 1996)
Extrusion and Deposition of Semi-Solid Metals (EDSSM; aka. SSM-SFF)	Deposits a semi-solid metal through a nozzle (similar to Fused Deposition Modeling)	# 1 - 7	(Rice et al., 2000)
Laser Engineered Net Shaping Techniques (LENS)	Melting powdered metals with a high-powered Nd:YAG laser. Metal powder is fed into laser beam by nozzle. Direct Metal Deposition (DMD)	# 1, 3, 7	(Laeng et al., 2000), (Keicher, 1998), (Hedges and Keicher, 2002), (Mazumder et al., 1999), (Weerasinghe and Steen, 1983)
Shape Deposition Manufacturing (SDM)	Combination of laser cladding (LENS process) with subtractive machining	# 1, 5, 7	(Merz et al., 1994)
Ultrasonic Object Consolidation (UOC)	Solid-state joining techniques deposit layers of tape to form solid aluminum parts, followed by trimming step	# 2, 4 - 6	(Solidica, 2004)
Layered Object Manufacturing (LOM)	Selectively cuts stacks of sheet metal and fuses the layers together	# 3 - 6	(Nakagawa, 1985)
Computer-aided Manufacturing of Laminated Engineering Materials (CAM-LEM)	Similar to LOM, selectively cuts layers from green tapes. Offers "cut-then-stack" technology where robot arm assembles pre-cut layers. Offers more complex internal geometry and wide material selection.	# 3 - 6	(Liu et al., 1997), (CAM-LEM, 2004)

It is important to note that SLM (Pham et al., 2003; Brooks et al., 2005), EBM (Cansizoglu et al., 2006), and DLMS have been recently been used to create parts with trussed or cellular material (Figure 2.3).

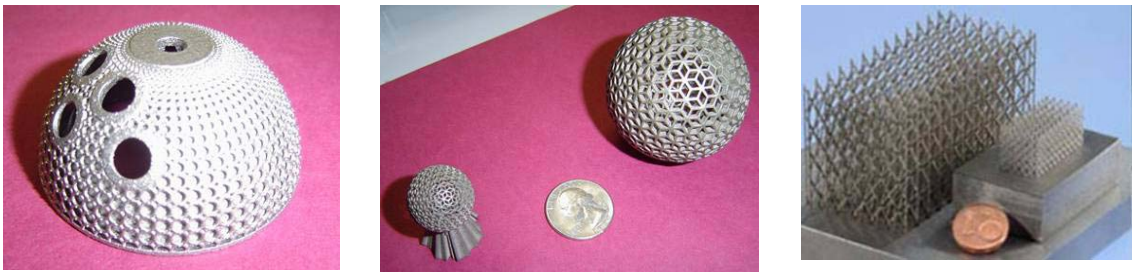

(a) (b) (c)

Figure 2.3 – Cellular Materials Created with Direct Metal AM Technologies; (a) EBM, (b) DMLS, (c) SLM

These technologies offer a sufficiently small feature size for the creation of cellular materials, and they offer a fully-dense part directly out of the powder bed. However, these technologies do suffer from limitations.

- It should be reiterated that these specific AM technologies raster a one-dimensional energy source (e.g., laser or electron beam spot) over a powder bed of metal and are therefore slow.
- The use of a high-powered energy source can introduce residual stresses, which arise from the high thermal gradients present in the material during part fabrication (Kruth et al., 2004a). This can lead to curling and/or warping during the build; as such, support structures which can be difficult to remove from small cells, must be added to the part geometry.
- Defects on bottom-facing surfaces and an overall poor surface finish typically arise due to the surface tension of the molten metal, which dominates at the small sizes required to achieve good surface finish, and creates the potential for capillary instabilities (Rice et al., 2000).

- Further problems arise when building over loose powder (which is common when creating overhanging surfaces), because the conductive heat transport is significantly larger than when building over previously melted powder – this will result in sagging overhanging structure (Kruth et al., 2007). This same effect can cause delaminations, buckling, and warping of cellular mesostructure when building surrounding walls over or around it (Rehme et al., 2007).
- In addition, the entire powder bed must be pre-sintered before a layer is deposited; this pre-sintered powder can be difficult to remove from the cells of the finished part.
- Finally, these processes are generally expensive (due to a dependence on a high-powered energy source) and have slow build rates (due to a dependence on rastering a one-dimensional pattering spot). These limitations provide opportunity for further investigation and potential improvement.

Although currently available metal-based AM technologies do not offer an ideal means of creating cellular materials (for technical and economical reasons), the concept of fabricating a part through additive means should not be ignored since it provides the greatest freedom in the design and manufacture of artifacts.

2.3 MANUFACTURING LINEAR CELLULAR ALLOYS: REDUCTION OF METAL OXIDES VIA THERMAL CHEMICAL PROCESSING

In this subsection, the Linear Cellular Alloy (LCA) manufacturing process (as described in Section 1.3.3) is investigated in further detail an effort to find a means of bypassing the limitations (as identified in Section 2.2.7) found in directly producing metal artifacts via sintering, melting, or cladding with high-powered energy sources.

LCAs, developed by the Georgia Tech Lightweight Structure's group, are extruded honeycomb-like materials, characterized by their thin cell walls and varied cross-section topology (Figure 2.4).

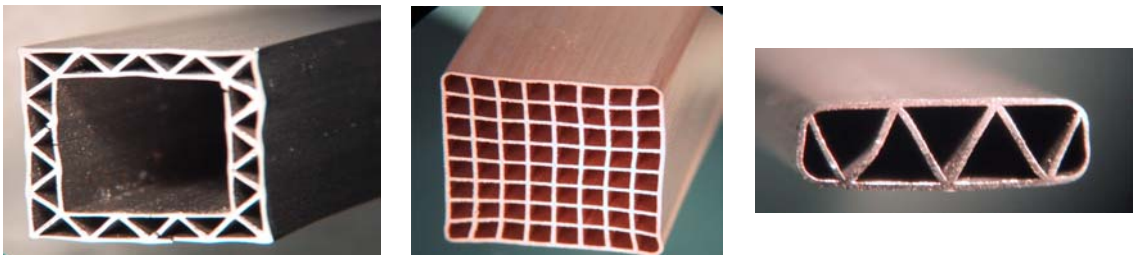

(a) Square Annulus **(b)** 8x8 Square Cell, Cell Size = 1.4 mm **(c)** Triangular Core Panel, 10 mm width

Figure 2.4 – Linear Cellular Alloys (Cochran et al., 2002)

2.3.1 Manufacturing Linear Cellular Alloys

The LCA manufacturing process (illustrated in Figure 2.5) begins with a metal oxide-based ceramic paste (containing lubricants, binders, and other additives) that is extruded through an interchangeable die (at room temperature). The ceramic green body is then dried, and processed in a reducing atmosphere to chemically convert the precursor into a metallic artifact (Cochran et al., 2003). The reducing agent is typically a gas (e.g., hydrogen or carbon monoxide), which reacts with the oxygen and forms water vapor, which is then removed from the system.

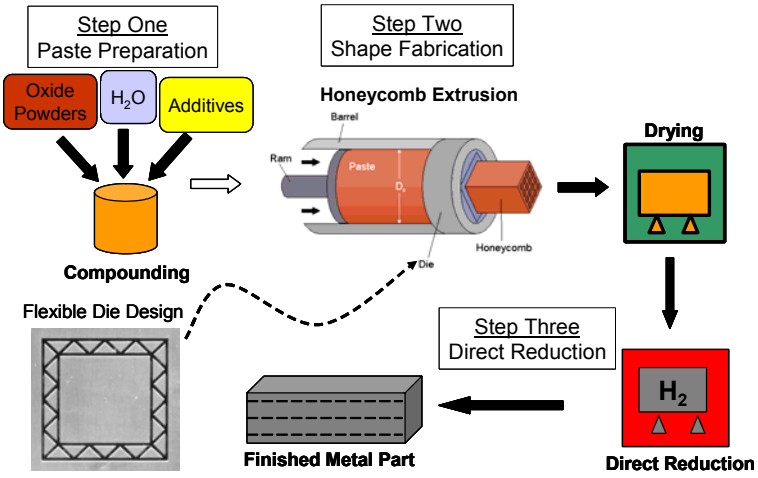

Figure 2.5 – Linear Cellular Alloy Manufacturing Process (Cochran et al., 2002)

Many metal oxides can be processed with this reduction technique. The primary requirement for a metal oxide is that it must be reducible at moderate temperatures (below the melting points of the materials involved) with a partial pressure of oxygen no lower than 10^{-16} atm. Unfortunately some elements such as Ti and Al are stable under these conditions; hence, they cannot be introduced into the alloy as an oxide, and must be added in a secondary process. With this technique, Cochran et al. have successfully processed a number of transition metal oxides (Fe, Ni, Co, Cr, N Cu, Mo, W, Mn, and Nb), as well as many engineering alloys including stainless steel, maraging steel, Inconel, and Super Invar (Cochran et al., 2000).

With the Linear Cellular Alloy (LCA) manufacturing process it is feasible to fabricate honeycomb structures with wall thickness as small as 50 times the average metal oxide particle size. This translates to thin-walled extrusions with cell sizes in the range of 0.5 to 2.0 mm with a web thickness of 50 to 300 microns (Cochran et al., 2002). These small features are accomplished, in part, by the shrinkage (and large increase in density) that is accompanied with the reduction process. Shrinkage is typically on the order of 30 to 70% by volume; this can be advantageous when fine geometric features are desired that would otherwise would be difficult or expensive to fabricate (Cochran et al., 2000).

2.3.2 Critical Analysis of the Linear Cellular Alloy Manufacturing Process

Strengths

Aside from the geometric benefits that are gained from using the extrusion process, reducing metal oxide powders has provided benefits as it produces parts of high quality. Through metallurgical characterization Cochran and coauthors have demonstrated that

"the direct reduction metal is comparable to conventionally processed counterparts" (Cochran et al., 2002). In addition, copper parts have demonstrated high thermal conductivity, and high strength and energy absorption have been demonstrated for maraging steel cellular structures. No other lightweight structure manufacturing approach demonstrates comparable values in properties (Cochran et al., 2002).

Chemical reduction of metal oxide green parts to metal has the potential to alleviate many of the limitations found in the direct-metal AM of cellular materials. An implementation of this post-processing technique is economically efficient, as the cost differential between a metal oxide powder and its metal counterpart is usually better than a 1-to-10 ratio (Cochran et al., 2000). Also, fine oxide powders are readily available in a pure and stable form. Compared to pure metal powders, metal oxides are safer as they are neither carcinogenic nor explosive.

Limitations

This novel process is not without its limitations however. As with other manufacturing techniques, certain process components impose constraints on a designer.

One major concern with the process is the large amount of shrinkage that green parts undergo. The extrusion process requires the addition of a binding agent, which must be totally removed in the drying process. Generally, this can result in the formation of cracks, laminations, and other flaws. Relatively large mounts of shrinkage can occur and disrupt dimensional stability and cause warping. As such, the parts may need to be fixtured during firing to maintain targeted tolerances, straightness and/or roundness, and to combat retained stresses and flaws (Cochran et al., 2003).

While a wide-range of geometries can be theoretically made using this process, the structure must be open for the article to survive the conversion process and emerge as a monolithic product. In general, the requirement for the geometry is to have a high surface-to-volume ratio and a highly open access to the interior. Multiple openings provide an unrestricted passage of both the reducing agents (hydrogen) to and the reaction products (water) from the interior (Cochran et al., 2003). Cochran and coauthors note that honeycombs are better suited to survive the large shrinkage that occurs during the reduction process. "The constant web thickness insures an equal coercion force to keep the material from separating or cracking, a phenomenon often observed where two neighboring unit cells were joined with a substantially smaller cross section" (Cochran et al., 2000). For this reason, it is not recommended to use this processing technique with parts that have a large variety in the cross-sectional dimensions.

While this processing technique is capable of producing parts with mechanical properties similar to their conventionally processed counterparts, the mechanical properties are heavily dependent on the manufacturing defects created by the process. Porosity can range from 5% for extruded/reduced maraging steel to 15% for extruded/reduced Inconel alloys (Cochran et al., 2000). This porosity is partially caused by low sintering temperatures (which are needed so that the constituent materials do not melt). Furthermore, the presence of porosity and the lack of Ti and Al in the alloys reduces tensile strength, strain at failure (Cochran et al., 2000), and the thermal properties of the finished part (Church et al., 2001).

A comparison of mechanical properties between bulk materials made conventionally and through direct reduction is presented in Table 2.14. While the data

presented in Table 2.14 shows some considerable weak points in the mechanical properties of the reduced alloys, it should be noted that the data is from 2000, and that the process is continuously improving.

Table 2.14 – Comparison of the Composition and Properties of Extrusion/Reduction Alloys with Regular Alloys (Cochran et al., 2000)

Composition Comparison				
Maraging Steel 350		Element %	Inconel 617	
Regular Alloy	Direct Reduction		Regular Alloy	Direct Reduction
Balance	Balance	Fe	-	-
18.0	18.0	Ni	Balance	Balance
-	-	Cr	22.0	22.0
12.5	10.0	Co	12.5	12.5
4.2	4.0	Mo	9.0	9.0
1.6	-	To	0.5	-
0.1	-	Al	1.0	-
-	-	C	0.1	-
Bulk Property Comparison				
8.0	7.61 – 7.73	Density (g/cc)	8.27	6.99
2450	1250	UTS (MPa)	-	-
2400	1200	Tensile Strength (Mpa)	760	350
186	160	Modulus of Elasticity (GPa)	211	80
6.0	1-2	Strain at Failure (%)	56	15
480 C for 3-6 hrs	480 C for 5 hrs	Heat Treatment	1200 C	1175 C

A final critique of the process is that it is very difficult to process functionally graded materials. Because a sintering post-process is needed, and because different materials have different firing temperatures and shrinkage kinetics, those graded materials produced thus far by the LCA process have had poor geometric quality.

2.4 PRIMARY RESEARCH HYPOTHESIS

From observing the design limitations imposed by current cellular material manufacturing techniques (Section 1.2), a primary research question was presented in Section 1.3:

Primary Research Question:

How to manufacture three-dimensional, low-density cellular metal structures while maintaining designer freedom in the selection of the material and the design of the part mesostructure and macrostructure?

In Sections 2.2 and 2.3, two existing methods for creating parts of designed mesostructure are presented: the creation of metal components through the reduction of metal oxide powders, and the flexible manufacture of artifacts through layer-based additive manufacturing. These approaches serve as a technical basis for this research.

In an effort to provide more freedom in the design and manufacture of the part macrostructure, we look to layer-based additive fabrication as a way to form metal oxide powders. The combination of the best traits of additive manufacturing and reduction of metallic oxide powders (Table 1.2) is a very promising solution to the limitations of existing cellular material manufacturing techniques. The capability of AM to selectively place material throughout a part alleviates the macrostructure limitations found in the LCA manufacturing process. Conversely, the extensive material selection and excellent material properties found in the metal oxide reduction technique (Cochran et al., 2002) are a perfect complement to the material troubles found in traditional AM processes and the (post-)processing issues found in direct metal AM technologies.

From these points, a primary research hypothesis is formulated:

Primary Research Hypothesis:

Three-dimensional, low-density cellular metal structures of any macrostructure, mesostructure, or material can be manufactured via layer-based additive manufacturing of metal oxide ceramic material followed by post-processing in a reducing atmosphere.

The combination of these processes is feasible. The forming of metal oxide powders to create metal artifacts through reduction is not only limited to extrusion. The inventors of the process note that other forming methods are suitable, including slurry coating of sacrificial cores, slurry casting methods (slip, pressure, centrifugal, tape, and gel casting), and dry pressing (Cochran et al., 2003). The infusion of AM into the existing process chain adds opportunities for strategic material placement and custom macrostructure. Furthermore, other successful examples of such combination exist, such as the slurry-based three-dimensional printing of a tungsten carbide mixture with post-processing in a reduction atmosphere to create tungsten carbide-cobalt (Kernan et al., 2003).

2.5 MANUFACTURING PARTS WITH DESIGNED MESOSTRUCTURE VIA ADDITIVE MANUFACTURING AND REDUCTION OF METAL OXIDES: A REQUIREMENTS LIST

The development of a research hypothesis narrows the design space that was initially outlined at the beginning of this chapter. By choosing to use a layer-based additive fabrication approach, new requirements must be added to the list that was presented in Table 2.1. The choice of using AM to create cellular materials in a green state from metal oxide powders that are suitable for reduction and sintering in a post-

processing step also adds additional requirements and constraints to the to-be-designed manufacturing process.

2.5.1 Geometry

The decision to implement an AM process to create parts with designed mesostructure imposes several additional requirements that fall underneath the "Geometry" heading of the requirements list presented in Table 2.1. Obviously, the process must be able to create the small, intricate, and complex features typical of cellular materials (cell sizes in the range of 0.5 – 2 mm and wall thicknesses as small as 200 μm). However, the constraint of using an AM process requires a specific consideration for its ability to handle the difficulties that arrive from building complex geometry in an additive manner. Specifically, the process must be able create overhanging structures, internal voids, and high-aspect ratio features. Furthermore, one must be able to create trusses that are angled to the build plane. A specific type of overhanging feature, angled trusses are difficult to create in an additive fashion since the combination of acute angles (θ), thin trusses (diameter t), and large layer thicknesses ($LT_2 > LT_1$) can lead to non-overlapping layers as shown in Figure 2.6.

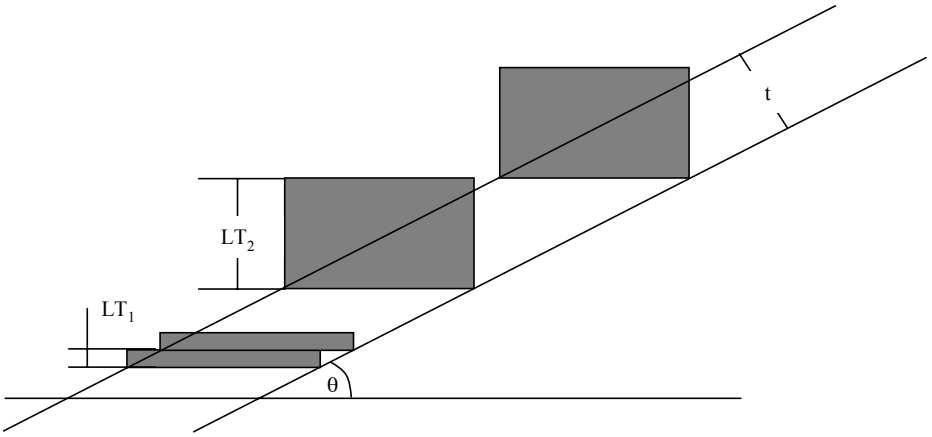

Figure 2.6 – Difficulty in Producing Angled Trusses with Additive Manufacturing

By explicitly stating these requirements, a designer is made conscious of the unique challenges in creating designed mesostructure via AM.

In the context of AM, the mesostructure geometry is relayed to the workstation as a series of two-dimensional cross sections. As such, in addition to the requirements associated with the overall desired geometry, the process must be able to successfully create cross-sections typical of cellular materials. Three representative cellular material geometries are presented in Figures 2.7 – 2.9: a chiral honeycomb structure (wall thickness = 1.5 mm), a swept cellular matrix (wall thickness = 1.5 mm; cell size = 2.25 mm), and a trussed structure (truss diameter = 1.5 mm). Characteristic cross-sections of each type of cellular material are also shown for both principal build directions.

(a) (b) (c)

Figure 2.7 – Cross-section of Chiral Honeycomb; (a) as built, (b) x-y orientation, (c) y-z orientation

(a) (b) (c)

Figure 2.8 – Cross-section of Swept Periodic Cellular Material; (a) as built, (b) x-y orientation, (c) y-z orientation

(a) (b)

Figure 2.9 – Cross-section of Trussed Cube; (a) as built, (b) x-y orientation

Although different in mesostructure topology, the cross-sections of the periodic cellular structures shown in Figure 2.7 and Figure 2.8 are similar, as they are composed of continuous lines. The trussed cube (Figure 2.9) is unique in that it requires very small discrete depositions of energy and/or material to successfully produce this cross-section. As such, a distinct requirement is added to the list to specify the need for a process to be able to deposit the wide variety of cross-sections needed to realize all topologies of designed mesostructures.

2.5.2 Material

The decision to create metal artifacts from metal oxide ceramic particles via thermal chemical post-processing places new constraints to the design space in the context of material processing requirements. Specifically, the system to be designed must be able to process all of the transitional metal oxides that can be processed with the current LCA manufacturing process (Fe, Ni, Co, Cr, N Cu, Mo, W, Mn, and Nb), as well as their mixtures which result in many engineering alloys (including stainless steel, maraging steel, Inconel, and Super Invar). As described in Section 2.3.1, alumina and titanium dioxide are not included in this demand since they cannot be readily reduced.

It is also important that the process is able to work with metal oxide powder particles of less than or equal to 50 μm. This is important …. Smaller particles lead to better sintering, smaller grains, and better material props

2.5.3 Production

One major drawback of most AM technologies is their inability to create artifacts at rates that are competitive with traditional manufacturing techniques. As such, a constraint on the minimum acceptable deposition rate is added to remind the designer of the overall goal of a high production capacity. The conception of this requirement will likely affect the choice of working principle for the "patterning" sub-function since one-dimensional patterning techniques are typically incapable of depositing material and/or energy at a sufficient rate.

Another drawback that is frequently present when AM technologies construct cellular materials is the inability for the user to get rid of the unpatterned and/or support material that becomes trapped in the parts' internal geometry during its build. Because excess metal oxide powder would sinter along with the part, it is crucial that all support material is removed from the ceramic green part before firing.

2.5.4 Quality Control

Many AM technologies suffer from anisotropic material properties due to the layered fabrication process. Because it is important that the parts created by the to-be-designed process are comparable to those made by more traditional manufacturing processes, a requirement is added in which isotropic material properties are demanded. Furthermore, in order to create the intricate, complex geometry typical of cellular materials, an AM process must have a high deposition accuracy (+/- 0.05 mm), a high z-

resolution (layer thickness ≤ 0.1 mm), and the ability to create minimum feature size of at least 0.2 mm.

In order to create a high-quality finished structure, it has been determined that the metal oxide ceramic green part created by the process must have a ceramic solids loading greater than 40 vol.%. This is an important constraint since a high green density directly relates to lower shrinkage during firing, and less porosity in the finished part.

The preliminary requirements list presented in Table 2.1 includes a "wish" that the process would not require a post-processing step. This wish has since been removed due to the decision to shape metal oxide powders via AM and reduce and sinter the resulting green part in order to create metal artifacts.

2.5.5 The Requirements List

The requirements list presented in Table 2.1 has been updated for the to-be-designed AM process and is presented in Table 2.15.

Table 2.15 – Requirements List for a Process for the Manufacture of Metal Parts of Designed Mesostructure via Reduction of Metal Oxide Powders

D/W	*Requirement*
	Geometry
D	Able to process any macrostructure geometry
D	Able to process complex geometry: - overhanging features - internal voids - high-aspect ratio structures
D	Able to process small cell sizes (0.5 – 2 mm)
D	Build small features and wall thicknesses (as small as 200 μm)
D	Build trusses from 0.5 mm – 10 mm in diameter
D	Construct trusses that are inclined at ≥ 35 degrees from the build direction
D	Able to create cross-sections representative of designed mesostructure: - circular depositions with diameter as small as 0.5 mm - 200 μm minimum feature size
	Material
D	Able to process all transitional metal oxides (excluding alumina and titanium oxide)
D	Process powder particles with diameter ≤ 50 μm
W	Minimize amount of effort required to adapt to a new material
W	Able to process standard working material (i.e., material is not proprietary or require specialized formulation)
	Production
D	Build envelope is 250 x 250 x 250 mm or larger
D	Deposition rate should be ≥ 10 cm^3/hr
D	Supporting material must be able to be removed from part with minimal effort (if applicable)
	Quality Control
D	Finished parts have ≥ 95% relative density
D	Ceramic green parts have ≥ 40 vol% ceramics solids loading
D	Material properties are comparable to standard
D	Material properties of finished part are isotropic
D	Minimize surface roughness before finishing (≤ 0.02 mm Ra)
D	Maximize accuracy (≥ +/- 0.05 mm)
D	Minimize z-resolution (≤ 0.1 mm)
	Operation
W	Does not require special operating environment
W	Minimize operator interaction
	Recycling
W	Minimize environmental impact by minimizing wasted material
W	Reusable wasted material
	Costs
D	Minimize cost of technology and technology maintenance by avoiding expensive technologies such as lasers and electron beams
D	Minimize cost of material
W	Easily scaled for large applications

2.6 DISSERTATION ROADMAP

The design process begins in this chapter with the Clarification of Task phase. Preliminary requirements for the realization of parts of designed mesostructure are offered in Section 2.1. A critical analysis of the existing manufacturing techniques which are capable of producing parts of designed mesostructure (direct-metal additive manufacturing, Section 2.2, and linear cellular alloy manufacturing, Section 2.3) provides the foundation for the generation of the primary research hypothesis (Section 2.4). In Section 2.5, the requirements list for the design task is generated through a systematic consideration of the various factors that affect the successful completion of the design task. The creation of this requirements list marks the end of the Clarification of Task phase of the design process.

The requirements list is a crucial component of the design task, as it provides direction during the conceptual design phase (Chapters 3 and 4), and the basis for the selection of the principal solution (Chapter 5). As seen in Figure 2.10, the conceptual design phase begins in the next chapter with the abstraction of the requirements list in an effort to create a solution-neutral statement of the crux of the design task.

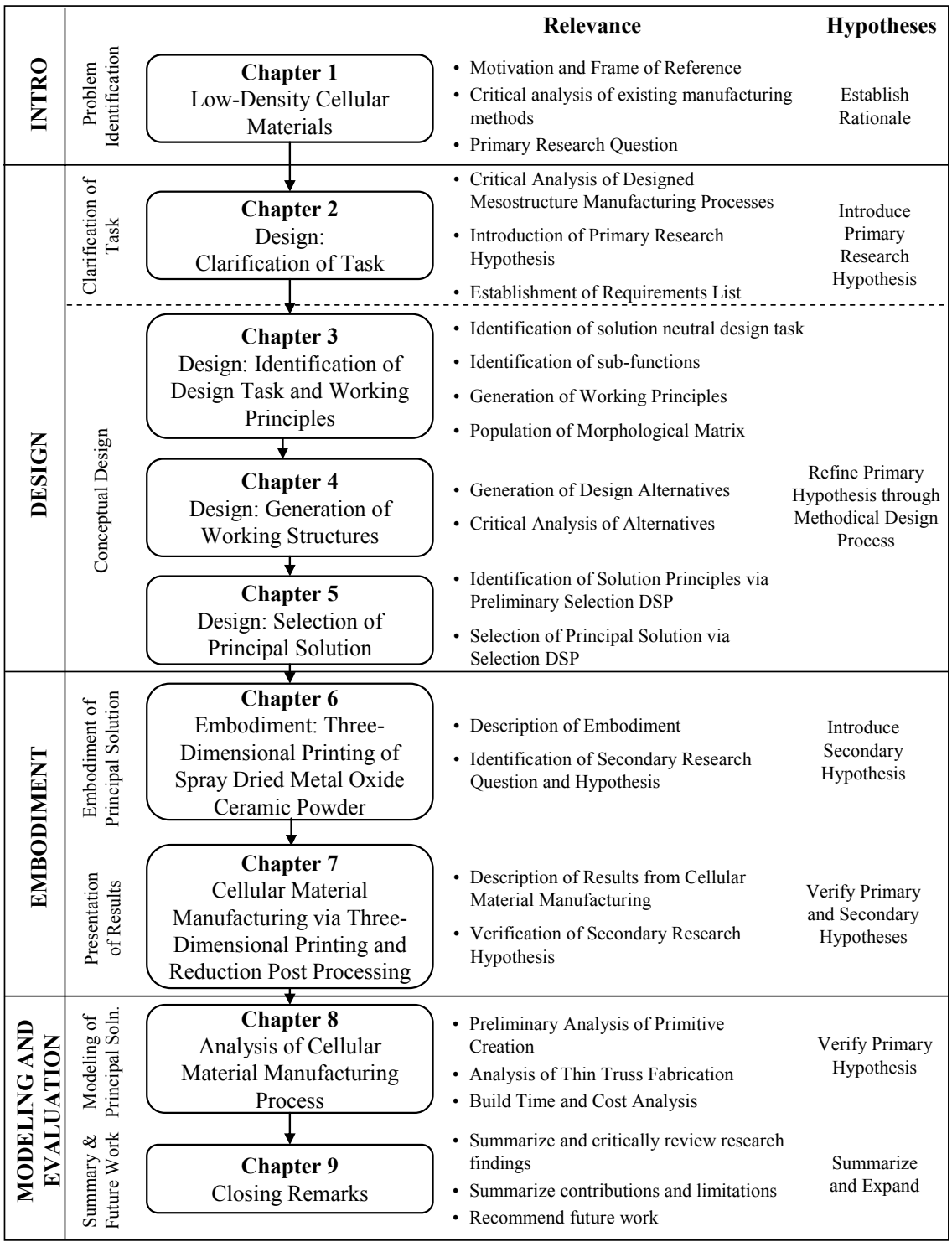

Figure 2.10 – Dissertation Roadmap

CHAPTER 3

DESIGN: IDENTIFICATION OF DESIGN TASK AND WORKING PRINCIPLES

With a list of design requirements and constraints established, conceptualization of the design solution may begin. This chapter begins with the identification of the crux of the design task, which is accomplished through a systematic abstraction of the design requirements. The primary and secondary functions of the to-be-designed manufacturing process are then identified through abstraction of the essential tasks that are required for the successful achievement of the listed requirements (Section 3.2). Conceptualization of a design solution begins with the ideation of physical principles that can satisfy each sub-function of the process. More concrete embodiment of these principles is then provided through the generation of working principles, which are ideated via research and critical analysis of a wide variety of ceramic manufacturing processes (Section 3.3). These working principles are combined through the use of morphological matrices in order to prepare for the generation of working structures. These working structures are detailed and critically analyzed in Chapter 4.

3.1 IDENTIFYING THE DESIGN TASK

Following the design methodology as outlined by Pahl and Betiz (Appendix A) (Pahl and Beitz, 1996), the first stage of the conceptual design phase is the identification of the crux of the design task. This is accomplished through a systematic abstraction of the design requirements that were identified at the closure of the Clarification of Task phase (Table 3.1, originally presented in Table 2.14).

Table 3.1 – Requirements List for a Process for the Manufacture of Metal Parts of Designed Mesostructure via Reduction of Metal Oxide Powders

D/W	*Requirement*
	Geometry
D	Able to process any macrostructure geometry
D	Able to process complex geometry: - overhanging features - internal voids - high-aspect ratio structures
D	Able to process small cell sizes (0.5 – 2 mm)
D	Build small features and wall thicknesses (as small as 200 μm)
D	Build trusses from 0.5 mm – 10 mm in diameter
D	Construct trusses that are inclined at ≥ 35 degrees from the build direction
D	Able to create cross-sections representative of designed mesostructure: - circular depositions with diameter as small as 0.5 mm - 200 μm minimum feature size
	Material
D	Able to process all transitional metal oxides (excluding alumina and titanium oxide)
D	Process powder particles with diameter ≤ 50 μm
W	Minimize amount of effort required to adapt to a new material
W	Able to process standard working material (i.e., material is not proprietary or require specialized formulation)
	Production
D	Build envelope is 250 x 250 x 250 mm or larger
D	Deposition rate should be ≥ 10 cm^3/hr
D	Support material must be able to be removed from part with minimal effort (if applicable)
	Quality Control
D	Finished parts have ≥ 95% relative density
D	Ceramic green parts have ≥ 40 vol% ceramic solids loading
D	Material properties are comparable to standard
D	Material properties of finished part are isotropic
D	Minimize surface roughness before finishing (≤ 0.02 mm Ra)
D	Maximize accuracy (≥ +/- 0.05 mm)
D	Minimize z-resolution (≤ 0.1 mm)
	Operation
W	Does not require special operating environment
W	Minimize operator interaction
	Recycling
W	Minimize environmental impact by minimizing wasted material
W	Reusable wasted material
	Costs
D	Minimize cost of technology and technology maintenance by avoiding expensive technologies such as lasers and electron beams
D	Minimize cost of material
W	Easily scaled for large applications

3.1.1 Abstraction of Requirements

There is great care taken in the Pahl and Beitz systematic design process to avoid "design fixation" - a premature commitment to a (often conventional) solution to a design

problem. The first effort in assisting a designer with avoiding this fixation is the use of a systematic abstraction process to emphasize what is general and essential in the design task instead of focusing on what is particular or incidental. Pahl and Beitz argue that such generalization leads straight to the crux of the design task and, if properly formulated, can assist a designer in the identification of the overall function and essential constraints of the design problem without prejudicing the choice of a particular solution.

There are five stages in the abstraction exercise:

1. Eliminate personal preferences.
2. Omit requirements that have no direct bearing on the function and the essential constraints.
3. Transform quantitative into qualitative data and reduce them to essential statements.
4. Generalize the results of the previous step.
5. Formulate the problem in solution-neutral terms.

Each sequential step assists a designer in systematically abstracting the essential design task. At each step a designer should ask, "What properties must a solution have?" and "What properties must a solution not have?"

Step One: Eliminating Personal Preferences

In this first step, a designer is tasked to eliminate all personal preferences from the initial requirements list (Table 3.1). For this design problem, the majority of the "wishes" were removed from the initial requirements. Such items as "minimize amount of effort required to adapt to a new material," "able to process standard working material," "does not require special operating environment," and "reusable wasted

material" are a reflection of the author's personal preferences, and are not crucial to the success of the essential design task. The remaining wishes "minimize operator interaction" and "minimize environmental impact by minimizing wasted material' are not eliminated as they reflect the key design requirement of creating a manufacturing process which is cost and time efficient. The updated requirements list is presented in Table 3.2.

Table 3.2 – Requirements List with Personal Preferences Removed

D/W	*Requirement*
	Geometry
D	Able to process any macrostructure geometry
D	Able to process complex geometry: - overhanging features - internal voids - high-aspect ratio structures
D	Able to process small cell sizes (0.5 – 2 mm)
D	Build small features and wall thicknesses (as small as 200 μm)
D	Build trusses from 0.5 mm – 10 mm in diameter
D	Construct trusses that are inclined at ≥ 35 degrees from the build direction
D	Able to create cross-sections representative of designed mesostructure: - circular depositions with diameter as small as 0.5 mm - 200 μm minimum feature size
	Material
D	Able to process all transitional metal oxides (excluding alumina and titanium oxide)
D	Process powder particles with diameter ≤ 50 μm
	Production
D	Build envelope is 250 x 250 x 250 mm or larger
D	Deposition rate should be ≥ 10 cm^3/hr
D	Supporting material must be able to be removed from part with minimal effort (if applicable)
	Quality Control
D	Finished parts have ≥ 95% relative density
D	Ceramic green parts have ≥ 40 vol% ceramic solids loading
D	Material properties are comparable to standard
D	Material properties of finished part are isotropic
D	Minimize surface roughness before finishing (≤ 0.02 mm Ra)
D	Maximize accuracy (≥ +/- 0.05 mm)
D	Minimize z-resolution (≤ 0.1 mm)
	Operation
W	Minimize operator interaction
	Recycling
W	Minimize environmental impact by minimizing wasted material
	Costs
D	Minimize cost of technology
D	Minimize cost of maintenance
D	Minimize cost of material
W	Easily scaled for large applications

Step Two: Requirements with Direct Bearing on Function and Essential Constraints

The second abstraction step involves eliminating those requirements that have no direct bearing on the critical function and/or the overall function of the to-be-designed manufacturing process. The result of this elimination is the identification of those requirements which state the most crucial functions of the AM process.

All requirements related to geometry are kept since this design task is focused in creating an AM technology which is dedicated to the realization of a special class of geometry. The ability to process ceramic metal oxide materials is identified as a crucial requirement in this step, as these materials are compatible with the previously identified reduction and sintering post-production process (Section 2.3). Finally, due to the emphasis on creating a machine which has speeds and costs typical of production-level processes, those requirements relating to deposition rate, deposition quality, and technology cost are retained.

It is important to note that the ceramic solids loading requirement is kept in this stage. This is considered a crucial functional requirement as green parts with poor solids loading will result in finished parts that do not meet other quality requirements (material properties, density, shrinkage, etc.).

The resultant amended requirements list is presented in Table 3.3.

Step Three: Transforming to Qualitative Data and Essential Statements

The third step of the abstraction process is the removal of all quantitative requirements and the transformation of the requirements into qualitative statements of essential needs. The results of this step are shown in Table 3.4.

Table 3.3 – List of Requirements Which Have Direct Bearing on Process's Function and Essential Constraints

D/W	*Requirement*
	Geometry
D	Able to process any macrostructure geometry
D	Able to process complex geometry: - overhanging features - internal voids - high-aspect ratio structures
D	Able to process small cell sizes (0.5 – 2 mm)
D	Build small features and wall thicknesses (as small as 200 μm)
D	Build trusses from 0.5 mm – 10 mm in diameter
D	Construct trusses that are inclined at ≥ 35 degrees from the build direction
D	Able to create cross-sections representative of designed mesostructure: - circular depositions with diameter as small as 0.5 mm - 200 μm minimum feature size
	Material
D	Able to process all transitional metal oxides (excluding alumina and titanium oxide)
	Production
D	Deposition rate should be ≥ 10 cm^3/hr
	Quality Control
D	Ceramic green parts have ≥ 40 vol% ceramic solids loading
	Costs
D	Minimize cost of technology

Table 3.4 – Qualitative List of Requirements

D/W	*Requirement*
	Geometry
D	Able to process any macrostructure geometry
D	Able to process complex geometry: - overhanging features - internal voids - high-aspect ratio structures
D	Able to process small cell sizes
D	Build small features and wall thicknesses
D	Build trusses with a wide variety of diameters
D	Construct angled trusses
D	Able to create cross-sections representative of designed mesostructure
	Material
D	Able to process all transitional metal oxides (excluding alumina and titanium oxide)
	Production
D	Fast deposition rate
	Quality Control
D	Ceramic green parts have high volume % ceramic solids loading
	Costs
D	Minimize cost of technology

Step Four: Generalization of Requirements

This penultimate abstraction step is the conscious generalization of the list of the requirements. For example, all references to specific geometries are removed and replaced with "able to process any mesostructure topology and complex internal geometries." The need for a high volume percentage of ceramic solids loading in the green part is now abstracted to the true fundamental requirement, "ceramic green parts are suitable for thermal-chemical post-processing." The resultant list of requirements is displayed in Table 3.5.

Table 3.5 – Generalized Process Requirements

D/W	*Requirement*
	Geometry
D	Able to process any macrostructure geometry
D	Able to process any mesostructure topology and complex internal geometries
D	Able to create cross-sections representative of designed mesostructure
	Material
D	Able to process all transitional metal oxides
	Production
D	Fast deposition rate
	Quality Control
D	Ceramic green parts are suitable for thermal-chemical post-processing
	Costs
D	Technology is cost-effective

3.1.2 Crux of the Design Problem

The fifth and final step of the systematic abstraction process is the formulation of the design problem in solution-neutral terms. Through the completion of the previous four steps, the essential requirements of the to-be-designed manufacturing process have been identified, primarily through the elimination of those secondary requirements that do not directly impact the process's crucial functions.

The process must be able to (i) realize any macrostructure geometry, (ii) realize mesostructures typical of cellular materials, (iii) process ceramic metal oxide materials,

(iv) create ceramic green parts that are suitable for the reduction post-process, and must do this in a (v) cost-efficient and (vi) time-efficient manner. From these essential requirements, the following solution-neutral design task is identified.

Design Task:

Design a layer-based additive manufacturing process that can be used to efficiently (in terms of cost and time) realize metal oxide ceramic green parts of any macrostructure geometry, any cellular mesostructure topology, and that are suitable for thermal-chemical post-processing.

3.2 FUNCTION STRUCTURE CREATION

With a solution-neutral design task formulated, the conceptual design phase can continue. Direct ideation and generation of design alternatives and solutions cannot begin; the primary and secondary essential functions of the to-be-designed process must first be identified. The identification of essential functions provides a framework in which to proceed with ideation. There are three separate steps in this portion of conceptual design: the identification of primary functions, the identification of secondary functions, and the generation of a function structure to illustrate the relationship amongst the functions.

3.2.1 Identification of Primary Functions

The task of identifying the to-be-designed process's primary functions begins with identifying the fundamental inputs and outputs of the process. As can be seen in Figure 3.1, the fundamental task of the process is to convert raw material (a ceramic metal oxide material) into a green part with cellular mesostructure via the addition of some form of

energy to convert the raw material to a solid part as per the information and signals provided by the .stl file (a data format that consists of triangulated facet information of the solid body).

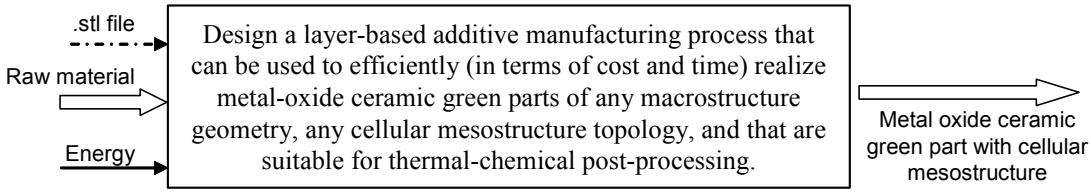

Figure 3.1 – Basic Function Structure for a Process for the Additive Manufacture of Metal Parts of Designed Mesostructure via Reduction of Metal Oxide Powders

From this statement of the process's overall primary function, a series of sub-functions can be identified through the ideation of the process's essential tasks.

3.2.2 Identification of Sub-Functions

The essential primary task of any AM process is the conversion of raw material to a series of connected solid primitives in a layer-based, additive manner in order to create a finished product. Primitives are typically created by the patterning of material and/or energy in such a manner as to change the phase of (or solidly join) the raw material in order to create a green part. Once a layer is completed, the process must have a means of providing additional material to the work part so that the next layer can be created. Finally, there must be a means of supporting the part during its creation so as to allow the realization of the complex geometry and mesostructure that is typical of cellular materials.

These essential tasks are listed in Table 3.6 in conjunction with their corresponding sub-functions. Sub-functions are identified by identifying those functions that must be fulfilled in order for any RP machine, no matter the embodiment, to function properly.

Table 3.6 – Mapping Essential Tasks to Process Sub-Functions

Crux of Design Problem	Essential Tasks	Sub-Functions
Design a layer-based additive manufacturing process that can be used to efficiently (in terms of cost and time) realize metal-oxide ceramic green parts of any macrostructure geometry, any cellular mesostructure topology, and that are suitable for thermal-chemical post-processing.	Provide metal-oxide ceramic raw material for primitive creation	Store material
	Pattern material and/or energy in order to initiate phase change and create primitives for realization of cross-sectional layers	Pattern material
		Pattern energy
		Create primitive
	Add material for creation of next layer	Provide new material
	Provide support structure for the creation of complex geometries typical of cellular materials	Support previously deposited material

These sub-functions are described below (initially described in Section 2.2.1):

vi. *store material* – each AM technology relies on a starting material that will be consolidated to form the final part (e.g., powder, tape, resin, slurry, etc.).

vii. *pattern material* & *pattern energy* – these sub-functions are the heart of an AM technology as they correspond to the way in which each layer of the part is developed. The process can involve creating primitives by directly depositing and patterning material onto a substrate. Alternatively, the process can selectively pattern energy in order to transform the raw material into finished primitives. Finally, the process can pattern both the material and energy simultaneously in order to create solid primitives.

viii. *create primitive* – each AM technology requires the input of some form of energy or solid-state joining process in order to transform/shape the raw material into the desired part. Energy is typically used to change the phase of the stored material in order to create each cross-section (e.g., liquid to solid, gas to solid, etc.). This sub-function entails such working structures as polymerization, sintering, melting, and freezing.

ix. *provide material for next layer* – as an additive fabrication process, each AM technology must have a method of supplying material for the manufacture of

each layer. While some technologies directly deposit material, most use a recoating process to prepare for additional layers.

x. *support previously deposited layer* – many AM technologies have a method of supporting deposited material to ensure stability, and to be able to build complex geometry such as overhangs.

3.2.3 Function Structure

The sub-functions are arranged into a function structure in Figure 3.2. The function structure assists a designer in seeing the fundamental inputs and outputs of each functional relationship. Originally shown in Figure 2.1, this version has been modified to show the thermal/chemical reduction post-process that will be employed to convert the ceramic green part to a metal finished part.

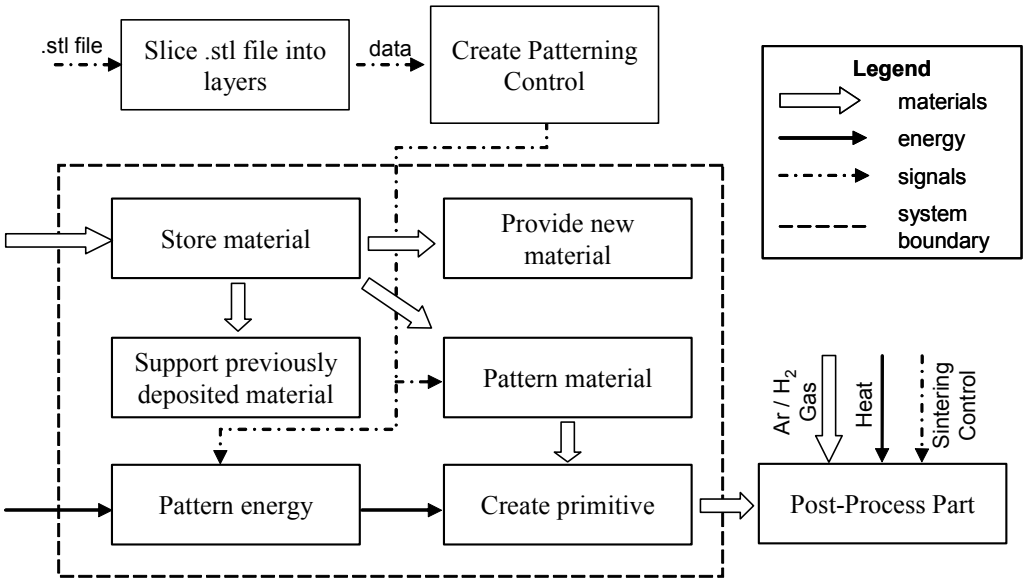

Figure 3.2 – Function Structure for a Process for the Additive Manufacture of Metal Parts of Designed Mesostructure via Reduction of Metal Oxide Powders

3.3 GENERATING WORKING PRINCIPLES

With the function structure created, the process of ideating solution principles for the design problem may begin. Just as done with the formulation of the overall design task in Section 3.1, Pahl and Beitz suggest a series of abstraction exercises to force a designer to avoid design fixation for the ideation process. This abstraction process is illustrated in Figure 3.3.

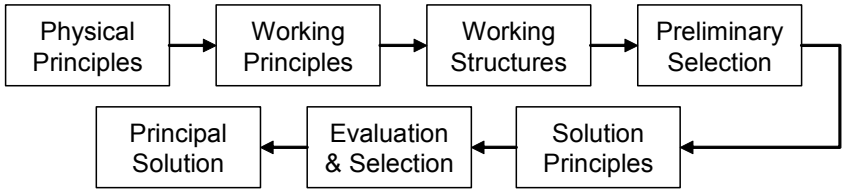

Figure 3.3 – Progression of Abstraction in the Ideation of Design Problem Solutions

Generic physical principles that can be used to fulfill the process's sub-functions must first be identified. These principles are then concretized and combined into working principles. Working principles are specific, slightly embodied solutions for the more generic physical principles. Pahl and Beitz state that these principles must "reflect the physical effect needed for the fulfillment of a given function" (Pahl and Beitz, 1996). These principles are later combined in various arrangements to create working structures (in Chapter 4).

In this sub-section, physical principles are first identified for each sub-function. These principles are kept at a very high level of abstraction so that fixation is not a concern during the generation of working principles. Working principles for each physical principle are then ideated for each physical principle. With the end goal of embodying a solution for the design task in the time frame set for this research, the author's search for working principles is limited to research of existing manufacturing

techniques. It is important to note, however, that this research is not limited to existing ceramic AM methods; instead the search is scoped by the research of all AM methods (both commercial and those in development), traditional ceramic manufacturing methods, and other miscellaneous existing process suited for specific sub-functions (primarily, "create primitive").

Figure 3.4 is offered at the beginning of this sub-section as a guide for the reader. Physical principles are listed for each sub-function in the form of a morphological matrix.

	Physical Principles					
Store Material	Solid		Liquid		Gas	
Pattern Material	1D material patterning		2D material patterning		No material patterning	
Pattern Energy	1D energy patterning		2D energy patterning		No energy patterning	
Create Primitive	Sinter	Solidify melt	Evaporate	Initiate polymerization	Initiate chemical reaction	Freeze
Provide New Material	Recoat layer			Direct material addition		
Support Previously Deposited Material	Bed of Material		Thin trusses of build material	Sacrificial support material		5-axis deposition

Figure 3.4 – Physical Principles of Additive Manufacturing Process Sub-Functions

3.3.1 Store Material

This sub-function details the phase of the raw material before it is transformed into a solid primitive for the creation of a solid green part. Generally, the working principles for this sub-function do not have a direct impact on the ability of an AM process to successfully manufacture parts. However, because the primary concern in the direct AM of ceramics is in creating a green part with a sufficient solids loading percentage for it to

be suitable for sintering and reduction (i.e., to easily reach fully density and to minimize warping, curling, and shrinkage), the successful embodiment of this sub-function is crucial to the overall success of the manufacturing process. The creation of physical and working principles for this sub-function is outlined in Table 3.7.

Table 3.7 – Working Principle Progression for "Store Material" Sub-Function

Sub-Function	Physical Principle	Working Principle
Store Material	Solid	Single-phase powder
		Two-phase powder
		Coated powder
		Tape / Sheet
		Wire / Rod
	Liquid	Molten material
		Binder / structural powder suspension
	Gas	Two phase gas

Solid

This physical principle describes working principles in which the raw material is stored in its solid form; either in its original form, or in a processed form such as a compact or a sheet or tape.

- *Single-phase powder* – The most straight-forward embodiment of this specific working principle, metal-oxide ceramic solid material can be introduced to the system as a single-phase powder. Once introduced into the process, this powder will require the addition of either energy or secondary material to bind the structural material together so that primitives can be formed. Single-phase ceramic powder is used in traditional ceramic manufacturing processes such as die pressing, and in additive manufacturing processes such as direct metal laser sintering (DMLS), selective laser melting (SLM) (Kruth et al., 2004b), electron beam melting (EBM) (Cormier et al., 2004a), and three-dimensional printing (3DP) (Michaels et al., 1992). It is important to note that there is a fundamental,

physical limit to the green part density one can achieve with this working principle, as powders have a tap or packing relative density around 75% due to the presence of interstitial voids between particles. The packing density is dependent upon particle size, size distribution, and morphology. In powder bed-based AM processes, powder bed density is typically around 45 vol%, with densities as high as 55 vol% being reported (Utela et al., 2006).

- *Two-phase powder* – This working principle details the introduction of a secondary phase to the structural material. This second phase is typically used as a binder material that can be selectively activated during the patterning process in order to bind the structural material together. In laser sintering (LS), for example, the secondary phase is selectively melted via the patterning of laser energy (Agarwala et al., 1995). Because it has a lower melting temperature than the structural material, primitives are created by the binding of the primary structural material phase (Greulich, 1997). Utela and coauthors have introduced a secondary binder material into the powder bed of 3DP and selectively activate the binder via the selective printing of a liquid solvent. Great care is taken in sufficiently mixing the two phases homogenously; however, it has been shown that the materials can segregate due to density discrepancies, causing powder bed heterogeneity and poor resultant part properties (Beaman et al., 1997).
- *Coated powder* – The third powder-based working principle is similar to the "two-phase powder" principle in that a second binder material phase that, upon later selective patterning of material or energy, can be used to create primitives by binding structural material together. This principle involves coating the

individual structural powder particles with the second phase material (for example, via spray-drying). This is often preferred over two-phase powder systems since homogeneity of the powder bed is assured. However, a debinding step is needed to remove the binder which can leave a porous part. This principle has been employed in the LS of silicon carbide (Evans et al., 2005). Coated powders are also typically used in the creation of ceramic green parts through dry pressing.

- *Tape / sheet* – This working principle describes the introduction of solid material in the form of a thin tape or sheet to the manufacturing process. Ceramic materials have been shaped into this form of raw material via the tape casting process for several decades. Tape casting is used to produce a green body which consists of a thin layer of dried ceramic suspension (Ring, 1996). The process typically involves the smoothing or flattening of the ceramic slurry via travel along conveyors and underneath doctor blades. The resultant green layers can be cut or punched into a near-net shape and sintered. The sheets can also be stacked to make multi-layer parts, such as done for ceramic capacitors. The advantage of this principle in the context of AM is that working with a sheet of material can increase the deposition rate as entire layers of material could be processed at once. This principle can be found in Ultrasonic Consolidation (UOC) (Solidica, 2004), Layered Object Manufacturing (LOM) (Bender et al., 2001; Das et al., 2003), Computer-Aided Manufacturing of Laminated Engineering Materials (CAM-LEM) (Liu et al., 1997), stereolithography

(Himmer et al., 1997), and 3D System's upcoming VFlash AM process (3D, 2007).

- *Wire / rod* – This principle is similar to the "tape / sheet" principle in that it is a solid form of a ceramic suspension. Instead of being formed into a sheet, this principle entails the extrusion of the suspension to form a thin filament. This product is then dried and stored as a solid material. The wire or rod is typically introduced into AM process through extrusion patterning as seen in the Fused Deposition Modeling (FDM) process (Agarwala et al., 1996) and the Electron Beam Welding process (Watson et al., 2002).

Liquid

Working principles of the "liquid" physical principle detail ways in which structural material is introduced into the manufacturing process in a liquid form. If these working principles are incorporated into a working structure, it is necessary to solidify the liquid material so that primitives and layers can be successfully created.

- *Molten material* – Observed in AM techniques such as Multi-Phase Jet Solidification (MJS) (Greul et al., 1996), Semi-Solid Metal Solid Freeform Fabrication (SSM-SFF) (Rice et al., 2000), and direct molten aluminum printing (Orme et al., 2000), this working principle involves the introduction of the solid material as a melt. Once deposited onto the substrate, the molten material cools and solidifies to form a layer. This is feasible with metallic materials, but is an infeasible candidate for ceramics due to their extremely high melting temperatures (e.g., 2050 C for Al_2O_3; 2800 C for MgO). However, plasma

spraying is used in the ceramics industry to deposit ceramic coatings frequently, and has been investigated as an AM process (Aljdelsztajn et al., 2005).

- *Binder / structural powder suspension* – This specific embodiment of the "liquid" physical principle is much more feasible than melting ceramics. This working principle details the introduction of ceramic metal-oxide particles into the manufacturing process as a suspension in an either aqueous or polymer-based solution. Suspensions require either a phase-change, an activation of the polymer, or evaporation of the solvent in order to create solid primitives. Working with ceramic suspensions is very common in traditional ceramic manufacturing techniques such as slip casting, filter pressing, sedimentation casting, extrusion, and injection molding (Ring, 1996). Ceramic suspensions have also been used in several ceramic AM processes such as slurry-based three-dimensional printing (S-3DP) (Grau et al., 1997), Freeze-Form Extrusion Fabrication (FFEF) (Huang et al., 2006), stereolithography (SL) (Griffith and Halloran, 1994b), and direct inkjet printing (Sirringhaus and Shimoda, 2003). It is important to note that there is a physical limit to the amount of powder that can be introduced into the suspension before it is too viscous to be processed. This problem is even more aggravated when attempting to suspend the fine ceramic particles that are necessary for the creation of quality finished parts. The stability of the suspension is also critical; particulate settling in the suspension can lead to heterogeneous density distribution in finished parts. Finally, powder/binder suspensions are further hampered by the amount of effort that is required to adequately suspend the ceramic powder in the solution;

not only does successful suspension require extensive experimentation and knowledge of materials engineering and chemistry, but the solution is unique to each material that the AM technique will process.

Gas

The final physical principle for the "store material" sub-function is to store the material as a gas. While this seems to be an unlikely manner in which to create solid primitives, the use of gas phase reactors is a common manner of synthesizing high-purity ceramic powders. Solid ceramic coatings can also be deposited onto substrates from a gaseous phase via chemical vapor deposition. Furthermore, this process has been adapted to the realm of AM via Laser Chemical Vapor Deposition (LCVD) wherein a gaseous phase is used to create solid depositions through the selective application of intense laser energy (Johnson et al., 2003). Selective Area Laser Deposition Vapor Infiltration (SALVDI) is another AM process which employs the "gas" working principle (Crocker et al., 1999). While gaseous phases can result in the deposition of high purity solids, not every material can be synthesized from a gaseous phase – only a few oxides (silica, titania, and alumina), carbides, nitrides, and borides have been produced by laser synthesis (Ring, 1996).

Because solids can only be synthesized from the initiation of a chemical reaction between multiple gaseous compounds, only one working principle is suggested as a proper embodiment for this working principle: "two-phase gas." This embodiment suggests the presence of multiple gaseous materials in the manufacturing environment. Such an example, the synthesis of alumina via laser synthesis, is provided below:

$$AlCl_3 + \frac{3}{2}O_2 \longrightarrow Al_2O_3(s) + \frac{3}{2}Cl_2 \qquad [3.1]$$

3.3.2 Pattern Material

This sub-function encompasses those processes which selectively deposit material in order to create a primitive or layer of the green part. Since it is possible that a process may not create layers by patterning material, a physical principle entitled "no material patterning" is included. The progression of abstraction for the creation of the working principles is outlined in Table 3.8.

Table 3.8 – Working Principle Progression for "Pattern Material" Sub-Function

Sub-Function	Physical Principle	Working Principle
Pattern Material	1D Material	1D extrusion
		1D powder deposition
	2D Material	2D suspension ejection
		2D tape / sheet
		2D powder deposition
	No Material Patterning	No material patterning

<u>One-Dimensional Material Patterning</u>

This physical principle entails the creation of layers via the selective patterning of material in one-dimensional raster scans. The speed of these one-dimensional patterning techniques is inherently limited by the machines' scanning speed. It is not likely that scanning a single deposition spot will ever be economically competitive with traditional manufacturing technologies.

- *One-dimensional extrusion* – A traditional ceramic green part manufacturing process, extrusion involves the continuous pushing of a ceramic slurry or paste through a die. Either through the aid of a heated nozzle or through the high shear rate imposed upon the viscous paste use, the polymer binder is melted or softened enough to aid flow through the nozzle. The slurry solidifies upon deposition onto a substrate thus creating a solid part. While the extrusion processes found in traditional ceramic manufacturing methods employ

differently shaped dies to create different geometries (as found in the aforementioned Linear Cellular Alloys, described in Sections 1.3.3 and 2.3.1), the extrusion process found in AM technologies such as FDM, MJS, Robocasting (Morissette et al., 2000), contour-crafting (Khoshnevis et al., 2001), and extrusion free-forming (Vaidyanathan et al., 1999) employ robotic control to control the deposition pattern. It is important to note that because the paste must have specific rheological properties for proper extrusion behavior, there is a physical limit to the solids loading content (and hence viscosity) of the paste. AM extrusion has been shown to process pastes with around 40 vol% solids loading (Lewis, 2000; Grida and Evans, 2003).

- *One-dimensional powder deposition* – Another embodiment of the 1D material patterning principle is the concept of selectively depositing powder onto a substrate. Li and Yang have developed a means of selectively depositing fine particles by using ultrasonic waves to discharge them from micro capillary tubes (Li et al., 2002). Yang and Evans have also performed research in this direction (Yang and Evans, 2004). A piezoelectric droplet ejector with micronozzles has also been shown to be able to selectively deposit lines of solid particles 260 μm wide (Percin and Khuri-Yakub, 2003). Although these technologies have yet to be used for the creation of substantial three-dimensionl geometry, researchers are beginning to implement this technology in an AM context (Lu et al., 2006).

Two-Dimensional Material Patterning

This physical principle entails the creation of layers via the patterning of material in a two-dimensional pattern; this can include the creation of whole layers at once, or the

deposition of two-dimensional layer segments. Two-dimensional patterning is inherently faster than one-dimension patterning as large portions of a cross-sectional layer can be processed in a single motion.

- *Two-dimensional suspension ejection* – This working principle involves the use of a series of print heads to selectively eject small droplets of material onto a substrate. Although dependent on the diameter of the nozzle, droplets are typically around 80 microns in diameter. It should be noted that this principle does not truly pattern material in a two-dimensional manner; instead, it involves the patterning of several one-dimensional parallel lines of material from an array of individual printing nozzles. Specific embodiments of this principle include drop-on-demand printing (selectively ejecting distinct droplets) and continuous printing (selective deflection of a continuous stream of droplets). AM processes that employ this working principle include 3DP (Sachs, 2000), aqueous direct inkjet printing (IJP-A) (Blazdell et al., 1995), hot-melt direct inkjet printing (IJP-W) (Slade and Evans, 1998), and UV direct inkjet printing (IJP-UV). Because this patterning principle processes ceramic powder suspensions, it is similar to extrusion in that there is a physical limit to the suspensions' solids loading that can be processed. Relative to extrusion, droplet ejection requires much more rigorous rheological constraints as individual droplets must be formed from very small nozzles with minimized satellite formation. Surface tension and viscosity of the suspension play critical roles in the successful formation of droplets due to the low pressure used for droplet ejection (Ainsley et al., 2002). 35 vol% solids loading is the maximum fraction

jetted with a polymeric carrier (Seerden et al., 2001), while only 15 vol% has been jetted with an aqueous carrier (Wright and Evans, 1999). The primary advantage of this principle is that it is an extremely scalable technology; the quantity of printing nozzles can be increased with very little increase in overall cost. One can imagine creating an array of print heads that would cover the entire width of the working area, such that only one linear stage is needed to sweep along the area, and thus increasing the deposition rate (and therefore reducing build time) significantly.

- *Two-dimensional tape / sheet* – This working principle involves patterning material by placing a two-dimensional tape or sheet directly on the workpiece. Both the LOM and CAM-LEM AM processes employ this working principle by patterning entire layers at once. UOC also employs this principle by selectively patterning several small strips of material over the cross-sectional area. No matter the specific embodiment, patterning two-dimensional swatches of material has been used to dramatically reduce build time.
- *Two-dimensional powder deposition* – Seen in the Electrophotographic Printing (EP) AM process, this working principle involves the deposition of two-dimensional selective patterning of powder (Karlsen and Reitan, 2003). In EP, this is accomplished by charging a roller electrically and then discharging the roller as it passes over the substrate. As such, entire layers of powder can be selectively patterned at once. This working principle is also observed in the Desktop Factory AM machine, which is being sold for only $5000 (Desktop, 2007). One disadvantage with this specific embodiment is that the powder must

be electrically conductive in order for it to be successfully deposited; this is not a common feature of most ceramics.

No Material Patterning

In order to be able to represent those working structures that do not feature material patterning, "no material patterning" is offered as a working principle. For example, many powder bed AM processes such as LS, EBM, SLM, and others do not selectively pattern material.

3.3.3 Pattern Energy

This sub-function details those processes which selectively deposit energy in order to create a primitive or entire layer of the green part. Typically, this patterned energy initiates a change of phase of the raw material in order to transform it to a solid primitive. Similar to the "pattern material" sub-function, the "pattern energy" physical principles are classified by the dimension of patterning. Working principles for "pattern energy" are further distinguished by the type of energy used to form solid primitives. These embodiments are presented in Table 3.9.

Table 3.9 – Working Principle Progression for "Pattern Energy" Sub-Function

Sub-Function	Physical Principle	Working Principle
Pattern Energy	1D Energy	1D light source
		1D heat source
	2D Energy	2D light source
		2D heat source
		2D ultrasonic welding
	No Energy Patterning	No energy patterning

One-Dimensional Energy Patterning

This physical principle involves rapid patterning of a point source of energy. Primitives are typically created by rastering the point source over the cross-sectional area in order to create a single layer. Patterning via rastering a single point is not an

economically efficient means of production due to the limited speed of operation and control of the energy patterning mechanisms (e.g., galvanometer mirrors and/or linear stages).

- *One-dimensional heat source* – In order to create primitives through such physical principles as sintering, melting, or polymerization, heat needs to be able to be selectively delivered into the build volume. Lasers are suitable embodiments of this working principle because of their small spot size, ease of use, and accuracy of control. Whether gas (e.g., CO_2) or solid-state (e.g., Nd:YAG), lasers of certain wavelengths (typically in the infrared range) and power can be used to selectively add energy to cut, heat, or melt single points within the build volume. Electron beams are another embodiment of this working principle, as they can be used to join powder particles through melting. This working principle is used to create solid primitives in several AM processes including LS, LENS, SLM, and EBM.
- *One-dimensional light source* – Because some polymers can be activated via exposure to certain wavelengths of light, "one-dimensional light source" is presented as a feasible working principle. Just as noted above, lasers are a suitable embodiment for this principle since many different wavelengths can be delivered at various powers and spot diameters accurately and precisely.

Two-Dimensional Energy Patterning

This principle entails the patterning of energy in a two-dimensional pattern. This can include the creation of whole layers at once, or the deposition of two-dimensional

layer segments. Similar to the two-dimensional patterning of material, this physical principle inherently has an increased build rate over its one-dimensional counterpart.

- *Two-dimensional heat source* – This working principle details the application of heat to the work piece, typically through exposure to infrared light. This principle includes the selective patterning of heat via some sort of mask, or the exposure of the entire layer to heat. This working principle is found in the High Speed Sintering AM process where the entire powder bed is exposed to infrared light once the printing of a special receptor ink is completed (Hopkinson and Erasenthiran, 2004; Thomas et al., 2007).
- *Two-dimensional light source* – This working principle describes those processes that expose two-dimensional areas of the build-volume to light in order to create primitives or layers. The micro-stereolithography AM processes employs this working principle through the use of ultra-violet lamps, active LCD masks, or digital micro-mirror devices (Limaye and Rosen, 2006).
- *Two-dimensional ultrasonic welding* – A solid-state joining process, ultrasonic welding involves the use of a sonotrode that vibrates at ultrasonic frequencies, which upon application to the substrate, causes interface diffusion and deformation between materials, thus binding them together (White and Carmein, 2002). Because the sonotrode has a relatively large footprint, it occupies a two-dimensional area. One benefit of the ultrasonic welding process is that it operates at room-temperatures and therefore does not impose any residual stresses into the workpiece. However, this process has only been

shown feasible for metallic sheets, and is therefore not an available option for the creation of ceramic green parts.

No Energy Patterning

In order to be able to represent those working structures that do not feature energy patterning, "no energy patterning" is offered as a working principle. AM process that do not directly pattern energy include extrusion processes (FDM, MJS, FEFF, etc.).

3.3.4 Create Primitive

This sub-function entails the manner in which the raw material is transformed or shaped into a series of primitives that will form the desired part once all layers are patterned. These principles are ideated by asking, "What physical principles can (trans)form loose, raw material into solid primitives?" Principles of this sub-function are typically some form of energy that changes the phase of the stored raw material in order to create each cross-sectional layer. Embodiments of each physical principle are presented in Table 3.10.

Table 3.10 – Working Principle Progression for "Create Primitive" Sub-Function

Sub-Function	Physical Principle	Working Principle
Create Primitive	Initiate Polymerization	Polymerization via catalyst
		Polymerization initiation via solvent
		Photopolymerization
		Thermal polymerization
		Introduce polymer to bind
	Solidify Melt	Solidify melt
	Sinter	Solid-state sintering
		Liquid-phase sintering
	Freeze	Freeze
	Evaporation	Evaporate solution
	Cutting and Joining	Joining and cutting
		Cutting and joining
	Initiate Chemical Reaction	Chemical reaction via catalyst
		Chemical reaction via heat

Initiate Polymerization

This physical principle describes the joining of raw material by the initiation (and sequential termination) of polymerization in order to create a solid primitive. This principle is embodied by the several methods of initiating polymerization.

- *Polymerization via catalyst* – This working principle describes the initiation of monomer cross-linking via the addition of a catalyst or hardening agent. The introduction of a secondary phase to initiate polymerization is common to epoxies.
- *Polymerization via solvent* – This embodiment describes the introduction of a solvent as a means of partially dissolving a polymer matrix. The partial dissolving can deform the polymer particles, causing them to neck and bind together. Solid primitives result once the solvent evaporates and the polymer dries. In ceramic green body manufacturing, solvents are used as a means of lowering paste viscosity during extrusion. This principle has been employed in 3DP as a means of initiating polymerization in the powder bed (Utela et al., 2006; Carreno-Morelli et al., 2007).
- *Photopolymerization* – Photopolymerization is the initiation of cross-linking of monomers via light-induced irradiation. This working principle is featured in SL: an ultraviolet laser scans over a vat of resin which is cured by the photochemical process where photoiniators cleave apart from the absorption of the UV light and subsequently break the double bonds of the monomers in the vat for polymerization to occur (Griffith and Halloran, 1994b).

Photopolymerization has also been used to create ceramic green tapes in the tape casting process (Chartier et al., 1997).

- *Thermal polymerization* – A common way to initiate polymerization is the introduction of energy in order to melt or soften the polymer to induce deformation and necking of the polymer particles. A solid primitive remains from the polymer once it cools and hardens. This working principle is found in the heated extrusion nozzles of FDM and the heated printing nozzles of hot-melt direct inkjet printing AM processes. This principle is also found in some forms of stereolithography were infrared energy is delivered to a thermosetting resin via a laser or 2D mask (Jardini et al., 2003).
- *Introduce polymer to bind* – This working principle describes the application of a polymer onto the working material. Solid primitives are created as the polymer sets upon drying, as seen in 3DP. Furthermore, polymer adhesives can also be introduced to bind layers together as featured in LOM.

Solidify Melt

This principle details the creation of primitives via melting, which entails the joining of particles by heating them past their melting point (thus changing their phase to liquid) and then cooling the resultant melt pool to a solid. This principle is found in AM processes such as MJS, SLM, and DMLS. As indicated in Section 3.3.1, however, this is an unlikely working principle for ceramic AM, as ceramic powers have an extremely high melting point.

Sinter

Sintering is the joining of powder particles by heating them (below their melting point) until they adhere to each other. This is typically identified by observing necking between particles caused either through solid-state diffusion or through viscous liquid flow of the particle surface or of a secondary solid binder phase (Kruth et al., 2003).

- *Solid-state sintering* – Solid-state sintering (SSS) is a specific embodiment of sintering and involves necking between particles solely due to diffusion of atoms along the particle surface at elevated temperature. SSS is typically a very slow process due to the slow kinetics of mass diffusion (Kruth et al., 2003). A wide variety of materials can be processed with SSS, but a post-processing operation is required to improve part characteristics (Kruth et al., 2004b). Furthermore, solid-state sintering of ceramic powder does not result in a green part, but instead a dense ceramic finished part which cannot be converted to a metal via reduction. Phenix Systems in France has commercialized a LS-like system that realizes SSS with an Nd:YAG laser source (Phenix, 2005). Parts with accuracy of +/- 50 μm (per 120 mm) and a minimum feature size of 300 μm have been reported using this process.
- *Liquid-phase sintering* – Liquid phase sintering is the necking of particles due to liquefying a secondary binder material so as to bind the structural material. Liquid phase sintering requires a lower temperature, and is faster than solid state sintering since mass transport can occur much more rapidly due to liquid flow and particle rearrangement; for these reasons, liquid phase sintering is much

more frequently used than solid state sintering in AM applications (Agarwala et al., 1995). This working principle is featured primarily in the LS AM process.

Freeze

This principle embodies the creation of primitives via the freezing of a liquid phase to a solid state. Freeze-drying is employed to synthesize ceramic powders (Ring, 1996). In the context of AM, Huang and coauthors have used freeze-drying to extrude ceramic suspension with a high percentage solids loading (60 vol%) (Huang et al., 2006). Fu and coauthors have processed ceramic components via freeze-spray processing (Fu et al., 2006).

Evaporation

This principle describes the creation of solid primitives via the evaporation of a solvent from a suspension. This principle is employed by the aqueous direct inkjet printing AM process (IJP-A). This process features the jetting of an aqueous solution containing ceramic particles followed by an increase in temperature to evaporate the liquid carrier (Evans, 2001). While the process can achieve very high resolution, evaporation is slow and therefore severely limits the build rate.

Cutting and Joining

This physical principle describes the creation of primitives via the physical cutting of larger solids into smaller items and physically joining the resultant smaller pieces. This process ("*cutting and joining"*) is featured in the CAM-LEM process. This principle also encapsulates the opposite working order ("*joining and cutting"*), as seen in the LOM and UOC AM processes. Joining is typically accomplished via the introduction of a polymeric binder, solid state joining techniques, or welding.

Initiate Chemical Reaction

This principle entails the creation of solid primitives through the initiation of a chemical reaction. This principle is unique to those reactions that yield a solid primitive from the combination and subsequent chemical reaction of two or more distinct raw materials.

- *Chemical reaction via catalyst* – Similar to the initiation of polymerization via the introduction of a catalyst, this working principle entails the introduction of a catalyst to initiate a chemical reaction.
- *Chemical reaction via heat* – This working principle describes the initiation of a chemical reaction via the introduction of energy. This working principle is found in the LCVD process where solid deposits of metals and ceramics have been patterned via the use of a laser to initiate a chemical reaction (Johnson et al., 2003).

3.3.5 Provide New Material

This sub-function entails the manner in which a supply of raw material is provided to the system so that a new layer can be created. The physical and working principles are displayed in Table 3.11.

Table 3.11 – Working Principle Progression for "Provide New Material" Sub-Function

Sub-Function	Physical Principle	Working Principle
Provide New Material	Recoat Layer	Recoat by spreading
		Recoat by spraying
		Recoat by dipping
	Direct Material Addition	Direct material addition
		Directly place layer

Recoat Layer

New material can be added by coating the previously deposited layer with a supply of fresh raw material. This coating can then be selectively patterned in order to create the new part cross-section.

- *Recoat by spreading* – This working principle details recoating via spreading new material onto the workpiece. Embodiments of this principle include a counter-rotating roller as seen in powder-bed technologies such as 3DP, LS, DMLS, SLM, EBM, as well as a doctor blade as seen in AM technologies such as SL.
- *Recoat by spraying* – This working principle details recoating by spraying new material through nozzles. This working principle is embodied through the use of inkjet printing nozzles in slurry-based Three-Dimensional Printing (S-3DP). This principle has also been suggested for the recoating of the viscous resins used in stereolithography (Geving et al., 2000). Finally, plasma spraying and freeze-spraying of ceramics are traditional manufacturing processes that could be used in an AM context by employing this working principle (Aljdelsztajn et al., 2005; Fu et al., 2006).
- *Recoat by dipping* – Another principle for recoating is to submerge the part in a suspension and allow the raw material to flow onto and around the part. Careful control can ensure that a single layer thickness is added to the working part. This working principle is employed by several various stereolithography AM processes. This principle is not as feasible when working with suspensions which are loaded with ceramics as the viscosity of the suspension would most likely be too great to effectively recoat the part.

Direct Material Addition

This principle encapsulates those working structures that directly add, and typically selectively pattern, material onto the substrate in order to create each new layer.

- *Direct material addition* – This working principle involves those embodiments that directly and selectively add material to the workpiece. This principle can be seen in AM processes such as LENS and direct inkjet printing.
- *Directly place layer* – This working principle encapsulates those processes that directly and selectively place an entire layer of raw material for processing. LOM, CAM-LEM, and UOC directly place entire sheets of raw material for pattering, while electrophotographic printing (EP) selectively places a layer of new material via its electrostatically charged roller.

3.3.6 Support Previously Deposited Material

This sub-function describes the manner in which each layer is supported during the build process. This is a crucial sub-function for the development of complex cellular mesostructure via additive manufacturing due to the frequent necessity of constructing overhanging and high-aspect ratio features.

Table 3.12 – Working Principle Progression for "Support Previously Deposited Layer" Sub-Function

Sub-Function	Physical Principle	Working Principle
Support Previously Deposited Layer	Bed of Material	Bed of build material
	Thin Trusses of Build Material	Thin trusses of build material
	Sacrificial Support Material	Dissolvable support material
		Breakable support material
		Pyrolizable support material
	5-Axis Deposition	5-axis deposition

Bed of Material

One manner of supporting previously deposited material is to build the part in a bed of the raw material, thus allowing the unpatterned material to serve as a framework for

support. This unpatterned material would need to be physically removed from the finished part. This principle is found in all powder bed AM processes including 3DP, SLM, EBM, and LS. This principle is also employed in those AM processes that work with extremely viscous slurries including the Optoform stereolithography process.

Thin Trusses of Build Material

This principle describes the creation of small, fibrous, truss-like support structures with build material as a means of supporting overhanging features. This principle requires the selective patterning of these special sub-structures and their physical removal once the part is completed. This principle can be found in the SL process and sometimes in the IJP-W process.

Sacrificial Support Material

This principle describes the inclusion of a secondary material that is used solely for the purpose of supporting built material. This support material is to be removed at the conclusion of the part build.

- *Dissolvable support material* – This working principle entails the use of a secondary support material which can be dissolved during post-processing via a solvent. It is necessary to note that the solvent must be carefully chosen so as to only dissolve the support material and not the structural material. This working principle has been employed in the FDM process via Stratasys's WaterWorks material (a water soluble support material) (Stratasys, 2007).
- *Breakable support material* – This principle describes the creation of support structure from secondary support material which can be removed by minimal physical effort. Just as with the "thin trusses of build material" principle, this is

not a feasible means of supporting the realization of cellular mesostructure since it would be very difficult to remove.

- *Pyrolizable support material* – This principle describes the deposition of support material which is burnt away during the sintering process. This working principle has been successfully implemented in IJP-A wherein carbon has been selectively deposited as a support material and then burnt away during sintering (Mott et al., 1999).

5-Axis Deposition

This physical principle is the one feasible alternative for creating complex mesostructure without the need for an explicit means of support. This principle describes the selective creation of primitives in a multiple degree-of-freedom deposition process that results in the creation of parts with sufficient structural strength such that a means of support is not needed. This principle can be found in the LENS (Hedges and Keicher, 2002) and LCVD AM processes.

3.4 MORPHOLGICAL MATRIX

With working principles outlined (from the systematic embodiment of physical principles, presented in Figure 3.4), the generation of working structures can begin. Working structures are created by the organization and combination of working principles with the aid of a morphological matrix. Morphological matrices provide a framework in which to categorize working principles by sub-function (Zwicky, 1967). In this scheme, the sub-functions and the appropriate working principles are entered into the rows of the matrix. By systematically combining a working principle fulfilling a specific

sub-function with the working principle for a neighboring sub-function, one obtains an overall solution in the form of a working structure. Only those working principles that are compatible are combined.

All of the working principles presented in Section 3.3 are combined into a morphological matrix in Figure 3.5.

Returning to the information presented for each working principle detailed in Section 3.3, it is clear that there are several principles that are not a feasible means of realizing metal-oxide ceramic green parts with cellular mesotructures. In order to generate valuable design solutions, these select working principles must be removed from the morphological matrix before the generation of working structures can commence.

The following working principles are removed (listed along with their respective sub-functions and physical principles):

- *Store material: liquid : molten material* – Detailed in Section 3.3.1, this principle is not suitable for the realization of ceramic green parts due to the fact that it is extremely difficult to liquefy ceramics via melting (due to either the inability to achieve liquid flow with certain ceramics, or an extremely high melting temperature).
- *Store material*: *gas: two-phase gas* – The only manner in which solid depositions can result from a gaseous raw material is through specific chemical reactions initiated by thermal energy (as detailed in Section 3.3.1). The result of these chemical reactions is a fully dense, sintered ceramic part. Those AM processes which utilize this working principle, SALVDI (Crocker et al., 1999) and LCVD (Johnson et al., 2003), are capable of creating complex structures with very

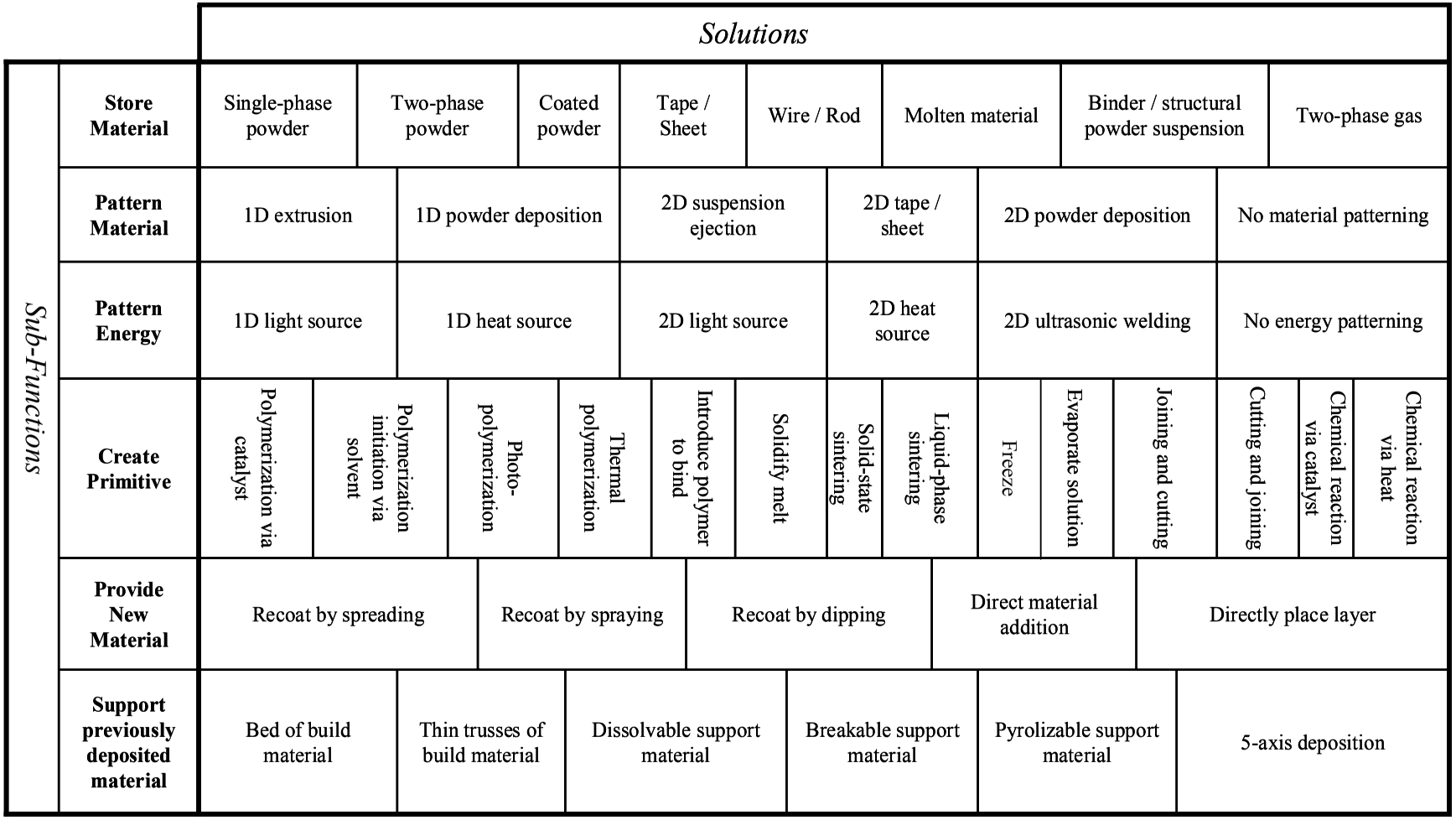

Figure 3.5 – Preliminary Morphological Matrix

small feature sizes (20 μm), although somewhat slowly (100 μm per second) (Tay et al., 2003). The resultant parts of both processes are a high purity, fully-dense, sintered ceramic part. As such, they are not suitable for further post-processing in a reducing atmosphere. This is because it is extremely difficult for the reducing agent (a hydrogen gas for example) to diffuse through the solid structure. Furthermore, it would be difficult for the oxygen to diffuse out of the solid, and could cause severe part warpage and/or cracking during the inevitable shrinking. As such, this working principle is not suitable for the to-be-designed manufacturing process.

- *Pattern energy: 2D energy patterning: 2D ultrasonic welding* – This principle (presented in Section 3.3.3) is not a feasible means for realizing ceramic green parts as the solid-state joining process does not work with ceramic materials.
- *Create primitive: Sinter: solid-state sintering* – As described in Section 3.3.4, solid-state sintering is not suitable for the to-be-designed manufacturing process as it is slow and does not result in a ceramic green part that is suitable for reduction post-processing.
- *Create primitive: solidify melt* – Just as the "store material" sub-function should not be realized via "molten material", the "create primitive" sub-function should not be realized via "solidify melt." The extremely high melting temperature of ceramics makes this principle infeasible for the manufacturing process.
- *Create primitive: freeze* – This working principle is eliminated from the morphological matrix because, although it is a standard method for synthesizing ceramic powders, it has not been shown to be an efficient method for realizing

three-dimensional ceramic structures. Specifically, the low-binder content in the green part prevents the creation of complex parts due to warping and shrinkage during sintering and debinding.

The updated morphological matrix, which has these principles removed, is presented in Figure 3.6.

3.5 DISSERTATION ROADMAP

The focus in the beginning of the conceptual phase of the design process is abstraction of design requirements so that a solution-neutral design task can be formulated (Section 3.1). The focus on abstraction continues in the development of a general function structure for the to-be-designed process (Section 3.2). Physical principles are defined for each sub-function, and are used for the creation of working principles (Section 3.3). These working principles are then used to populate a morphological matrix (Section 3.4), which provides a framework for the systematic generation of working structures.

As can be seen in the dissertation roadmap (Figure 3.7) working structures are generated in Chapter 4. Once working structures are generated and analyzed, a selection decision must be made so as to identify the principal solution (Chapter 5).

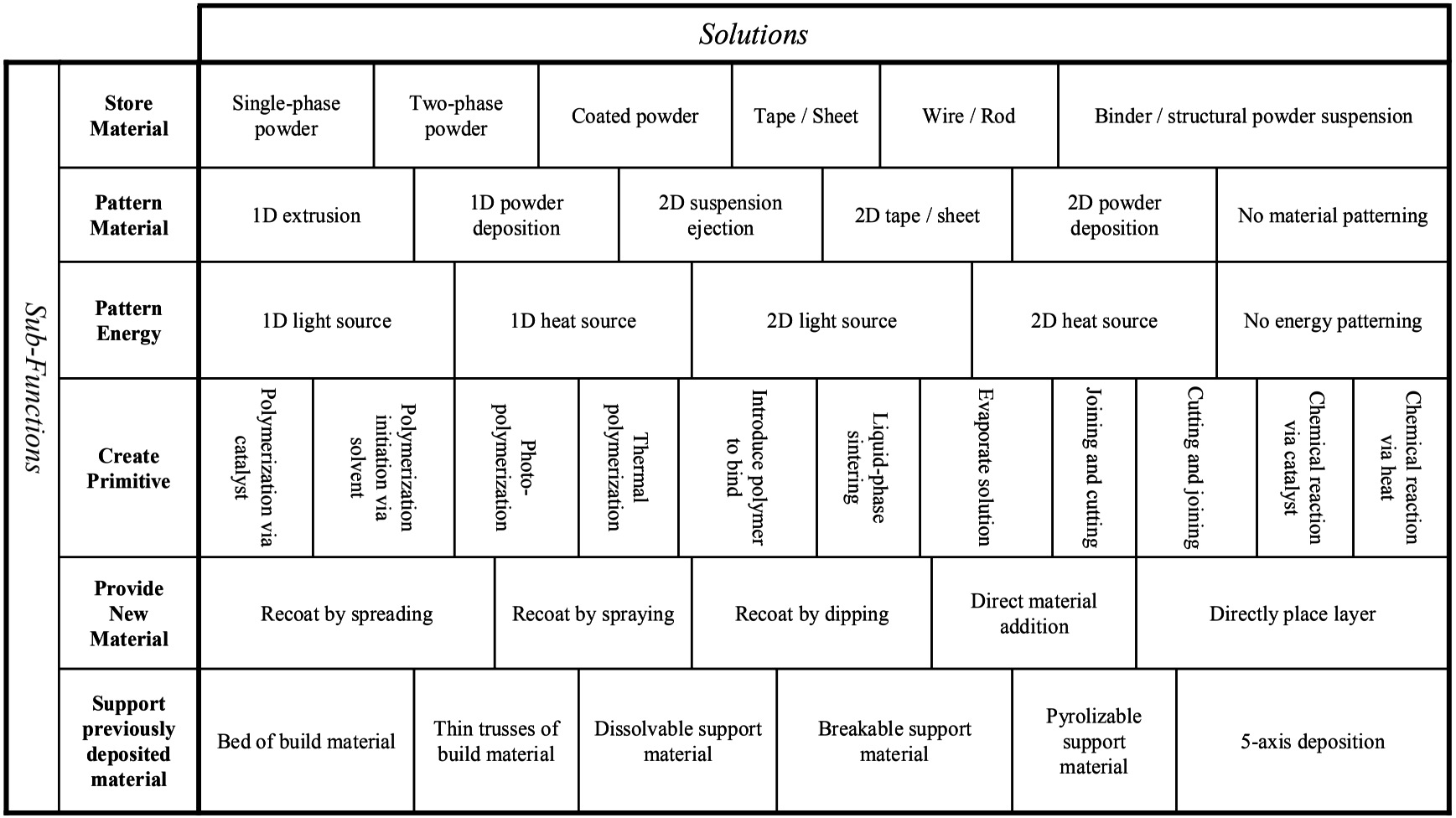

Figure 3.6 – Morphological Matrix

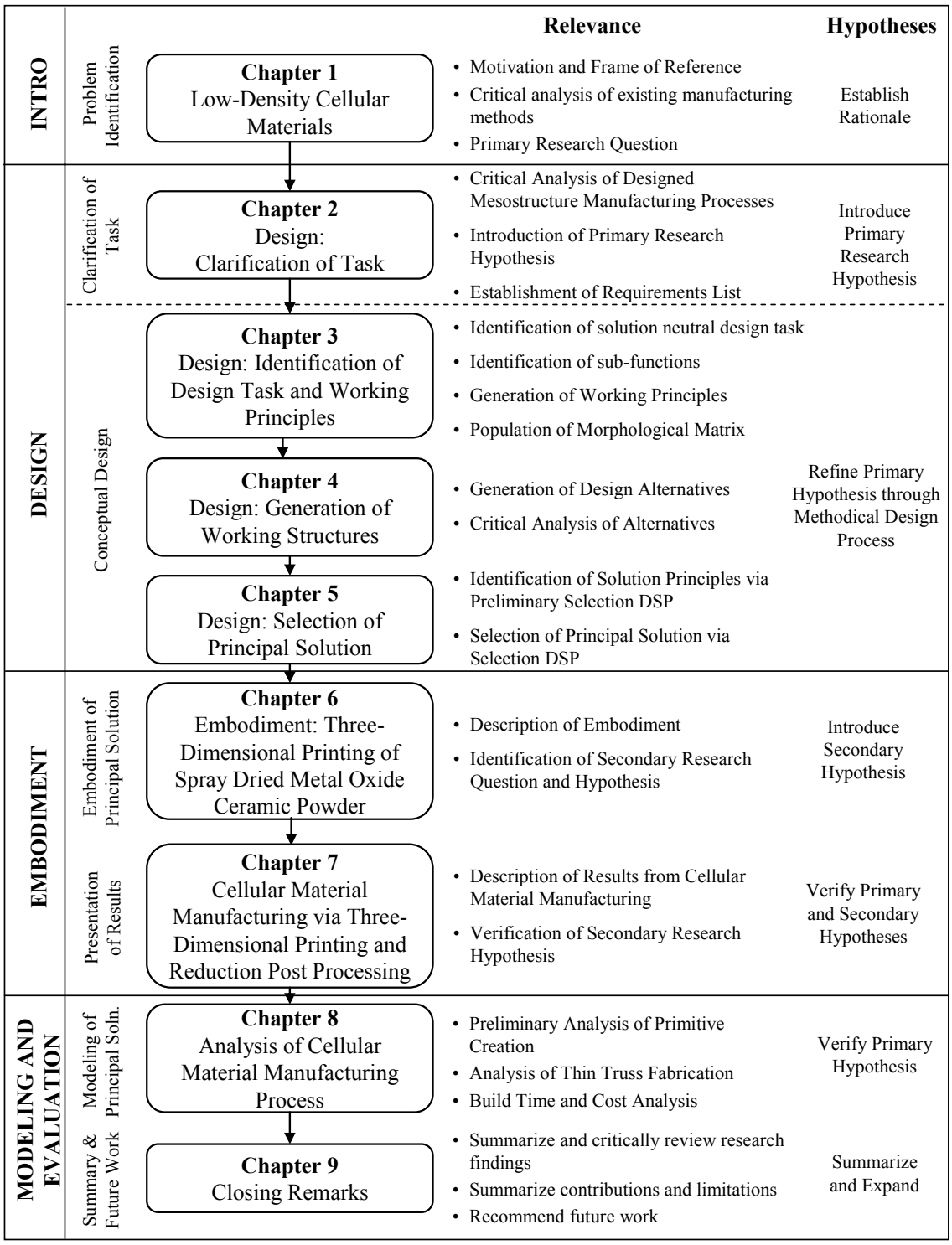

Figure 3.7 – Dissertation Roadmap

CHAPTER 4

DESIGN: GENERATION OF WORKING STRUCTURES

As shown in Figure 3.3, with working principles generated from the identified physical principles (Section 3.3), the generation of working structures can begin. Working structures are generated via combining a working principle from each sub-function with the aid of a morphological matrix (Section 3.4, Figure 3.6). In this chapter, working structures are generated and are critically analyzed. While summaries and reviews of existing ceramic AM techniques are available in the literature (Halloran, 1999; Tay et al., 2003), the review presented in this chapter is unique in that it is organized by function and is done in the specific context of manufacturing cellular materials (as seen in (Williams et al., 2005b)).

The working structures generated by this conceptual design exercise are grouped by the common use of certain working principles. These categories include one-dimensional energy patterning (Section 4.1), two-dimensional energy patterning (Section 4.2), material patterning (Section 4.3), indirect material printing (Section 4.4), and direct material printing (Section 4.5). Each sub-section is closed with a list of process properties that will serve as criteria for the selection of the solution principle (presented in Chapter 5). These criteria include: production cost, deposition rate, minimum feature size, z-resolution (layer thickness), surface roughness, green part solids loading, available working materials, and a judgment of the processes' ability to make (and support) the complex geometries typical of cellular materials. References are provided when available. Because each working structure is in the midst of various stages of

development, there are occasions in which these metrics are only noted with qualitative engineering data.

4.1 ONE-DIMENSIONAL ENERGY PATTERNING WORKING STRUCTURES

In this section, two working structures are presented: laser sintering (LS, Section 4.1.1) and stereolithography (SL, Section 4.1.2). These processes are grouped together because they employ the use of the one-dimensional energy patterning working principle (as shown in Figure 4.1).

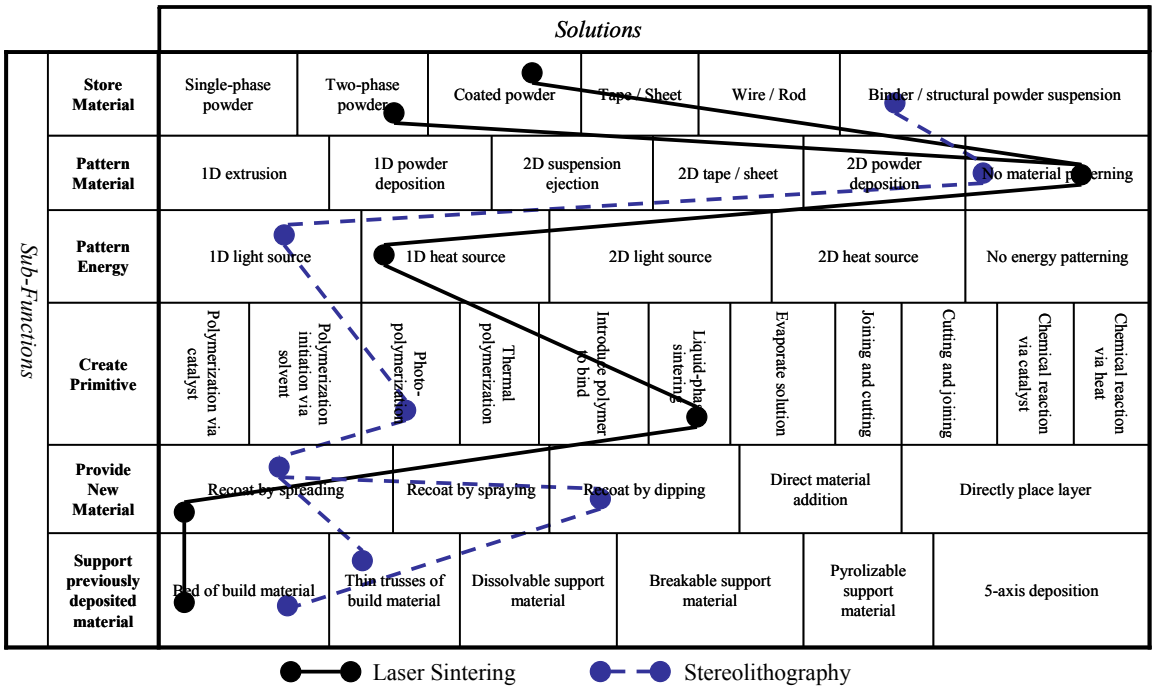

Figure 4.1 – 1D Energy Patterning Working Structures

4.1.1 Laser Sintering (LS)

Laser Sintering (LS) involves the use of a high powered laser beam (typically 100-200 W CO_2 laser) to selectively fuse particles of a powder bed together in order to create solid primitives (Bourell et al., 1995). Specifically, the thermal energy from the laser

beam induces liquid-phase sintering (LPS) on a polymer that is either coating, or mixed with, the ceramic particles. The partial melting and subsequent necking of the polymer causes the creation of a solid primitive. The binder can either be an organic polymer or a low melting inorganic salt (Tay et al., 2003). The reason for the indirect approach is that laser sintering of high melting point ceramics requires a high level of laser energy and can create large thermal gradients, and thermal shock, which can cause difficulty in forming a continuous shape (Subramanian and Marcus, 1995).

Once a layer has been successfully patterned, an elevator platform lowers the part and the new material for the next layer is added onto the working powder bed from a reservoir of fresh powder via a spreading mechanism (typically, a counter-rotating roller or scraper blade). This process repeats until the entire part is created. Once the part is removed from the powder bed, and excess unpatterned material is removed, the part undergoes debinding, sintering, and often infiltration post-processing in order to fully densify the ceramic part. Researchers have successfully formed a wide variety of materials with LS, including alumina, zirconium silicate, silicon / silicon carbide, silicon sand, and other metal-matrix composites including Ti/SiC (Tay et al., 2003).

In the context of manufacturing cellular materials, the primary strengths and weaknesses of this working principle reside in its use of a powder bed. The primary benefit of using a powder bed is that no support structure is needed to create complex geometry as the non-fused powder remains in place to act as a support itself. Furthermore, changing from one material to another is simpler than in many of the suspension-based AM techniques, given the dry solid nature of the starting material (i.e., no suspension control is needed) (Tay et al., 2003). However, it should be noted that

each distinct material requires different heating and laser parameters due to each powders' various absorptance values (absorptance of a material is the ratio of the absorbed laser radiation to the incident radiation) (Tolochko et al., 2000).

Despite these advantages, the use of a powder also imposes some limitations. For example, while the presence of the powder bed circumvents the need for support structures, it prevents the ability to process cellular materials with closed cells or small channels due to enclosed material and/or the inability to sufficiently remove un-sintered material. The major limitation in working with a powder bed is the inherent high level of residual porosity that is present in the green part (Klocke and Ader, 2003). This porosity is resultant of the use of a powder bed which typically contains less than 50 vol% solids loading due to the inefficient packing of spherical particles. Hot isostatic pressing and/or infiltration is often used as a means of increasing the final part's density.

Furthermore, the surface finish obtained by using a powder bed is sensibly rougher compared to parts obtained by powder compaction, and surface finishing (only possible on accessible surfaces) is necessary (Vaucher et al., 2002). In fact, Klocke and Ader have shown that simultaneously improving surface finish and green part density are conflicting objectives: increasing laser power increases the density of the part since more energy is delivered into the powder and larger melt pools fill up the porous structures of the previous layers; however the surface roughness also increases (Klocke and Ader, 2003). As such, ceramic LS is typically only used for the creation of molds for the indirect production of ceramic parts (Deckard and Claar, 1993).

It should also be noted that the process is somewhat wasteful, as any unsintered powder not used in the process should be disposed in order to achieve the highest quality

parts. Recycled powders must be sieved to remove agglomerates, which interfere with the smooth application of the next level of powder. This is not sufficient however, as recent research has shown that the use of recycled powder leads to poor surface finish and poor material properties (Sewell et al., 2007).

Finally, the use of one-dimensional thermal energy to create ceramic primitives introduces the same limitations found when creating metal parts. First and foremost, the need to raster a one-dimensional laser spot across the entire part cross-section in order to create a layer inherently limits build speed. Most importantly, the use of thermal energy to initiate sintering introduces thermal gradients, and thus residual stresses, to the part during its fabrication (Mercelis and Kruth, 2006). The presence of residual stresses, and the resultant warping and curling, can make the processing of thin walls (a common feature of cellular materials) very difficult. In order to minimize the amount of energy needed to initiate the LPS, the powder bed is typically heated to close to its sintering temperature, thus only requiring a small amount of energy to begin solidification. This procedure may also help in reducing residual stress development and to relieve stresses that have been established during fabrication (Tay et al., 2003). However, pre-heating the powder bed only exacerbates the difficulties in removing un-patterned powder from small cellular passages.

The process properties of the current embodiment of the laser sintering working structure are presented in Table 4.1.

Table 4.1 – Laser Sintering Process Properties

Stat	Value	Reference
Production Cost ($)	314,000 – 700,000	(Wohlers, 2006)
Deposition rate (cm^3/hr)	Scan speed is 10 m/sec; deposition limited by 1D deposition, powder recoating, and material bed pre-heat process	
Minimum feature size (mm)	0.1	
Z-resolution (mm)	0.02 – 0.15	(Kruth et al., 2004b)
Surface Roughness (μm, Ra)	Sandy appearance; Worse than powder compact compaction	(Vaucher et al., 2002)
Green part solids loading (vol %)	~ 50	
Working materials	All ceramics	
Support / Complex Geometry	Somewhat limited (powder bed)	

4.1.2 Stereolithography (SL)

One of the most widespread AM techniques, stereolithography (SL), involves the creation of solid primitives via the use of an ultra-violet (UV) laser to selectively cure a photopolymer resin. Photocurable resins contain a photoinitiator that generates free radicals in the presence of UV light. The resin monomer is polymerized when attacked by the free radicals. Once exposure to UV light ceases, the reaction stops due to oxidation. The depth of cure, C_d, is given by Equation 4.1 where D_p is the penetration depth of the resin, E_{max} is the peak value of exposure of the laser beam, and E_c is the critical energy density below which polymerization will not occur. D_p and E_c are material properties of the resin.

$$C_d = D_p \ln\left(\frac{E_{\max}}{E_c}\right) \qquad [4.1]$$

The reaction occurs in a vat of the resin. Once a layer is rastered by the UV laser spot (and thus solidified), the part is lowered into the vat and a new layer of fresh material is precisely added either by spreading with a doctor blade or dipping. Overhanging geometry is supported by the creation of thin truss-like strands of the build material,

which must be physically removed during post-processing (making cleaning of cellular materials extremely difficult).

Parts created by SL are distinguished by the excellent surface finish and fine detail (minimum feature size of 700 μm). These quality metrics result from the combined use of a resin vat (layer thicknesses of 50 – 100 μm) and a UV laser source with a small spot size (75 μm).

Recognizing the limited working material selection for the process, a decade of research has been conducted to find ways of processing ceramics with this technology. To create ceramic parts with this technology, fine-grained ceramic particles are combined with a monomer and photoinitiators to create a modified photopolymer resin. High shear mixing is used to combine the particles and the resin; this is followed by prolonged ball-milling in order to ensure homogeneity (Griffith and Halloran, 1995). Through the careful control of dispersants, researchers have been able to successfully create stable working resins with approximately 50 vol% ceramic powders (Brady et al., 1996). Since no shrinkage occurs during curing, the ceramic volume fraction in the solid cured body is the same as the ceramics loading of the fluid SL suspension before curing (Griffith and Halloran, 1994b).

After the green part is made by selective curing with the UV laser, the part is sintered at high temperatures (usually optimized by thermogravimetric analysis). Parts typically undergo ~15% linear shrinkage; results have given densities as high as 96% theoretical density (Hinczewski et al., 1998b). The resultant parts show no sign of layered processing; however, some cracking and delamination during sintering has been observed (Brady et al., 1996). While SL ceramic parts benefit from the process's inherit

high resolution, good surface finish, and high-density green parts, the process suffers from two major limitations: a limited selection of working materials and high resin viscosity.

The main flaw with this layer-based approach to free-forming ceramic parts stems from its inability to process many different types of ceramics. Most ceramics are incompatible with the principle of using UV radiation to cure photopolymer suspensions; specifically, the UV radiation cannot be absorbed at a great enough depth (150-200 μm) to achieve curing and binding between layers. Griffith and Halloran note that the lack of absorption of the UV radiation, and the resulting small cure depth, comes from the suspension's turbidity due to light scattering as shown in Figure 4.2 (Griffith and Halloran, 1994b).

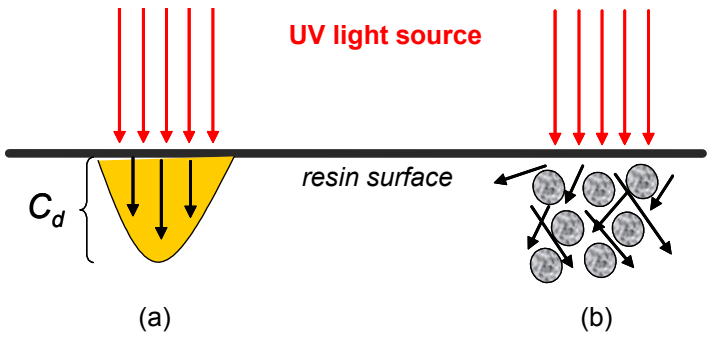

Figure 4.2 – Depth of Resin Curing with (a) standard resin, (b) resin loaded with ceramic particles

Powder suspensions can have a very high turbidity due to light scattering, even if the ceramic itself is transparent to UV. Scattering has also been shown to contribute to larger line-widths and elliptical curvature thus increasing the process's realizable minimum feature size (Brady et al., 1996). This problem is exacerbated by the need to have a high-solids loading in the suspension (Griffith and Halloran, 1996). Experiments have shown that the cure depth, C_d, is a function of the volume concentration of powder

(there is a linear relationship between the C_d and the inverse of the concentration of the ceramic), an experimentally determined scattering efficiency term (Q), the particle diameter (d), and the refractive index difference (Δn) between the UV curable solutions (n_o) and the ceramic powder (Griffith and Halloran, 1994b; Griffith and Halloran, 1996; Hinczewski et al., 1998a). Halloran et al. have shown that the scattering phenomena is dominated by the refractive index difference between the ceramic material and the resin (Griffith and Halloran, 1997; Brady and Halloran, 1998) as seen in Equation 4.2.

$$C_d = \frac{2d}{3Q}\frac{n_o^2}{\Delta n^2}\ln\left(\frac{E_{\max}}{E_c}\right) \qquad [4.2]$$

Due to this limitation, only three ceramics have been successfully processed using SL: alumina (Al_2O_3), silica (SiO_2), and PZT (Griffith and Halloran, 1996; Hinczewski et al., 1998b) as their refractive indices (1.56 and 1.418 for alumina and silica, respectively) are close enough to the value of 1.5 for typical resin (for reference, titanium dioxide and iron oxide have refractive indices of around 2.5). Many researchers have attempted silicon nitride, but the cure depth was too small to claim a success (Griffith and Halloran, 1994b; Zimbeck et al., 1996). In fact, Jang and co-authors published a paper solely regarding their failure with attempted curing of barium titanate in hexanediol diacrylate (HDDA) (Jang et al., 2000). It should be noted that, in their patent filing, Moussa and co-authors propose coating the particles so as to minimize UV absorbency and/or scattering (Moussa et al., 2003).

The need to increase the suspension's solids loading for a high quality finished part creates another problem: it dramatically increases the suspension's viscosity, thus making it very difficult to process in an AM context. The Optoform process, a variant of the SL

process, works with suspensions with 67% volume loading (Doreau et al., 2000; Clarinval et al., 2007). As a result, the Optoform process does not require a build vat because the resin is viscous enough to support overhanging features, much like a powder bed. The viscosity of these loaded resins poses a large problem for layer recoating: support structures are needed due to the large stresses posed by the recoating scraper blade and the viscous resin (Clarinval et al., 2003). Dispersants and diluents are also often added to alleviate this problem (Hinczewski et al., 1998a). The rise in viscosity is much greater if submicron powder must be used, because dispersion of these fine powders becomes increasingly difficult (Griffith and Halloran, 1994a). This is especially troublesome when trying to build the complex geometry typical of cellular materials, as it would be impossible to remove the viscous unpatterned resin from extremely small microchannels or honeycombs.

A final flaw of this process is the use of a one-dimensional patterning principle. The selective scanning of a single point of energy limits the overall build speed of the process due to physical limits to galvanometer speed and control.

The process properties of the current embodiment of the stereolithography working structure are presented in Table 4.2.

Table 4.2 – Stereolithography Process Properties

Stat	Value	Reference
Production Cost ($)	186,000 – 784,000	(Wohlers, 2006)
Deposition rate (cm^3/hr)	375-750	(Clarinval et al., 2007)
Minimum feature size (mm)	0.2 – 0.7	(Himmer et al., 1997); (Doreau et al., 2000)
Z-resolution (mm)	0.025 – 0.150	(Doreau et al., 2000)
Surface Roughness (μm, Ra)	Better than powder bed processes due to resin carrier and small z-resolution	
Green part solids loading (vol %)	50 – 60	(Brady et al., 1996); (Doreau et al., 2000; Clarinval et al., 2007)
Working materials	Only UV transparent ceramics (e.g., silica, alumina)	
Support / Complex Geometry	Limited by support structures and viscous resin	

4.2 TWO-DIMENSIONAL ENERGY PATTERNING WORKING STRUCTURES

The fundamental limitation of the working structures presented in the previous sub-section is the manner in which energy is patterned in only one dimension. In order to alleviate this limitation, and thus increase the fabrication speed, recent research has focused in using various techniques in order to pattern energy in two-dimensions (Figure 4.3). There can be two separate embodiments of this principle; the difference lies in the choice of using a masking device (such as a digital micro-mirror display, DMD) to selectively pattern the energy across the working material.

4.2.1 Two-Dimensional Sintering (HSS)

As can be seen in Figure 4.3, two-dimensional sintering (also known as High Speed Sintering, or HSS) has an almost identical working structure to that of LS (Figure 4.1) – both systems induce liquid-phase sintering in a powder bed in order to create the solid part. The differences between the two sintering approaches lie in the manner in which both energy and material is patterned.

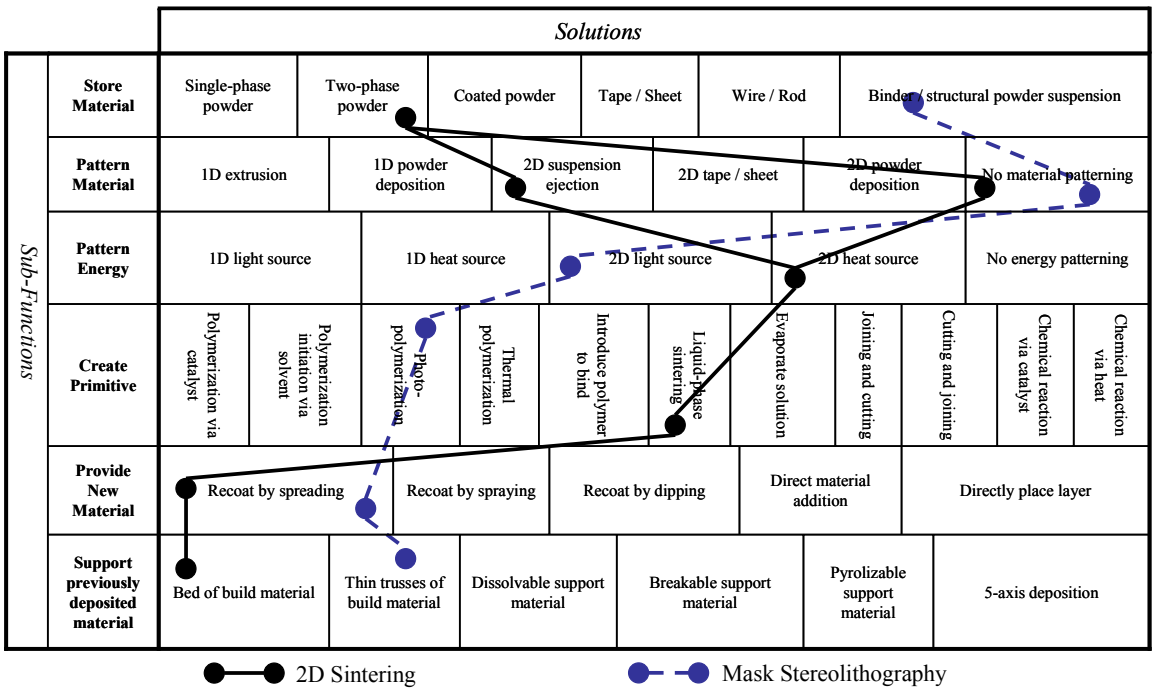

Figure 4.3 – 2D Energy Solution Patterning Working Structures

First introduced by Hopkinson and Erasenthiran, HSS involves the selective two-dimensional patterning of infrared energy (typically via an infrared source, such as a 2 kW short wave infrared lamp, and a DMD) onto a powder bed containing a mixture of nylon powder and carbon black powder (Hopkinson and Erasenthiran, 2004). Due to the fact that carbon black absorbs infrared energy at a higher rate than nylon, and heats up more quickly than nylon, the particles of carbon black heat up and transfer energy to surrounding particles of nylon by conduction and radiation. Thus LPS is initiated at those points in the powder bed that are exposed to the infrared energy. Similar to LS, the green part consists of ceramic powder held together by a polymer matrix. Via this embodiment, an entire layer can be processed in just 30 seconds (5 seconds for sintering, 5 seconds for powder deposition, 5 seconds for pre-heating, and 15 seconds for depositing a radiation absorbing material) (Hopkinson and Erasenthiran, 2004).

Another embodiment of this process (also shown in Figure 4.3) is the selective printing of a carbon black-based suspension onto a powder bed of nylon powder (Hopkinson and Erasenthiran, 2006). IR energy is then patterned non-discriminately to the entire powder bed (usually via a simple IR lamp), thus initiating LPS between those particles that are coated with the printed liquid.

To date, this process has only been used to process nylon powder. However, it is not difficult to imagine a variation of the process in which ceramic powder is used instead of nylon powder. In order to use LPS as the "create primitive" working principle, the ceramic powder would have to be combined (or blended) with a polymer powder, as pure ceramic powder will not begin sintering with such a small amount of energy input. As such, the solids loading of the ceramic green part will likely be relatively low for either embodiment; since dry powder beds naturally have a maximum solids loading of ~50 vol%, the coating of the ceramic powder, or inclusion of a second phase will significantly lower that percentage. Although not fully realized as of this writing, the inventors of the process do note that ceramic filler powder could be introduced into the existing embodiment as a means to increase part strength (Hopkinson and Erasenthiran, 2006).

Not only is this process ten times faster than traditional LS, its inventors have noted that the resulting parts have superior mechanical properties relative to its LS-processed counterparts. Furthermore, due to the lack of a laser, it is estimated that HSS is five times cheaper than LS (Hopkinson and Erasenthiran, 2004). It should be noted, however that there is 20% linear shrinkage during sintering of each layer, which could cause issues with process repeatability, accuracy, and control.

As the process is still in early stages of its development, there has not been quantitative data published about its minimum feature size or surface finish. Whether selectively depositing material via a print head, or selectively depositing energy via a DMD mask, both embodiments provide sufficient resolution for the realization of those features common to cellular materials. In fact, it is safe to assume that the powder particle size is the limiting constraint. The powder particle diameter (along with the wetting characteristics of the jetted carbon suspension) is also likely to be the limiting constraint on the parts' surface finish. Finally, like all working structures that employ the powder-bed working principle, certain cellular mesostructures may not be realizable due to the concern of trapped unpatterned material.

The process properties of the current embodiment of the two-dimensional sintering working structure are presented in Table 4.3.

Table 4.3 – Two-Dimensional Sintering Process Properties

Stat	Value	Reference
Production Cost ($)	140,000	(Hopkinson and Erasenthiran, 2004)
Deposition rate (cm^3/hr)	Extremely fast due to 2D energy deposition. Limited only by powder recoating process	
Minimum feature size (mm)	Limited by size of powder particles used and resolution of printer; ~ 0.1	
Z-resolution (mm)	0.1	(Hopkinson and Erasenthiran, 2004)
Surface Roughness (μm, Ra)	Surface finish similar to LS (and other powder bed technologies)	
Green part solids loading (vol %)	Similar to other powder bed technologies, ~50	
Working materials	All ceramics	
Support / Complex Geometry	Moderate; (powder bed)	

4.2.2 Mask Stereolithography (M-SL)

This working structure is identical to that of SL except, instead of patterning UV light via a one-dimensional laser spot, the UV energy is supplied selectively across the

entire cross-sectional layer at once. This principle is typically embodied by the use of a DMD mask – each cross-section is represented as a bitmap image that is projected onto the resin surface. The photopolymer resin cures wherever exposed to the UV radiation.

Aside from the obvious build time improvement from curing an entire layer at once, the use of the DMD enables the creation of parts with feature sizes as small as 1-2 μm (Zhang et al., 1999; Sun and Zhang, 2002). Entire layers can be cured in 5 to 10 seconds with this working principle; higher UV light intensity could decrease this time further. Bertsch and coauthors report a build speed of 2 mm per hour in the vertical direction (layer thickness of 10 μm) (Bertsch et al., 2004). Furthermore the absence of the need for a UV laser significantly lowers the production cost.

Researchers have been able to make ceramic microstructures with the use of M-SL devices by suspending ceramic nanoparticles in photocurable resin (up to 75 wt%). However, the large viscosity of the resulting paste requires that external supports are built around the structure so they are not damaged from the recoating process (a carefully designed and controlled doctor blade recoat) (Bertsch et al., 2004). The need for such supports severely limits the cellular mesostructures which can be realized.

The largest limitation of this working structure is the same as that of SL – the inability to fabricate ceramic green parts of any ceramic material due to the refraction of the UV radiation (caused by incompatibility between the indices of refraction of the resin and the ceramic powder, as described in Section 4.1.2). The light scattering and refraction also results in poorer feature definition at small scales (Zhang et al., 1999). Successfully made ceramic microcomponents by M-SL include silica, alumina, and lead zirconate titanate (PZT) (Zhang et al., 1999; Sun and Zhang, 2002).

Recent research in the community has shown the creation of green parts of TiO_2. This recent success has been attributed to the use of acrylate resins, which have refractive indices (1.45 at 366 nm) that are closer to that of ceramic powders. However, since acrylate resins directly polymerize, they leave a large volume of polymer to be removed during the binder burnout stage. Polymer contents in the 40-50 volume percent range make polymer burnout much more difficult (Griffith and Halloran, 1994a).

The process properties of the current embodiment of the mask stereolithography working structure are presented in Table 4.4.

Table 4.4 – Mask Stereolithography Process Properties

Stat	Value	Reference
Production Cost ($)	Lower than SL process due to lack of laser	
Deposition rate (cm^3/hr)	Faster than SL process due to 2D deposition of energy	
Minimum feature size (mm)	0.001	(Zhang et al., 1999)
Z-resolution (mm)	0.01	(Bertsch et al., 2004)
Surface Roughness (μm, Ra)	Better than SL due to small z-resolution	
Green part solids loading (vol %)	~ 40	(Bertsch et al., 2004)
Working materials	Limited to those that are transparent to UV	
Support / Complex Geometry	Limited (support structure and viscous resin)	

4.3 MATERIAL PATTERNING WORKING STRUCTURES

While those structures in the previous sub-sections featured the patterning of energy as the primary means of primitive creation, those featured in this section employ the selective patterning of material as a means of realizing cross-sectional layers (Figure 4.4).

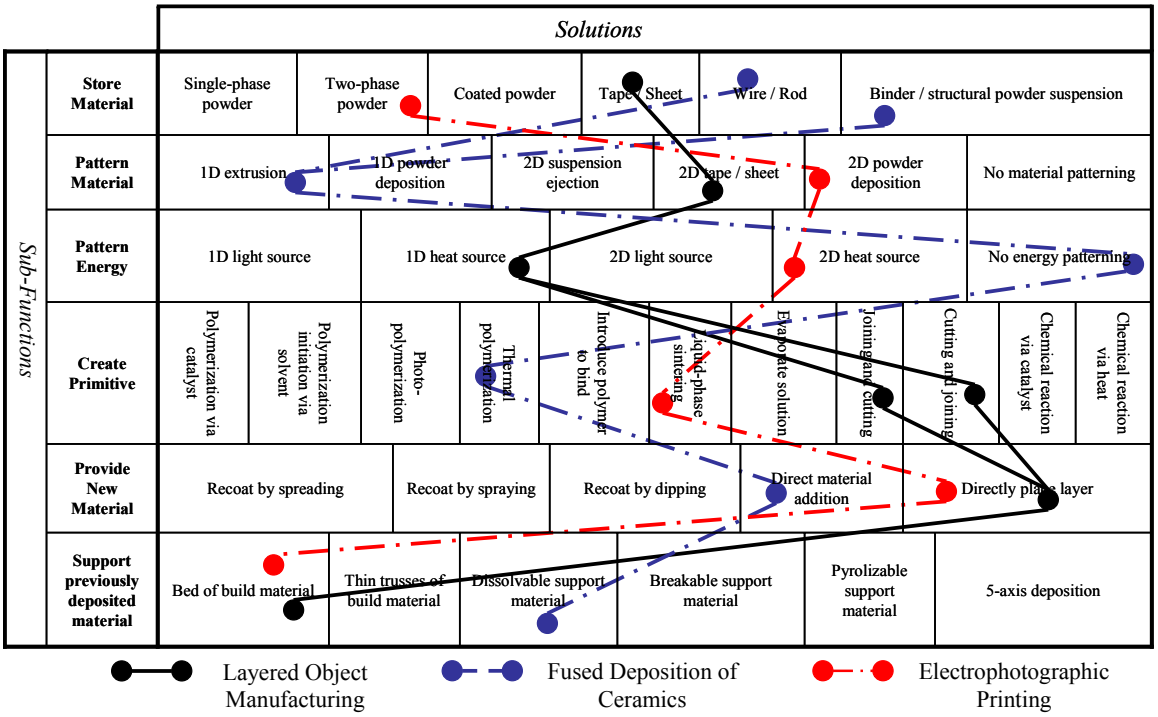

Figure 4.4 – Material Patterning Working Structures

4.3.1 Fused Deposition of Ceramics (FDC)

In ceramic Fused Deposition Modeling (FDM), a thermoplastic polymer is extruded through a small diameter nozzle using the solid polymer strand as the extrusion ram. This technique is used for processing polymer and wax parts. The same approach, applied to ceramic suspensions in a polymer or wax carrier, is known as Fused Deposition of Ceramics (FDC). This process features filaments comprised of ceramic particles in thermoplastic binders that are extruded through a heated nozzle (McNulty et al., 1998). The suspensions' rheology must be carefully optimized in order to balance issues related to drying, spreading, and of course, viscosity (King et al., 1998). The filament is extruded at a temperature just above its melting point; it then solidifies due to the decrease in pressure and temperature as it exits the nozzle. The extruded suspension partially remelts previously deposited layers and promotes strong bonding between the

layers. After the green part is formed, the binder is burned out, and the part is sintered to its final density (typically 98% with 18% linear shrinkage, (Vaidyanathan et al., 1999)). Since green FDC parts are similar to injection molded green ceramic parts (both require post-processing such as binder removal and densification) many ceramics have been successfully deposited with FDC including silicon nitride, silica, alumina, and lead-zirconium titanate (McNulty et al., 1998).

The process typically features two separate extrusion heads: one for the extrusion of structural material, the other for the extrusion of a sacrificial support material. This enables the creation of complex geometry and overhangs. This process's "direct material addition" and "dissolvable support structure" (Stratasys, 2007) working principles enable it to successfully create any complex cellular mesostructure. Furthermore, there is very little material waste during or after part production (Tay et al., 2003).

Unfortunately, there are two features of this process which fundamentally limit the density of the green parts that can be realized from its use. The first is related to a physical limit on the suspension viscosity it can process (which is a common theme of all AM processes which work with powder/binder suspensions). Because extrusion processes do not have to create small droplets as in direct inkjet printing, their green parts often feature a higher solids loading percentage. The solids loading is limited however by the need to extrude through a small nozzle – typically 250-500 μm in diameter. Most FDC suspensions are limited to a solids loading of 50-65 vol%.

The other limiting feature of extrusion which results in poor green part density is related to process control. Porosity plagues most parts made with FDC due to poor optimization of material flow, filament/roller slippage, liquefier head motion (start-stop

motion), and build/fill strategies. Poor material flow control and slippage can cause over/underfilling of the layer and poor bonding between adjacent road depositions or adjacent layers (Jafari et al., 2000). Furthermore, because it is hard to suddenly stop and start the extrusion head motion and filament feed, sub-perimeter voids are created when trying to fill-in curved boundaries via rastering. As seen in Figure 4.5, these voids appear due to the tool path preventing road depositions from completely meshing with the cross-section's boundary contours.

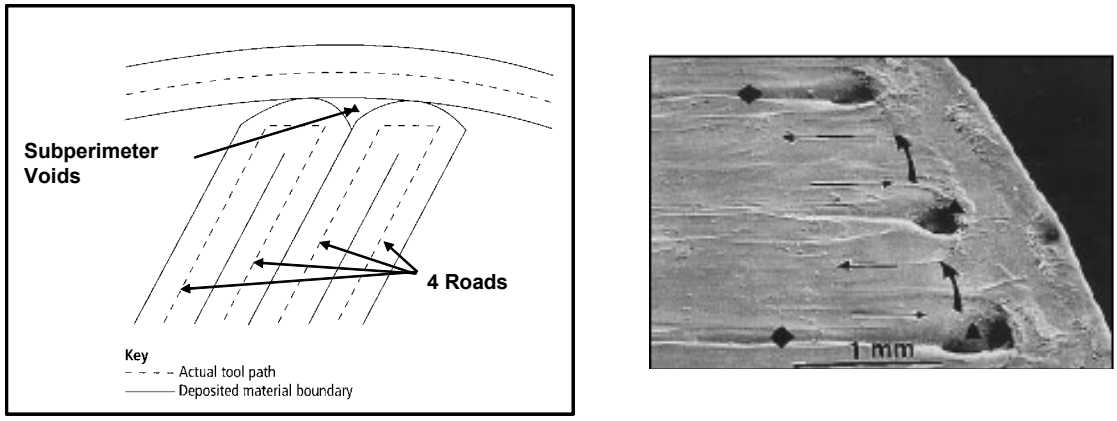

(a) (b)

Figure 4.5 – Subperimeter Voids in Fused Deposition of Ceramics; (a) illustration, (b) SEM image (Agarwala et al., 1996)

These processing difficulties are aggravated by further deficiencies:

- Problems associated with extrusion flow control (sudden starting and stopping) are heightened with the need to extrude the viscous ceramic-filled suspension.
- Deposits made by the FDC process (known as "roads") are larger than other AM processes. Due to material flow, the width of the deposit is usually 1.2 to 1.5 times the diameter of the nozzle (therefore, around 0.75 mm) (Agarwala et al., 1996).

- Sharp edges of cross-sections tend to be filleted because the material yields behind the extrusion nozzle.
- Due to the requirements of the hardware control, curves in the x-y plane are linearized, thus giving curves a chorded effect.
- There are often density gradients in the filament due to suspension settling or filament slippage. Thus, resultant depositions can be non-homogeneous throughout the part (Jafari et al., 2000).

Not only do the above listed limitations constrain the realizable green part density, they severely hinder the process's ability to realize cellular materials. As shown, in Figure 4.6 (and shown in Figure 2.9), the to-be-designed process must be able to create layers which can contain several discrete points with diameters as small as 1.5 mm in order to realize trussed mesostructure. This type of small, discrete deposition is extremely difficult to achieve with extrusion-based processes because they are not suited for the start-stop motions needed for point-like depositions.

(a) (b)

Figure 4.6 – Cross-section of Trussed Cube; (a) as built, (b) x-y orientation

In addition to the density problems listed above, FDC parts also suffer from poor surface finish. Large layer thicknesses (~0.5 mm) provide a stair-stepping effect for curvature in the z-direction. Although most surface defects can be eliminated by post-processing, internal defects result in strength limitation which cannot be eliminated after

part fabrication (Agarwala et al., 1996). Furthermore, the part's bottom surface is rough once it is removed from the foam substrate. Finally, the removal of support structure leaves burrs on the finished part.

Of course, like other one-dimensional patterning techniques, extrusion-based fabrication is limited by the nozzle's scan speed. The process is further limited, however, by the slow extrusion rate of the specific filament which is much slower than laser scanning speeds.

Other embodiments of this extrusion-based approach to freeforming ceramics include Multi-phase Jet Solidification (MJS) (Greulich et al., 1995) (Lenk, 2000), Extrusion Freeforming (EFF) (Vaidyanathan et al., 2000), and Contour Crafting (CC) (Khoshnevis et al., 2001). These technologies are capable of extruding more viscous solutions (since they extrude a powder-binder mixture or liquefied substance instead of feedstock). In an effort to improve the minimum feature size capable of extrusion, Grida and Evans have modified existing EFF technology to extrude thin fibers (> 100 μm) of ceramic suspensions through hypodermic needles. The authors were unable, however, to extrude thinner fibers since they would solidify before contacting the previously deposited layers (Grida and Evans, 2003). The selective extrusion of ceramic gelcasting suspensions is also a promising research direction (Morissette et al., 2000). Support structures for overhangs are not needed if the slurry sets immediately upon extrusion (Li and Lewis, 2003).

Finally, it is noted that FDC and its variants have been successfully used to make cellular mesostructures. However, work towards producing cellular materials with extrusion processes have been limited to indirect fabrication via lost mold techniques

(Bandyopadhyay et al., 1999) or to direct fabrication of periodic lattice structures created by a serpentine extrusion pattern, as seen in Figure 4.7 (referred as "log-piles" in (Grida and Evans, 2003), as shown in (Lewis, 2000), (Chi et al., 2006) and (Smay et al., 2002b)).

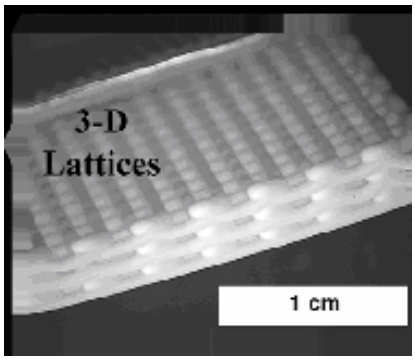

Figure 4.7 – Lattice Structure "Log Piles" Made via FDC (Smay et al., 2002a)

The process properties of the current embodiment of the fused deposition of ceramics working structure are presented in Table 4.5.

Table 4.5 – Fused Deposition of Ceramics Process Properties

Stat	Value	Reference
Production Cost ($)	18,900 – 250,000	(Wohlers, 2006)
Deposition rate (cm^3/hr)	Slow due to 1D material deposition; nozzle is cleaned every 5 layers	
Minimum feature size (mm)	0.2	(Agarwala et al., 1996)
Z-resolution (mm)	0.5	
Surface Roughness (μm, Ra)	Very poor	
Green part solids loading (vol %)	< 50	
Working materials:	All ceramics (related to ceramic injection molding)	
Support / Complex Geometry	Moderate; (dissolvable support structure, but unable to deposit all cross-sections representative of cellular materials)	

4.3.2 Layered Object Manufacturing (LOM)

Layered Object Manufacturing (LOM) features the patterning of an entire layer of material at one time. The working material for ceramic LOM is commercially available

green ceramic tape layers. These ceramic tapes typically contain fine ceramic particles (0.5 μm in diameter) in a proprietary binder system (solids loading around 56 vol%) (Bender et al., 2001). These tape layers are unrolled onto the working bed where a CO_2 laser quickly cuts the outline of each layer of the part. A heated roller is passed over the layer, thus activating the tape's binder system and laminating the sheet to the previous layer (Griffin and Dautenbach, 1995; Klosterman et al., 1999). The outside of the layer is cut into small blocks the laser to become the support structure. The process repeats generating a solid object enclosed within and supported by blocks of the excess material. The finished part is then removed from the working bed by physically removing the surrounding cubes of support material (Halloran, 1999). The green part is then post-processed via a debinding step and a sintering stage. Klosterman and coauthors note that pressure must be applied during binder burnout and pyrolysis to counteract delamination and bloating that result from outgassing and the relaxation of residual stresses imparted during the lamination step (Klosterman et al., 1998).

Another embodiment of this process is the Computer-Aided Manufacturing of Laminated Engineering Materials (CAM-LEM) method (Liu et al., 1997). This process is identical to that of LOM, but instead of stacking the layers and then cutting them, each layer is pre-cut and then robotically stacked onto the working part for lamination. This method has several advantages over traditional LOM. First, the sheets can be cut at an angle by 5-axis laser cutting, thus allowing a better approximation to vertically curved surfaces via tangent cutting and trajectory smoothing (Halloran, 1999). Furthermore, internal voids within each layer can be easily produced, thus allowing for the creation of hollow parts.

Because of their use of ceramic tapes, which have a well-established manufacturing history, LOM and CAM-LEM can process almost any ceramic material. These methods have successfully been used to create parts made of alumina, silicon nitride, lead-zirconate titanate, and zircinia toughed alumina (Liu et al., 1999). Halloran reports that the quality of LOM ceramics is comparable with conventional ceramic materials (Halloran, 1999). However, it has also been reported that LOM parts suffer from density gradients, delamination, and anisotropic material properties (Bender et al., 2001; Das et al., 2003). Klosterman reports that all evidence of a layered structure is absent in the part after sintering and infiltration (Klosterman et al., 1999).

In the context of manufacturing cellular materials, the fundamental limitation of this process is the manner in which complex geometry is supported. While the excess material cut from the part provides support during the process, it is impossible to retrieve this material from internal voids. Even CAM-LEM's "cut-and-stack" approach proves to be troublesome for the complex cross-sections of cellular materials; it would be extremely difficult to robotically place the small features that are typical of cellular material cross-sections.

The process properties of the current embodiment of the layered object manufacturing working structure are presented in Table 4.6.

Table 4.6 – Layered Object Manufacturing Process Properties

Stat	Value	Reference
Production Cost ($)	69,500 – 179,500	(Wohlers, 2006)
Deposition rate (cm^3/hr)	Fast	
Minimum feature size (mm)	Small	
Z-resolution (mm)	0.2	(Bender et al., 2001)
Surface Roughness (μm, Ra)	Poor due to large z-resolution	
Green part solids loading (vol %)	55	(Liu et al., 1997)
Working materials:	All ceramics	
Support / Complex Geometry	Limited (material trapped in voids)	

4.3.3 Electrophotographic Printing (EP)

Electrophotographic Printing (EP) is another AM process which is capable of patterning an entire layer of material at once. The patterning working principle employed by EP is very similar to that seen in photo-copying. A photoreceptor plate or drum is charged to a specific charge density via a corona device. An electrostatic image of the part layer is created o the photoreceptor by light exposure, using a computer controlled LED printer head. The photoreceptor is aligned over the powder bed where the electrostatic charge causes the powder to be attracted to the plate in the exact shape of the part layer. The layer of powder is then deposited on the building table. Overhanging structures are created by the selective deposition of a secondary support powder. The printed layers are then compacted and sintered via an appropriate method (e.g., electric contact sintering, plasma-activated sintering, or microwave sintering) (Karlsen and Reitan, 2003).

In order to produce a green part instead of a sintered part, it would be best to work with either a powder mixture (or coating) of ceramic and polymer. The polymer could undergo LPS and thus serve as a binder material for the ceramic powder.

Conceptually, this principle offers many advantages including direct material addition and two-dimensional material patterning (entire layers have been fabricated in less than five seconds). However, potential problems with adapting this process to the realization of ceramic powders include the porosity of printed parts and the quality of adherence of the support powder to the build powder. Furthermore, it has been reported that the available surface finish does not meet that of molded or machined parts, and that the dimensional accuracy and repeatability are not acceptable. Concerns about the

technique's ability to process non-conductive materials are valid; however, Karlsen and Reitan have reported preliminary success with alumina and silicon nitride.

The process properties of the current embodiment of the electrophotographic working structure are presented in Table 4.7.

Table 4.7 – Electrophotographic Printing Process Properties

Stat	Value	Reference
Production Cost ($)	Relatively cheap due to having copy machine technology base	
Deposition rate (cm^3/hr)	Very fast; 2D energy and material deposition. Recoating directly applies new layer	
Minimum feature size (mm)	Limited by powder size due high resolution corona charging	
Z-resolution (mm)	0.1	(Karlsen and Reitan, 2003)
Surface Roughness (μm, Ra)	Similar to other powder based technologies	
Green part solids loading (vol %)	Slightly lower than powder bed technologies.	
Working materials	Limited to materials which can be electrostatically charged	
Support / Complex Geometry	Moderate (powder bed)	

4.4 INDIRECT MATERIAL PRINTING WORKING STRUCTURES

Indirect material printing involves the selective deposition of a liquid binder into a bed of powder via jetting (Figure 4.8). The binder is deposited through traditional inkjet print heads; thus the process is commonly referred to as Three-Dimensional Printing (3DP). The binder does not impart a phase change to the powder in the bed; instead, it simply acts as a method of joining individual powder particles together to create a solid deposition. Once a layer is printed, the powder bed is lowered and a new layer of powder is spread onto it (typically via a counter-rotating rolling mechanism) (Sachs et al., 1993b). This process (printing binder into bed; recoating bed with new layer of powder) is repeated until the green part is completed. The green part is typically left in the powder bed after its completion in order for the binder to fully set and for the green part

to gain strength. Post-processing involves removing the part from the powder bed, removing unbound powder via pressurized air, and sintering the green part in order to burn off the binder and densify the part. There are three existing variants of 3DP: powder-based 3DP (Section 4.4.1), slurry-based 3DP (S-3DP, Section 4.4.2), and 3DP using a photopolymer as a binder (UV-3DP, Section 4.4.3), as shown in Figure 4.8.

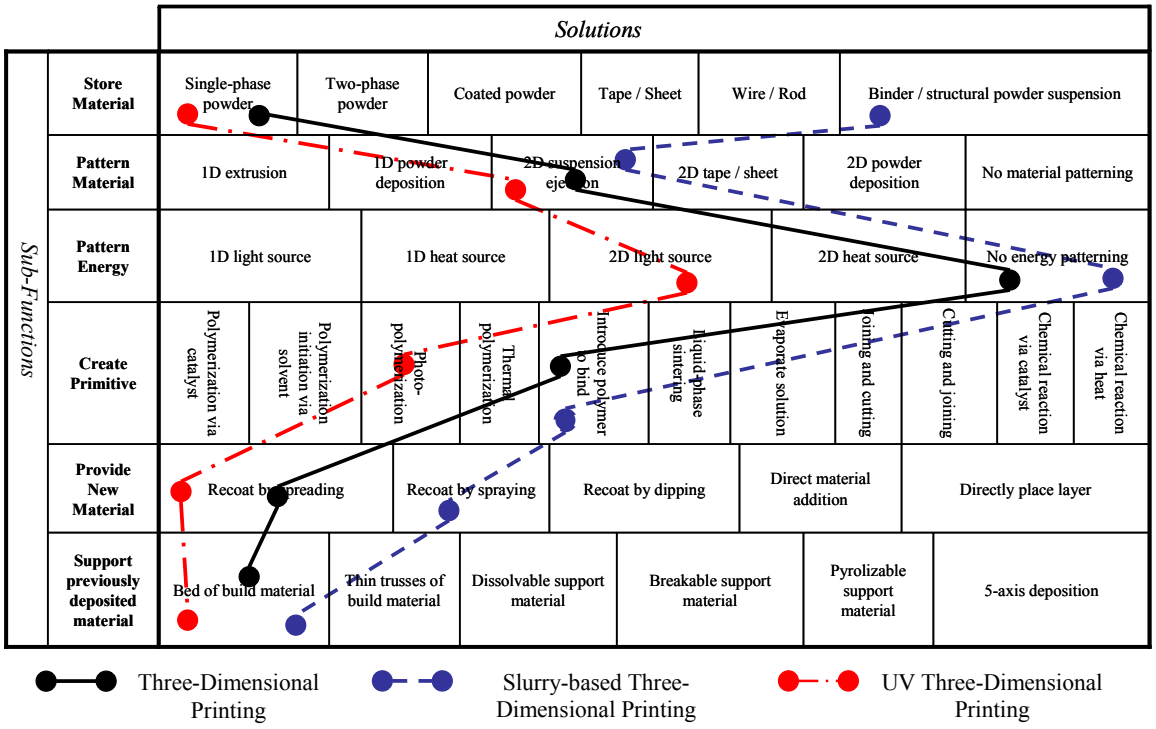

Figure 4.8 – Indirect Printing Working Structures

4.4.1 Three-Dimensional Printing (3DP)

Traditional powder-based 3DP of ceramics involves the selective printing of a binder over a bed of ceramic powder (Yoo et al., 1993). The spherical powder particles are bonded together as spherical binder droplets enter the porous media and form necks between the particles. The powder particles can be pulled together more tightly as the liquid dries due to each droplet's desire to minimize its surface energy through the reduction of its surface to volume ratio and the minimization of the area of its

liquid/vapor interface. Cima and coauthors attribute the resultant powder bed densification to the particles sliding over one another due to the capillary forces imparted by the liquid's surface tension (Cima et al., 1992).

Green parts created by this process are subjected to a thermal decomposition prior to sintering to remove the polymer binder. The first report of using 3DP for the fabrication of ceramics was in 1993; fired components were reported as typically greater than 99.2% dense (Yoo et al., 1993).

Just as in LS (Section 4.1.1), 3DP's use of a powder bed is the source for both advantages and disadvantages in the context of manufacturing cellular materials. Just as in other powder bed AM technologies, complex geometries are able to be realized without the need for secondary support structures since unpatterned powder in the bed provides sufficient support for overhanging structures. However, the presence of unpatterned powder does preclude the fabrication of hollow (closed skin) structures, and can limit the size of cells and/or channels (as the powder must be removed prior to post-processing).

Because 3DP does not have a suspension-based working principle for its "store material" sub-function, it is relatively easy to process multiple types of materials. A primary benefit of the 3DP working structure is that any ceramic powder can be processed; alumina, silica, and titanium dioxide have been made with this process (Uhland et al., 2001). Yoo and coauthors comment that "the effort involved in processing new materials systems using 3DP is minimal as compared to other (AM) processes. Powder/binder combinations that are used for conventional powder processing can often be used in 3DP since inkjets can be adapted to print a variety of

binders" (Yoo et al., 1993). Furthermore, unbound powder can be recycled for subsequent builds.

Commenting on the freedom potentially posed by the 3DP process, Cima and coauthors note that large amounts of matter can be deposited in selective regions of a component on a 100 μm scale with the process. Furthermore, multiple jets containing different material composition or concentration could be employed to prepare components with composition and density variation on a fine scale (Cima et al., 1992). In addition, compared to tradition ceramic forming processes, much less organic binder is required in the 3DP process "since the binder is used only to hold the green part together rather than plasticize the powder mass;" thus avoiding the troubles of non-uniform powder packing and uncontrolled shrinkage and distortion during sintering (Yoo et al., 1993).

Of course, just as in LS, the use of a powder bed can cause poor part surface finish and the inability to grade material across the part cross-section. The largest disadvantage in working with a powder bed is the poor green part density that results from the porous nature of the powder bed. Yoo and coauthors attempted to increase the density of the working powder bed by using submicron ceramic powders (specifically, alumina), which had a lower apparent and tap density than other common 3DP powders. Unfortunately, the fine powders needed for good powder bed density did not generally flow well enough to spread into defect-free layers (Yoo et al., 1993). Furthermore, Sachs and coauthors found that spreading fine powders conventionally resulted in layers that were inhomogeneous and had low particle packing density. As such, the recoating process was modified to include an additional pass with the roller that pressed on the dry powder. As

a result, they were able to achieve 40% packing density in the powder bed. In addition, the high velocity of each droplet onto the powder bed surface can cause ballistic ejection of the particles in a fine powder bed (thus cutting a trench into the powder surface), resulting in poor part surfaces and high porosity. This can be combated by increasing the cohesive strength of the powder bed by adding moisture to it prior to printing (Yoo et al., 1993). Generally, dry 3DP is limited to working with particles 20 μm or greater (Sachs et al., 1993b).

Since green part density is normally inadequate with the use of dry powders, isostatic pressing is implemented after the printing process. After printing, green parts typically have a density of 35%; isostatic pressing improves density by 15% before firing (Yoo et al., 1993). Unfortunately, the isostatic pressing needed to improve green part density when using a dry power bed in the 3DP process limits the topologies that can be made.

The minimum feature size that can be created by the 3DP process is dependent on both the powder and the binder being used. While the primitive size is primarily dependent on the size of the binder droplets used, it is also dependent on the drop spreading, its infiltration into the powder bed, and the powder shrinkage upon the binder drying (Sachs et al., 1993b; Holman et al., 2002a). Roughly, the volume of the primitive formed is twice that of the printed droplet; this follows from the fact that the droplet occupies the void space between the powder particles which is typically 50 percent of the total volume (Sachs et al., 1992).

The main advantage of 3DP, in the context of manufacturing cellular materials, lies in its economic considerations. Simply put, the 3DP process does not require high

energy, does not involve lasers or any toxic materials and is relatively cheap and fast (Carrion, 1997). Part creation rate is limited to approximately twice the binder flow rate. A typical inkjet nozzle delivers approximately 1 cm^3/min of binder; thus a machine with a 100 nozzle printhead could create up to approximately 200 cm^3/min of printed component. Sachs suggests that, because commercial inkjet printers exist with up to 1600 nozzles, there is reason to hope that 3DP could be used as a production process (Sachs et al., 1993a).

The process properties of the current embodiment of the three-dimensional printing working structure are presented in Table 4.8.

Table 4.8 – Three-Dimensional Printing Process Properties

Stat	Value	Reference
Production Cost ($)	19,900 -180,000	(Wohlers, 2006)
Deposition rate (cm^3/hr)	Relatively fast. Scalable array of print heads; slightly slowed by recoating	
Minimum feature size (mm)	0.4	(Sachs et al., 1992)
Z-resolution (mm)	0.1	(Grau et al., 1997)
Surface Roughness (μm, Ra)	Similar to other powder bed technologies	
Green part solids loading (vol %)	50	
Working materials	All ceramics	
Support / Produce complex geometry	Somewhat limited (powder bed)	

4.4.2 Slurry-based Three-Dimensional Printing (S-3DP)

In order to be able to process fine powders (< 20 μm) in the powder bed, and thus improve sintering characteristics of the green part, research of ceramic 3DP shifted away from working with dry powders to working with a slurry-based working material (S-3DP, Figure 4.8). In this approach, layers of raw material are first deposited by inkjet printing a layer of slurry over the build area. The slurry is then dried via infrared heating, hot-air

heating, or microwave heating techniques (Sachs et al., 1993b). Once the slurry is dried, binder is selectively printed in order to define each cross-sectional layer of the part.

The use of an aqueous suspension as a working material medium provides many qualitative advantages over dry powder 3DP. Grau and coauthors note that the densities and microstructures (pores of 0.1 μm, (Holman et al., 2002b)) of Al_2O_3 powder beds prepared by the S-3DP process compare favorably with those prepared by slip casting (Grau et al., 1997). The microstructural inhomogeneities known to characterize compacted dry powders are absent with the use of the suspension (Tay et al., 2003). The surface finish of the green part is much better than those created via traditional 3DP due to the smooth texture of the suspension and due to working with layer thicknesses as small as 10 μm (Grau et al., 1997). Alumina, and silicon nitride have been processed with this technique with green part density as high as 67 vol%.

In fact, this manufacturing process has been used to make green parts suitable for the reduction post-process. Kernan and coauthors have used the slurry-based 3DP process to fabricate parts of cobalt oxide precursor material, which is then processed in a reducing atmosphere to create a part of tungsten carbide-cobalt. They report good dimensional control (within one binder droplet diameter) and a final part density comparable to the equivalent conventionally processed material; however, binder print-through on the bottom surfaces resulted in a poor surface finish (Kernan et al., 2003).

The main limitation of slurry-based 3DP stems from the manner in which it fabricates parts in a bed that results composed of dried ceramic slurry. Just as in dry powder 3DP, the unpatterned material provides ample support for the part during construction, but it also makes part retrieval very difficult. Of course, with S-3DP, part

retrieval is very difficult given the large packing density and the cohesion of the dried slurry. In order to separate the part from the unpatterned material, the powder bed must be submerged in water. Moon and coauthors note that an "audible explosion" occurs when the powder bed is submerged in pure water due to pressure build up from the air that is trapped inside its pores (Moon et al., 2000). The requirement of high bed packing density opposes the requirement of efficient separation of the part from the unpatterned material. In the context of creating cellular materials, this is a very large limitation as it may prove to be impossible to successfully remove the unprinted slurry from microchannels and other internal features. Furthermore, switching between working materials can be very difficult as each material must be carefully dispersed in the colloidal suspension.

Just as in dry powder-based 3DP, the economics of this process are its strength as it employs a two-dimensional patterning working principle that does not require a large amount of energy or a laser source. Although it patterns material in two-dimensions, it is not as fast traditional 3DP for two reasons: (i) each layer must be patterened twice (once for the deposition of the slurry, and once for the deposition of the binder), and (ii) the deposited slurry must completely dry before the binder is deposited. It is important that the slip doesn't dry too quickly, or the deposited lines won't stitch together; instead, the lines must slip cast slow enough so that the inter-arrival time of slurry lines ensures that the lines merge together nicely (Kernan et al., 2003). The drying times will depend on the specifics of the powder, binder, and solvent used, but drying times on the order of 0.1 – 10 seconds per layer can be expected (around 10 times slower than traditional 3DP)

(Sachs et al., 1992). Uhland and coauthors report a drying time of 30 seconds per layer using an IR heat lamp (Uhland et al., 2001).

The process properties of the current embodiment of the slurry-based three-dimensional printing working structure are presented in Table 4.9.

Table 4.9 – Slurry-Based Three-Dimensional Printing Process Properties

Stat	Value	Reference
Production Cost ($)	Slightly more expensive than 3DP as additional print heads are needed for slurry deposition	
Deposition rate (cm^3/hr)	Very slow due to drying of slip cast after each deposited layer	
Minimum feature size (mm)	0.15	(Grau et al., 1997)
Z-resolution (mm)	0.01	
Surface Roughness (μm, Ra)	Slightly better than powder bed processes	
Green part solids loading (vol %)	67	(Grau et al., 1997)
Working materials	Any ceramic (that can be successfully suspended)	
Support / Produce complex geometry	Very limited (viscous compacted powder bed)	

4.4.3 UV Three-Dimensional Printing (UV-3DP)

This working structure is the combination of the fundamental principles of SL (Section 4.1.2) and 3DP (Section 4.4.1). The process involves the selective deposition of a photopolymer into a bed of ceramic powder. The bed is then flashed by a UV light source to cure the photopolymer.

Wang and coauthors have begun development on a system with a working principle similar to that described here. In their work, they jet a photoinitiator-filled epoxy onto a bed of proprietary thermoplastic polymer powder. When combined, the two materials undergo a chemical reaction and create a solid lamina which is suitable for exposure to UV radiation. The powder is employed in their work because the dissolution of the powder into the resin makes it easier to process than the resin alone. Furthermore, the

presence of the powder increase the viscosity of the jetted fluid, which controls the droplet spreading and hence increases the printing resolution (Wang et al., 2007).

The combination of these principles brings together the two principal advantages of SL and 3DP, which coincidentally complement two disadvantages of each respective technique. Specifically, the excellent green part strength found in SL is combined with the two-dimensional patterning of 3DP. Unfortunately, this combination also brings forth each process's limitations; namely, the inability to process multiple ceramics due to UV scattering, and the difficulty in removing unpatterned material from the green part due to the powder bed working principle.

The process properties of the current embodiment of the UV three-dimensional printing working structure are presented in Table 4.10.

Table 4.10 – UV Three-Dimensional Printing Process Properties

Stat	Value	Reference
Production Cost ($)	Slightly more than 3DP due to UV light requirement	
Deposition rate (cm^3/hr)	Slightly longer than 3DP due to need for curing	
Minimum feature size (mm)	Similar to 3DP	
Z-resolution (mm)	0.1	(Wang et al., 2007)
Surface Roughness (μm, Ra)	Similar to 3DP	
Green part solids loading (vol %)	Similar to 3DP	
Working materials:	Only UV transparent ceramics.	
Support / Complex Geometry	Moderate (powder bed)	

4.5 DIRECT MATERIAL PRINTING WORKING STRUCTURES

Unlike indirect inkjet printing, the ceramic powders in direct inkjet printing are deposited directly from the print nozzle. This is accomplished via the selective deposition of individual droplets of a liquid suspension onto a substrate; the droplets undergo a phase change (evaporation, solidifcation, photopolymerization, or chemical reaction) upon contact and thus create a solid part (Figure 4.9). Two principal solutions

have been presented in the literature as a means for realizing the task for creating ceramic green parts via direct jetting: aqueous direct jetting (IJP-A, Section 4.5.1), and hot-melt direct jetting (IJP-W, Section 4.5.2). A third working structure is also presented in this grouping: direct jetting of a photopolymer (IJP-UV, Section 4.5.3)

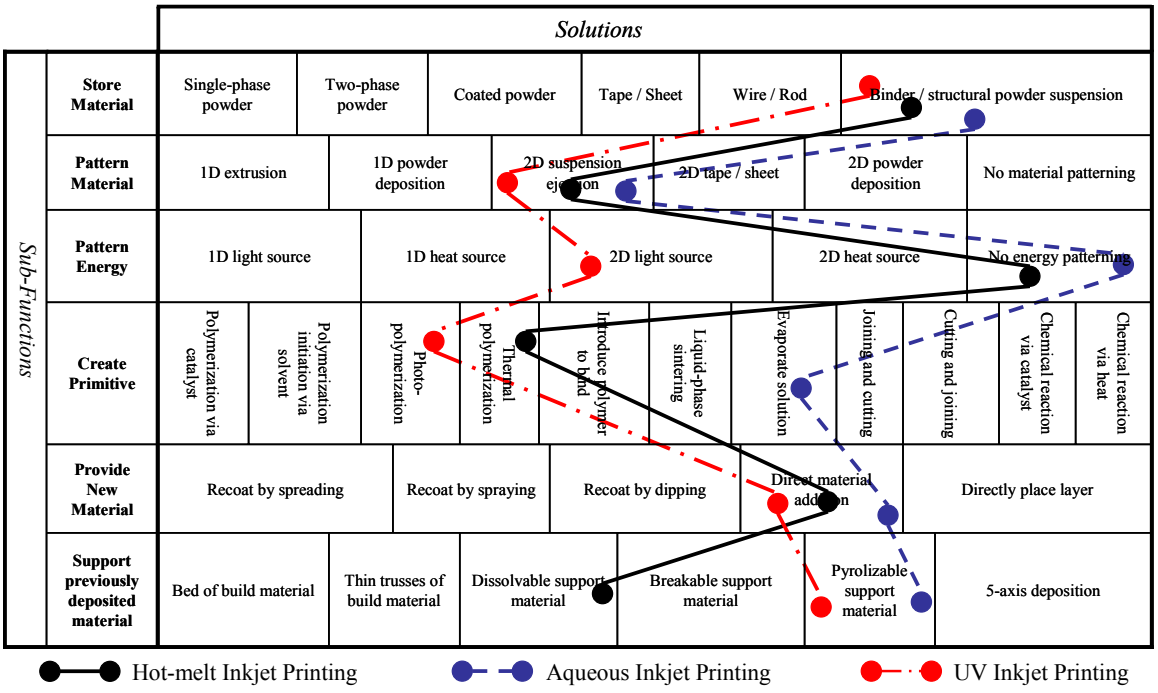

Figure 4.9 – Direct Printing Working Structures

4.5.1 Aqueous Inkjet Printing (IJP-A)

In aqueous direct inkjet printing, ceramic powder is thoroughly dispersed in an ink vehicle that contains dispersant to confer stabilization and a resin to confer mechanical strength on the printed part (Evans, 2001). The phase change principal solution featured in this technology is the evaporation of the aqueous portion of the dilute suspension; this is accomplished by a drying step that takes place immediately after the ink has been deposited onto the substrate. This drying step, embodied via the use of a hot-air blower, assists with the evaporation of the solvent and can take up to 20 seconds (Zhao et al.,

2002b). After evaporation, the solid particles remain; the layer-by-layer accumulation of these particles results in a three-dimensional ceramic green part. The green part is then dried and sintered to full density in order to form the final part.

In this work, aqueous inkjet printing is classified as a process with two-dimensional patterning of material; current embodiments of this technology feature an array of 500 deposition nozzles that print 70 mm across, thus eliminating the need for an x-stage (Zhao et al., 2002a). Furthermore, the process's individually controlled nozzles present opportunities for changing the part composition from point-to-point, thus producing graded materials throughout the part efficiently (Song et al., 1999). The presence of multiple nozzles also permits the deposition of support material (in addition to the standard build material) in order to construct overhanging features – a crucial component of additively manufacturing cellular materials (Mott et al., 1999).

There exist two different working principles for particle-laden droplet delivery in direct aqueous inkjet printing research: continuous and drop-on-demand (DOD) deposition. Continuous inkjet technology is characterized by electrically charging a continuous stream of ink droplets that have been ejected from a pressurized fine nozzle (Sirringhaus and Shimoda, 2003). The droplets acquire their charge from a high-voltage electric field; depending on the charge they have acquired, they are either deflected toward the substrate, or into an ink collection and recirculation system (Song et al., 1999). In piezoelectric DOD printing, a pressure wave in the ink chamber is generated by applying a voltage pulse to a piezoelectric stack or plate, resulting in the formation of droplets at the nozzles (Sirringhaus and Shimoda, 2003). In contrast to continuous

printing, droplets are formed only when individual pressure pulses in the nozzle cause the fluid to be expelled.

Initial direct ceramic inkjet printing made use of continuous printers. The droplet formation rate of continuous printers is typically much higher (64 kHz) than DOD printers, hence a higher ceramic deposition rate is possible (Song et al., 1999). Continuous printers also offer a lower resolution (Calvert, 2001). These advantages are offset, however, by the fact that the inks used in continuous printing must be capable of conducting an electrical charge. Furthermore, it has been found that the positioning of the droplets in continuous printing is very sensitive to inhomogeneities in the ink (such as agglomerates). For these reasons, recent work has shifted to DOD printers (Evans, 2001).

As can be expected, the formulation of the ink to be printed is the most crucial component of this technology. Song and coauthors offer four guidelines for the creation of ink suitable for aqueous direct jetting of ceramics (Song et al., 1999):

(i) *Rheological properties:* Regardless of the droplet delivery subsystem chosen, progress in direct aqueous inkjet printing of ceramics has been stymied by the strict viscosity requirements that the ceramic ink must satisfy in order to pass through printer nozzles that are 30-120 μm in diameter (Teng et al., 1997). Many researchers have prescribed several different successful viscosity ranges; it is generally agreed that the suspension to be printed should be less than 10-100 mPas (Song et al., 1999; Evans et al., 2001; Zhao et al., 2001; de Gans et al., 2004). Obviously, the particles suspended in the ink must be sufficiently dispersed in order to reduce viscosity and to prevent blockage of

the nozzles. Dispersant must be carefully introduced into the ink formulation; if the surface tension of the ink is less than 25 mNm^{-1} (Song et al., 1999; de Gans et al., 2004), the ink may seep out of the nozzle and prevent the consistent formation of droplets. Finally, if the ink is to be printed through a continuous droplet delivery system, the ink must be conductive.

(ii) *Powder dispersion and stability*: The particles suspended in the ink must be well dispersed and stabilized in order to prevent nozzle clogging and sedimentation within the feed lines. Nozzle clogging prevents the dispersion of ceramic; if this occurs in a multi-arrayed print head, defects can easily be introduced to the green part through the resulting material vacancy. Sedimentation can lower the solids loading of the printed suspension, which can result in an inhomogeneous green part (Zhao et al., 2002a). Many researchers look upon these hurdles with a positive light, claiming that the agglomerates that clog the nozzles and halt printing make the process "fail-safe" and offer "remarkable quality assurance opportunities" (Mott et al., 1999). Zhao and coauthors state that the lack of printed agglomerates also eliminates the sources of strength-limiting defects in ceramics (Zhao et al., 2001).

(iii) *Drying rate*: Once the ink is deposited onto the substrate, the printing process must pause in order for the ink to dry. The ink should have a sufficiently high drying rate in order to increase printing speed and edge quality and to prevent part sagging. Usually accomplished via hot air driers and volatile solvents in the ink itself, the drying process must be carefully controlled as it can affect

part microstructure (due to residual solvent) and part macrostructure (e.g., the deposition rate can fluctuate with changes in the drying rate) (Zhao et al., 2002b). This is a crucial facet of the printing process, as both Thornell and coauthors, and Windle and coauthors have had failed experiments (e.g., hollow structures and depositions greater than 20 layers, respectively) due to drying problems.

(iv) *Green strength*: The printed part must have sufficient strength and flexibility for handling and processing.

These properties are reliant on proper formulation (selection of the powder, solvent, dispersant, binder, and plasticizer) and processing (mixing, dispersion, filtering, and sedimentation) (Song et al., 1999).

In order to investigate the green part density obtained via aqueous direct jetting of ceramics, one must first define two different ceramic volume fractions: that of the green part created, and that of the ink deposited. The green part volume fraction is based on the pre-fired relative density obtained from the accumulated deposition of ink. Obviously, it is desired to have a large volume fraction of ceramic particles in the ink in order to have a large deposition rate; however, as discussed above, the ceramic volume fraction in the ink is limited because the ink must flow at high speeds through fine nozzles in order to create fine droplets.

Early aqueous direct jetting research featured ceramic ink volume fraction as low as 2.5 vol% (Mott et al., 1999; Song et al., 1999); in recent research however, this has increased to 15 vol% (see Table 4.11).

Table 4.11 – Comparison of Volume Fractions of Aqueous Direct Inkjet Printing Research

Ink Volume Fraction (vol %)	Green Part Volume Fraction (vol %)	Reference
5	49	(Xiang et al., 1997)
5.3	60	(Blazdell et al., 1995)
14	63	(Zhao et al., 2002a)
14.2	65	(Zhao et al., 2001)
15	60	(Wright and Evans, 1999)

Relative to all other ceramic additive manufacturing technologies, aqueous direct inkjet printing excels at creating ceramic green parts with high solids loading. Evans and coauthors note that pre-fired green parts formed from the dried aqueous suspensions are typically 50-70 vol% (corroborated by the data collected in Table 4.12). Furthermore, they observe that green parts created via this technology have a comparable volumetric composition to an injected molded ceramic and similar porosity after binder removal to a compacted body (Evans, 2001).

Although a volume fraction of 50 vol% is relatively large for ceramic additive manufacturing techniques, it is still rather porous. As a result, the green part experiences drastic shrinkage during sintering. Both Zhao (Zhao et al., 2001) and Xiang (Xiang et al., 1997) and their respective coauthors have observed a linear shrinkage of around 20% as the part sinters to 96% relative density.

Aqueous direct jetting has proven to offer high resolution in the x-y plane, with researchers reporting drop sizes (after drying) of ~30 μm (Blazdell et al., 1995; Zhao et al., 2001). Zhao and coauthors report creating walls of 170 μm thick with 170 μm spacing in between (Zhao et al., 2002a).

High resolution is also offered in the z-direction; the evaporation of the deposited ink leaves only the ceramic particles, thus layer thicknesses are extremely small (therefore offering more accurate curved profiles). Mott and coauthors report depositing

a layer thickness of only 0.4 μm; their setup required 1200 layers to make a 0.49 mm deposit (Mott et al., 1999). Similarly, Zhao and coauthors' embodiment of this technology processed 0.3 μm layers; 400 passes were required for a 0.7 mm deposit, and 3500 layers were required to make a 1 mm deposit (Zhao et al., 2002b). Xiang and coauthors also reported that 1000 passes were required to create a deposit 340 μm high (an average layer thickness of 0.34 μm) (Xiang et al., 1997).

It should be noted that the drying that takes place after each layer is deposited plays an important role in the formation of features. For example, the deposited droplets shrink to $1/10^{th}$ of their as-ejected size (Zhao et al., 2001). Furthermore, Zhao and coauthors report that drying issues caused non-uniform deposit height and prevented the formation of sharp right angles in the x-y plane (Zhao et al., 2002a).

Theoretically, any ceramic material can be printed via direct aqueous inkjet printing. Ceramic materials printed via this solution principle include TiO_2 (Xiang et al., 1997; Kim and McKean, 1998), ZrO_2 (Mott et al., 1999; Windle and Derby, 1999), and PZT (Thornell et al., 1999). Mott and coauthors also printed carbon as a support material, although they did encounter some settling issues (Mott et al., 1999). The fundamental constraint in printing a material via IJP-A is the ease at which it is suspended in an organic media. Significant effort and research is required in order to successfully suspend a significant amount of the powder in the aqueous carrier.

Like many other ceramic additive manufacturing processes, not much data has been presented regarding the material properties of the finished parts. Calvert and coauthors note that the final sintered product obtained from this technology tends to be weak due to the difficulty in obtaining good, uniform drying in the creation of the green bodies from

the dilute suspensions (Calvert, 2001). While drying causes many headaches for researchers, Zhao and coauthors state that the drying process avoids the accumulation of residual stress found in other ceramic processes, such as LS (Zhao et al., 2001).

From a high level of abstraction, 2D material patterning is inherently the fastest way to manufacture a part in a layer-by-layer fashion. By embodying the direct jetting solution principle such that multiple print heads span the entire y-stage (perpendicular to the print direction), an entire layer can be printed in a single pass.

Unfortunately, due to the inability to print a suspension that contains significant solids loading, aqueous direct jetting is an extremely slow manufacturing process simply because it requires thousands of printing passes to accumulate a significant material deposit (as discussed earlier). While small layer thicknesses are not reason enough for disregarding a technology, the time required for drying each individual layer, ranging from 20 s (Zhao et al., 2002b) to 60 s (Slade and Evans, 1998), however, seriously impedes the opportunity that this technology will become a viable manufacturing process. Furthermore, once the time required for flushing the nozzle every 100 passes (a necessary maintenance routine for preventing clogging and sedimentation (Mott et al., 1999; Zhao et al., 2002b)) is taken into account, it is apparent that the cycle time of the technology is severely limited.

Evans, however, argues that the slow nature of aqueous direct ink jet printing should not eliminate it as a manufacturing alternative. He suggests that the capability to concurrently shape microstructure and macrostructure, data-log every droplet for quality purposes, and to "confer ultimate individuation in a mass production process" might justify the process's low throughput (Evans, 2001).

While exact cost estimates are not provided in the literature, one can assume that the technology is inexpensive when compared to other AM technologies. This is primarily because it does not require the use of a laser or proprietary materials. In fact, many researchers in the literature have created testbeds by simply modifying off-the-shelf inkjet printers.

When exploring IJP-A at a functional level, it seems to be an excellent candidate solution principle for manufacturing cellular materials. Thanks to the inkjet deposition process, an entire layer of material can be deposited in a single pass. By directly depositing the material onto the substrate, concerns of excess material being trapped in voids is eliminated. By exploiting the technology found in today's color printers, multiple materials can be deposited in a build. This provides the capability to create graded materials (at the voxel level) and complex geometries such as overhangs and voids via the deposition of sacrificial support material.

At a lower level of abstraction, other advantages are discovered. The technology has the capability to achieve a high resolution in all 3 principal directions due to the small size of each droplet. The deposition process itself is very rapid, as drops are quickly ejected from nozzles and the print head is passed above the substrate. Most importantly, this technology also offers the highest green part solids loading out of all of the ceramic AM processes, therefore reducing concerns about the shrinkage and warping typically found during sintering of other additively manufactured ceramics.

Despite all these advantages, IJP-A is crippled by its embodiment. The use of an aqueous carrier in the ink coupled with the need to eject it from small nozzles limits the amount of ceramic particles that can be loaded into suspension due to viscosity

constraints. As such, several passes are required to create a substantial deposit. In addition, the reliance on evaporation as the phase change principle adds a significant delay to the deposition process as each layer must dry before the next layer is added. Furthermore, when problems with sedimentation, nozzle clogging, drying speed, and the shrinkage of deposited layers are accounted for, the promise of this technology quickly fades. The most telling evidence of this comes from reviewing the literature – of dozens of papers published thus far, the tallest part reported was 3 mm (Zhao et al., 2002a) ((Song et al., 1999) also reported a section 2.5 mm thick), with no complex structures presented.

The process properties of the current embodiment of the aqueous inkjet printing working structure are presented in Table 4.12.

Table 4.12 – Aqueous Inkjet Printing Process Properties

Stat	Value	Reference
Production Cost ($)	Scalable technology, based on IJP	
Deposition rate (cm^3/hr)	Fast 2D deposition, but slow drying and material accumulation	
Minimum feature size (mm)	0.03	(Blazdell et al., 1995; Zhao et al., 2001)
Z-resolution (mm)	0.007	(Zhao et al., 2002b)
Surface Roughness (μm, Ra)		
Green part solids loading (vol %)	50 – 65	(Zhao et al., 2001)
Working materials:	All ceramics (although must be suspended in carrier)	
Support / Complex Geometry	Yes (pyrolizable support material)	(Mott et al., 1999)

4.5.2 Hot-Melt Inkjet Printing (IJP-W)

Hot-melt or phase-change represents a second direct ink-jet printing working principle. Similar to aqueous direct inkjet printing, hot-melt printing is the creation of solid parts by the selective deposition of droplets of ceramic suspensions. Unlike aqueous printing, however, hot-melt printing features a particulate suspension in a low

melting point carrier fluid (typically paraffin wax based, thus the acronym IJP-W). This special suspension is printed at a temperature above its melting point. Instead of evaporating away a liquid portion of the suspension (as in done in aqueous direct jetting), deposits are created by cooling the heated droplets once they hit the substrate (Seerden et al., 2001). Overhanging features are supported through the deposition of special sacrificial material from a separate series of inkjet nozzles.

This variation of direct inkjet printing is much faster than aqueous printing because it does not require drying after each pass. Also, unlike aqueous printing, the deposits have significant thickness, and therefore require fewer patterning passes. An additional advantage of IJP-W printing is that the absence of evaporation as a phase-change (i.e., solidification) process leads to greater resistance to print head clogging (Wang and Derby, 2005).

The printed objects are ceramic green bodies that contain a substantial amount of wax. As such, the green parts must be dewaxed before sintering. As-printed bodies are packed in a bed of carbon black powder and are held at an elevated temperature for an extended period of time to remove the wax via capillary action (Ainsley et al., 2002). Once dewaxing is completed, the part is then post-processed via heat treating and sintering, typical of traditional ceramic processing.

The large majority of the research dedicated towards this technological development has been presented by Derby and his colleagues at the Manchester Materials Science Center at the University of Manchester. Their experimentation and realization of this process is primarily accomplished via a modified commercial drop-on-demand hot-melt inkjet printer (specifically, Solidscape's Modelmaker MM6 Pro (Solidscape, 2006)

and Sanders Design International's RTM) (Seerden et al., 2001). Unlike continuous printing, drop-on-demand inkjet printers only form drops when required. Individual drops of particle suspensions are typically created by pulsing pressure waves in a liquid-filled cavity via a piezoelectric actuator. The pressure pulse ejects drops from the open orifice of the print head (which usually contains the liquid by its own surface tension) (Derby and Reis, 2003a). Although continuous ink-jet printing operates at much faster droplet generation rates, drop-on-demand was chosen as the method for droplet delivery because (i) it does not require electrically conducting fluids, and (ii) there is no possibility of contamination during the recirculation process that is featured in continuous printing (Ainsley et al., 2002).

Like all other ceramic AM technologies, the biggest limitation of IJP-W is obtaining ceramic suspensions with a high enough solids loading in order to form green parts with high densities. Just as in aqueous direct jetting, the viscosity of a suspension, η, increases as the fraction of particles, ϕ, in suspension increases; following the Krieger-Dougherty model as shown in Equation 4.2 (where η_o is the viscosity of the unloaded carrier, ϕ_{max} is the maximum solids loading, and the parameter n describes the increase in viscosity with particle concentration) (Wang and Derby, 2005).

$$\eta = \eta_o \left(1 - \frac{\phi}{\phi_{\max}}\right)^{-n} \qquad [4.2]$$

Thus, there exists a fundamental tradeoff between the need to maximize the solids loading of the suspension and the need to minimize the suspension viscosity so that it is able to be reliably printed (Ainsley et al., 2002).

Through their research and experimentation, Derby and colleagues have identified that while the successful development of ceramic suspensions suitable for printing is dependent on the suspension's surface tension, density, and the printhead orifice's diameter, the viscosity of the suspension has the largest impact (Wang and Derby, 2005). Ink viscosity is the key parameter for successful inkjet printing of ceramics because of the very low pressures (100-500 kPa) that are used (Reis et al., 2005). Manufacturers' literature states that most commercial inkjet printing systems operate below some critical fluid viscosity (typically in the range of 10-50 mPa·s) (Wang and Derby, 2005). Specifically, for the Modelmaker 6 Pro printing platform, the upper viscosity limit is about 40 mPa·s (Ainsley et al., 2002).

Working within this constraint, Derby and coauthors have been able to successfully print ceramic suspensions containing 30-40 vol% solids by making strides in reducing the viscosity of the suspension and by altering the mechanics of the fluid jetting behavior (Seerden et al., 2001). The suspensions' viscosity have been reduced by three different techniques: (i) using suitable surfactants to stabilize the suspension, (ii) lowering the viscosity of the carrier wax (done by adding kerosene), and (iii) increasing the mean particle size (Ainsley et al., 2002). Increasing the mean particle size may seem non-obvious; however, it is known that, for particles of similar morphology, larger particles (maximum size 5 μm) show lower viscosity at the same fraction than do small particles when suspended (Ring, 1996). The mechanics of the jetting process can be altered by varying the frequency of the pressure pulse, the voltage applied across the piezoelectric, the shape of the driving pulse, the chamber dimension, and the temperature of the apparatus. In (Ainsley et al., 2002), Ainsley and Derby add an additional power supply

to the original system in order to increase the voltage pulse used to excite the piezoelectric actuator in order to print a suspension loaded with up to 40 vol% solids.

The acoustic properties of the suspension, namely the dynamic resonance behavior, also help to determine the printability of the suspension. In (Reis et al., 2005), Reis and coauthors analyze the loss mechanisms that occur when acoustic waves propagate through solid-liquid dispersions. In (Ainsley et al., 2002), Ainsely and coauthors discuss the relationship between the suspension's solids loading and the excitation frequency. A drawback of jetting is unveiled in their discussion: there is a large frequency range in which the suspensions will not print; if these ranges are entered, the face of the nozzle is wetted and will clog – as such, these ranges must be avoided, thus limiting the maximum speed of the printing process.

Seerden and coauthors modeled the fluid dynamics of the jetting process, and specified a range of printability for suspensions. This model shows that droplet characteristics are dictated by the ratio between the suspension's Reynolds number (Re) and the root of its Weber number (We) (this ratio is equivalent to the inverse of the Ohnesorge number) as shown in Equation 4.3 (Seerden et al., 2001)

$$1 < \frac{\mathrm{Re}}{\mathrm{We}^{1/2}} < 10 \qquad [4.3]$$

If this ratio is small, the viscosity is the dominant parameter and a large pressure pulse is required to eject a droplet. This leads to low droplet viscosity and shorter fluid column extensions before droplet ejection. A high value of the numerical grouping leads to very large liquid column extensions before droplet formation, which usually lead to satellite drop formation behind the main drop.

In (Ainsley et al., 2002), Ainsley and coauthors report a 18% linear shrinkage and a final relative density of 80% after sintering a green part created with a suspension of 40 vol% solids loading. The low final density came from the porosity associated with the printing process; specifically, the droplets did not uniformly spread on the substrate in order to sufficiently overlap. The authors noted that the beads deposited during the later stages of printing show different spreading behavior and leave larger voids between them. This limitation can be corrected through better understanding of the deposition process and careful process control.

It is interesting to note that, in IJP-W, the solids volume fraction of the deposited droplet is actually higher than the fraction of particles in the liquid drop. This is due to the shrinkage that takes place during the solidification of the printed drop (Wang and Derby, 2005). A liquid droplet having a solids volume fraction of 40% translates to a packing efficiency of 50% in the green part before sintering due to the shrinkage that occurs on wax solidification and wax removal (Seerden et al., 2001).

The droplets deposited by Derby and his colleagues through using the hot-melt direct jetting process are approximately 70 μm in diameter. In (Seerden et al., 2001) it is shown that walls less than 100 μm in thickness (prior to firing) were fabricated with 30 vol% alumina ink. Seerden and coauthors present photos of the parts, which exhibited good resolution of vertical corners and edges.

Derby and colleagues have successfully printed ZrO_2, PZT, and Al_2O_3 using hot-melt direct jetting. They note that, "in principle, given suitable surfactants, stable printable suspensions of any material available in powder form can be developed (Derby and Reis, 2003b)." Although one should be able to suspend any given material, it is not

guaranteed that it is feasible. In their work with PZT, for example, Wang and Derby note that making a suspension with PZT that won't settle after a few hours is very difficult due to the fact that the powder has a higher density than the carrier fluid (Wang and Derby, 2005). As is common with all AM techniques which process ceramic suspensions, each new material requires careful control of colloidal chemistry.

Despite several papers on the processing of ceramic parts through IJP-W, there is very little information shared regarding the material properties of the finished parts. Successful grain growth is an important characteristic of ceramic processing. Generally, small powder particles are preferred in ceramics processing as they lead to easier sintering and smaller grains, thus leading to better material properties. In this process, however, there exists a lower limit on particle size, since (as discussed earlier) the suspension's viscosity greatly increases with smaller particles. It is reported in (Wang and Derby, 2005) that significant grain growth and "very little" porosity are observed in a part created with a suspension of 35 vol% PZT.

Unfortunately, there has been no published work concerning the surface finish of the fired ceramic parts created through direct hot-melt printing.

Although no time or cost estimates for the direct jetting of ceramic suspensions via hot-melt printing have been described in the literature, one can look at technically-similar machines that are commercially available. Due to the lack of a laser, this technology is cost-effective relative to other AM processes (SL, LS, LENS, EBM, etc.). Solidscape's line of hot-melt printers range from $40k-$50k (Solidscape, 2006).

In IJP-W, material is directly deposited by a parallel array of multiple nozzles; thus, material can be deposited very quickly. Just as in other 2D material printing via inkjets,

one can imagine having an array of hundreds of nozzles that can print the entire width of the part in one pass, thus eliminating the need for an x-stage. Furthermore, unlike aqueous direct jetting, the individual droplet deposits formed with hot-melt printing are substantial – a typical layer thickness is 0.127 mm. It should be noted that it is not uncommon for direct jetting machines to incorporate multiple passes per layer in their process plan. This is done in order to compensate for any nozzles that might be clogged during building.

IJP-W of ceramic suspensions holds a lot of promise for the additive manufacture of cellular green parts. Unlike indirect inkjet printing, direct jetting can be used to fabricate objects where the composition is controlled at the level of a voxel defined by the deposited droplet size (Song et al., 1999; Reis et al., 2005). Although graded materials may prove to be difficult to process via the reduction process seen in the manufacture of Linear Cellular Alloys, this feature keeps the system open for future discoveries and uses.

Another advantage that this process has over indirect ink-jet printing is the direct addition of material. By not having to work in a powder bed, there is no concern about the successful removal of unbound support material. In direct inkjet printing, overhanging structures are supported by a sacrificial support material that is deposited by an independent set of inkjet heads. In the work of Ainsley and coauthors, Solidscape's commercial support material, "Protosupport" (a low-melting point wax), is used as a support material and has shown to be easily leached away during post-processing (Ainsley et al., 2002).

The major limitation of this process is the low solids loading featured in the processed parts. There exists a tradeoff, however; as in IJP-A, which can process parts

with a much higher solids loading, features very slow deposition (due to drying and small layer thicknesses) and several processing inefficiencies (clogging nozzles, frequent nozzle flushes, etc.).

The process properties of the current embodiment of the hot-melt inkjet working structure are presented in Table 4.13

Table 4.13 – Hot-Melt Inkjet Printing Process Properties

Stat	Value	Reference
Production Cost ($)	40,000	(Solidscape, 2006)
Deposition rate (cm^3/hr)	Very high; direct material addition (no recoating)	
Minimum feature size (mm)	0.1	(Seerden et al., 2001)
Z-resolution (mm)	0.127	
Surface Roughness (μm, Ra)	Better than powder bed technologies	
Green part solids loading (vol %)	40	(Ainsley et al., 2002)
Working materials	All ceramics (although must be successfully suspended in carrier fluid)	
Support / Complex Geometry	Yes (pyrolizable support material)	

4.5.3 UV Direct Inkjet Printing (IJP-UV)

This final direct printing working structure features yet another embodiment of the photopolymerization working principle (as seen in SL, Section 4.1.2, and in MSL, Section 4.2.2). In this concept, inkjet print heads are used to selectively deposit a photopolymer suspension of ceramic powders. Once deposited onto the substrate, UV bulbs are used to quickly flash the part surface and thus solidify the newly deposited primitive. The curing of individual droplets of UV resin provides drop-by-drop control over material deposition. Overhanging features can easily be supported by the deposition of a secondary sacrificial support material. Just as the case with the other inkjet-based concepts, a large array of printing nozzles can be used, allowing for the printing of an

entire layer in just a few seconds. Furthermore, the absence of a laser source significantly reduces the cost of the technology.

While the working principles in this strucuture allow for the realization of small features, complex mesostructure, and strong green parts, there are a few distinct disadvantages. Primarily, the use of the "photopolymerization" working principle limits the list of ceramic materials that can be processed due to the high index of refraction of the ceramic particles. Furthermore, as with other direct inkjet concepts, the viscosity of a suspension of photopolymer and ceramic nanoparticles would most likely be too great for traditional inkjet print heads. It should be noted that there have been promising initial results in the realm of jetting viscous materials via ultrasonic MEMs nozzles that might alleviate this limitation. (Meacham et al., 2004; Fedorov and Degertekin, 2005; Meacham et al., 2005).

Objet has commercialized an AM machine which embodies this working structure (Objet, 2005). However, their line of working material does not include ceramic-filled suspensions due to the limitations identified above (Sagi and Libermann, 2007).

The process properties of the current embodiment of the UV inkjet printing working structure are presented in Table 4.14.

Table 4.14 – UV Inkjet Printing Process Properties

Stat	Value	Reference
Production Cost ($)	39,900 – 170,000	(Wohlers, 2006)
Deposition rate (cm^3/hr)	Slightly slower than IJP-W because of flashing every layer	
Minimum feature size (mm)	Same as IJP-W	
Z-resolution (mm)	0.016	(Sagi and Libermann, 2007)
Surface Roughness (μm, Ra)	Same as IJP-W	
Green part solids loading (vol %)	Slightly less than IJP-W due to larger viscosity of carrier fluid	
Working materials	Only UV transparent ceramics	
Support / Complex Geometry	Yes (pyrolizable material)	

4.6 DISSERTATION ROADMAP

With the working structures detailed and critically analyzed (Sections 4.1 – 4.5), the conceptual design process continues with the selection of the principal solution. This important decision is separated into two separate phases: (i) a preliminary selection decision is made first to identify those alternatives that are most-likely-to-succeed based upon the design requirements established in Chapter 3, and (ii) a selection decision is made to identify the principal solution. As seen in Figure 4.10, this selection process takes place in Chapter 5. Once the principal solution is identified, the design phase of this research will close, and the embodiment of the selected solution principle will begin (Chapter 6).

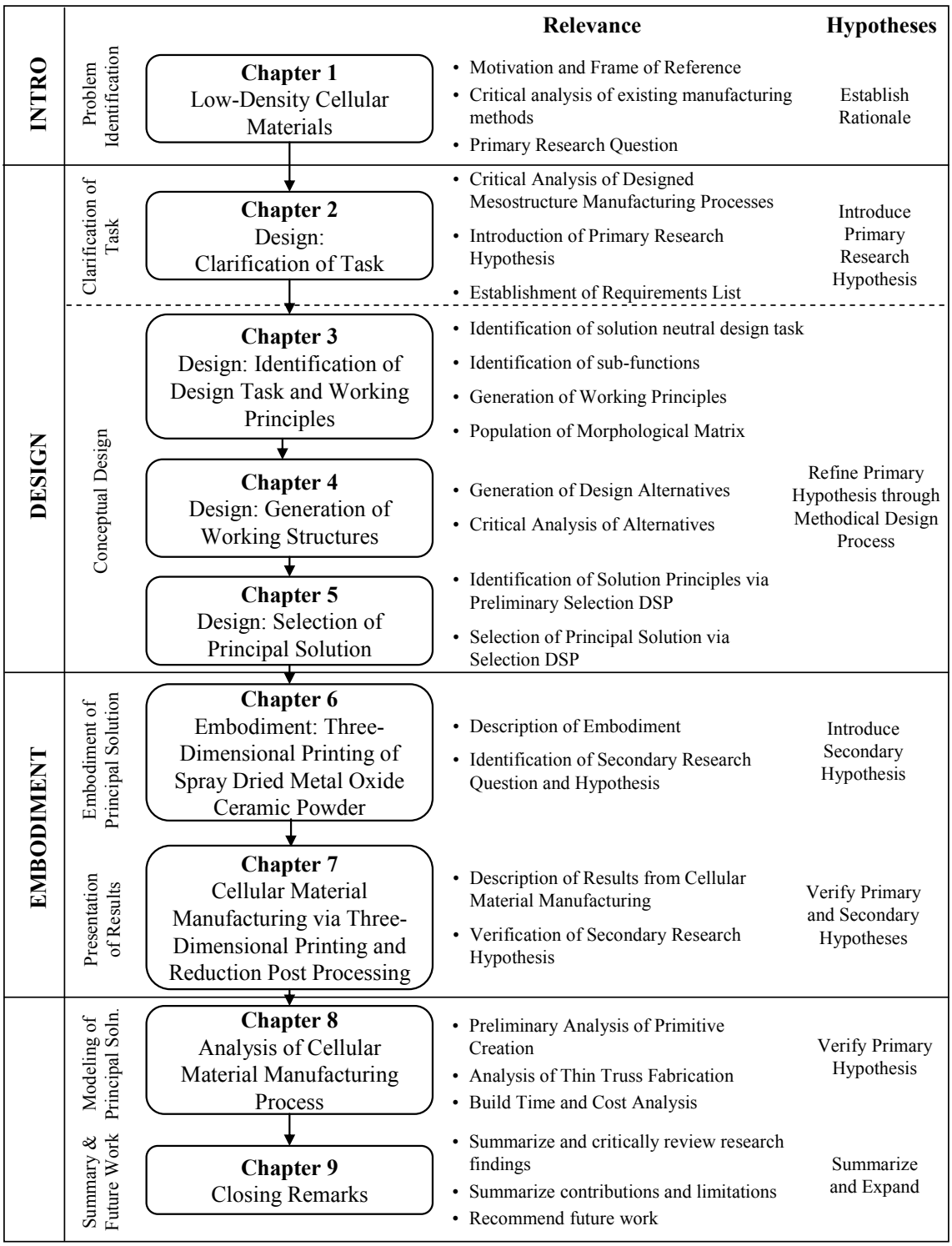

Figure 4.10 – Dissertation Roadmap

CHAPTER 5

DESIGN: SELECTION OF PRINCIPAL SOLUTION

The final stage of the conceptual design phase is focused in selecting the principal solution from a set of solution principles that is to be further embodied in the remainder of the design process. Mistree, Lewis, and Stonis suggest that this selection phase should be divided into a three step process (Mistree et al., 1994):

i) Use the available information to identify the more promising "most-likely-to-succeed" working structures. This is accomplished by formulating and solving a preliminary selection Decision Support Problem (DSP) which provides a framework in which to make selection decisions in the face of soft (i.e., primarily qualitative) engineering data (Section 5.1).

ii) Establish the functional feasibility of these most-likely-to-succeed concepts and develop them into candidate alternatives. This process is aimed at increasing the amount of hard information that can be used to characterize the suitability of the alternative for selection.

iii) Select a candidate alternative that best satisfies the identified design task and requirements (Section 3.1). This is accomplished by formulating and solving a selection DSP. The selection DSP has been designed to utilize both the hard and the soft information that is available. This is done in Section 5.2.

The result of these three steps is the identification of the principal solution which is deserving of further embodiment and research.

5.1 IDENTIFICATION OF SOLUTION PRINCIPLES: PRELIMINARY SELECTION

Due to the lack of sufficient quantitative engineering data presented for each alternative, it is not possible to proceed immediately with a full engineering selection process. Mistree and coauthors propose the preliminary selection Decision Support Problem (DSP), a technique for making selections in a complex, multi-faceted design environment (Mistree et al., 1994). A brief overview of the preliminary selection of ceramic AM technologies for the realization of green ceramic cellular parts can be found in (Williams et al., 2005b).

5.1.1 The Preliminary Selection Decision Support Problem

The preliminary selection DSP provides a designer a framework in which most-likely-to-succeed concepts can be identified through the systematic comparison of alternatives based upon soft engineering data. The DSP representing preliminary selection is stated as follows:

Given	A set of concepts
Identify	The principal criteria influencing selection. The relative importance of the criteria.
Capture	Experience-based knowledge about the concepts with respect to a datum and the established criteria.
Rank	The concepts in order of preference based on multiple criteria and their relative importance.

The preliminary selection DSP consists of eight distinct steps:

i) Describe the components and provide acronyms (Section 5.1.2)

ii) Describe each generalized criterion and provide acronyms and specify the relative importance of the specific criteria (Section 5.1.3)

iii) Choose a datum with which all other concepts will be compared (Section 5.1.4)

iv) Capture experience-based knowledge through comparison of concepts. Justify decisions (Section 5.1.4)

v) Repeat steps iii and iv for several datums in order to dispel any prejudice (Appendix C)

vi) Evaluate the merit function for each concept within each generalized criterion and determine rank (Section 5.1.5)

vii) Include interactions between generalized criteria and compute the overall merit and determine the overall rank (Section 5.1.5)

viii) Post-solution analysis: Determine the most likely to succeed concepts (Section 5.1.6)

The first two steps are described in Sections 5.1.2 and 5.1.3. Steps 3-4 are demonstrated in Section 5.1.4. The results of the process's final two steps are presented in Sections 5.1.5 - 5.1.6.

5.1.2 Description of Concepts

Working structures are described in detail and critically analyzed in the context of realizing cellular materials in Chapter 4. Each concept to be evaluated is listed in Table 5.1 along with its acronym, the section of this dissertation in which it is detailed, and a brief description of the technology.

Table 5.1 – List of Working Structures

Category	Concept	Acronym	Section	Brief description
1D Energy Patterning	Laser Sintering	LS	4.1.1	Laser selectively initiates liquid-phase sintering on polymer powder that is blended with (or coating) ceramic powder.
	Stereolithography	SL	4.1.2	Laser selectively initiates photopolymerization on resin surface.
2D Energy Patterning	2D Sintering	HSS	4.2.1	IR light is selectively patterned in 2D via a mask onto a ceramic/polymer powder blend.
	Mask Stereolithography	MSL	4.2.2	UV light is selectively patterned in 2D via a mask onto a ceramic/photopolymer suspension.
Material Patterning	Fused Deposition of Ceramics	FDC	4.3.1	Ceramic/polymer suspension is extruded from a heated nozzle onto a substrate.
	Layered Object Manufacturing	LOM	4.3.2	Cross-sectional layers are cut from ceramic green tape via a laser and are fused together with a heated roller.
	Electrophotographic Printing	EP	4.3.3	Similar to photocopying, entire cross-sectional layers of coated ceramic powder are deposited onto a substrate and sintered.
Indirect Material Printing	Three-Dimensional Printing	3DP	4.4.1	Polymer binder is selectively printed onto a bed of ceramic powder.
	Slurry-based Three-Dimensional Printing	S-3DP	4.4.2	A ceramic suspension is jetted onto a substrate and dried. Primitives are created by printing a polymer binder onto the resultant slip.
	UV Three-Dimensional Printing	UV-3DP	4.4.3	Photopolymer is jetted onto a bed of ceramic powder. A UV lamp is used to cure the jetted polymer.
Direct Material Printing	Aqueous Direct Inkjet Printing	IJP-A	4.5.1	An aqueous ceramic suspension is jetted onto a substrate. A heat source evaporates the carrier fluid, leaving behind a small ceramic solid primitive.
	Hot-Melt Direct Inkjet Printing	IJP-W	4.5.2	A ceramic suspension is jetted onto a substrate. The polymer carrier cools and solidifies.
	UV Direct Inkjet Printing	IJP-UV	4.5.3	A suspension of photopolymer and ceramic powder is jetted onto a substrate. A UV lamp is used to cure the jetted suspension.

5.1.3 Selection Criteria

Criteria around which a preliminary selection decision can be made must be identified. In order to ensure that the design requirements are taken into account, selection criteria are created based on the requirements list created in the "Clarification of Task" design phase (presented in Table 2.14). Those requirements which are most crucial to the success of the design can be found in an abstracted version of the initial

requirements list which contains a list of the generalized process requirements (Table 3.5).

Generally, manufacturers desire that the process be efficient, cost effective, and able to make parts from a wide variety of materials with small features, complex geometry, a high green solids loading, and a good surface finish. The specific criteria to be used in this preliminary selection decision are presented in Table 5.2 (acronyms are provided as suggested by the preliminary selection DSP framework).

Table 5.2 – Preliminary Selection Criteria

Category	Criteria	Acronym	Description	Preference (+1)
Economics	Cost of technology	TECHCOST	The cost of purchasing and operating the technology.	Low cost
	Rate of deposition	DEPRATE	The amount of volume deposited per unit time.	High rate of deposition (shortened build time)
Performance	Minimum feature size	MINFEAT	The smallest feature able to be produced by the technology	Able to make small features
	Complex geometry	COMPGEO	The ability of the technology to create complex geometry (e.g., overhangs and small channels) with minimal post-processing.	Able to make cellular mesostructure
	Surface finish	SURFIN	Quality of surface able to be produced by the machine.	Small surface roughness
Materials	Solids loading of green part	GREENLOD	The percentage of the green part volume that is ceramic material.	Large solids loading
	Material selection	MATSEL	The number of ceramic materials able to be processed by the technology.	Large selection of working materials

This list represents criteria that are specific to manufacturing parts of all classes (low cost, high rate of material deposition, multiple materials), as well as criteria that are specific to manufacturing parts of designed mesostructure (extremely small features, excellent surface finish, and complex geometries).

The relative importance of the specific selection criteria is represented by a set of weighting values that will be used in the calculation of the overall merit function. In

order to evaluate the sensitivity of the final decision on the assignment of preferences, two separate scenarios with different values for relative importance are established in Table 5.3. Scenario A represents an equal weighting for each specific criterion within its "generalized criteria" grouping.

Table 5.3 – Scenarios for the Relative Importance of Specific Criteria

		Scenario	
Generalized Criteria	***Specific Criteria***	**A**	**B**
Economics	TECHCOST	0.5	0.4
	DEPRATE	0.5	0.6
Performance	MINFEAT	0.3	0.35
	COMPGEO	0.3	0.5
	SURFIN	0.3	0.15
Materials	GREENLOD	0.5	0.35
	MATSEL	0.5	0.65

Scenario B represents a more accurate viewpoint of our opinion of the relative importance of each specific criterion. In the context of economics, it is slightly more important to design a process which is capable of producing parts quickly than it is to produce them cheaply; this is because a shortened processing time will lead to a higher production capacity and thus result in a lower production cost. In the context of machine performance, the ability to create complex cellular mesostructure is the most important requirement, while surface finish is the least important. Finally, in the context of materials, it is more important to be able to process a wide variety of ceramics than it is to have a higher green part solids loading.

5.1.4 Comparison of Concepts

The Preliminary Selection DSP involves a series of comparisons between each working structure alternative and a chosen datum in the context of the different selection criteria. The concepts are evaluated against the datum as inferior (-1), equal (0), or superior (+1) (based upon the criteria preference listed in Table 5.2). Since the

comparisons are based upon soft engineering data, this three-point scale is appropriate; at this point in the design process a designer can only identify that one concept is preferred over another, but cannot quantitatively identify by how much the concept is preferred. It is noted that value assessments are subjective and experience-based; however, this is not a shortcoming – evaluation procedures are meant to enhance an engineer's decision making ability. The scores are then summed and normalized within each category, utilizing the relative importance for each criterion presented in Table 5.3.

This systematic comparison procedure is repeated for multiple datums in order to dispel any prejudice. These additional comparisons are presented in Appendix C. A sample comparison matrix, wherein LS is the chosen datum, is given in Table 5.4.

Table 5.4 – Comparison Matrix for LS Datum

	LS	SL	HSS	MSL	FDC	LOM	EP	3DP	S-3DP	UV-3DP	IJP-A	IJP-W	IJP-UV
ECONOMICS													
TECHCOST	0	0	1	1	1	0	1	1	1	1	1	1	1
DEPRATE	0	0	1	1	1	1	1	1	1	1	-1	1	1
Score A	0.00	0.00	1.00	1.00	1.00	0.50	1.00	1.00	1.00	1.00	0.00	1.00	1.00
Score B	0.00	0.00	1.00	1.00	1.00	0.60	1.00	1.00	1.00	1.00	-0.20	1.00	1.00
Normalized Score A	0.00	0.00	1.00	1.00	1.00	0.50	1.00	1.00	1.00	1.00	0.00	1.00	1.00
Normalized Score B	0.17	0.17	1.00	1.00	1.00	0.67	1.00	1.00	1.00	1.00	0.00	1.00	1.00
PERFORMANCE													
MINFEAT	0	0	1	1	-1	0	0	1	1	1	1	1	1
COMPGEO	0	-1	0	-1	1	-1	1	0	-1	0	-1	1	1
SURFIN	0	1	0	1	-1	-1	0	0	1	0	1	1	1
Score A	0.00	0.00	0.33	0.33	-0.33	-0.66	0.33	0.33	0.33	0.33	0.33	0.99	0.99
Score B	0.00	-0.35	0.35	0.00	0.00	-0.65	0.50	0.35	0.00	0.35	0.00	1.00	1.00
Normalized Score A	0.40	0.40	0.60	0.60	0.20	0.00	0.60	0.60	0.60	0.60	0.60	1.00	1.00
Normalized Score B	0.39	0.18	0.61	0.39	0.39	0.00	0.70	0.61	0.39	0.61	0.39	1.00	1.00
MATERIALS													
GREENLOD	0	0	0	-1	-1	1	0	0	1	0	1	-1	-1
MATSEL	0	-1	0	-1	0	0	-1	0	0	-1	0	0	-1
Score A	0.00	-0.50	0.00	-1.00	-0.50	0.50	-0.50	0.00	0.50	-0.50	0.50	-0.50	-1.00
Score B	0.00	-0.65	0.00	-1.00	-0.35	0.35	-0.65	0.00	0.35	-0.65	0.35	-0.35	-1.00
Normalized Score A	0.67	0.33	0.67	0.00	0.33	1.00	0.33	0.67	1.00	0.33	1.00	0.33	0.00
Normalized Score B	0.74	0.26	0.74	0.00	0.48	1.00	0.26	0.74	1.00	0.26	1.00	0.48	0.00
OVERALL SCORE - Scenario 1													
Sum of Scores, A	0.36	0.24	0.76	0.53	0.51	0.50	0.64	0.76	0.87	0.64	0.53	0.78	0.67
Rank, A	12	13	3	8	10	11	6	3	1	6	8	2	5
Sum of Scores, B	0.43	0.20	0.78	0.46	0.63	0.56	0.65	0.78	0.80	0.62	0.46	0.83	0.67
Rank, B	12	13	3	10	7	9	6	3	2	8	10	1	5

Mistree and coauthors stress the importance of recording a designer's viewpoints and underlying reasons for the decisions made in this preliminary selection process. An

example of the justifications for the generalized criterion where LS is the datum is provided below.

Economics

- TECHCOST: LS, SL, and LOM are determined to contain more expensive technologies than the other alternatives due to their incorporation of high-powered lasers.
- DEPRATE: LS is determined to have an equivalent deposition rate as SL due to the need to raster a 1D laser spot. While FDC also rasters a 1D deposition area, it does not require powder/resin recoating and is therefore determined to be faster. LOM also rasters a 1D laser spot, but it only has to trace the cross-sectional boundary, and is therefore faster than LS. The other 2D patterning technologies are deemed to be faster; IJP-A is the exception since the volumes of its deposited primitives are extremely small (and thus accumulation of layers takes much longer).

Performance

- MINFEAT: SL is determined to have the same minimum feature size because both technologies use similar laser patterning techniques. The masking technologies found in HSS and MSL are capable of obtaining smaller features than LS due to their use of DMD masks. Due to its large diameter extrusion nozzle, FDC has the largest minimum feature size of all of the technologies. Finally, inkjet printing technologies are capable of creating slightly smaller primitives due to the small deposition nozzles used in these technologies.

- COMPGEO: The employment of the "powder bed" working principle prevents the creation of extremely small cellular channels by using LS. HSS and 3DP also use powder beds, and thus have equivalent limitations. SL's use of lattice structures to support overhangs prevents a user from making all types of cellular mesostructure, and is therefore deemed inferior. S-3DP and MSL are also deemed inferior due to the manner in which they fabricate parts in a viscous vat of a ceramic suspension, which is hard to remove from a green cellular part. EP, FDC, and IJP methods are capable of depositing a secondary sacrificial material that can be removed either through dissolving or pyrolysis and are therefore rated as superior to LS (primarily due to their embodiment of the "direct material addition" working principle of the "support previously deposited material" sub-function). However, because parts of significant size or quality have yet to be created by IJP-A, it is rated inferior to LS.
- SURFIN: Powder bed technologies such as LS, HSS, EP, 3DP, and UV-3DP have poor surface finishes from creating green parts from dry powder. Conversely, those concepts which work with suspensions such as SL, MSL, and S-3DP, are capable of creating parts with a better surface finish. Although FDC and LOM both work with a ceramic slurry, its surface finish capability is deemed inferior to LS because of the large z-resolution which can result in significant stair-stepping for parts with curved macrostructure. Finally, IJP processes are deemed to have better surface quality than LS due to their small z-resolutions.

Materials

- GREENLOD: All powder bed technologies which work with dry powders are deemed to have similar solids loading values. While those concepts that employ the "powder bed" working principle are able to offer a very high solids loading (when compared to those that work with suspensions such as IJP and FDC), S-3DP and LOM offer a higher green part solids loading because of the manner in which they work with very dense ceramic slips and tapes (respectively).
- MATSEL: As with all other powder bed technologies, LS can work with any ceramic material. EP is the lone exception of powder bed technologies, sine it requires the use of a material that can be electrostatically charged. Finally, all concepts which employ the "initiate photopolymerization" working principle are deemed inferior to LS because they are only capable of processing UV-transparent ceramics.

5.1.5 Evaluation of Merit Function

Multiple weighting schemes are employed in the Preliminary Selection DSP to address the interaction of the generalized selection criteria and their relative importance. The weighting schemas for each scenario are presented in Table 5.5.

Table 5.5 – Scenarios for the Relative Importance of Generalized Criteria

	Scenario Number				
Generalized Criteria	**1**	**2**	**3**	**4**	**5**
Economics	0.33	0.2	0.2	0.6	0.2
Performance	0.33	0.2	0.6	0.2	0.4
Materials	0.33	0.6	0.2	0.2	0.4

The first scenario represents an equal preference weighting for the three generalized criteria. Scenarios 2 – 4 represent a strong preference towards satisfying each individual generalized criterion. Finally, Scenario 5 represents an accurate portrayal of the

preferences expressed in the design task. Specifically, it is of utmost importance to design a process that is able to fabricate cellular green parts of any ceramic material; the economics of the process are slightly less important.

Normalized scores for each concept are computed by multiplying the normalized score of each concept's attribute category (Table 5.4) by the weighting values (Table 5.5). The summed score serves as the merit function for each generalized concept. For example, the merit function results for Scenario 1 for the LS datum are shown at the bottom of Table 5.4. The results for all scenarios from the LS datum are graphically shown in Figure 5.1.

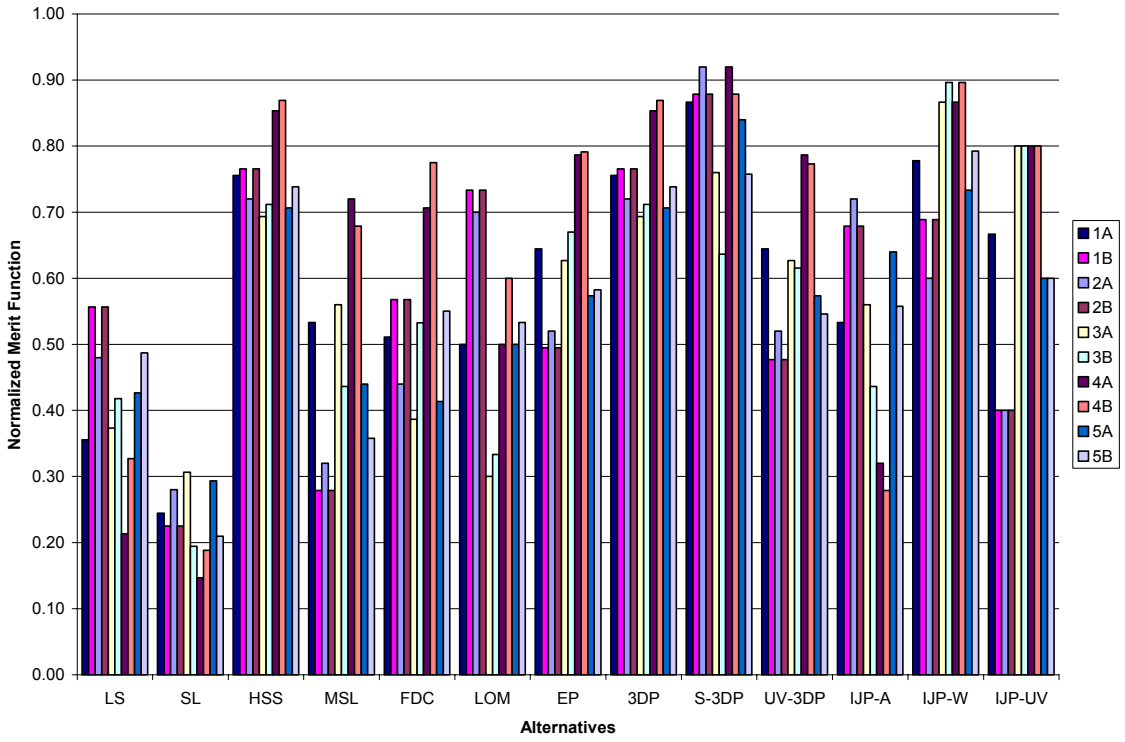

Figure 5.1 – Graphical Representation of Evaluated Merit Functions for LS Datum

Since the "B" scenarios (Table 5.3) are a more accurate portrayal of the preferences stated by the design requirements, Figure 5.1 is reformatted to only include those scenarios (Figure 5.2).

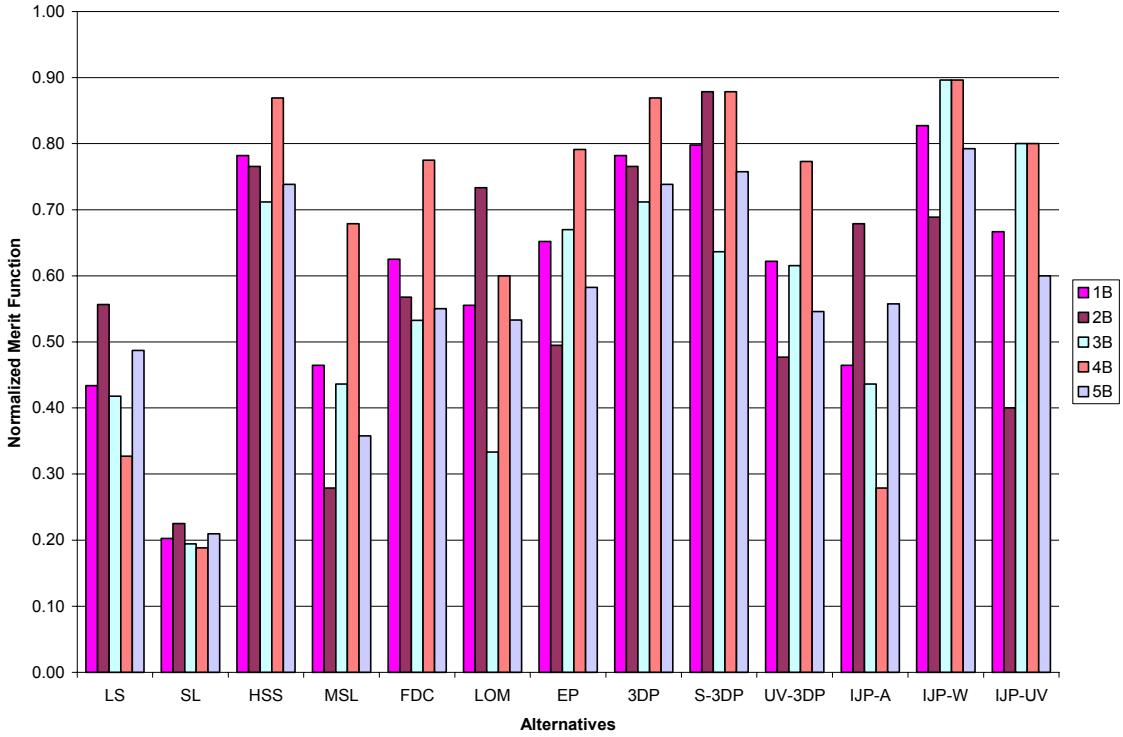

Figure 5.2 – Graphical Representation of Evaluated Merit Functions for "B" Scenarios of LS Datum

Each alternative is ranked from the merit function values for each scenario. Ranking results for the LS datum are shown in Table 5.6. Looking broadly across all of the scenarios (Figure 5.1 and Table 5.6), IJP-W, S-3DP, 3DP, and HSS are identified as the most likely to succeed technologies for the scenarios when LS is set as the datum.

This step is repeated in a similar manner using multiple datums for all weighting scenarios in order to dispel any prejudice (Appendix C). Once the comparison process is repeated for multiple datums, the average overall merit function for each of the alternatives for all weighting scenarios is calculated. These results are shown in Table

5.7. Rank ordering these values results in a list of most-likely-to-succeed technologies, as presented in Table 5.8.

Table 5.6 – Rankings of Concepts for the LS Datum

	Scenario Number									
Alternative	**1A**	**1B**	**2A**	**2B**	**3A**	**3B**	**4A**	**4B**	**5A**	**5B**
LS	12	12	9	8	11	11	12	11	11	11
SL	13	13	13	13	12	13	13	13	13	13
HSS	3	3	2	2	4	3	3	3	3	3
MSL	8	10	12	12	8	9	8	9	10	12
FDC	10	7	10	7	10	8	9	7	12	8
LOM	11	9	5	4	13	12	10	10	9	10
EP	6	6	7	9	6	5	6	6	7	6
3DP	3	3	2	2	4	3	3	3	3	3
S-3DP	1	2	1	1	3	6	1	2	1	2
UV-3DP	6	8	7	10	6	7	6	8	7	9
IJP-A	8	10	2	6	8	9	11	12	5	7
IJP-W	2	1	6	5	1	1	2	1	2	1
IJP-UV	5	5	11	11	2	2	5	5	6	5

Table 5.7 – Averaged Overall Merit Functions for Preliminary Selection

	Scenario Number									
Alternative	1A	1B	2A	2B	3A	3B	4A	4B	5A	5B
LS	0.358	0.391	0.495	0.545	0.364	0.381	0.215	0.248	0.429	0.463
SL	0.219	0.154	0.251	0.183	0.274	0.174	0.131	0.106	0.263	0.179
HSS	0.637	0.695	0.662	0.727	0.586	0.645	0.662	0.714	0.624	0.686
MSL	0.408	0.374	0.245	0.225	0.547	0.481	0.431	0.418	0.396	0.353
FDC	0.461	0.540	0.477	0.572	0.403	0.533	0.503	0.517	0.440	0.552
LOM	0.533	0.578	0.680	0.719	0.320	0.347	0.600	0.669	0.500	0.533
EP	0.626	0.647	0.535	0.530	0.566	0.635	0.775	0.775	0.551	0.583
3DP	0.659	0.683	0.675	0.720	0.599	0.637	0.702	0.692	0.637	0.678
S-3DP	0.731	0.664	0.839	0.798	0.663	0.573	0.692	0.621	0.751	0.686
UV-3DP	0.420	0.410	0.372	0.336	0.476	0.486	0.412	0.409	0.424	0.411
IJP-A	0.736	0.667	0.841	0.800	0.777	0.689	0.588	0.513	0.809	0.745
IJP-W	0.750	0.817	0.610	0.710	0.790	0.864	0.850	0.877	0.700	0.787
IJP-UV	0.517	0.559	0.310	0.336	0.650	0.710	0.590	0.633	0.480	0.523
	Overall Merit Function									

Observing the results shown in Table 5.8, it can be seen that five of the concepts are consistently preferred over the other eight. These five concepts are two-dimensional sintering (HSS), three-dimensional printing (3DP), slurry-based three-dimensional printing (S-3DP), aqueous direct inkjet printing (IJP-A), and hot-melt direct inkjet printing (IJP-W).

Table 5.8 – Rankings for the Averaged Overall Merit Function

	Scenario Number									
Alternative	1A	1B	2A	2B	3A	3B	4A	4B	5A	5B
LS	12	11	8	8	11	11	12	12	10	10
SL	13	13	12	13	13	13	13	13	13	13
HSS	5	2	5	3	6	4	5	3	5	3
MSL	11	12	13	12	8	10	10	10	12	12
FDC	9	9	9	7	10	8	9	8	9	7
LOM	7	7	3	5	12	12	6	5	7	8
EP	6	6	7	9	7	6	2	2	6	6
3DP	4	3	4	4	5	5	3	4	4	5
S-3DP	3	5	2	2	3	7	4	7	2	4
UV-3DP	10	10	10	10	9	9	11	11	11	11
IJP-A	2	4	1	1	2	3	8	9	1	2
IJP-W	1	1	6	6	1	1	1	1	3	1
IJP-UV	8	8	11	11	4	2	7	6	8	9
	Overall Merit Function									

5.1.6 Post-Solution Analysis: Lessons Learned

Several generalized preferences are extracted from the comparison exercises completed for this preliminary selection process (performed for the LS datum in Section 5.1.4, and for multiple datums in Appendix C). When observing the working structures of the five selected concepts, it is clear that they share many working principles (or conversely, avoid the employment of many similar principles). As such, lessons learned from the preliminary selection exercise are presented in the context of the sub-functions of the to-be-designed process.

Store Material

The function labeled "store material" represents how the raw material for the building of the part is stored before being processed. Generally, one would not expect that the working principles listed for this function would have a direct impact on the ability of an AM process to manufacture cellular materials. However, since the primary concern in direct AM of ceramics is in creating a green part with a sufficient solids loading percentage for it to be suitable for sintering and reduction (i.e., to easily reach full

density and to minimize warping, curling, and shrinkage), the manner in which the raw material is provided to the system is of utmost importance.

The relation between this requirement and the working principle chosen for the "store material" sub-function is no more apparent than in the "powder/binder suspension" principle. Those technologies that employ this working principle, such as direct inkjet printing, extrusion, and stereolithography, produce parts that have a relatively low solids loading percentage. The primary reason for this is that suspensions become extremely viscous as the solids loading percentage increases (especially when attempting to suspend very fine particles). Because most patterning or recoating techniques have a set range of suspension viscosities in which they can process materials, this phenomenon poses a very large constraint. Examples of this limitation include:

- Derby and coauthors have only been able to successfully inkjet print suspensions of ceramic powder in a thermoplastic polymer that contain ~35 vol.% solids (Seerden et al., 2001).
- Inkjet printing of aqueous ceramic suspensions has reached a maximum of only 15 vol.% (Wright and Evans, 1999).
- Without the need to form droplets, extrusion techniques have processed slurries with ~40 vol.% ceramics (maximum of ~55 vol.%) (Lewis, 2000; Grida and Evans, 2003).

An exception to this observation is S-3DP, which works with a slurry, and yet its solids loading capability is its largest strength, due to its centering on the slip-casting technique. However, its use of the slip-casting technique is also the source of its major limitations:

(i) delicate cellular materials cannot be successfully removed from the dense dried slip bed, and (ii) its build time is very long (Cima et al., 1992; Moon et al., 2000).

The use of powder/binder suspensions is further hampered by the amount of effort that is required to adequately suspend the ceramic powder in the solution. Not only does successful suspension require extensive experimentation and knowledge of materials engineering and chemistry, but the solution is unique to each material that the AM technique will process. Taking all of these limitations into account, it is difficult to recommend the use of powder/binder suspensions for the "store material" function.

Working with a powder form of the raw material seems to be a more appropriate working principle for the manufacture of cellular materials. If used in a powder bed, the maximum solids loading of the green part is no longer a function of rheology of a suspension; instead, it is a function of the tap density of the powder (dependent on particle size and shape). Utela and coauthors report powder beds with solid loading as high as 55 vol% in their work with 3DP (Utela et al., 2006).

Pattern Material & Pattern Energy

These "patterning" sub-functions capture the act of selectively depositing (or patterning) material and/or energy to create the final part. The working principles are categorized by their dimension of deposition.

One-dimensional patterning refers to those processes that have single point material deposition methods such as extrusion (e.g., FDC) or laser-based energy deposition methods (e.g., SL and LS). The speed of patterning found in one-dimensional processes is constrained by the fundamental limit of the machines' scanning speed. It is simply not

possible to scan a single deposition spot fast enough to be economically competitive with traditional manufacturing technologies.

Two-dimensional patterning techniques do not suffer from this limitation as they entail processes that are able to pattern large portions of a cross-section in one motion. This can include the delivery of energy through a mask (e.g., M-SL, HSS), the patterning of large portions of material (e.g., LOM), and even printing methods (e.g., the IJP and 3DP process families) which feature several parallel one-dimensional depositions of material or binder. EP is an example of a process that patterns both energy and material in two-dimensions. Two-dimensional patterning processes are preferred for manufacturing not only because of the aforementioned concerns regarding process throughput, but also because they are capable of being scaled cost effectively since they do not require an expensive laser element (Carrion, 1997). As such, two-dimensional patterning methods were consistently preferred in the preliminary selection exercise.

In addition to their influence on the economics of the process, the working principles of the "patterning" sub-functions have a direct influence on the minimum feature size that the process can fabricate. This is crucial for the realization of cellular materials, in that the process must be able to fabricate parts with cell sizes in the range of 0.5 – 2 mm and wall thicknesses as small as 200 μm. These requirements resulted in consistent preference towards inkjet printing-based working principles or masking-based working principles since these principles (IJP and 3DP, M-SL and HSS) can create features as small as 100 μm with 100 μm layer thicknesses (Seerden et al., 2001; Moon et al., 2002). Conversely, extrusion-based principles (e.g., FDC) were consistently disfavored due to their inability to deposit viscous ceramic slurry in the form of small,

discrete primitives that are typical of the cross-sections of trussed cellular materials as described in (Section 4.3.1).

Finally, it can be generally accepted that "material patterning" is slightly more preferred over "energy patterning" since patterning of material is typically cheaper and more scalable than energy patterning since specialized energy sources are not needed.

Create Primitive

This function describes the need for a delivery of some form of energy to transform, shape, or change the phase of the raw material to obtain the desired part. While most working principles developed for this sub-function do not directly limit the manufacture of cellular materials, some are more preferred than others.

Photopolymerization, found in stereolithography-based processes (SL, 3DP-UV, IJP-UV), is not a feasible means of processing most ceramics. As detailed in Section 4.1.2, photopolymerization typically cannot occur in ceramic-loaded photocurable resins since the solid particles in the powder/resin suspension refract the UV radiation and thus prevent the resin from absorbing enough energy to surpass its critical exposure level. As such, only those ceramics which have refractive indexes close to that of the resin are able to be processed (e.g., alumina, silica, and PZT (Griffith and Halloran, 1996; Hinczewski et al., 1998b)). This large limitation is the primary reason why no SL-based working principle was selected as most-likely-to-succeed.

In direct aqueous inkjet printing, deposition of material occurs by evaporating the solvent from a printed droplet of a dilute (5-14 vol.%) ceramic suspension (Slade and Evans, 1998). While green parts created by this process typically have a volume fraction of 60%, the low solids content of each individual deposition results in layer thicknesses

as small as 0.7 μm (Zhao et al., 2002b). Not only is this process extremely slow (each layer must be thoroughly dried by a hot-air blower for up to 20 seconds), but no depositions of over 1 mm in height have been reported (Zhao et al., 2002b). Thus, in this particular embodiment, the "evaporation" working principle is not a preferred way of realizing ceramic green parts.

It became evident through the selection process that the "cutting and joining" and "joining and cutting" working principles (as seen in the LOM and CAM-LEM processes, Section 4.3.2) were not preferred as they are not efficient methods of creating cellular geometry. This decision is due both to the resultant trapped structural material and the inability to place precut layers that are of the typical topology of cellular mesostructure.

Finally, it should be noted that the "sintering" working principle, although capable of processing many different ceramic materials, is not preferred since heat affected zones caused by thermal processing are difficult to control, which can result in non-uniform depositions, warping, and residual stresses in the final part (Tang, 2002).

Provide New Material & Support Previously Deposited Material

In the context of using AM to fabricate cellular materials, the sub-functions "provide new material" (the manner in which new layers of material are supplied to the process) and "support previously deposited material" (the manner in which deposited material and overhanging geometry are stabilized) are somewhat coupled. The complex internal geometry of cellular materials prohibits the use of an AM technique that constructs support structure that must be manually removed (e.g., the fibrous supports built during stereolithography).

Although the use of a powder bed eliminates the need for support structures as the un-patterned powder can support complex geometry, the un-patterned material can be trapped, or at the least, be very troublesome to remove with specific cellular geometries (e.g., microchannels found in cellular honeycombs, skinned cellular structures, etc.). Therefore, the most appropriate way for the internal voids found in cellular materials to be realized in an AM process is to construct support structures with a separate dissolvable or pyrolizable material (or through processing self-supporting material as seen in the extrusion of colloidal ceramic gels (Smay et al., 2002b)). Examples include Stratasys' WaterWorks™ water soluble support materials for its extrusion process (Stratasys, 2007) and Mott and coauthors' use of a carbon suspension as a fugitive mechanical support in aqueous direct inkjet printing (Mott et al., 1999). Since selective deposition of different materials can only be achieved with direct material addition, this "provide new material" working principle is preferred over those that involve recoating.

Summary

From this analysis, it can be summarized that there exist working principles of each sub-function which are not appropriate for an AM process which is dedicated to the realization of cellular materials. These select principles are highlighted in red in Figure 5.3 along with those principles that are preferred (highlighted in green), and those that are not preferred because they impose minor limitations to the geometries that can be realized (highlighted in yellow).

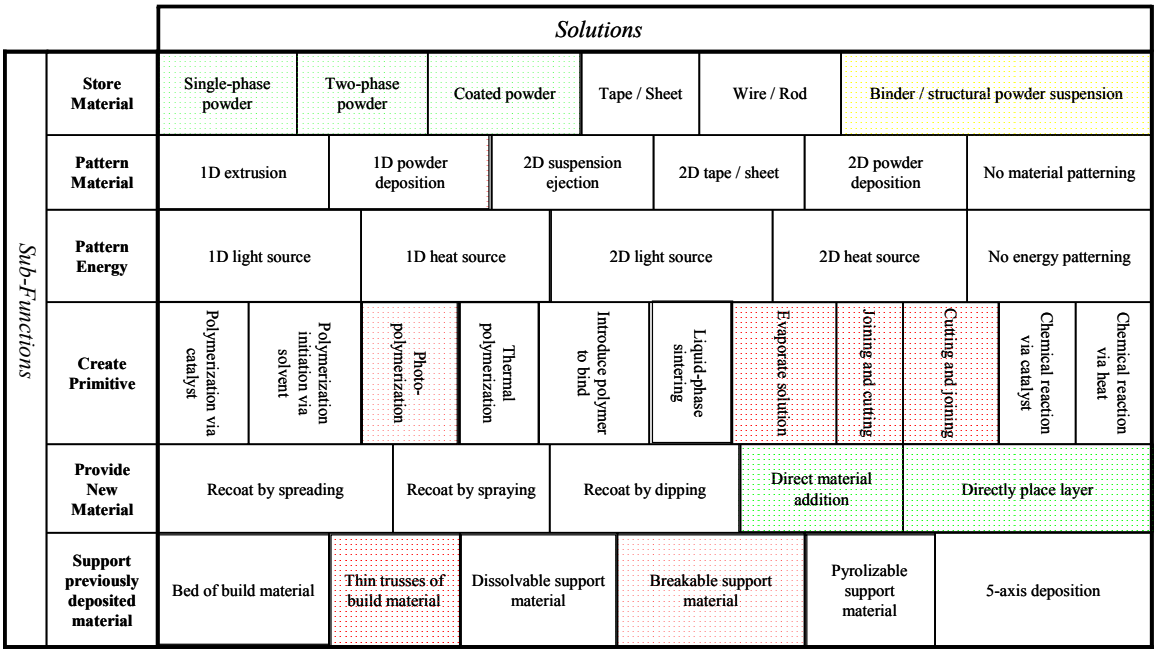

Figure 5.3 – Morphological Matrix with Highlighted Working Principles; (green) preferred, (yellow) not preferred, (red) should be avoided

When the five selected principles' working structures are overlaid onto this color-coded morphological matrix (Figures 5.4 and 5.5), it is clear that none of the five principles are ideal.

With five "most-likely-to-succeed" principles identified, conceptual design can close with the selection of the principal solution for the to-be-designed process. Because none of these five principles is clearly preferred over the other, a systematic selection exercise must be completed in order to identify the preferred tradeoffs between the selection criteria and to select the principal solution.

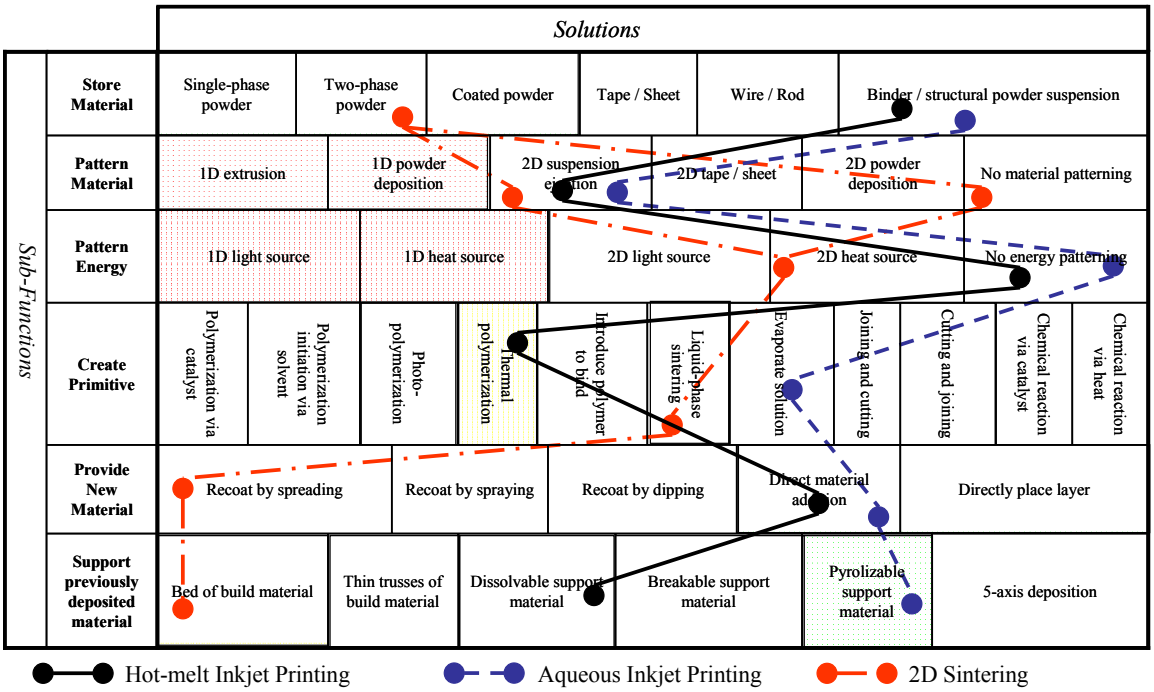

Figure 5.4 – IJP-W, IJP-A, and HSS Working Structures Overlaid on Morphological Matrix with Highlighted Working Principles; (green) preferred, (yellow) not preferred, (red) should be avoided

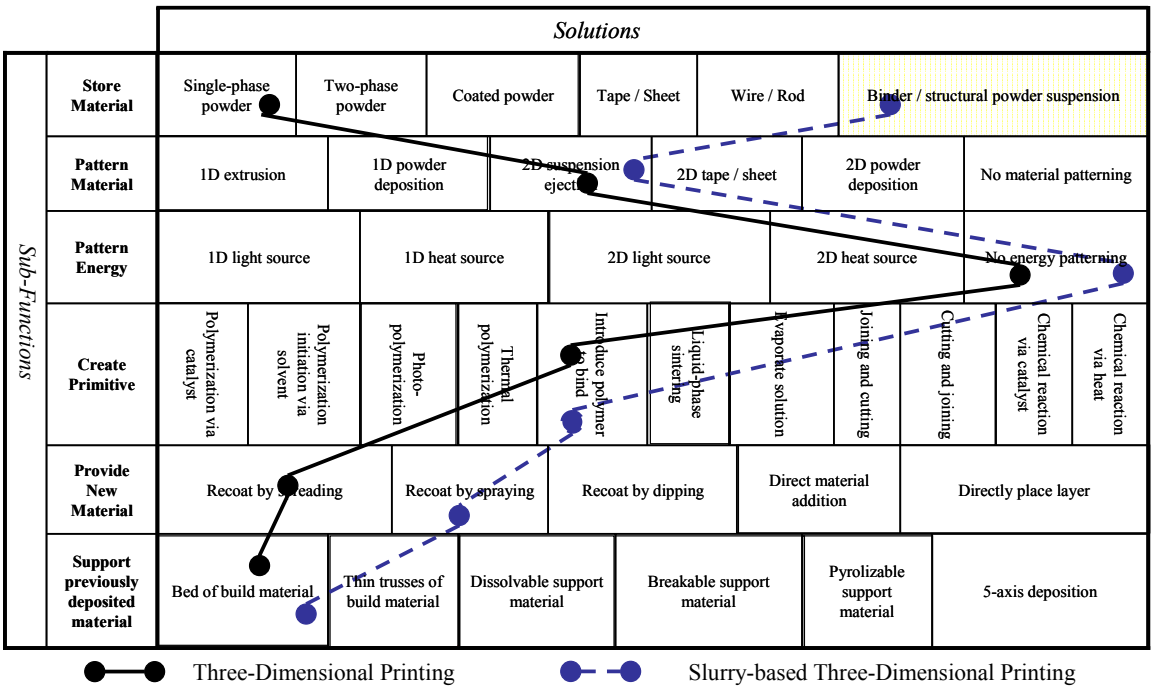

Figure 5.5 – 3DP and S-3DP Working Structures Overlaid on Morphological Matrix with Highlighted Working Principles; (green) preferred, (yellow) not preferred, (red) should be avoided

5.2 SELECTION OF PRINCIPAL SOLUTION

With the "most-likely-to succeed" alternatives identified, the principal solution must be selected. In order to make a selection decision amongst multiple attributes with varying levels of importance, one must quantitatively capture both the science based "hard" engineering information as well as the experience-based "soft" information. Most importantly, a designer needs a framework in which to make a selection decision that takes both types of information into account. Mistree and coauthors propose the selection Decision Support Problem (DSP), a systematic framework for making such selection decisions (Mistree et al., 1994).

5.2.1 The Selection Decision Support Problem

The selection DSP provides a designer a framework in which to identify the "best" concept from a set of feasible working structure alternatives. The selection DSP facilitates the ranking of alternatives based on multiple attributes of varying importance. The order indicates not only the rank by also by how much one alternative is preferred to another. The DSP representing selection is stated as follows:

Given: A set of concepts

Identify: The principal attributes influencing selection.

The relative importance of each attribute.

Rate: The alternatives with respect to each attribute

Rank: The feasible alternatives in order of preference based on the attributes and their relative importance.

The selection DSP consists of six distinct steps:

i) Describe the alternatives and provide acronyms.

ii) Describe each attribute, specify the relative importance of the attributes and provide acronyms

iii) Specify scales, rate the alternatives with respect to each attribute. Justify allocation of ratings.

iv) Normalize the ratings. Identify formula used.

v) Evaluate the merit function for each alternative.

vi) Post-solution sensitivity analysis. Validate/verify decision model and determine change in solution for small changes. Determine the "best" concept.

The first two steps are described in Sections 5.2.2. Step 3 is demonstrated in Section 5.2.3. The merit function is evaluated in Section 5.2.4, and a sensitivity analysis is preformed in Section 5.2.5.

5.2.2 Description of Alternatives and Selection Attributes

Five alternatives were identified at the closure of the preliminary selection exercise: HSS, 3DP, S-3DP, IJP-W, and IJP-A (detailed in Table 5.1). Since it is not immediately clear as to which of these five alternatives is ideal for the specific requirements of this design task, these five alternatives are the focus in the more rigorous selection DSP.

The attributes that have been identified for use in solving the selection DSP are listed in Table 5.9. The list of attributes is based on those used in the preliminary selection exercise (Table 5.2); however, three new attributes are added to better reflect additional design requirements: the effort involved in preparing the raw material (MATPREP), the size of the powder processed (POWSIZ), and the residual stress introduced to the green part by the process (RESTRESS). Furthermore, the material

selection attribute (MATSEL), which represents the number of ceramic materials that are able to processed, has been removed from the list of selection attributes, since each of the alternatives can process any ceramic material. The type of scale used to model each attribute is listed in Table 5.9 along with the preference and the range for each decision.

Table 5.9 – Selection Attributes

Attributes	Acronym	Description	Scale Type	Preference	Range
Cost of technology	TECHCOST	The cost of purchasing and operating the technology.	Ratio	Smaller number	5 – 500 ($k)
Rate of deposition	DEPRATE	The amount of volume deposited per unit time.	Composite (relative importance)	Larger number	0 – 1
Minimum feature size	MINFEAT	The smallest feature able to be produced by the technology	Ratio	Smaller number	10 – 500 (μm)
Complex geometry	COMPGEO	The ability of the technology to create complex geometry (e.g., overhangs and small channels) with minimal post-processing.	Ordinal converted to interval	Larger number	0 - 10
Surface finish	SURFIN	Quality of surface able to be produced by the machine.	Composite (relative importance)	Larger number	0 – 1
Solids loading of green part	GREENLOD	The percentage of the green part volume that is ceramic material.	Ratio	Larger number	10 – 80 (vol %)
Material preparation	MATPREP	The amount of effort to process a new material type	Composite (relative importance)	Larger number	0 - 1
Powder size	POWSIZ	Size of powder that can be processed	Ratio	Smaller number	1 – 100 (μm)
Residual stress	RESTRESS	Residual stresses introduced into green part during fabrication	Composite (relative importance)	Larger number	0 - 1

The relative importance of each attribute is decided by using the comparison method, wherein each attribute's importance is compared quantitatively (1 for more important, 0 for less important, and ½ for equal importance). A dummy attribute is introduced so that the least important attribute exerts some influence on the evaluation of alternatives. Cycling was avoided through careful definition of the "equal preference" measure. The points are totaled and normalized; the attribute which receives the highest

score is the most important attribute. This method of comparison is preferred over simple ranking methods since it reflects the quantitative difference in preference. The relative importance of the attributes is presented in Table 5.10.

Table 5.10 – Relative Importance of Attributes

Attributes	TECHCOST	DEPRATE	MINFEAT	COMPGEO	SURFIN	GREENLOD	MATPREP	POWSIZ	RESTRESS	DUMMY
TECHCOST		1	0.5	1	0	1	0	0	0	0
DEPRATE	0		0	1	0	1	0	0	0	0
MINFEAT	0.5	1		1	0	1	0	0	0	0
COMPGEO	0	0	0		0	1	0	0	0	0
SURFIN	1	1	1	1		1	0.5	0.5	0	0
GREENLOD	0	0	0	0	0		0	0	0	0
MATPREP	1	1	1	1	0.5	1		0.5	0	0
POWSIZ	1	1	1	1	0.5	1	0.5		0	0
RESTRESS	1	1	1	1	1	1	1	1		0
DUMMY	1	1	1	1	1	1	1	1	1	
Sum	5.5	7	5.5	8	3	9	3	3	1	0
Normalized Sum	0.122	0.156	0.122	0.178	0.067	0.200	0.067	0.067	0.022	0.000
Rank	4	3	4	2	6	1	6	6	9	10

After much deliberation, it is determined that the solids loading of the green part (GREENLOD) is the most important attribute for the to-be-designed AM process. A large solids loading has the most influence on the quality of the finished part – poor solids loading can lead to significant shrinkage, warping, cracking, and porosity, which leads to poor mechanical properties. The ability to produce complex geometry (COMPGEO) is extremely important as well; the ability to fabricate cellular materials is the prime objective of this AM process. The ability to deposit primitives/layers quickly (DEPRATE) is deemed slightly more important than the cost of the technology (TECHCOST) since a high deposition rate will inherently reduce the cost of production in the long term future of the to-be-designed-machine. Finally, surface finish (SURFIN), material preparation time (MATPREP), powder size (POWSIZ), and residual stress introduced to the green part during fabrication (RESTRESS), were deemed to be relatively insignificant as they reflect secondary (or tertiary) requirements.

5.2.3 Specification of Scales and Rating of Alternatives

One way in which the selection DSP differs from the preliminary selection DSP is that a designer is able to make decisions with both "hard" and "soft" engineering data. This is important in the selection of the alternatives presented as each of them currently exist in various stages of development. 3DP and IJP-W, for example, have been commercially offered for several years (although a ceramic option in either has not). This contrasts greatly with HSS, which has only recently been introduced to the research community, and has yet to be used to process ceramics.

In order to cope with these varying fidelities of information and still be able to make rigorous and methodical selection decisions, a variety of scales are used. The attributes describing technology cost (TECHCOST), minimum feature size (MINFEAT), green part solids loading (GREENLOD), and powder size (POWSIZ) are measured in physical units, and are therefore evaluated using a ratio scale. The attributes which describe deposition rate (DEPRATE) and surface finish (SURFIN) can also be measured in physical units; however, because there is not any "hard" engineering data available in the literature for all five alternatives, a composite scale is used. A composite scale is also used for the evaluation of the SURFIN, MATPREP, and RESTRESS attributes. A composite scale is used instead of a simple interval ranking scale because it can be used to model the collective preference associated with a number of related sub-attributes. The ability of the process to fabricate complex cellular geometry, COMPGEO, is judged using an ordinal converted to interval scale. This is used because it is possible for the designer to articulate a definite and measurable degree of preference for the various alternatives with this somewhat qualitative attribute.

With the scales specified, the alternatives can now be rated with respect to each attribute.

Composite Attribute Ratings for DEPRATE

The ratings for the DEPRATE attribute are presented in Table 5.11.

Table 5.11 – Composite Attribute Ratings for DEPRATE

Alternatives	**HSS**	**3DP**	**S-3DP**	**IJP-W**	**IJP-A**	**Dummy**
HSS		0.5	0	0.5	0	0
3DP	0.5		0	0.5	0	0
S-3DP	1	1		1	0	0
IJP-W	0.5	0.5	0		0	0
IJP-A	1	1	1	1		0
Dummy	1	1	1	1	1	
Sum	4	4	2	4	1	0
Normalized Sum	0.267	0.267	0.133	0.267	0.067	0.000
Rank	1	1	4	1	5	6

The use of a composite scale allows for the display of equal preference for 3DP, IJP-W, and HSS. IJP-A and S-3DP have very slow build rates due to their need for a drying cycle for each layer. Furthermore, the IJP-A process has a very small primitive size, thus increasing the overall build time of an entire part. IJP-W should be faster than HSS and 3DP because it does not require extra recoating passes after each layer; however, it is slowed by the need to heat the build chamber prior to fabrication – thus the three are deemed equal in this attribute.

Interval Scale Ratings for COMPGEO

The interval scale used for rating the five alternatives for the COMPGEO attribute is presented in Table 5.12. The different levels in the scale allow a designer to distinguish between those alternatives which can provide complex mesostructure and the amount of post-processing effort needed.

Table 5.12 – Ordinal – Interval Scale for COMPGEO

Ordinal Scale	Description	Rating
Complex; No Post-Processing	Can meet all established mesostructure requirements (small cells and walls, overhanging structure, etc.) with no post-processing.	10
Complex; Minor Post-Processing	Can meet majority of mesostructure requirements with minor post-processing.	7
Average Complexity	Can meet some mesostructure requirements with significant post-processing effort.	4
No Complexity	Cannot realize green parts featuring cellular mesostructure	1

The resultant ratings are presented in Table 5.16. IJP-W is deemed to have the highest rating because it can create complex geometry with the aid of a sacrificial support material which can easily be removed through pyrolysis. A sacrificial support can also be introduced in the IJP-A process; however, because it has yet to be used to fabricate a finished part over 2 mm (Section 4.5.1), it is given a very low rating in this attribute. Similarly, while S-3DP is capable of creating complex cellular mesostructure, it is given a low rating because it is impossible to retrieve the finished part from the dried slip-cast material bed. 3DP and HSS are given moderate ratings due their ability to fabricate parts of cellular mesostructure with the aide of a post-processing (removal of unpatterned powder).

Composite Attribute Ratings for SURFIN

The ratings for the SURFIN attribute are presented in Table 5.13. IJP-A is deemed to offer the best surface finish because of its extremely small primitives. IJP-W and S-3DP are rated higher than HSS and 3DP because shaping primitives with a suspension generally result in a better surface finish than working with dry powders.

Composite Attribute Rating for MATPREP

The ratings for the MATPREP attribute are presented in Table 5.14. HSS and 3DP, as powder-based technologies, are chosen as the top alternatives with respect to this

rating, as the other alternatives require copious amounts of effort in successfully suspending ceramic powders.

Table 5.13 – Composite Attribute Ratings for SURFIN

Alternatives	HSS	3DP	S-3DP	IJP-W	IJP-A	Dummy
HSS		0.5	1	1	1	0
3DP	0.5		1	1	1	0
S-3DP	0	0		0	1	0
IJP-W	0	0	1		1	0
IJP-A	0	0	0	0		0
Dummy	1	1	1	1	1	
Sum	1.5	1.5	4	3	5	0
Normalized Sum	0.100	0.100	0.267	0.200	0.333	0.000
Rank	4	4	2	3	1	6

Table 5.14 – Composite Attribute Ratings for MATPREP

Alternatives	HSS	3DP	S-3DP	IJP-W	IJP-A	Dummy
HSS		0.5	0	0	0	0
3DP	0.5		0	0	0	0
S-3DP	1	1		0	0	0
IJP-W	1	1	1		0	0
IJP-A	1	1	1	1		0
Dummy	1	1	1	1	1	
Sum	4.5	4.5	3	2	1	0
Normalized Sum	0.300	0.300	0.200	0.133	0.067	0.000
Rank	1	1	3	4	5	6

Composite Attribute Rating for RESTRESS

The ratings for the RESTRESS attribute are presented in Table 5.15. The one alternative which could potentially introduce residual stresses into the green part is HSS due to its use of thermal energy to create primitives.

Rating of Alternatives

The attribute ratings, the bounds, the type of scale, and the preference for higher or lower numbers for each alternative are shown in Table 5.16. The values used in the ratio scales for the TECHCOST, MINFEAT, GREENLOD, and POWSIZ attributes are provided in the description of each alternative in Chapter 4.

Table 5.15 – Composite Attribute Ratings for RESTRESS

Attributes	HSS	3DP	S-3DP	IJP-W	IJP-A	Dummy
HSS		1	1	1	1	0
3DP	0		0.5	0.5	0.5	0
S-3DP	0	0.5		0.5	0.5	0
IJP-W	0	0.5	0.5		0.5	0
IJP-A	0	0.5	0.5	0.5		0
Dummy	1	1	1	1	1	
Sum	1	3.5	3.5	3.5	3.5	0
Normalized Sum	0.067	0.233	0.233	0.233	0.233	0.000
Rank	5	1	1	1	1	6

Table 5.16 – Attribute Ratings (A_{ij})

	Attributes								
Alternatives	TECHCOST	DEPRATE	MINFEAT	COMPGEO	SURFIN	GREENLOD	MATPREP	POWSIZ	RESTRESS
HSS	140	0.27	100	6	0.10	50	0.30	25	0.07
3DP	30	0.27	100	6	0.10	55	0.30	25	0.23
S-3DP	35	0.13	150	2	0.27	65	0.20	10	0.23
IJP-W	40	0.27	150	9	0.20	35	0.13	1	0.23
IJP-A	35	0.07	30	2	0.33	65	0.07	1	0.23
Type	R	I	R	O - I	I	R	I	R	I
Preference	L	H	L	H	H	H	H	L	H
Upper Bound	500	1	500	10	1	80	1	100	1
Lower Bound	5	0	10	0	0	10	0	1	0
Units	k$	None	μm	None	None	vol %	None	μm	None

Normalization of Alternatives

The various attribute ratings, A_{ij}, are on scales that are not uniform. For example, for some attributes a larger rating would indicate a preference whereas for others a lower rating would indicate preference. Furthermore, the upper and lower bounds on the scales are not the same. Therefore, it is necessary to convert the attribute ratings to scales that are uniform. This is achieved by converting the attribute rating to a normalized rating, R_{ij}. The normalized scales range from 0 to 1 with a higher number indicating a preference.

For those attributes in which preference is indicated by larger numbers, Equation 5.1 is used to normalize the value.

$$R_{ij} = \frac{A_{ij} - A_j \min}{A_j \max - A_j \min} \qquad [5.1]$$

For those attributes in which preference is indicated by smaller numbers (e.g., TECHCOST, MINFEAT, and POWSIZ), Equation 5.2 is used to normalize the value.

$$R_{ij} = 1 - \frac{A_{ij} - A_j \min}{A_j \max - A_j \min} \qquad [5.2]$$

In Equations 5.1 and 5.2, the variable *i* represents the alternative and the variable *j* represents the attribute.

The normalized attribute ratings are presented in Table 5.17.

Table 5.17 - Normalized Attribute Ratings (R_{ij})

	Attributes								
Alternatives	TECHCOST	DEPRATE	MINFEAT	COMPGEO	SURFIN	GREENLOD	MATPREP	POWSIZ	RESTRESS
HSS	0.73	0.27	0.82	0.60	0.10	0.57	0.30	0.76	0.07
3DP	0.95	0.27	0.82	0.60	0.10	0.64	0.30	0.76	0.23
S-3DP	0.94	0.13	0.71	0.20	0.27	0.79	0.20	0.91	0.23
IJP-W	0.93	0.27	0.71	0.90	0.20	0.36	0.13	1.00	0.23
IJP-A	0.94	0.07	0.96	0.20	0.33	0.79	0.07	1.00	0.23

5.2.4 Evaluation of Merit Function

The merit function values are calculated using Equation 5.3, the normalized ratings (Table 5.17), and the normalized relative weights of the attributes (Table 5.10). Equation 5.3 is presented as

$$MF_i = \sum_{j=1}^{n} I_j R_{ij} \qquad i = i, \ldots, m \qquad [5.3]$$

where:

m = number of alternatives

n = number of attributes

I_j = relative importance of j^{th} attribute

R_{ij} = rating of alternative i for the attribute j

MF_i = value of merit function for alternative *i*

The merit function values are presented together in Table 5.18. The merit function values are altered +/- 5% to investigate their proximity to one another. From this exercise it is seen that all of the merit function values for each alternative are very close to one another; specifically, aside from S-3DP, all alternatives' merit function values overlap the highest value (0.575 of 3DP) within a 5% differential.

Table 5.18 – Merit Function Values and Final Rankings for the Alternatives

Alternatives	Merit Function Values	5% Increase	5% Decrease
HSS	0.530	0.556	0.503
3DP	0.575	0.604	0.546
S-3DP	0.512	0.538	0.487
IJP-W	0.568	0.596	0.539
IJP-A	0.534	0.560	0.507

It is observed from Table 5.18 that the 3DP and IJP-W alternatives have the highest merit function values, although the difference in these values is very small (1.2%); thus further analysis is needed to select the principal solution.

5.2.5 Sensitivity Analysis

In order to assist in the completion of the selection decision, a sensitivity analysis is performed in order to determine the effect on the solution due to small changes in the values of the relative importances and also to changes in the attribute ratings.

Sensitivity of Solution to Changes in Attribute Importance

To evaluate the sensitivity of the solution to changes in the relative importance of the attributes the following steps are followed:

- The top two alternatives are identified for further analysis (3DP & IJP-W)

- The relative importance of each attribute is increased or decreased by 5% so as to affect the merit function of the second ranked alternative (IJP-W) favorably with respect to the first ranked alternative (3DP)
- The revised merit functions are then computed

As per the attribute ratings presented in Table 5.17, for those attributes in which IJP-W is rated higher than 3DP (COMPGEO, SURFIN, & POWSIZE), the relative importance of the attribute (presented in Table 5.10) is increased by 5%. Similarly, the relative importance of those attributes in which IJP-W is rated lower than 3DP are decreased by 5%.

Table 5.19 – Merit Function Values When Attributes Changed in Favor of IJP-W

Alternatives	Merit Function Values	5% Increase	5% Decrease
HSS	0.522	0.548	0.496
3DP	0.565	0.593	0.537
S-3DP	0.500	0.525	0.475
IJP-W	0.566	0.594	0.538
IJP-A	0.520	0.546	0.494

From this exercise it is clear that the 3DP and IJP-W alternatives can almost be considered equivalent.

Sensitivity of Solution to Changes in Alternative Ratings

To evaluate the sensitivity of the solution to changes in the ratings of the alternatives in each attribute, the following steps are followed:

- The top two alternatives are identified for further analysis (3DP & IJP-W)
- The rating of each attribute *i,j* is changed by +/- 5% and the merit function is recalculated.

The results from changing each attribute rating for every alternative is presented in Table 5.20. The attribute rating changes to the 3DP (-5%) and the IJP-W (+5%) are highlighted.

Table 5.20 – Merit Function Values for 5% Change in Alternative Ratings

	HSS	HSS	3DP	3DP	S-3DP	S-3DP	IJP-W	IJP-W	IJP-A	IJP-A
Attributes	5%	-5%	5%	-5%	5%	-5%	5%	-5%	5%	-5%
TECHCOST	0.534	0.525	0.581	0.569	0.519	0.507	0.572	0.561	0.540	0.528
DEPRATE	0.532	0.528	0.577	0.573	0.514	0.512	0.569	0.565	0.535	0.533
MINFEAT	0.535	0.525	0.580	0.570	0.517	0.508	0.571	0.562	0.540	0.528
COMPGEO	0.535	0.525	0.581	0.570	0.515	0.511	0.575	0.559	0.536	0.532
SURFIN	0.530	0.530	0.576	0.575	0.514	0.512	0.567	0.566	0.535	0.533
GREENLOD	0.536	0.524	0.582	0.569	0.521	0.505	0.570	0.563	0.542	0.526
MATPREP	0.531	0.529	0.576	0.574	0.513	0.512	0.567	0.566	0.534	0.534
POWSIZ	0.532	0.527	0.578	0.573	0.516	0.510	0.570	0.563	0.537	0.531
RESTRESS	0.530	0.530	0.576	0.575	0.513	0.513	0.567	0.566	0.534	0.534
Max / Min	0.536	0.524	0.582	0.569	0.521	0.505	0.575	0.559	0.542	0.526

From this data, it can be observed that IJP-W is the preferred selection when changes to the TECHCOST and COMPGEO ratings. The results of Table 5.20 are shown graphically in Figure 5.6. It is important to observe that the best merit function value for IJP-W (a 5% increase to the COMPGEO attribute rating) is equal to the unaltered merit function value of 3DP (0.575).

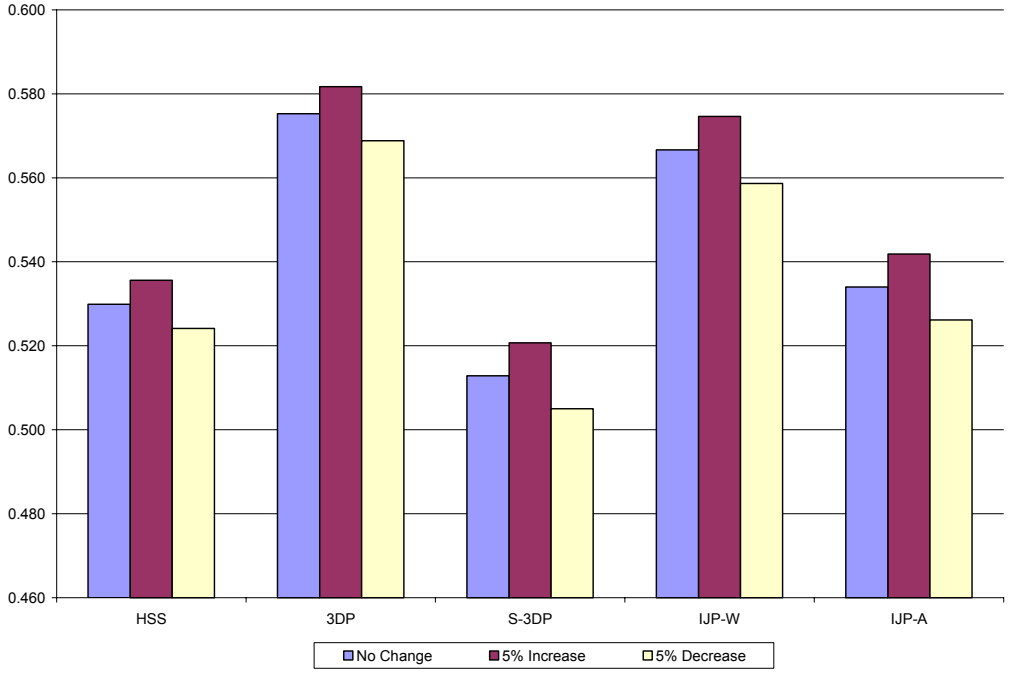

Figure 5.6 – Variations in Merit Function Values

5.2.6 Post-Solution Analysis: Lessons Learned

The selection DSP is a decision framework that is used to assist a designer in making a selection decision amongst several alternatives that are identified as "likely to succeed." After taking into account both hard and soft engineering data, and modeling a designer's preferences for the relative importance of the attributes, it is observed that IJP-W and 3DP are equally appropriate for the design requirements established in Chapter 3. Furthermore, there is little to distinguish these two alternatives, even following a sensitivity analysis. How can this issue be resolved? How can a decision be made?

In an effort to answer these questions, the results are further investigated:

- It is odd that the merit function values for the IJP-A and S-3DP alternatives are so relatively similar to that of IJP-W and 3DP. While the results are not mathematically incorrect (the high solids loading offered by these alternatives compensates for their other deficiencies), they do not accurately represent a designer's intuition – these alternatives' COMPGEO ratings are so low, that they should not even be considered as feasible alternatives. Thus, it is possible that the COMPGEO attribute should be weighted in a different manner so as to heavily penalize the inability to create parts of cellular mesostructure.
- Similarly, the GREENLOD attribute should be altered so as to place more preference for higher solids loading – it is very difficult to achieve full density from a green part with a solids loading of less than 45 vol%, thus IJP-W should be penalized much more for its solids loading of 35 vol%.
- It is clear that the solids loading limitation of the IJP-W process is its greatest fault. If this attribute could be improved, IJP-W would be the clear choice as it

offers the ability to make complex geometry with minor post-processing, parts with good surface finish, and with an economically scalable technology. Such an improvement is not possible, however, because of the physical limitations that exist on jetting viscous, highly-loaded ceramic suspensions. It is doubtful that a jetted suspension could ever result in a green part with a solids loading greater than that which can be achieved using a dry powder bed.

Ideally, with an infinite amount of time and resources, further engineering investigation would be expended in order to make a more informed decision. However, with the information available to the author, it is decided that the IJP-W alternative is the inferior alternative because of its aforementioned solids loading limitation. The 3DP alternative offers a much higher solids loading in its green parts and is capable of producing complex cellular mesostructure with only a slight limitation in cell size caused by the use of a powder bed. It is also a very economically scalable technology and is able to process any ceramic material with very little pre-processing.

5.3 DISSERTATION ROADMAP

Following the critical analysis of current cellular material manufacturing technologies (Chapter 1), the following primary research question was posed:

Primary Research Question:

How to manufacture three-dimensional, low-density cellular metal structures while maintaining designer freedom in the selection of the material and the design of the part mesostructure and macrostructure?

Following a critical analysis of the existing manufacturing techniques which can fabricate materials of designed mesostructure (including direct-metal additive manufacturing approaches), the following primary research hypothesis was offered in Chapter 2:

Primary Research Hypothesis:

Three-dimensional, low-density cellular metal structures of any macrostructure, mesostructure, or material can be manufactured via layer-based additive manufacturing of metal-oxide ceramic material followed by post-processing in a reducing atmosphere.

With the conceptual design portion of the design phase of this research complete (Chapters 3 and 4), the primary research hypothesis can now be updated to reflect the selection of the principal solution (as determined in Chapter 5):

Updated Primary Research Hypothesis:

Three-dimensional, low-density cellular metal structures of any macrostructure, mesostructure, or material can be manufactured via three-dimensional printing of metal-oxide ceramic powder followed by post-processing in a reducing atmosphere.

With the design phase of this research complete, the embodiment and analysis of the selected solution principle can now begin. As can be seen in Figure 5.7, the primary research hypothesis is verified through the use of three-dimensional printing to create green parts and reduction post-processing to create metal cellular parts of designed mesostructure in Chapter 6.

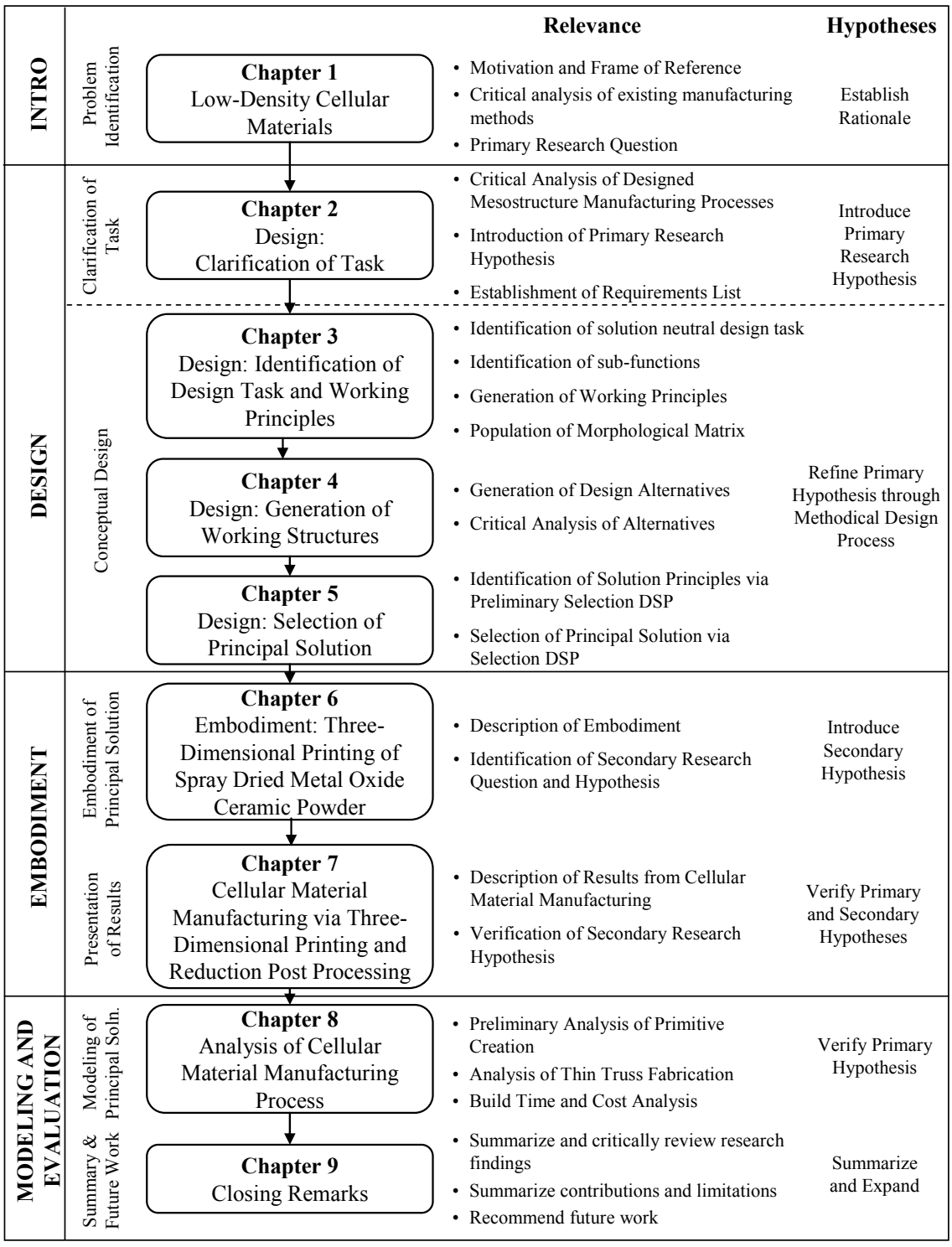

Figure 5.7 – Dissertation Roadmap

CHAPTER 6

EMBODIMENT: THREE-DIMENSIONAL PRINTING OF SPRAY DRIED METAL OXIDE CERAMIC POWDER

With the conceptual design process complete and a principal solution selected, the embodiment phase of the research can begin. In this chapter the details of the embodiment of the principal solution, three-dimensional printing (3DP), are described. This description entails a presentation of the manner in which the commercial 3DP process is altered in order to be suitable for the specific intent of manufacturing cellular materials, as indicated by the design requirements identified in Chapter 3. From this embodiment effort, a secondary research question and hypothesis concerning improving finished part density are introduced. In Section 6.2, the specific concrete embodiment details (e.g., machine, material, and post-processing specifications) are presented. This description of embodiment also serves as the detailing of the experimental setup used to verify the research hypotheses (Chapter 7).

6.1 ADAPTING THE THREE-DIMENSIONAL PRINTING PROCESS FOR THE CREATION OF GREEN CERAMIC PARTS OF DESIGNED MESOSTRUCTURE

The solution principle selected at the closure of the conceptual design phase, three-dimensional printing (3DP), is described in Section 4.4.1 and is shown graphically in the context of a morphological matrix in Figure 6.1.

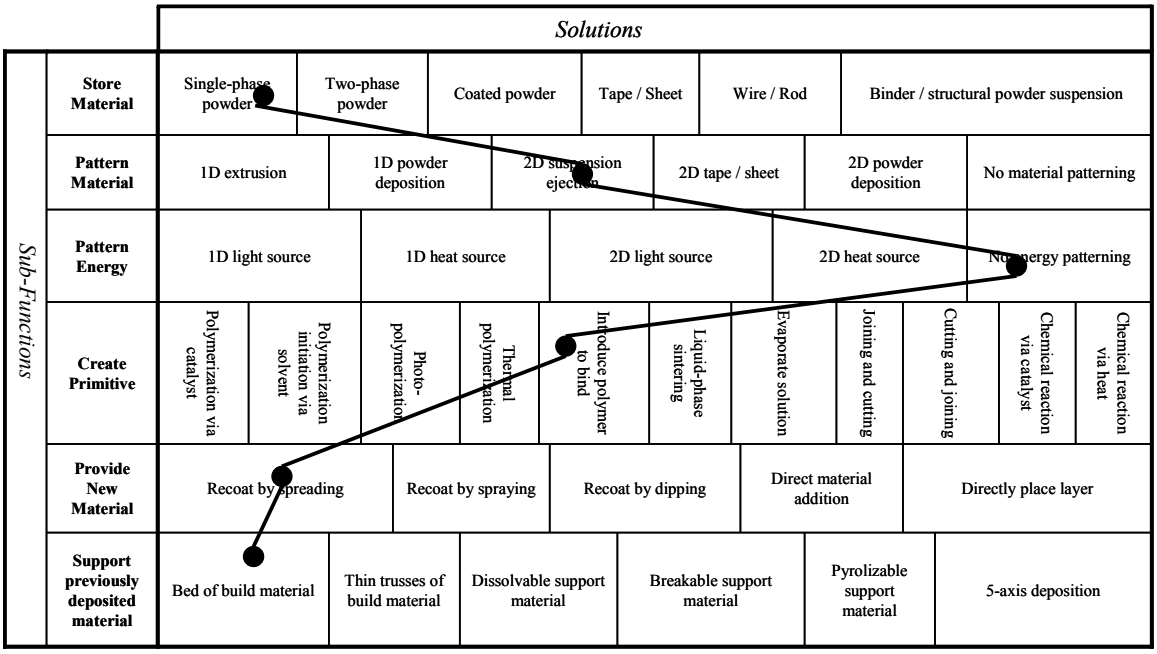

Figure 6.1 – Three-Dimensional Printing Solution Principle

The embodiment phase of the design process, as described by Pahl and Beitz, focuses in the configuration of the working principles (size, shape, arrangement, etc.) of the selected principal solution. This approach, meant for usage in "original design" scenarios is not appropriate for this research task because the selected solution principle has been embodied commercially (Sachs et al., 1993b). As such, the embodiment effort in this research is centered in "adaptive design," which entails adapting the embodiment of known working principles for new and/or changed design requirements. Commercially available 3DP technologies were primarily designed to process plaster-based powder systems for the realization for a wide variety of part geometries, thus opportunities exist for the adaptation of the embodiment of 3DP for the fabrication of metal-oxide ceramic green parts of cellular mesostructure. These opportunities can be identified by exploring the further investigation of the working principle employed by each sub-function.

6.1.1 Store Material

As discussed in Section 5.1.6, the working principle chosen for the "store material" sub-function can have a significant impact on the ability of an AM process to fabricate ceramic green parts with a high solids loading. The raw material processed in 3DP is dry powder, which is the preferred working principle for this sub-function, as it is possible to get a high solids loading in the green part and also has minimal material pre-processing needs (i.e., doesn't require colloidal chemistry know-how to create a finely tuned suspension). This preference is shown graphically in Figure 6.2 by the green shading applied to the powder-based working principles (adapted from Figure 5.5).

Store Material	Single-phase powder	Two-phase powder	Coated powder	Tape / Sheet	Wire / Rod	Binder / structural powder suspension

Figure 6.2 – Preferred Working Principles for "Store Material" Sub-Function (adapted from Figure 5.5)

There are two decisions to be made in the embodiment of this sub-function: (i) the morphology of the powder particles, and (ii) the selection of one of the three powder-based working principles – single-phase powder, a mixture of powder and binder particles (two-phase powder), or powder coated with a binder material (coated powder).

The powder morphology decision includes the selection of the size, shape, and size distribution of the powder particles. This series of decisions not only directly affects the density of the green parts that can be fabricated by the process, but it also affects the parts' surface finish and minimum feature size. The following characteristics are desired for processing green parts from ceramic powder via 3DP:

- *Particle size*: Generally, in ceramics processing, fine particles are preferred over coarse particles because they have better sintering characteristics, which result in a finished part with a higher relative density and better material properties. In the context of 3DP, fine particles are preferred because their use ensures a better surface finish, smaller features, and a smaller z-resolution (layer thickness) (Lanzetta and Sachs, 2003). Due to its recoating process, however, 3DP cannot process dry powders with particle size less than 20 μm (Sachs et al., 1993b). Many possible deposition mechanisms are possible for dry powders but most require that the powder flow easily when only a small amount of shear is applied. While this kind of flow behavior is characteristic of granulated powders or where the particle size is ~ 50 μm, the flow of finer particles is dominated by interparticle forces (due to their high surface area) which produce aggregates of particles and prevent their free motion (Sachs et al., 1992). In the context of 3DP, this results in layers filled with defects upon recoating the powder bed (Yoo et al., 1993). Furthermore, a powder bed composed of fine particles is also susceptible to ballistic ejection (resulting in the cutting of a trench through the bed) due to the large kinetic energy of the deposited binder droplets in the 3DP process.
- *Size distribution*: The powder bed of 3DP could be characterized as "loose random packing" (as opposed to "dense random packing") because the powder bed is not vibrated after the deposition of each layer to maximize settling and minimize porosity. This packing configuration can have packing densities in the range of 0.57 – 0.61 with monosized particles. As known from traditional

ceramic powder processing, the distribution of the size of the powder particles is a key variable for increasing the powder bed density. A continuous distribution between minimum and maximum particle sizes can significantly increase packing density due to the fine particles filling the interstitials of the coarse particles (Rahaman, 2003). Generally, it is preferred to have a wide distribution of particle sizes; however, as the width of particle size distributions increases, the scale over which density fluctuations occur also increases – this is crucial as packing uniformity is an important aspect of good sintering characteristics (shrinkage control and the prevention of the formation of defects in the final component) (Yoo et al., 1993). Furthermore, it is known that little is gained beyond the use of ternary mixtures because fine particles do not locate into their ideal positions to maximize the packing density (Rahaman, 2003). Lanzetta and Sachs have shown the use of bimodal powders (a 25 wt% addition of fine particles to coarse powder) to significantly increase the packing density and the surface finish of parts created by 3DP (Lanzetta and Sachs, 2003).

- *Particle shape*: Generally, smooth, spherical particles are preferred in 3DP because they are easier to recoat; their smooth surfaces lead to high flowability and reduced interparticle friction. High flowability also leads to a higher powder bed density. The ability of spherical particles to pack together well also results in high quality surface finishes for 3DP-created parts (Lanzetta and Sachs, 2003). Furthermore, spherical powders require much less binder to form a solid deposit than other particle shapes since the necks between the particles have small area and only small amounts of binder are required per neck to

effectively bond the particles (i.e., for a given amount of binder, spherical particles result in a larger primitive) (Cima et al., 1992). While the use of faceted powders in the 3DP process may result in smaller features, the large particle rearrangement that results from the introduction of a binder droplet (due to the low packing density) could cause a large amount of linear shrinkage and poor dimensional control.

From the above list it is clear that fine, spherical powder particles, with a moderate range in size distribution are the preferred embodiment for this working principle. However, as stated above, it is not possible to process fine dry particles with the standard 3DP "single-phase powder" embodiment. Large powder sizes (> 20 μm) have been used in the 3DP process but resulted in green parts featuring only 35% solids loading (Yoo et al., 1993).

The incongruity that exists between the requirement for fine particles and the inability to process them via the chosen principal solution provides an opportunity for the formulation of a secondary research question:

Secondary Research Question:

How can the density of metal parts created by the thermal-chemical conversion of ceramic green parts fabricated by three-dimensional printing be improved?

A corresponding research hypothesis can be formulated through further investigation of the available working principles for the "store material" sub-function.

The 3DP process has been augmented to process fine particles by working with a suspension of ceramic powder and binder (S-3DP), described in Section 4.4.2. S-3DP

has been used to create parts with a green part density of up to 67% and z-resolution as small as 10 μm. Of course, as stated in Section 5.1.6, this embodiment cannot be used to realize cellular materials because delicate features cannot be retrieved from the dried slip and the build time is extremely slow due to the need to deposit and dry each layer. (Moon et al., 2000).

As described in Section 3.3.1, the "two-phase powder" working principle features the mixture of binder particles with structural ceramic particles. This working principle has been incorporated in 3DP processing by Utela and coauthors (Utela et al., 2006). Specifically, they combine powdered acetate alumoxane with powdered alumina in a 3DP powder bed and activate the in-bed binder by selectively printing a mixture of water and isoproponal (Utela et al., 2006). Unfortunately, this working principle does nothing to alleviate 3DP's inability to process fine powders. Furthermore, Beaman and coauthors note that simply mixing two materials together can potentially lead to highly variable powder and part properties since mixed materials can segregate by density (Beaman et al., 1997).

The final powder-based working principle listed in Figure 6.2, "coated powder," describes coating the structural ceramic material with secondary binder material. Solid primitives can be made from this raw material by either printing a binder material into the powder bed, or by activating the binder that is coating the structural material. Coated powders are preferred over simple two-phase mixtures because powder bed homogeneity is assured. Furthermore, in Laser Sintering, the strength of green parts made from coated particles has been shown to be higher than that of parts made using a powder mixture at the same polymer content (Badrinarayan and Barlow, 1991).

In the context of the secondary research question, coated powders present a significant advantage because it is possible to combine several fine particles into a single granule via coating with a binder material. This can be achieved via spray drying. Illustrated in Figure 6.3, spray-drying is the process of spraying a slurry composed of fine powder particles and a binder into a warm drying medium to produce powder granules that are relatively homogeneous (Reed, 1995).

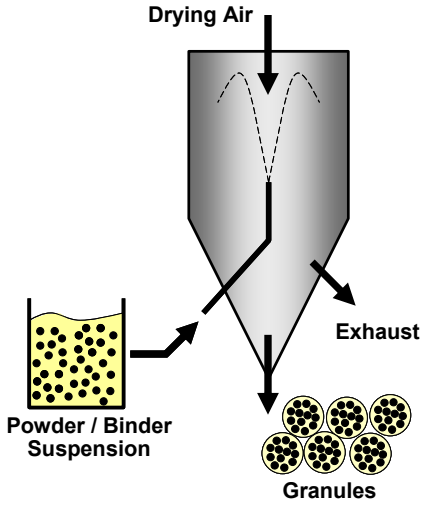

Figure 6.3 – Illustration of Spray-Drying Process

The use of spray-dried granules make it possible to work with fine particles (~60 vol.%, 1 – 5 μm ceramic particles per granule) thus improving sintering, decreasing porosity, and decreasing grain size in the finished part. Furthermore, spray-dried granules are nearly spherical and typically on the order of 30 μm in diameter; therefore they flow very well and are easily recoated in the 3DP process (Cima et al., 1995). While the porous nature of spray-dried granules is detrimental in that it slightly decreases the solids loading possible for a green part, it is beneficial for the manufacture of cellular materials since smaller printed primitives result from the increased absorption of the jetted binder (Cima et al., 1992). For these reasons, "coated powder" is chosen as the embodiment for the

"store material" sub-function. It should be noted, however, that Cima and coauthors warn that, while fine powders can be used in the form of spray-dried granules, one should be wary of the large shrinkage that accompanies their use (Cima et al., 1995).

6.1.2 Pattern Material

One of the primary reasons why 3DP was selected as the principal solution for the identified design task is its ability to quickly create primitives due to its two-dimensional patterning technique (the preferred class of working principles, as shown in Figure 6.4 and described in Section 5.1.6).

Pattern Material	1D extrusion	1D powder deposition	2D suspension ejection	2D tape / sheet	2D powder deposition	No material patterning
Pattern Energy	1D light source	1D heat source	2D light source		2D heat source	No energy patterning

Figure 6.4 – Preferred Working Principles for "Patterning" Sub-Functions (adapted from Figure 5.5)

The inkjet printing process employed by the 3DP process is preferred not only because it is capable of rapidly creating solid primitives, but because it is capable of doing so cost-effectively and in a manner which can readily be scaled for larger applications. The embodiment decision that must be made for this sub-function is the determination of the type of jetting technology to be used. As described in Section 4.5.1, there are two different existing embodiments of the inkjet printing concept: continuous jetting and drop-on-demand (DoD) jetting.

Continuous inkjet technology is characterized by electrically charging a continuous stream of ink droplets that have been ejected from a pressurized fine nozzle (Sirringhaus and Shimoda, 2003). The droplets acquire their charge from a high-voltage electric field;

depending on the charge they have acquired, they are either deflected toward the substrate, or into an ink collection and recirculation system (Song et al., 1999).

In piezoelectric DoD printing, a pressure wave in the ink chamber is generated by applying a voltage pulse to a piezoelectric stack or plate, resulting in the formation of droplets at the nozzles (Sirringhaus and Shimoda, 2003). The pressure pulse ejects drops from an open orifice, which normally contains the liquid by surface tension. In contrast to continuous printing, droplets are formed only when individual pressure pulses in the nozzle cause the fluid to be expelled, and spatial control is achieved by mechanically positioning the print head above the desired location before drop ejection (Derby and Reis, 2003a).

Continuous printers offer a higher rate of deposition than DoD printers and require less energy to form a drop (Song et al., 1999). However, the inks used in continuous printing must be capable of conducting an electrical charge. Furthermore, DoD printheads yield smaller drops (droplet size of continuous = $2d_{orifice}$; droplet size of DoD = $d_{orifice}$), allowing a higher process resolution than the continuous jet. Another advantage of the DoD technology is that it has a better performance in vector printing; the execution of curved trajectories and the associated speed changes require controlling the drop frequency in a wide range, which is only possible with DoD (Lanzetta and Sachs, 2003). For these reasons DoD printing is chosen as the embodiment for the "2D Material Patterning" working principle.

6.1.3 Create Primitive

One of the key advantages of the 3DP process (and other powder-based processes) is its ability to process almost any ceramic material. This ability stems primarily from the

manner in which it creates solid primitives – the selective application of binder into a powder bed. As described in Section 5.1.6 (and shown in Figure 6.5), this working principle is preferred because it is economically scalable (does not require high amounts of energy or an expensive piece of equipment and is relatively fast), does not introduce residual stress to the green part during fabrication (as is done in thermal energy-based principles), and is easily adapted to other materials.

Create Primitive	Polymerization via catalyst	Polymerization initiation via solvent	Photo-polymerization	Thermal polymerization	Introduce polymer to bind	Liquid-phase sintering	Evaporate solution	Joining and cutting	Cutting and joining	Chemical reaction via catalyst	Chemical reaction via heat

Figure 6.5 – Preferred Working Principles for "Create Primitive" Sub-Function (adapted from Figure 5.5)

The successful embodiment of this working principle requires several decisions. The primary decision is the selection of the material that is to be printed. More detail-oriented decisions include printing process parameters such as droplet size, viscosity, surface tension, and impact velocity, as well as deposition frequency and printhead scan speed. These decisions are important since the geometry of the solid primitives created by 3DP are influenced by the microstructure and surface finishes of the powder bed as well as physical properties of the binder and printing conditions (Moon et al., 2002). The influences of the various binder characteristics are listed below:

- *Surface tension and rheology* – Surface tension and rheology are the two most important properties controlling the size and shape of binder droplet and jet reliability. Low surface tension binder has a high penetration rate and penetration depth, but it spreads more easily and thus reduces printing resolution (Grau et al., 1997). High surface tension droplets produce spherical primitives, while low

surface tension droplets give cylindrical shaped primitives. Furthermore, the binder impact size is inversely proportional to the square root of viscosity due to viscous energy dissipation (given constant jet velocity, drop size, and surface tension). Generally, as viscosity increases, primitive size decreases (Moon et al., 2002).

- *Wetting behavior* – The wetting difference between the binder-printed region and the unprinted region of the powder bed is also another important aspect of the binder system. Lamination defects and surface roughness are observed when the wetting behavior differs substantially between the binder printed and unprinted regions. This wetting behavior difference depends on the properties of the binder materials. For example, alcohol-based or aqueous-alcohol mixed slurries have a much lower contact angle and wet the binder printed regions more uniformly.
- *Molecular weight* – The molecular weight of the binder is also important. Moon and coauthors discovered that higher molecular weight binders have difficulty in penetrating the pores of a powder layer, but produced stronger parts when compared with lower molecular weight binder (Moon et al., 2002).
- *Binder basis* – Moon and coauthors suggest that aqueous binder systems are preferred over solvent-based binders because of improved jet reliability. Furthermore, water-based binder can be tailored to a wide range of surface tensions and viscosities, whereas the solvent-based binder tends to have a relatively low surface tension (Moon et al., 2002).

As stated in Section 6.1.1, the chosen embodiment for the "store material" sub-function is spray-dried metal oxide powders since they provide a means for processing

fine particles. An additional advantage in using spray-dried particles is that the binder used to form granules can be activated in the powder bed, thus eliminating the need for printing a polymeric binder. Thus, in order to form a deposit, all which is required is printing of an aqueous solution into the powder bed – this solution partially dissolves the polymer binder coating, thus causing the granules to deform and to form necks with one another. This deformation decreases the distances between individual ceramic particles, which improves the sintering characteristics of the green part.

Perhaps most important in this "binding" working principle is that it is modular – all granules that are spray-dried with the same binder coating will behave similarly with the solvent, regardless of the ceramic material chosen as the core powder. As such, there is no requirement for individualized binder formulation or powder/binder suspension.

From this investigation, a hypothesis for the secondary research question can be formulated:

Secondary Research Hypothesis:

The density of metal parts which result from the thermal-chemical conversion of ceramic green parts can be improved by creating primitives via printing a solvent into a bed of binder-coated powder particles.

The approach suggested by this hypothesis should provide a more dense final part in the designed manufacturing process than if single-phase powder were used in conjunction with a printed binder.

To summarize the information presented in the previous sub-sections, spray-dried granules present a manner in which finer particles can be processed in a dry state using

3DP. The granules are spherical and therefore flow and pack well during recoating; they also efficiently use binder during the creation of solid primitives. Furthermore, the binder coating of the granule can be activated via the presence of a solvent. It is hypothesized that as the solvent partially dissolves the granule surfaces, neighboring granules will deform, partially collapse, and form a solid primitive whilst bringing the ceramic fine particles closer together. Finally, this approach is preferred because it is modular – the same solvent can be used on various ceramic spray-dried granules as long as the coating is the same polymer. The creation of primitives via printing a solvent into a powder/binder mixture has been implemented in (Utela et al., 2006) and in (Carreno-Morelli et al., 2007).

6.1.4 Provide New Material & Support Previously Deposited Material

Provide New Material	Recoat by spreading	Recoat by spraying	Recoat by dipping	Direct material addition	Directly place layer	
Support previously deposited material	Bed of build material	Thin trusses of build material	Dissolvable support material	Breakable support material	Pyrolizable support material	5-axis deposition

Figure 6.6 – Preferred Working Principles for "Provide New Material" & "Support" Sub-Functions (adapted from Figure 5.5)

Unfortunately, as discussed in Sections 5.1.6, "recoat by spreading" and "bed of build material" are not preferred working principles for the "provide new material" and "support previously deposited material" sub-functions (shown in Figure 6.6). Principles such as "direct material addition" and "dissolvable / pyrolizable support material" are preferred because they provide a means of creating complex geometries without the need for manual support structure removal and/or cleaning. The powder bed present in 3DP is its most significant drawback and is a key compromise made in the selection process

presented in Chapter 4. It should be noted, however, that while this may place a limit on the size of voids that can be created and will prohibit the construction of closed cells, the use of highly-flowable spray-dried powder will minimize the difficulties in removing un-patterned powder.

6.2 SPECIFICATION OF EMBODIMENT

To reflect the slight change in the embodiment of the 3DP process for the research objective of this dissertation, an updated working structure is presented in Figure 6.7.

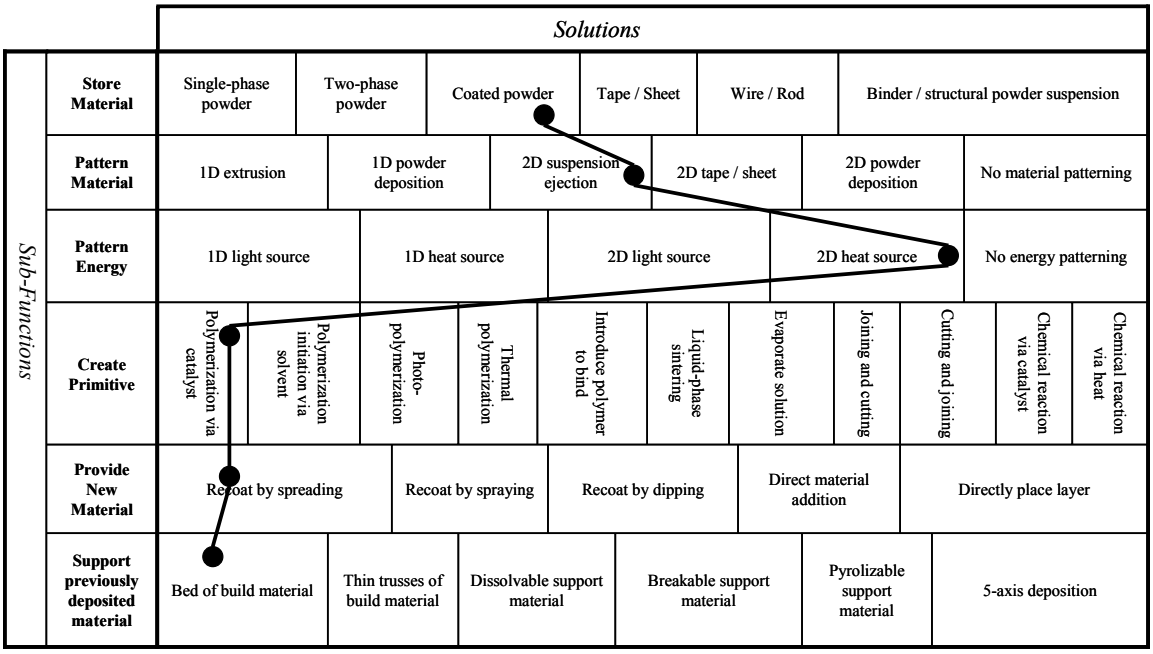

Figure 6.7 – Working Structure for 3DP of Ceramic Spray Dried Powders

In this sub-section, the specifications and details of the embodiment of the principal solution are presented. This discussion of embodiment also details the experimental set-up used for the verification of the primary and secondary research hypotheses. The description of embodiment is divided into three sections: that of the machine (Section 6.2.1), the material (Section 6.2.2), and the post-processing procedure (Section 6.2.3).

6.2.1 Specification of Machine

In order to leverage the developmental effort and progress made by those that have worked with 3DP in the past, a commercial 3DP machine is used as a platform for augmentation in the experimental work of this dissertation. The physical embodiment of the 3DP principal solution is illustrated in Figure 6.8.

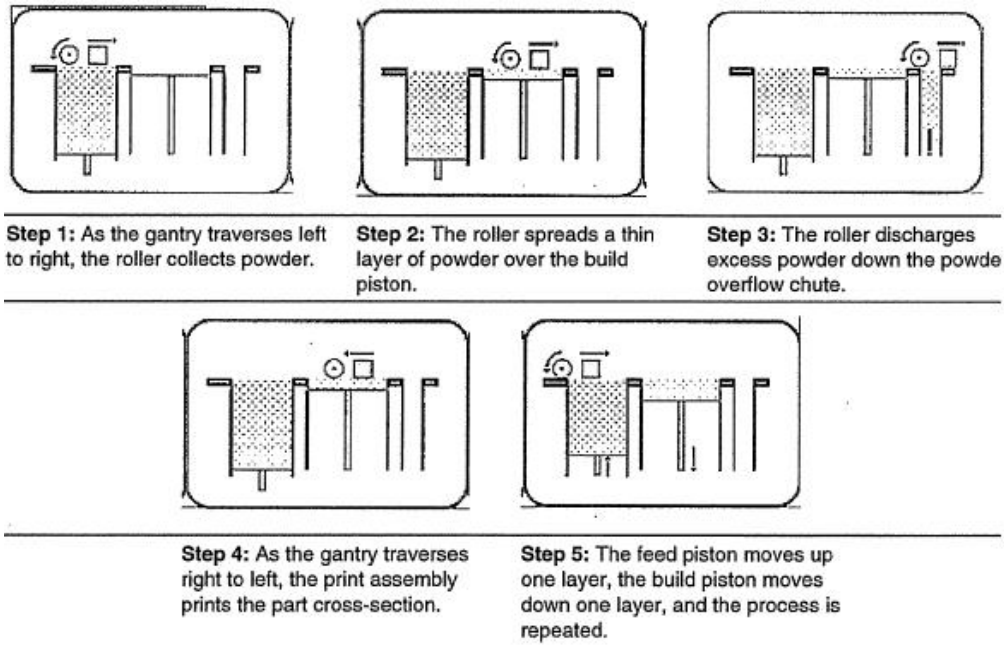

Figure 6.8 – Embodiment of 3DP: Physical Arrangement of Working Principles (ZCorporation, 1996)

As can be seen in the figure, a printhead gantry system is passed over a powder bed; as the printhead traverses perpendicularly to this motion, binder is printed into the powder in order to create each cross-section. After passing over the "build" powder bed, the feed powder piston rises a distance of one layer and a roller is used to move new powder onto the previously deposited layer. Excess powder from this recoating process is caught in an overflow container for easy reuse.

A ZCorp Z402 three-dimensional printer is employed in this research. This specific machine model is illustrated in Figure 6.9 (Z, 2007). A coordinate axis is overlaid onto the illustration for the aid of future discussion. Cross-sections are printed in continuous strips along the *y*-axis (the binder cartridge direction of travel), bands across the *x*-axis (the gantry direction of travel), and laminated layers along the *z*-axis (the build direction).

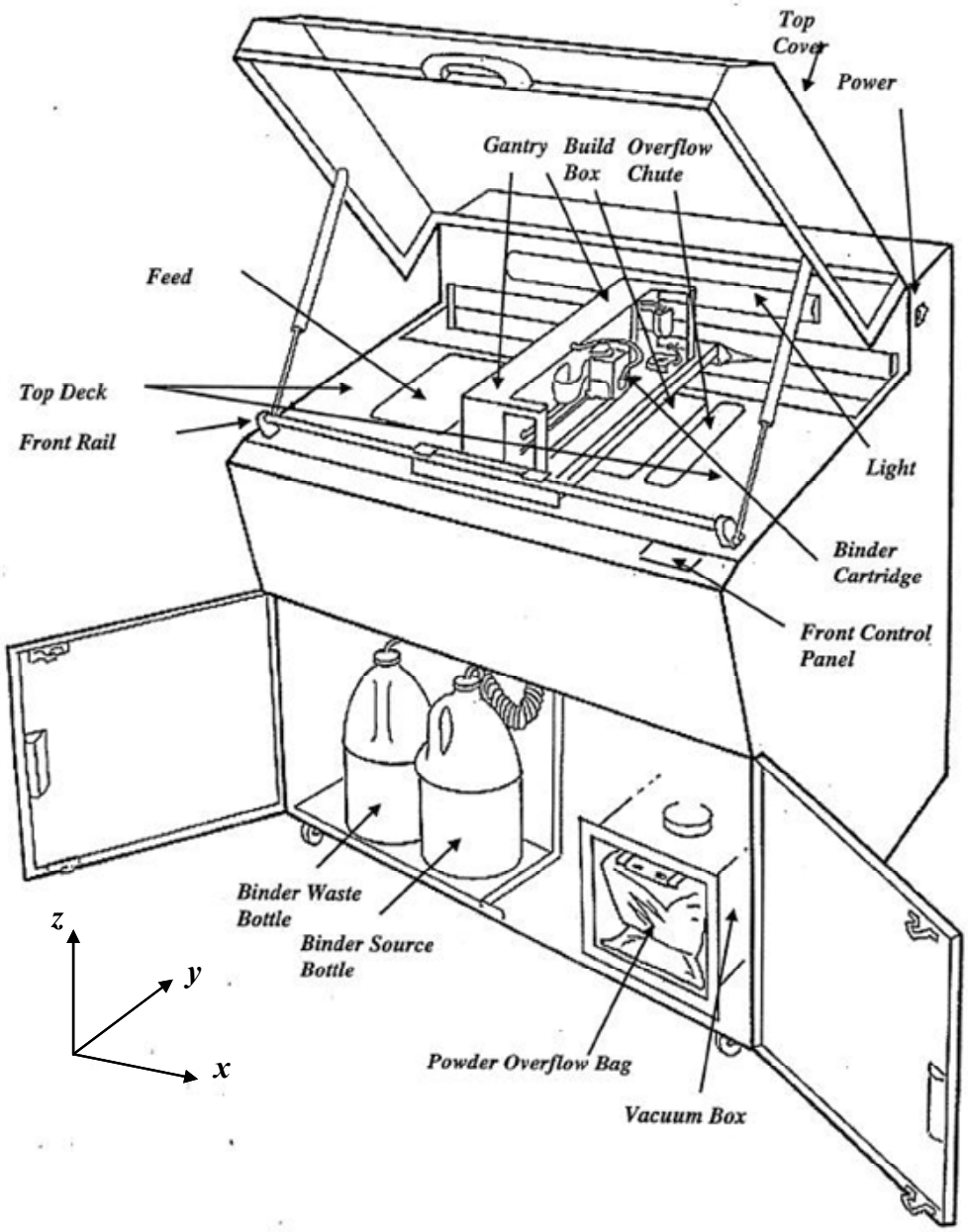

Figure 6.9 – Schematic of ZCorp Z402 Printer (ZCorporation, 1996)

The specifications of the Z402 printer are presented in Table 6.1. It should be noted that newer 3DP printer models are available that offer the user multiple (and larger) print heads, a higher printing resolution, a larger build volume, and a faster deposition speed. The Z402 is chosen for the experimental efforts of this research as it is more easily adapted to changes in working material (in both the powder bed and the printed binder).

Table 6.1 – ZCorp Z402 Machine Specification

Parameters	**Operational Range**
Layer Thickness Operating Range	0.089 – 0.2 mm
Resolution	11.18 dots/mm (300 dpi); 0.0847 mm droplet size; 128 print heads
Build Volume	20.3 cm x 25.4 cm x 20.3 cm
Deposition Speed	25.4 – 50.8 vertical mm per hour
Print Head	Bubble jet; drop-on-demand

Since commercially-available 3DP machines are designed to be "user-friendly," one major drawback of using them as an experimental apparatus is that the user is not given full freedom to change the entirety of the build parameters. The build parameters which are controllable by the user are presented in Table 6.2 along with the settings used for the experimental work.

Table 6.2 – Z402 3D Printer Process Parameter Settings

Parameter	**Setting**
Layer Thickness	89 μm; 102 μm; 200μm
Core Saturation	2
Anisotropic Scaling	0 *x*, 0 *y*, 0 z

As seen in the above table, three different layer thickness settings are used during experimentation so as to investigate the influence of this process parameter. This setting varies based upon the powder and solvent used during printing. Its specification is discussed in more detail in Chapter 7.

"Core saturation" refers to a specialized parameter that is unique to the ZCorp's embodiment of the 3DP principal solution. Due to problems with over-saturating the powder bed with binder (which can lead to poor surface finish, poor part strength, part distortion, and print-through errors), ZCorp employs a unique printing strategy:

- binder is first applied in high concentration around the edges of the part to create a strong "shell" around the exterior of the part
- within the parts, an infrastructure is created by printing strong scaffolding within part walls with a higher concentration of binder solution
- finally, the remaining interior areas are printed with a lower saturation, which gives them stability, but prevents over saturation.

Generally, this printing strategy results in a checkerboard pattern which is offset at every layer. The "core saturation" parameter refers to the amount of saturation applied to the interior of the parts' cross-sectional layers and varies from 1 to 2. Generally, thicker, bulkier parts are suggested to be printed at a lower setting while delicate parts are printed at a higher setting. Aware that spray-dried granules are more porous than the plaster powders that are typically used, and that the printer will be primarily used to print small features typical of cellular materials, the saturation level is set at its maximum value of 2. Other than this, no changes are made to the default printing setup.

An anisotropic scaling parameter is included as a variable parameter so as to provide a designer with the ability to cope with any shrinkage that might occur during printing due to humidity and temperature variations between operating environments. Since no shrinkage was observed in any of the printing experiments, this scaling factor is set to 0 for all three principal directions.

6.2.2 Specification of Material

As indicated in Section 6.1, three separate materials must be specified for the embodiment of the 3DP variant described in this research: the structural ceramic material to be used in the powder bed, the polymer binder that will coat the structural powder, and the solvent that will be printed into the powder bed.

Ceramic Material

While a wide variety of transition metal oxides can be reduced to metal using the reduction post-processing procedure described in Section 2.3, maraging steel has been chosen as the working material for the experimental portion of this dissertation. Maraging steel features high strength and high fracture toughness. Through small changes in the composition of its constituents, it is possible for the material to have a wide range of mechanical properties; thus one can imagine easily altering the mixture ratios in order to achieve specific design objectives. Maraging steel also has uniform, predictable shrinkage during heat treatment. Finally, its constituents are easily reduced (Table 6.3).

Table 6.3 – Reduction Reactions of Maraging Steel Constituents

$$Fe_3O_4 + 4H_2 \longrightarrow 3Fe + 4H_20 \quad [6.1]$$

$$Co_3O_4 + 4H_2 \longrightarrow 3Co + 4H_20 \quad [6.2]$$

$$NiO + H_2 \longrightarrow Ni + H_20 \quad [6.3]$$

Maraging Steel: Fe 18.5Ni 8.5Co 5Mo

A metal oxide powder system that will chemically convert to maraging steel upon reduction is created by combining iron oxide (Fe_3O_4), nickel oxide (NiO), cobalt oxide

(Co_3O_4), and molybdenum metal (Mo) powders (in the amounts listed in Table 6.4) and ball-milling them for 24 hours.

Table 6.4 – Maraging Steel Constituent Mixture

Constituent	Amount (g)	Density (g/cm^3)
Fe_30_4	1430.42	5.24
NiO	353.03	6.67
Co_3O_4	173.1	6.07
Mo	48.75	10.19
Mixture Total	2005.3	5.58

Binder Coating

The resultant fine powder mixture is then spray-dried so that granules can be formed. As illustrated in Figure 6.3, the binder material that will serve as granule coating must be selected. For this research, a water soluble poly-vinyl alcohol (PVA) is selected as the polymer coating. PVA is chosen as the binder because it is (i) a common binder that works well with almost an oxide ceramic, (ii) soluble in water, and (iii) the resulting parts have considerable strength and are handled easily in the green form (Morse, 1979). Specifically, the ceramic powders are spray-dried in Airvol 203 (now known as Celvol 203, offered by Celanese Chemicals), which has a bulk density of 0.6 g/cm^3 (Celanese, 2007).

The powder particles were spray-dried by Aero-Instant Spray-Drying Services of Brunswick, Georgia via a generous donation of services. A NIRO Mobile Minor spray-drier with a 30" diameter vessel was used. A rotary atomizer was used at 30,000 rpm in air with a low-vaned wheel. The target inlet temperature of the suspension was 300 C, and the outlet target temperature was 100 C. Two separate suspensions were processed, one with 2 wt% Airvol 203, and one with 4 wt%. The granules created with 2 wt%

Celvol 203 have a theoretical density of 4.79 g/cm^3, while the granules created with 4 wt% Celvol 203 have a theoretical density of 4.20 g/cm^3. Parts created from these two separate granule systems are compared in the experimental results presented in Chapter 7.

Once spray-dried, the resulting granules' flowability is tested. Using the Z402 3DP machine, the granules are able to successfully be recoated to form defect-free layers at the smallest layer thickness setting (89 μm). As a point of reference, previous tests with 100 μm alumina spray-dried granules were not able to be successfully processed with any layer thickness setting (the largest being 0.2 mm) – formed primitives were swept away during recoating. However, once these granules were sieved to 40 μm in diameter, problems with recoating were alleviated. As a general rule, the layer thickness setting should be around three times larger than the particle diameter.

Solvent

In order to realize the suggested embodiment, a solvent must be selected that will partially dissolve and deform the PVA binder that is coating the metal oxide particles. The selected solvent must also be suitable for jetting from the printheads of the Z402 machine; thus it must have compatible rheological properties (surface tension, viscosity, density, etc.) and operating conditions (jetting temperature, non-corrosive, etc.).

Several preliminary experiments with various solvents (distilled water, ethanol, isopropanol, and acetone) were performed wherein the solvents were manually deposited into a bed of the spray-dried granules (10 μL droplets; ~ 2.7 mm diameter). The resulting reaction was then observed under a microscope.

Interestingly, not even the most aggressive of the solvents was able to form a solid primitive with those granules that were prepared by spray-drying the 2 wt% PVA

solution. While the granules would clump together due to the surface tension of the solvent, they did not have the strength necessary for successful removal from the powder bed. It is concluded that a granule system composed by a 2wt% PVA coating is not sufficient for successful primitive forming via the deposition of a solvent. For this reason, all experiments with the 2wt% granules will be completed using the standard ZCorp ZB7 PVA-based binder.

This conclusion is validated through experimentation with those granules that are prepared with the 4 wt % PVA solution. Significant granule deformation is observed as the solvents are able to initiate partial dissolving and necking between the granules. Each solvent tested was able to sufficiently dissolve the 4wt% PVA coating and create a solid primitive suitable (upon drying) for easy removal from the surrounding unbound powder, as seen in Figure 6.10.

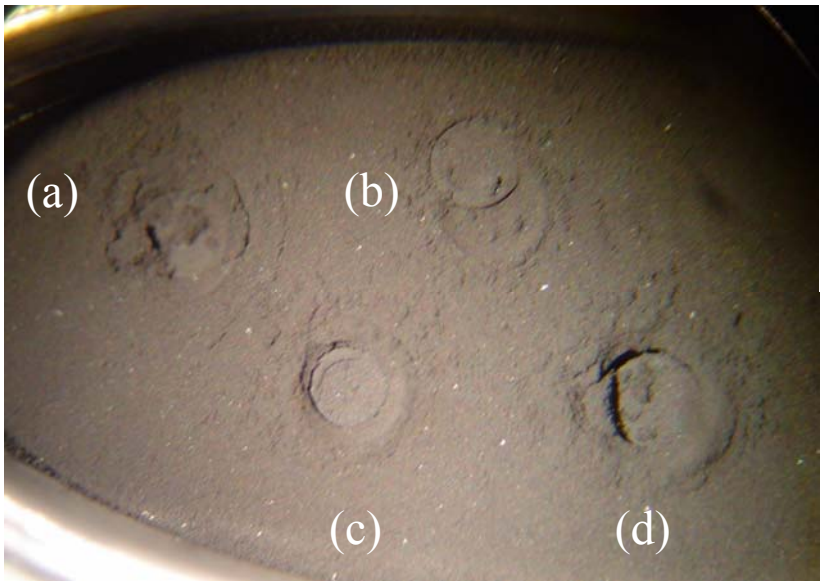

Figure 6.10 – Primitives Formed via the Manual Deposition of Various Solvents; (a) water, (b) ethanol, (c) denatured alcohol, (d) mixture of water and ethanol

Primitives were successfully formed with even the least caustic of the solvents tested: distilled water. Heated distilled water seemed to cause more deformation of the granules

than that of room temperature; however, operating temperature constraints on the printhead prevent this from being a feasible alternative.

Primitives created via the manual deposition of distilled water into the powder bed are seen in Figure 6.11. The general shape of the primitive shown in Figure 6.11 is typical of every solvent deposited into the bed. As seen in the profile view (Figure 6.11a), the primitives have a concaved top surface. This curvature is caused by the surface tension of the solvent, which pulls powder towards the center of the droplet. The profile views also show the mushroom cap shape of the primitive. This shape is due to the surrounding powder which sticks to the core primitive due to partial wetting. This phenomenon leads to a smooth top surface (Figure 6.11c and d).

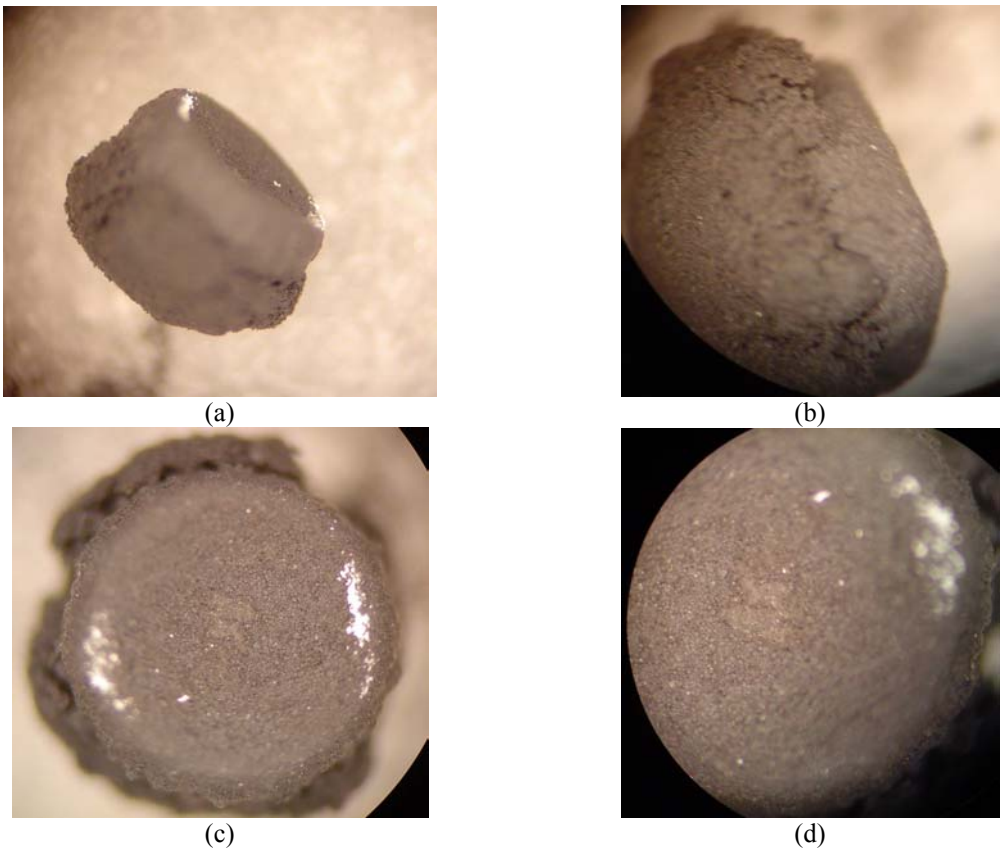

Figure 6.11– Primitives Created with Distilled Water; (a) & (b) profile view, (c) & (d) overhead view

As per the suggestions offered by Utela and coauthors, a mixture of 80% distilled water and 20% isopropyl alcohol is selected as the primary solvent for the granule system prepared with 4wt% PVA. This mixture, with a surface tension of 35 dynes/cm^2, has a more reliable performance in the printhead because the surface tension of plain distilled water is not within the bounds of the printhead (Utela et al., 2006). A manually-deposited primitive created with this mixture is shown in Figure 6.12.

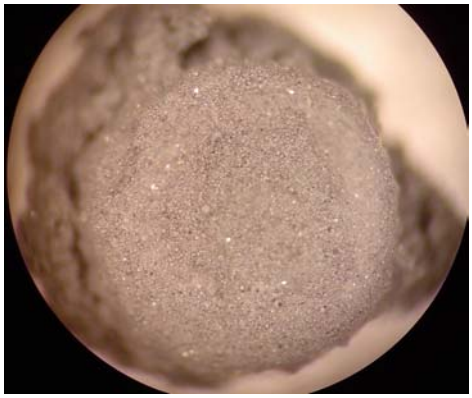

Figure 6.12– Primitive Created with Mixture of Distilled Water and Ethanol

The more aggressive solvents, such as acetone, were not chosen because they are incompatible with the printhead system of the ZCorp printer and have a surface tension that are not within the working range of the printheads.

6.2.3 Specification of Post-Processing Procedure

Once printing is completed, the green part is left in the powder bed for a minimum of 30 minutes to allow the binder to set and for the green parts to gain strength. Light from an infrared lamp (120 W) is often applied directly onto the powder bed surface in order to accelerate binder drying. The green parts are then transferred to a depowdering station where unbound pattern is carefully removed from the complex cellular geometry using the combination of compressed air and a vacuum nozzle.

Once depowdered, the green parts are transferred to an oven to further dry the binder. The oven is consistently set to 100 C, while the duration of drying is dependent on the size of the part (typically around 30 minutes).

Once depowdered and dried, the green parts are reduced and sintered in an atmosphere-controlled tube furnace in an Ar – 10% H_2 environment. The flow rate of the gas mixture is dependent on the size of the green part(s) being processed. The thermal-chemical conversion of the metal oxide green part to a metal finished part follows the sintering cycle presented in Figure 6.13.

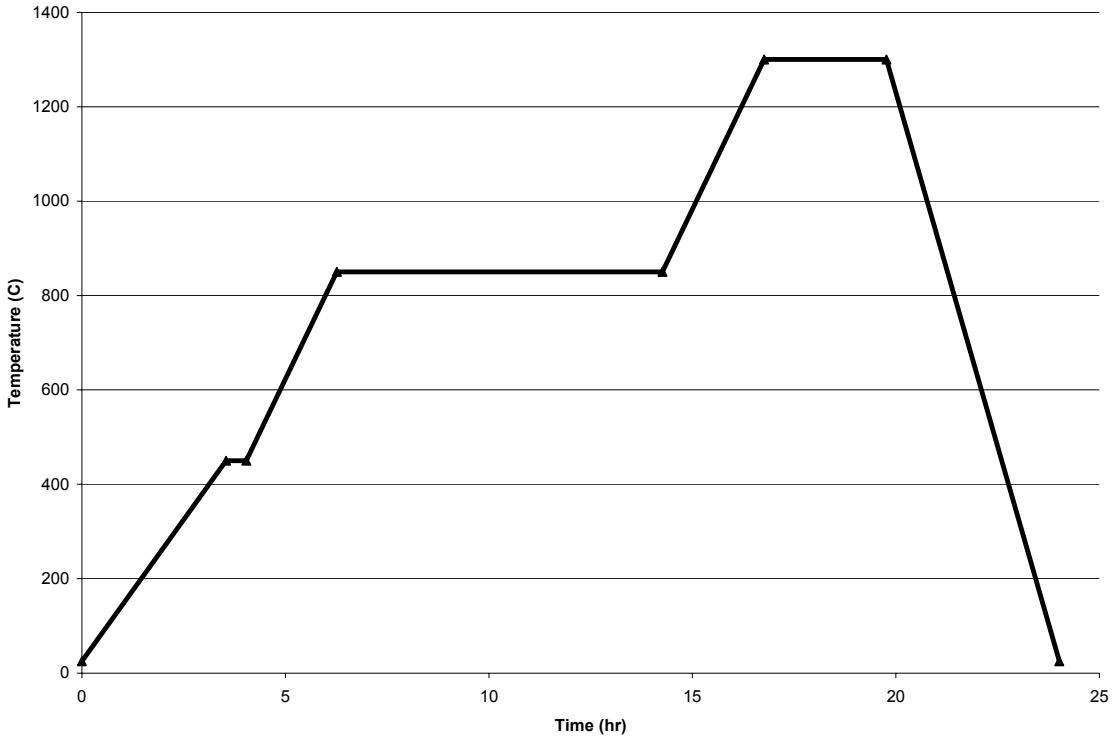

Figure 6.13 – Cycle for Reduction and Sintering of Maraging Steel

Debinding of the PVA binder occurs at 450 C (ramped from room temperature at 2 C/min); reduction of the metal oxide green part occurs at 850 C (ramped from debinding temperature at 3 C/min); sintering of the metal occurs at 1300 C (ramped from reduction

temperature at 3 C/min); and finally, the part is slowly lowered to room temperature at a rate of 5 C/min. During early experimentation with the process, the hold times for reduction and sintering were varied in order to determine ideal settings. It was discovered that a reduction hold of 8 hrs coupled with a sintering hold of 3 hours assured that finished parts would have all oxide phases completely removed and would be as dense as possible.

6.3 DISSERTATION ROADMAP

With the process's embodiment complete and the experimental setup detailed, experimentation can begin. As shown in Figure 6.14, the process's capability to realize parts of designed mesostructure is tested in Chapter 7 in an effort to verify both the primary and secondary research hypotheses.

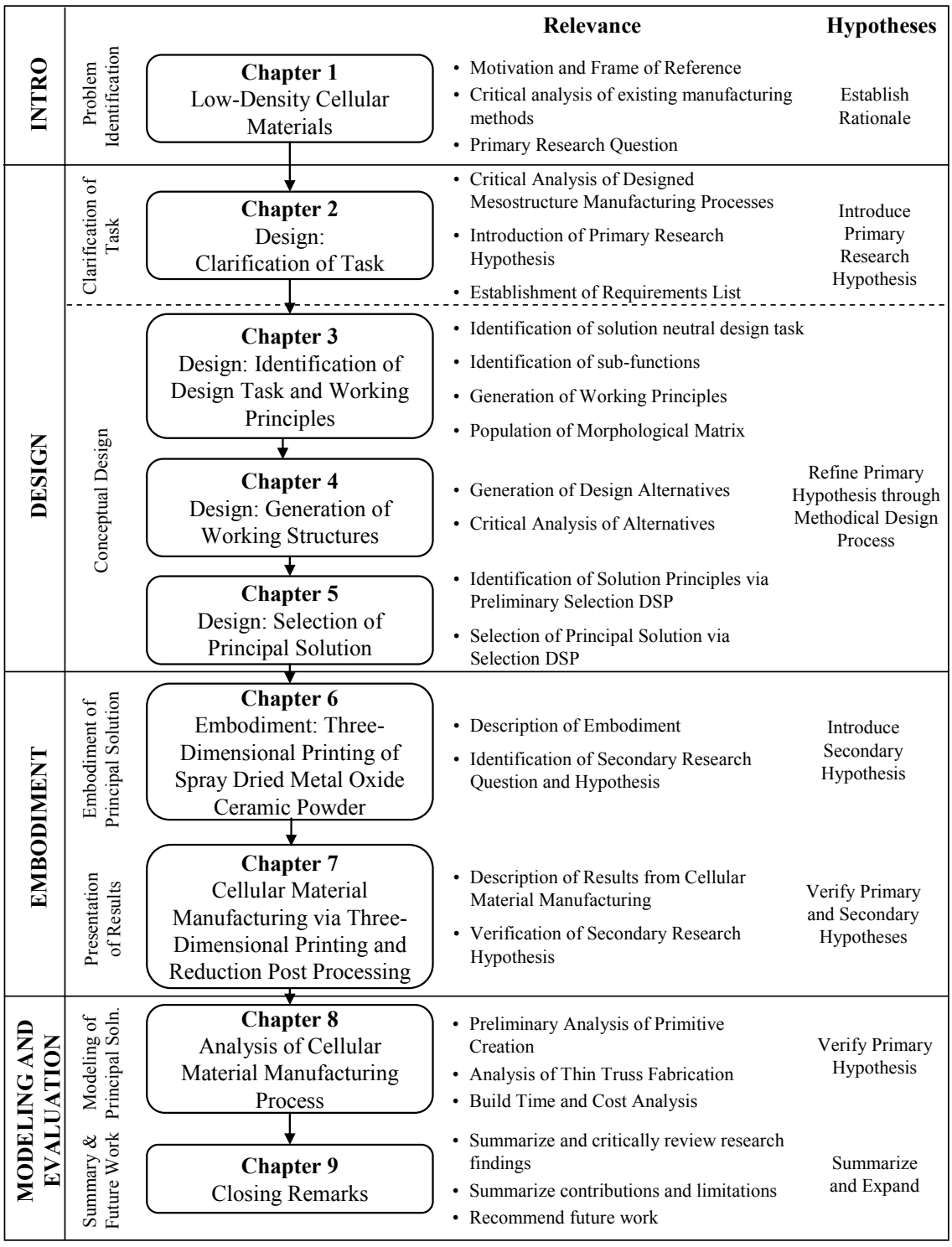

Figure 6.14 – Dissertation Roadmap

CHAPTER 7

CELLULAR MATERIAL MANUFACTURING VIA THREE-DIMENSIONAL PRINTING AND REDUCTION POST-PROCESSING

With the embodiment design phase complete and the experimental setup specified, the results of the experimentation are presented in this chapter. Specifically, initial results of processing maraging steel parts with the designed manufacturing process chain are presented in Section 7.1. The parts which result from the embodied manufacturing process chain are characterized in Section 7.2; this includes a description of the parts' phase, density, porosity, and shrinkage. The secondary research hypothesis is verified through this analysis. The primary research hypothesis is validated in Section 7.3 through the creation of parts featuring geometries typical of parts of designed mesostructure. Finally, a critical analysis of the manufacturing process chain is offered in Section 7.4.

7.1 INITIAL RESULTS

Following the embodiment outlined in Chapter 6, experimentation was initiated by making qualitative observations of the interaction of various binders and solvents with the 2 wt% and 4 wt% granule systems. The results of these initial experiments are detailed in Table 7.1.

Table 7.1 – Qualitative Observations of Solvent/Binder Interaction with Granule Systems

Granule System	Solvent / Binder	Layer Thickness	Result
2 wt%	ZB7 binder	0.089 mm	Some minor curling around edges of cross-section
	Water	0.089, 0.1, 0.27 mm	As described in Section 6.2.2, no solvent could initiate primitive formation due to an insufficient amount of binder.
4 wt%	ZB7 binder	0.089 mm	Minor curling around edges of cross-section
	80/20 vol% water/ethanol mixture	0.089 mm; 0.1 mm	Extreme curling at 0.089 mm layer thickness which caused part destruction during recoating; 0.01 mm layer thickness was sufficient
	Distilled water	0.089 mm; 0.1 mm	Distilled water performed well at both layer thickness settings

From the observations listed in Table 7.1, the following solvent/granule systems are identified as worthy of further investigation:

(i) 2 wt% + ZB7 binder at 0.089 mm layer thickness

(ii) 4 wt% + water/ethanol mixture at 0. 1 mm layer thickness

(iii) 4 wt% + distilled water at 0.089 mm layer thickness

(iv) 4 wt% + distilled water at 0.1 mm layer thickness

With these experimental material systems identified, sample parts were processed in order to evaluate the general success of the designed manufacturing process chain. Some of these sample parts are shown in Figure 7.1.

Additional qualitative observations are noted as a result of this initial experimentation:

- *Layer curling* – As mentioned in Table 7.1, deposited layers displayed significant curling and warping around edges, often resulting to a concave surface. This curling can be so significant as to cause protrusion from the powder bed which is significant enough as to interfere with the recoating roller (as was noted in Table 7.1 for the 4 wt% + water/ethanol mixture system). Curling was most

severe in the first layers deposited, and wasn't as prominent as fabrication continued. As such, bottom surfaces of parts created are curved. This curling issue is typical of 3DP and can be alleviated by careful tuning of the solvent's surface tension and wetting characteristics.

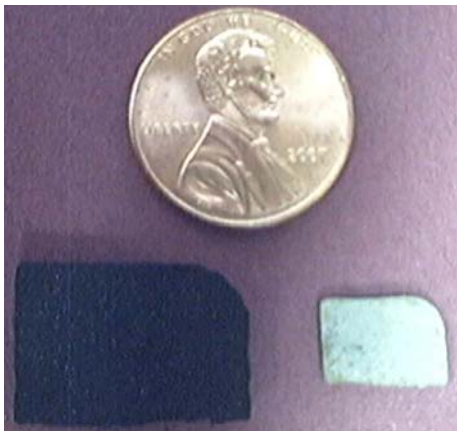

(a) 20 mm x 10 mm sample in green state (LHS) is 11.6 mm x 6.4 mm after post-processing (RHS)

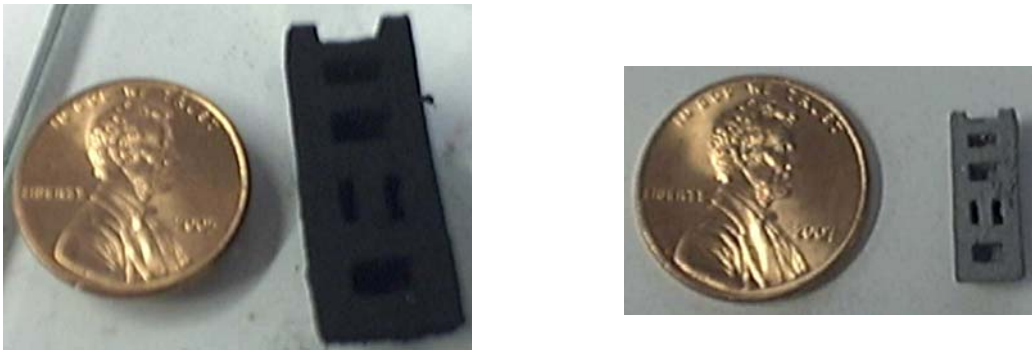

(b) 10 mm x 25 mm sample in green state (LHS) is 5.25 mm x 13.65 mm after post-processing (RHS)

Figure 7.1 – Sample Parts Created by the Designed Manufacturing Process Chain

- *Powder ejection* – Another characteristic issue found in 3DP is ejection of powder in the bed due to the deposition of the binder/solvent. This occurs solely in the initially created layers, when the powder bed is dry. As fabrication continues, the previously created layers in the powder bed are sufficiently saturated and compacted, thus eradicating powder ejection difficulties. Due to this problem, bottom layers are extremely porous and have poor resolution around the edges.

This problem can be alleviated through light wetting of the powder bed before wetting (via misting with water, or through deposition of metal salts), or by modifying size or molecular weight the spray-dried granules.

- *Green part fragility* – It is noted that the green parts are very fragile when removed from the powder bed. This is a common issue with all parts created by 3DP, as green parts are simply composed of compacted particles held together with a moderate amount of binder. It was discovered that increasing the parts' powder bed drying time significantly increases part strength. However, if left in the powder bed for too long, part cracking can occur due to the interference of part shrinkage with the constraints imposed by surrounding loose powder. The fragility of the green parts is a concern as it significantly increases the difficulty in post-processing parts with thin features (as is often the case with parts with designed mesostructure) – the use of compressed air to remove unbound powder can shear thin part members. Green part strength can be improved via an increased amount of deposited solvent (to activate additional binder) and/or the inclusion of a polymer suspended in the solvent system.
- *Surface finish* – As is true of all other parts created with a powder-based AM process, the surface finish of the parts created via the designed manufacturing process chain is observed to be very rough. This roughness is attributed to two factors: (i) loose granules that are partially wetted by the deposited solvent become attached to the part and remain after firing, and (ii) the use of compressed air to remove loose powder can damage surface finish and cause surface porosity due to the fragility of the green part.

- *Reduction to metal* – All of the sample parts were successfully converted to steel via the reduction and sintering post-processing process outlined in Section 6.2.3. Successful initial tests with magnetism verified that there was some presence of iron in the finished parts. Detailed tests of phase are presented in Section 7.2.1.
- *Shrinkage* – As can be seen in Figure 7.1, a significant amount of shrinkage is observed after the green part is fired. Initial experiments suggest a linear shrinkage of 45%. The large shrinkage is due to the low solids loading of the green part and the removal of the relatively large oxygen atoms through reduction. Further characterization of part shrinkage is offered in Section 7.2.4.
- *Structural integrity* – All of the sample parts fired held together during sintering. Although not surprising, this is a concern when firing ceramic green bodies with small binder content. Actually, it is unclear why ceramic green bodies retain their shape during sintering, as debinding occurs long before (and at a lower temperature than when) sintering begins. In this embodiment, it is likely that the green part is held together because of the presence of carbon residue from the pyrolized PVA binder in between particles after the debinding process.

7.2 PART CHARACTERIZATION

In order to obtain more quantitative results, and thus verify the research hypotheses presented in this work, the finished parts created through the completion of the designed manufacturing process chain are characterized with multiple, repeated tests. Specifically, the finished parts' phase, density, porosity, and shrinkage are analyzed.

7.2.1 Phase Identification

X-ray diffraction is used to identify the phases present in the parts created by the manufacturing process chain. The results from the test (completed with Molybdenum radiation) are presented in Figure 7.2.

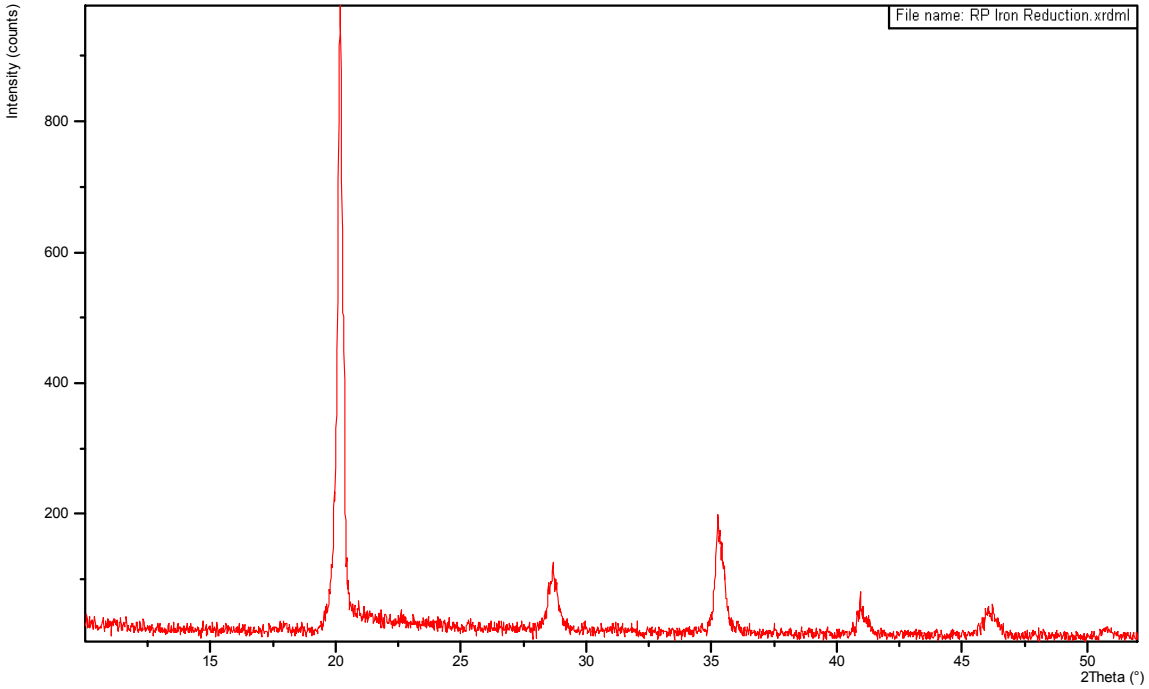

Figure 7.2 – X-Ray Diffraction Test Results of Maraging Steel Sample

As can be seen in Figure 7.2, count peaks occur at 2θ = 20.155, 28.651, 35.284, 40.97, 46.067, and 50.755. Using the JADE phase identification software, it is discovered that these results correspond to a BCC iron phase (power diffraction file # 00-0006-0696) with a figure of merit (FoM) of 3.5. From this it can be concluded that no oxide phase is present in the finished parts, thus the parts are fully reduced and are pure steel.

7.2.2 Density Analysis

In order to evaluate the quality of the parts created by the designed manufacturing chain, and in order to validate the secondary research question, an analysis of the parts' density is conducted. Density analysis is done via the Archimedes method; mass

measurements of samples are taken in their dry, suspended, and saturated states, and relative density is calculated (assuming maraging steel has a bulk density of 8.2 g/cm^3) along with the percentage of open porosity present in the part.

Relative Density of 2 wt% and 4 wt% Granule Systems

In an effort to verify the secondary research hypothesis (introduced in Section 6.1.3), the densities of three different powder/binder systems are analyzed – 2 wt% granules & ZB7 binder, 4 wt% granules & ZB7 binder, and 4 wt% granules & an 80/20 water/ethanol mixture. The results of this analysis are presented in Table 7.2. As can be seen in the table, several samples were created and measured for each powder/binder system to verify the repeatability of results.

Table 7.2 – Relative Density Measurements for 2 wt% and 4 wt% Granule Systems

Granule Binder Content	***Deposited binder / solvent***	***Relative density***	***Open porosity***
2 wt%	ZB7	63.8	39.4
		63.6	32.4
		63.4	32.4
	Average	**63.6**	**34.7**
4 wt%	ZB7	59.0	36.6
		59.3	35.7
	Average	**59.15**	**36.15**
	Water + Ethanol	64.3	34.7
		61.9	35.1
		61.5	33.4
	Average	**62.57**	**34.4**

It should be noted that the minor variations that exist within the sample groups of each powder/binder system can be attributed to either a small error in measurement (relative density and open porosity calculations are sensitive to the recorded mass measurements, especially to that of the saturated measurement which is the most inaccurate), and/or because each part was created in a different location in the powder bed (thus suggesting that powder bed density varies across the XY plane of the build volume).

As can be seen in Table 7.2, the 2 wt% and ZB7 powder/binder system provides the highest average relative density (at 63.6%). The 4 wt% granules & ZB7 binder pairing resulted in the lowest average relative density. This trend makes sense as one would assume that an increase in polymer content in the green part would result in a lower finished density due to the increased distance between ceramic particles in the green part. For this reason, the 4 wt% granule & ZB7 binder system is eliminated from further consideration.

As observed in Table 7.2, the use of a solvent in the 4 wt% granule system increases the density of the finished parts, and is very similar to that achieved in the 2 wt% & ZB7 binder system at 62.57% (a difference of only 1.6%). When compared to the use of ZB7 binder, the increased density found when using a solvent (a 5.5% difference) confirms the hypothesis that the use of a solvent with spray-dried granules increases part density.

From this set of experiments it is observed that there exists a balance between the amount of polymer content in the granule system and the act of introducing a solvent to bring particles closer together through partial dissolving: increasing the polymer content of the granules decreases the density of the part, but it provides an opportunity for increasing density through the application of a solvent in order to bring particles closer together. Decreasing polymer content provides a large final density, however, too little polymer prevents the use of solvents as a printing medium.

An additional qualitative difference which further distinguishes the two embodiment principles can be found in Figure 7.3, which contains parts created using the 2 wt% and 4 wt% granule systems. As can be seen by comparing the two samples in

Figure 7.3, the feature definition is much clearer on the part created with the 4 wt% granule system. This follows reason since the increased porosity of the granules of the 4 wt% system will result in smaller printed primitives, thus increasing the resolution of the printed parts.

Figure 7.3 – Comparison of Resolution of Parts Created with 2 wt% and 4 wt% Granule Systems

Thus, although the density found in parts created with the 4 wt% & solvent system is slightly less than that created with the 2 wt% & binder system, the accompanying improvement in feature definition might be of enough significance to a designer as to persuade him/her to work with the 4 wt% granule & solvent system.

Relative Density of Upper and Lower Part Segments of Various Granule/Binder Systems

Additional experiments are conducted in an effort to further understand the influence that the selection of the powder/binder embodiment has on final part density. Furthermore, in an effort to explore the effect of initial layer curling and powder ejection (as described in Section 7.1) on density, the sample featured in Figure 7.4 is built. As can be seen in Figure 7.4a, this part features a small indentation that allows for the selective removal of the bottom layers in its green state via careful incision with a razor blade.

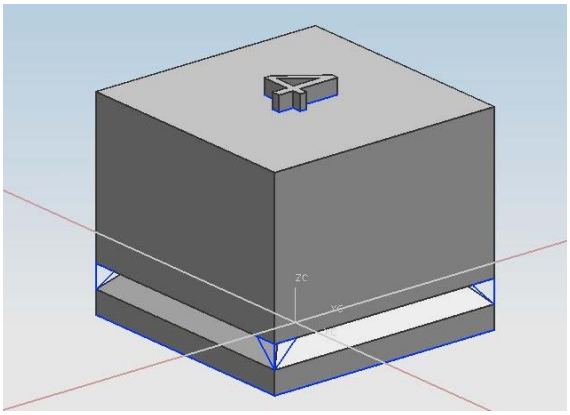

(a) CAD model for 4 wt% granule system

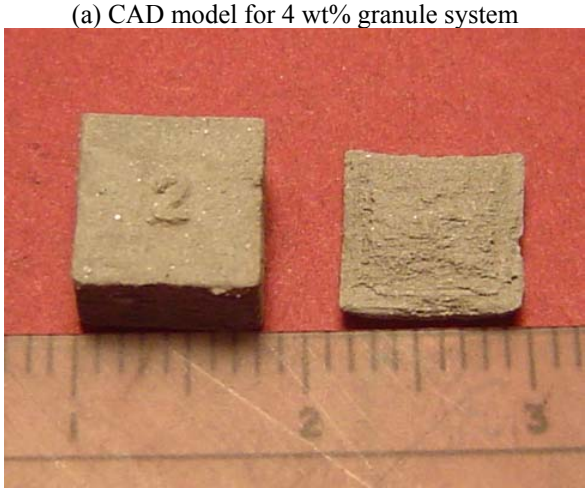

(b) Sintered and reduced test sample (2 wt% granule system)

Figure 7.4 – Density Test Piece

Once separated, the upper and lower sections of the sample are fired and analyzed (as seen in Figure 7.4b). The density measurements for the upper section of the sample are presented in Table 7.3. As can be seen in the table, two separate solvents are tested with the 4 wt% granule system at two different layer thicknesses – water with and without 20 vol% ethanol, and layer thicknesses of 0.089 mm and 0.102 mm. The data presented in Table 7.3 follows the same trend as that presented in Table 7.2 – those parts created via 4 wt% and a solvent are slightly less dense than that of the 2 wt% and binder system.

Table 7.3 – Relative Density Measurements of Upper Sections of Parts

Granule Binder Content	***Deposited binder / solvent***	***Relative density***	***Open porosity***
2 wt%	ZB7	63	35.6
		61.8	38.8
	Average	**62.4**	**37.2**
4 wt%	Water + Ethanol	54.7	43.2
		56.1	40.4
	Average	**55.4**	**41.8**
	Water @ 0.102 mm layer thickness	56.7	40.2
		55	47.9
	Average	**55.85**	**44.5**
	Water @ 0.089 mm layer thickness	50.6	47.4
		47.4	51.1
	Average	**49**	**49.25**

It was discovered that the separated lower layers of the test pieces are typically around 3% more dense than their upper layer counterparts. This increase in density is primarily due to the oversaturation of the lower levels due to the curling phenomenon.

It is important to note that the relative densities of the parts created in these secondary experiments (Table 7.3) are much lower than that presented in Table 7.2. The reason for this decrease (of 2.9% for 2 wt% & ZB7, and 11% for 4 wt% and solvent) is most likely due to the use of a different furnace in the experiments. The furnace used in the second set of density experiments (those results presented in Table 7.3) was unable to reach 1300 C, instead only consistently firing to 1250 C. While the second furnace was unable to reach the desired temperature, it is used because it offers a larger sintering environment (50 mm diameter tube compared to 10 mm diameter tube) and thus affords the creation of larger and more complex parts.

Discussion of Density Analysis

As can be seen in Table 7.2 and 7.3, the largest relative densities achieved in all of the trials are 63.6% (2 wt% & ZB7 binder) and 62.6% (4 wt% & solvent). In either scenario, a relative density of ~63% is simply not adequate for most engineering

applications. Generally, there are three potential sources for this result: (i) inadequate sintering schedule, (ii) poor green part density, and (iii) insufficient granule deformation.

It has been shown through experimentation in this work how vastly a small difference in sintering temperature can affect the final density of a part (compare Tables 7.2 and 7.3 with the difference in sintering histories discussed above). It should be noted that 1300 C is the maximum temperature at which the sintering hold can occur in this experimentation, since liquid phases from partial melting can be observed in maraging steel at around 1320 C. As such, the only variable left to change is the time at which the sintering temperature is held. However, in early experimentation, no significant difference in density was observed between a 6 hour hold and the 8 hour hold employed in the experimental setup. Thus, it is unlikely that additional holding time would further increase part density.

It is very likely that a large cause of the poor finished part density is due to a poor green part density. Although powder bed technologies have been shown to provide the largest solids loading in ceramic green parts created via AM, the final density measurements suggest that the green parts created with this process are sub-standard. As noted in Table 7.4, the 2 wt% granules have a theoretical density of 4.8 g/cm^3 and the 4 wt% granules have a theoretical density of 4.21 g/cm^3 (with a tap density of 21.3%). An estimate of the powder bed relative density is made by measuring the mass of the build powder bed of a known volume after a build is completed. These low bed densities are further complicated by the low solids volume % of each granule (84.3% for 2 wt% granules, and 72.4% for 4 wt% granules). It should be noted, however, that the powder bed relative density is not equivalent to the density of the green part; there is a

"significant increase" in powder packing density once the binder droplets impact the powder bed and granules are drawn closer together via the surface tension of the solvent (or binder) (Cima et al., 1992). It is safe to assume that the relative density of the green parts created in this experimental setup is in the range between 30-40 %.

Table 7.4 – Powder Bed Density Measurements

Weight %	Solids Volume %	Theo. Density (g/cm^3)	Tap Density (g/cm^3)	Tap Relative Density (%)	Powder Bed Density (g/cm^3)	Powder Bed Relative Density (%)
2	84.3	4.80	-	-	-	-
4	72.4	4.21	0.9	21.3	0.87	20.6

It is clear from this data that the green bed densities of 55 vol% reported by Utela and coauthors (Utela et al., 2006) are not realizable for this specific experimental setup. However, it should be made clear that this deficiency is not due to the overall manufacturing process design, and is instead an affect of the recoating working principle implemented in the ZCorp Z402 3D Printer (Utela and coauthors used a printing machine supplied by ExOne (ExHone, 2007)). It has been shown in literature that the powder bed density can be improved through press-rolling (Yoo et al., 1993), vibrating the powder bed (Sachs, 2000), or by using a bi-modal powder (Lanzetta and Sachs, 2003). In an effort to ensure that the green density deficiencies of this specific experimental setup are not due to the granules themselves, several pellets are pressed with each granule system at various pressures. The results are presented in Figure 7.5.

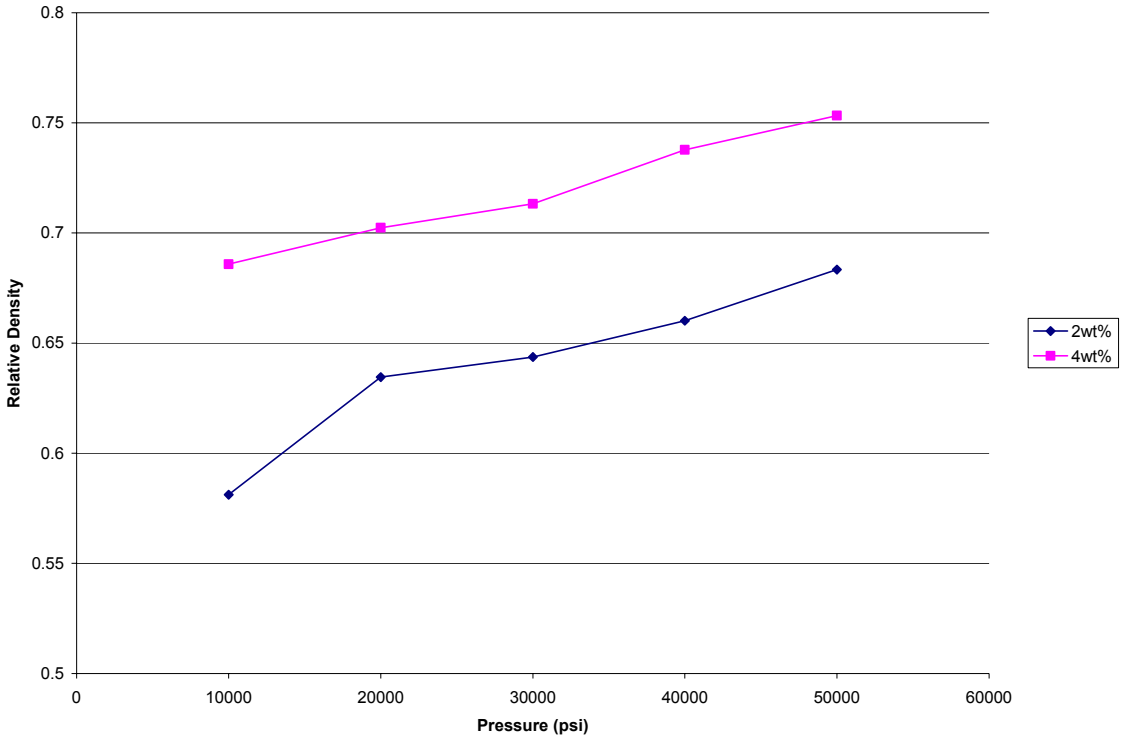

Figure 7.5 – Relative Density of Pressed Pellets at Various Pressing Pressures

As can be seen in the above figure, with sufficient pressure, the granules are able to be packed into a green form with high relative densities. As expected, as pressure is increased, the relative density of the granule compacts increase. It is interesting to note that the granules prepared with the 4 wt% PVA suspension pack at a higher relative density than that of 2 wt%; this is most likely due to their slightly larger size, and the increased deformability of the enlarged PVA coating.

A final reason for poor green part density is due to insufficient deformation of the spray-dried granules. As noted in Section 6.1.3, granule deformation decreases the distance of the ceramic particles, which directly affects the sinterability of the green part. In order to increase granule deformation, the amount of solvent introduced into the powder bed must be increased. Unfortunately, the Z402 3D Printer does not offer its

users the ability to increase the size of the droplets. Furthermore, there is no means of forcing the machine to print multiple times without recoating. As such, droplets of solvent (roughly 12 μL in volume) were manually deposited into the powder bed using a small syringe. In order to avoid over-saturation caused by large droplets, droplets were manually deposited at every third recoating pass (thus making the layer thickness of the manually created parts 0.267 mm). The resulting parts (roughly 4 mm in each dimension) are displayed in Figure 7.6. Their measured post-sintering relative densities are presented in Table 7.5.

Figure 7.6 – Parts Created via Manual Deposition of Solvent

Table 7.5 – Part Density as Result of Manual Solvent Deposition

Granule Binder Content	***Deposited Solvent***	***Relative Density (%)***	***Open Porosity (%)***
4 wt%	Water, manual	78.9	11.3
		80	11.7
		81.5	4.9
		83	7.9
	Average	**80.85**	**8.95**

As can be seen in the above table, the relative densities of the finished parts are much greater than that achieved through the standard setting of the Z402 printer (as compared to the data presented in Table 7.3; roughly a 25% increase). Compared to parts created with the 2 wt% & ZB7 binder system, parts created with a large amount of

solvent provide an 18.45% increase in relative density. Therefore, it can be concluded that, although not illustrated in the current embodiment (i.e., the use of a Z402 printer), the density of the finished green part can be increased through the deposition of a solvent in a bed of granules created via spray-drying with a polymer coating. Thus the secondary research hypothesis (presented in Section 6.1.3) is verified.

7.2.3 Porosity Analysis

In order to further evaluate the quality of the parts that is able to be realized using this manufacturing process chain, the porosity of the finished parts is investigated. This is accomplished by exploring the cross-sectional surface of each principal direction (parallel and perpendicular to the build-direction) for parts created from all of the granule/solvent systems presented in the previous sub-section.

Fully-processed part cross-sections are analyzed by first mounting samples in epoxy pucks, and then polishing them through a progression of grit sizes; thus obtaining a clean cross-sectional surface for microscopy. The samples presented in this section are prepared by polishing with the following SiC grit progression: 180, 280, 500, 800, 1200, and then 2400 grit. Following this progression, a 1 μm alumina suspension is used as a polishing substrate to further remove any remaining polishing defects.

X-Y Cross-Section

The X-Y cross-section provides an opportunity to analyze the porosity present in a typical cross-sectional layer fabricated by the process. Each sample presented in this sub-section is roughly 8 mm in dimension after sintering.

The micrographs for the 2 wt% + ZB7 granule/binder system are presented in Figure 7.7.

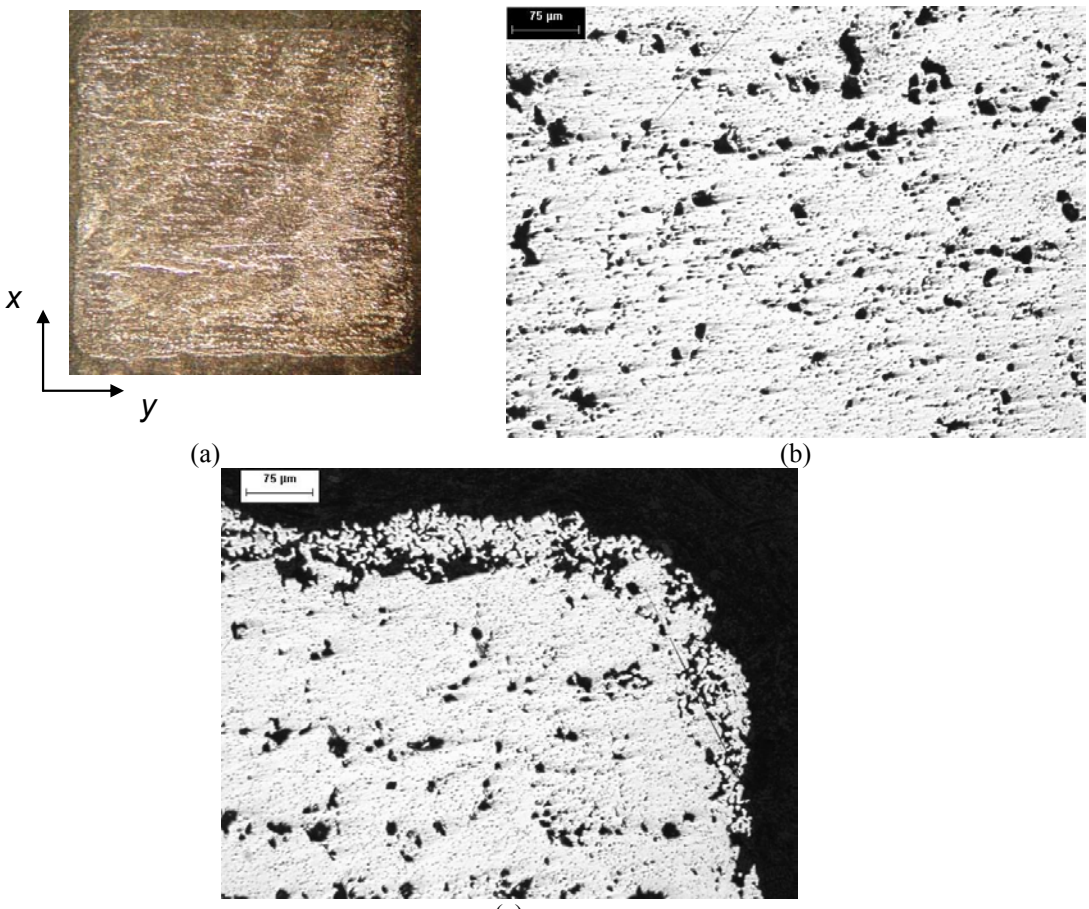

(a) (b)

(c)

Figure 7.7 – X-Y Cross-Section of 2 wt% + ZB7 Sample

As can be observed in Figure 7.7a and 7.7b, the pores are aligned parallel to the direction of the printhead travel (left to right for each figure, the *y*-axis as indicated in Figure 6.9). It is likely that the lines of pores are locations in which printed bands did not successfully overlap or "stitch" to one another. This can be due to a clogged print nozzle, but is more likely due to un-optimized binder characteristics (surface tension, wetting of granules, viscosity, droplet size, etc.) and associated process parameters (e.g., line overlap, as dictated by the gantry travel direction – the *x*-axis as shown in Figure 6.9).

A corner edge of the sample is shown in Figure 7.7c. It is interesting to note that several small pores exist along the perimeter of the sample. Furthermore, underneath that

porous surface, there exists a segment of very dense material (as compared to the center of the sample). From these observations it can be concluded that the dense perimeter is the boundary (or "shell") of the part (as described in Section 6.2.1), and that the porous perimeter is composed of granules that were attached to the part due to unwanted wetting during the binder deposition process.

The micrographs for the 4 wt% + water/ethanol mixture system are presented in Figure 7.8.

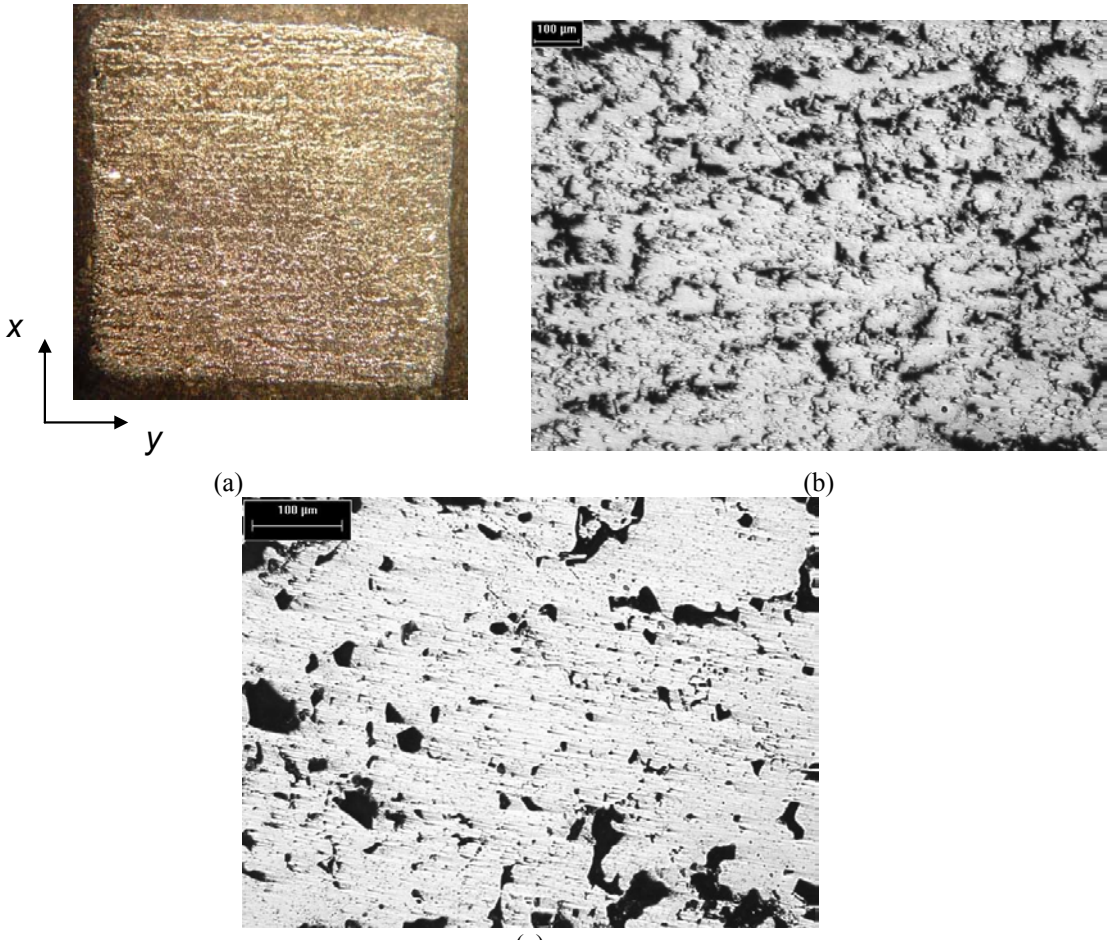

Figure 7.8 – X-Y Cross-Section of 4 wt% + Water/Ethanol Mixture Sample

This sample features more porosity than that presented in Figure 7.7 (as expected from the results presented in Table 7.1), and more pronounced pore alignment due to poor

stitching between printed bands (the print direction is left to right relative to samples shown in Figure 7.8).

The micrographs for the 4 wt% + water granule/binder system prepared at a layer thickness of 0.1 mm are presented in Figure 7.9.

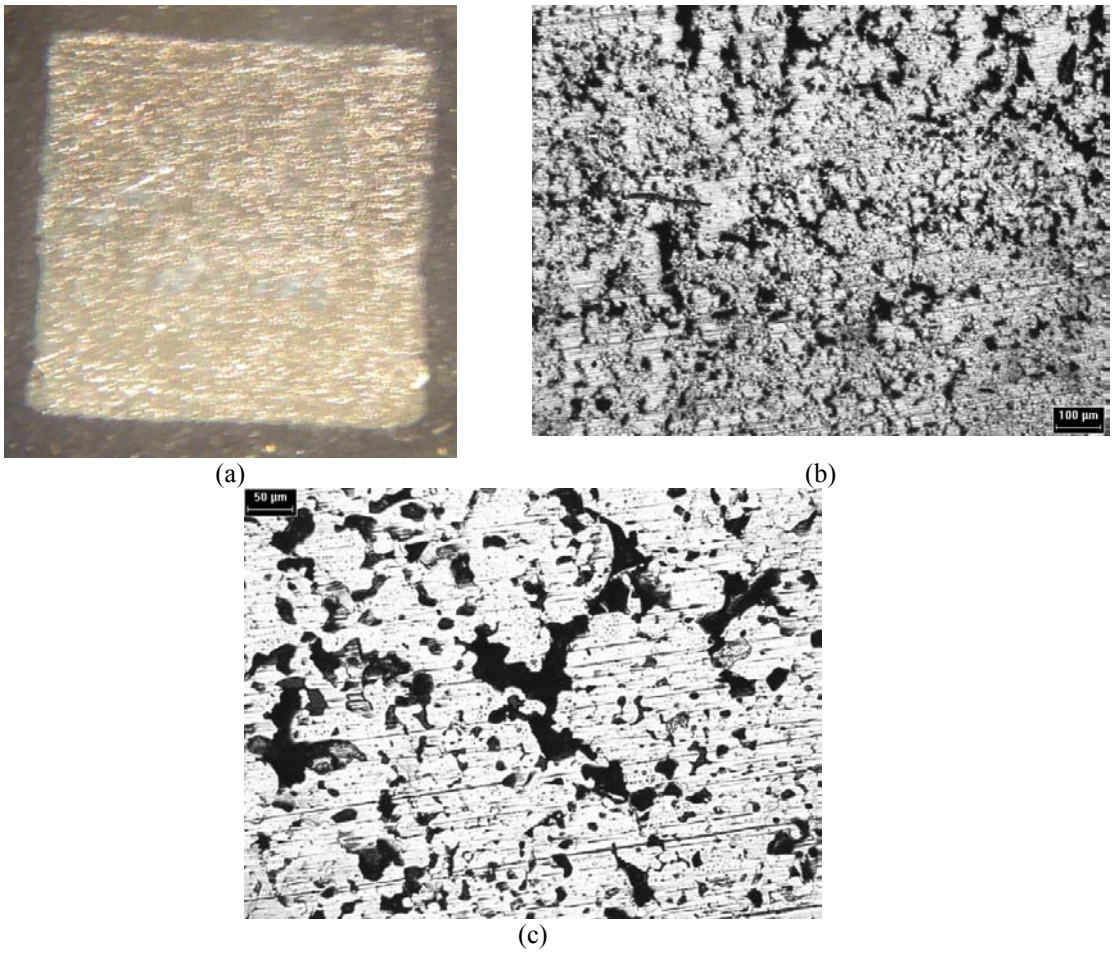

Figure 7.9 – X-Y Cross-Section of 4wt% with Water (at 0. 1 mm layer thickness) Sample

Unlike the two previous samples, there is an absence of aligned porosity due to banding effects in the sample presented above. In corroboration with the open porosity measurement of Table 7.3, there exists relatively more porosity in this sample than in the other two; however, the pores seem slightly smaller and more evenly dispersed.

The same observations can be made for the sample created by the 4 wt% + water granule/binder system prepared at a layer thickness of 0.089 mm. The micrographs for this system are presented in Figure 7.10.

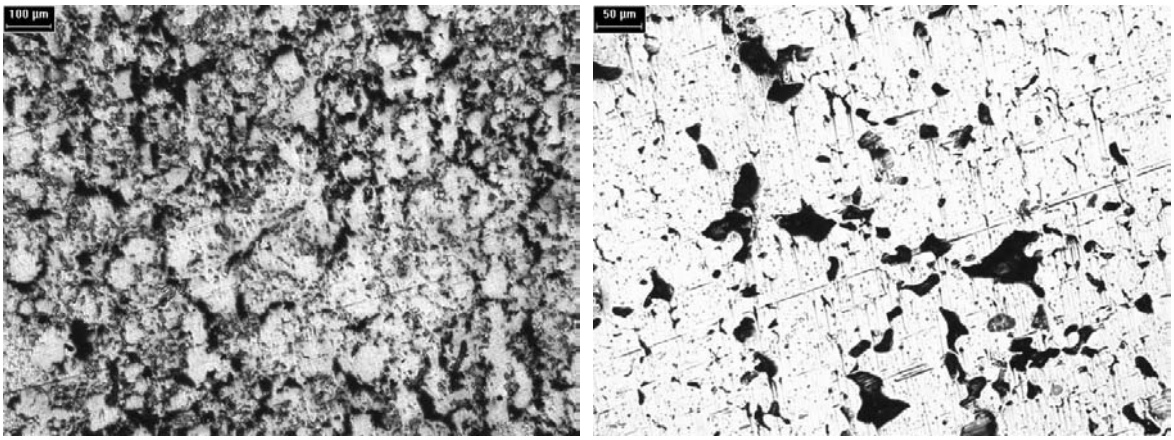

(a) (b)

Figure 7.10 – X-Y Cross-Section of 4wt% with Water (at 0. 089 mm layer thickness) Sample

These results are expected due to the increased viscosity and reduced surface tension of the water/ethanol mixture. As will be discussed in Section 8.1, both a reduction in surface tension and an increase in viscosity will result in an increased primitive size. This increased primitive size accounts for the lack of aligned porosity observed in those parts created with pure distilled water.

X-Z Cross-Section

The X-Z cross-section provides an opportunity to analyze the porosity that exists along the build direction of the part. Each sample presented in this sub-section is roughly 8 mm in width and 14 mm in length after sintering.

The micrographs for the 2 wt% + ZB7 granule/binder system are presented in Figures 7.11 – 7.14. It is clear from observing Figure 7.11 that there is a significant difference in the top surface of the sample relative to its bottom surface. It should be

noted that the length-wise lines in the sample are not relics of the manufacturing process, and are instead scratches from the polishing process.

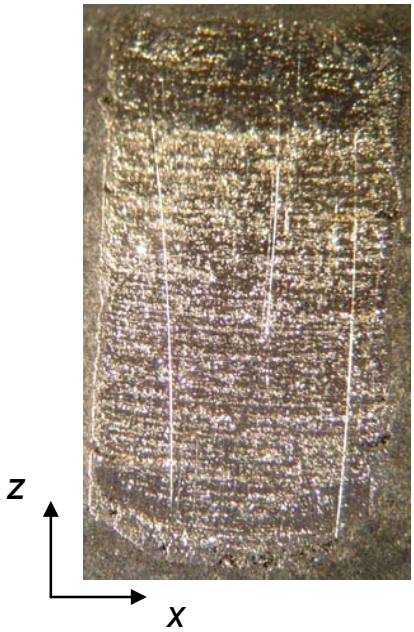

Figure 7.11 – X-Z Cross-Section of 2 wt% + ZB7 Sample (top surface on LHS)

From this figure it is possible to observe how each deposited layer exhibits curling along the edges of the sample. It is also possible to see the how the bottom (i.e., initially deposited) layers are severely warped from this curling. Most importantly, however, one can see relics of each layer, as pores are aligned along the layer surface. Finally, it is possible to see the increased part density along the "shell" (i.e., perimeter) of the part, as compared to the center or "core" of the part due to the increased saturation.

A magnified view of the top edge of the sample is provided in Figure 7.12. Compared to the center portion of the sample (Figure 7.13), it is clear that this section of the sample is much denser. It should also be noted that, similar to what was observed in Figure 7.7c, there is a collection of several small pores on the up-most surface – due

either to partially wetted granules, or to damage from post-processing with compressed air.

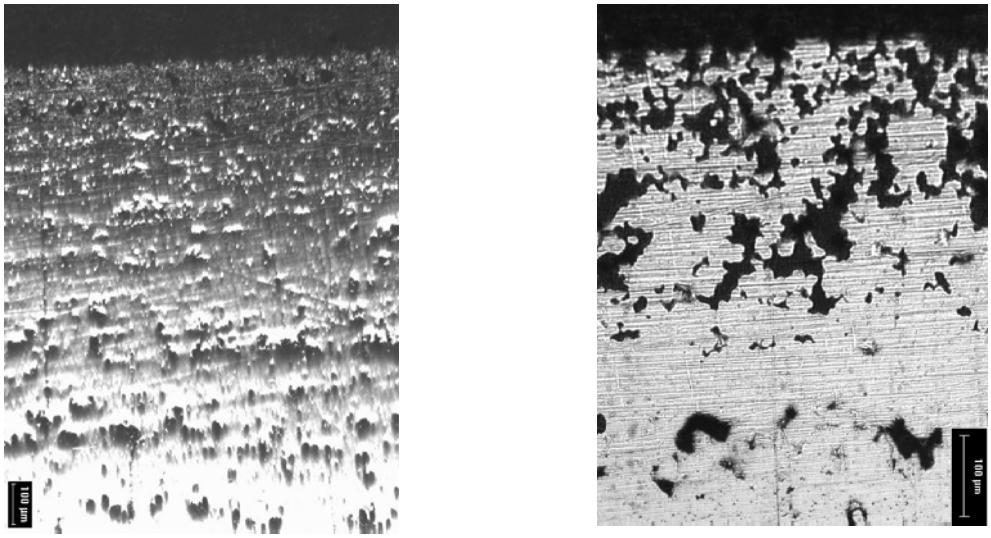

(a) (b)

Figure 7.12 - Top Surface of 2 wt% + ZB7 Sample

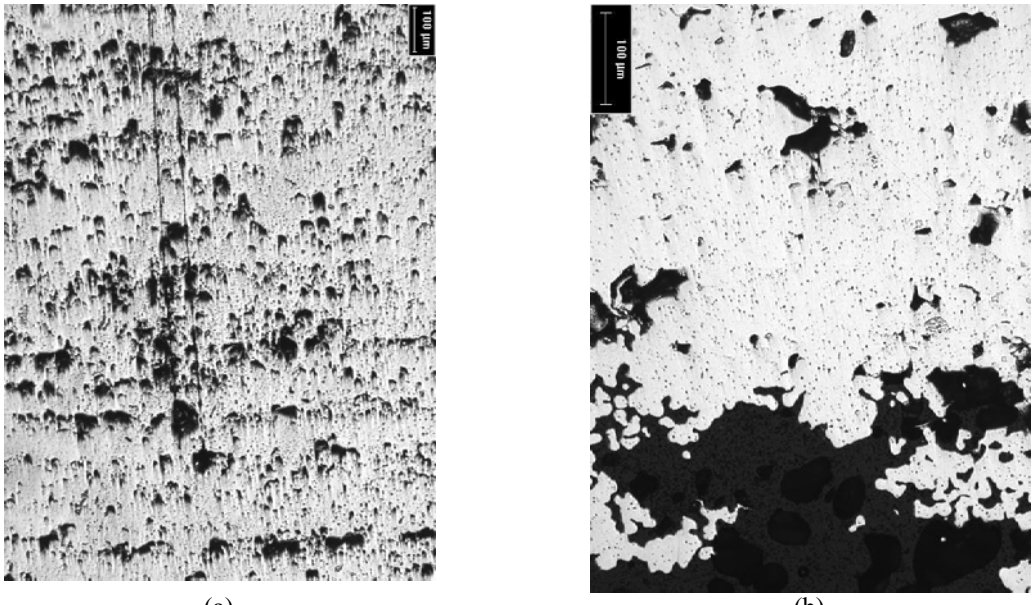

(a) (b)

Figure 7.13 – Center Section of 2 wt% + ZB7 Sample

At the center of the sample one can observe the presence of very large pores. Most importantly, it becomes clear that the pores are aligned perpendicular to the build direction (i.e., the *z*-axis in Figure 6.9), suggesting that they are relics of the layered

process. This feature suggests that the binder is not sufficiently penetrating the powder bed so as to fully fuse the layers together.

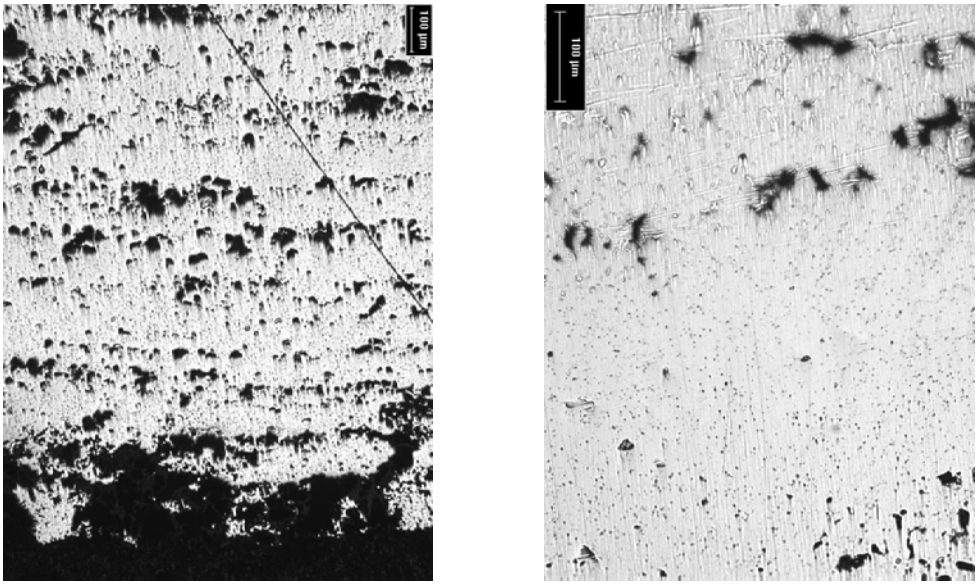

(a) (b)

Figure 7.14 – Bottom Surface of 2 wt% + ZB7 Sample

A magnified view of the bottom edge of the sample is provided in Figure 7.14. The large porosity of the bottom-most layer is due to powder ejection caused by the impact of the jetted binder. In Figure 7.14b, one can see the increased density and small pores present in the bottom layers which have been sufficiently more saturated with binder than that of the center of the sample.

The micrographs for the 4 wt% + water/ethanol mixture system are presented in Figure 7.15. Just as in Figure 7.11, it is observed that layer curling and porosity are aligned perpendicular to the build direction (*z*-axis).

Figure 7.15 – X-Z Cross-Section of 4wt% + Water/Ethanol Mixture Sample

The top surface of this sample is shown in Figure 7.16; a portion of the center section is shown in Figure 7.17. Just as observed in the previous sample, the top surface features a higher density and much smaller pores than the center section. These magnified images give one the ability to clearly see the large pores present throughout the part, as well as the manner in which said pores are aligned along each layer division.

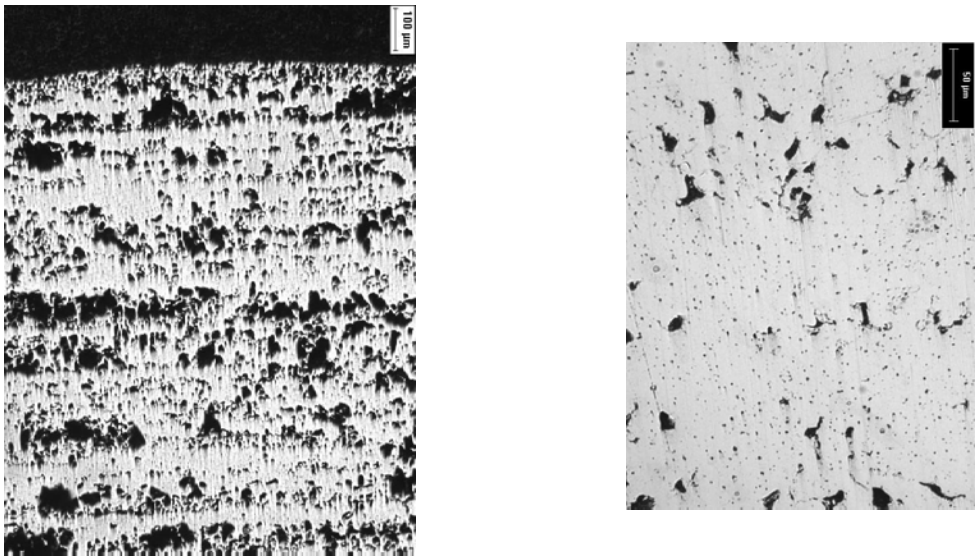

(a) (b)

Figure 7.16 – Top Surface of 4wt% with Water/Ethanol Mixture Sample

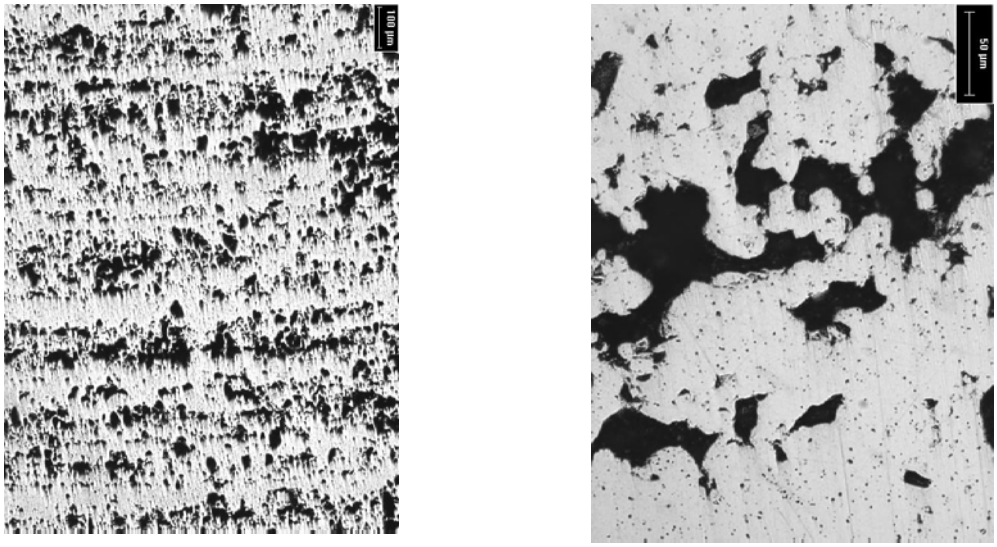

(a) (b)

Figure 7.17 – Center Section of 4wt% with Water/Ethanol Mixture Sample

Finally, views of the bottom surfaces of the 4 wt% granule samples composed via the deposition of distilled water (for both 0.1 and 0.89 mm layer thicknesses) is presented in Figure 7.18.

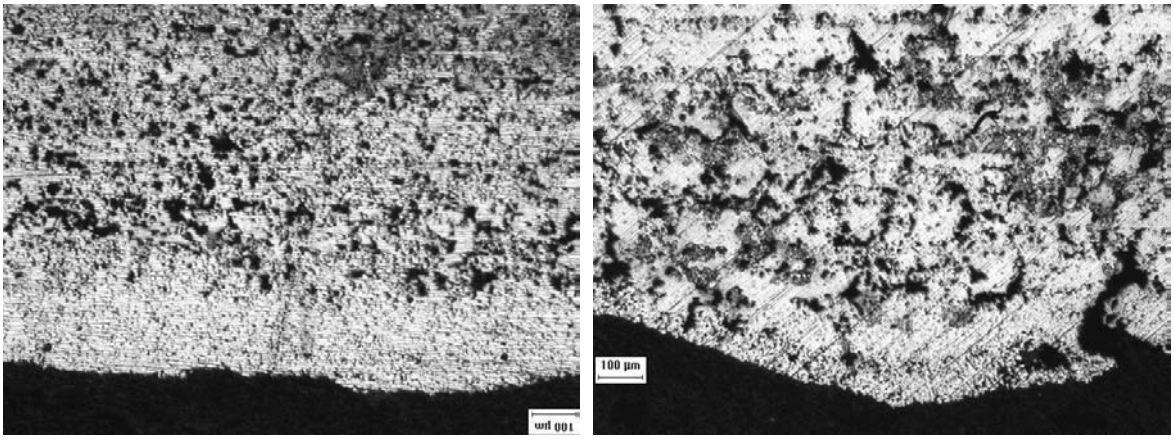

(a) (b)

Figure 7.18 – Bottom Surfaces of 4wt% with Water Samples; (a) 0.89 mm layer thickness, (b) 0.1 mm layer thickness

Unlike the previous samples, there is no clear definition of the layered process. The pores seem to be more homogenously distributed throughout the part. This is primarily

due to the higher surface tension of the solvent; thus increasing its rate and depth of penetration and better joining individual layers (as detailed in Section 8.1).

Discussion of Porosity Analysis

From the micrographs of the primary cross-sections of two different granule/binder systems, it is evident that the parts created by this process are extremely porous. Just as with the poor finished part density, it is likely that the root of this limitation is in inadequate saturation of the spray-dried granules with solvent. The deposition of additional solvent will promote increased granule deformation and thus reduce pore size. Furthermore, increasing the amount of solvent deposited into the powder bed and optimizing its characteristics (molecular weight, surface tension, volume, etc.) will improve the binding between layers, thus reducing the layered definition in the final part (as seen in the sample created with a solvent with higher surface tension).

7.2.4 Shrinkage Analysis

In order to characterize the shrinkage that parts undergo during post-processing, a specialized part is created (presented in Figure 7.19). The part consists of a 20 mm square coupon with four features: a cylindrical peg and three rectangular features aligned parallel, perpendicular, and at a 45^{o} orientation to the gantry motion (x-axis).

Percent linear shrinkage is calculated by comparing the difference of a feature's dimension in its sintered ($d_{sintered}$) and green states (d_{green}), as shown in Equation 7.1.

$$\% \text{ linear shrinkage} = \left(\frac{d_{green} - d_{sintered}}{d_{green}} \right) 100 \qquad [7.1]$$

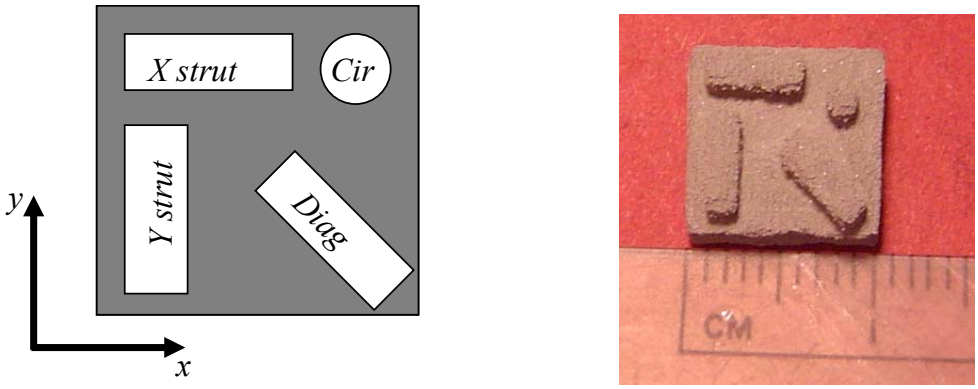

(a) (b)

Figure 7.19 – Shrinkage Test Piece; (a) illustration, (b) as built and fired

The amount of linear shrinkage measured for each dimension of each feature of the test piece pictured in Figure 7.19 is presented for the various granule/solvent systems in Table 7.6.

Table 7.6 – Linear Shrinkage for Various Granule/Solvent Systems for All Features of Shrinkage Test Piece

	2 wt% + ZB7	*4 wt% + Water/Ethanol*	*4 wt% + Water @ 0.1 mm*	*4 wt% + Water @ 0.089 mm*
Dimension	**% Linear Shrinkage**	**% Linear Shrinkage**	**% Linear Shrinkage**	**% Linear Shrinkage**
X	42.55	46.7	48.5	48
Y	42	45.6	46.5	46.6
Cir (diameter)	32.67	33.3	44	30
Diag, t	24.3	31.5	40	31.3
Diag, L	42.4	43.1	44.4	42.9
X strut, t	21.5	32.3	38.7	29.67
X strut, L	43.9	45.25	47.5	46.4
Y strut, t	23.67	37.5	44.7	40
Y strut, L	38.2	42.3	44.8	41.6

It should be noted that shrinkage in the *z*-axis is not included in this analysis as the curling errors (noted in Section 7.1) caused inaccurate dimensional measurements.

Upon first observation it is clear that the linear shrinkage experienced by the part is anisotropic. Upon further investigation, it becomes clear that there are two distinct ranges of shrinkage values for each binder/granule system. Closer inspection reveals that those dimensions aligned with the *x*-axis (gantry direction of motion) experience more

shrinkage than those aligned with the *y*-axis (print head direction of motion). This is primarily due to the banding phenomenon discussed earlier. Because the printheads' depositions do not sufficiently overlap, there exist segments of unbound powder that leave porosity upon firing and thus provide room for further shrinkage. It is important to note that it is likely that this problem is unique to this specific embodiment; different printing setups could account for this with a higher printing resolution, a better tailored printing medium, or via overlapping printheads.

Through further investigation of the results presented in Table 7.6, one can observe that there exists a difference in percent linear shrinkage between features with variable thicknesses. This is a primary concern when trying to take into account the shrinkage caused by reduction shrinkage. Because this range of shrinkage is reproducible, it is possible that the part could be tailored to compensate for this difference. Of course, it is possible that this is a limitation of any embodiment of this process, and hence part geometry would be limited to features with common thicknesses.

7.3 MANUFACTURING PARTS OF DESIGNED MESOSTRUCTURE

In an effort to characterize the proposed manufacturing process's capability of fabricating parts of designed mesostructure, several test pieces with geometries typical of this class of material were created. Specifically tests are conducted to verify that the designed mesostructure is capable of realizing parts of designed mesostructure: thin walls, small channels, angled trusses, and complex geometry.

The sample parts are presented in both their green and sintered forms in Figures 7.20 – 7.28. Due to the size limitations of the tube furnace used to reduce and sinter the parts, the green parts are no larger than 50 mm in their cross-section.

7.3.1 Thin Wall Test

The sample part shown in Figure 7.20 was created in order to discover the minimum wall thickness that is capable of being produced with the proposed manufacturing process. High-aspect ratio walls are prevalent in cellular materials as they provide channels for fluid flow in heat transfer applications as well as load bearing supports for structural applications. Because printing resolution is primarily dependent on the design of printhead, this test is not necessarily representative of the best possible result of this principal solution. After sintering and reduction, the minimum wall thickness successfully built with this embodiment of the process is 270 μm.

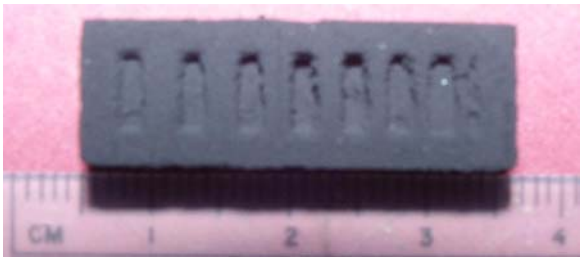

(a)

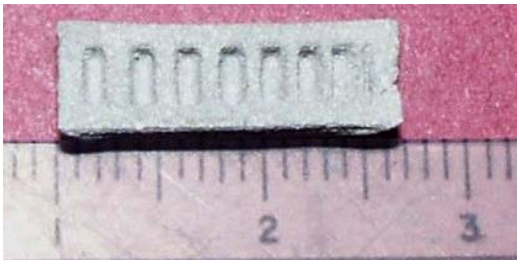

(b)

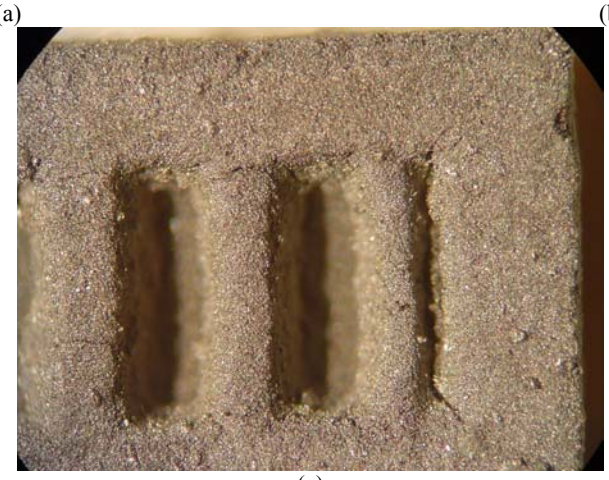

(c)

Figure 7.20 – Thin Wall Test Part: (a) green part, (b) & (c) sintered and reduced part

It should be noted that 270 μm is not the absolute minimum wall thickness that can be achieved with this principal solution; it is just the minimum that can be achieved with this embodiment. Smaller wall thicknesses could be realized via the use of newer print heads that have higher resolutions (i.e., the ability to deposit more "dots per inch").

7.3.2 Small Channel Test

The sample part shown in Figure 7.21 is created in order to test the ability of the process to realize parts with small channels and pores. While it is evident that the 3DP process has the resolution to create geometry with very small voids, these parts are used to test the ability of the green parts to withstand the rigorous depowdering that is necessary to remove the unbound powder. The trussed cube shown in Figure 7.22a features open channels that are 2 mm square and 10 mm in length (with intersecting channel openings) in the green state. After reduction and sintering, these channels shrink to roughly 1.1 mm square and 5.5 mm in length.

(a) (b) (c)

Figure 7.21 – Small Channel Test; (a) CAD representation, (b) green part, (c) sintered and reduced part

It is important to note the difficulty in cleaning this test piece. Unlike the standard ZCorp plaster powder, it is extraordinarily difficult to remove the unbound granules from small channels due to their higher packing fraction. Furthermore, the increased air

pressure needed to clean the channels often causes fracture of thin walls due to the fragility of the green part.

7.3.3 Angled Truss Test

As explained in Section 2.5.1, it is often a challenge to create trusses that are angled to the build plane in additive fabrication processes, since the combination of acute angles, thin trusses, and large layer thicknesses can lead to non-overlapping layers (as shown in Figure 2.6). In order to test the process's ability to create angled trusses, two test pieces were created.

The trussed channel shown in Figure 7.22 features two trusses (2 mm in diameter in green state; 0.92 mm in sintered and reduced state) angled at 45 degrees across a channel, and one truss horizontally spanning the channel.

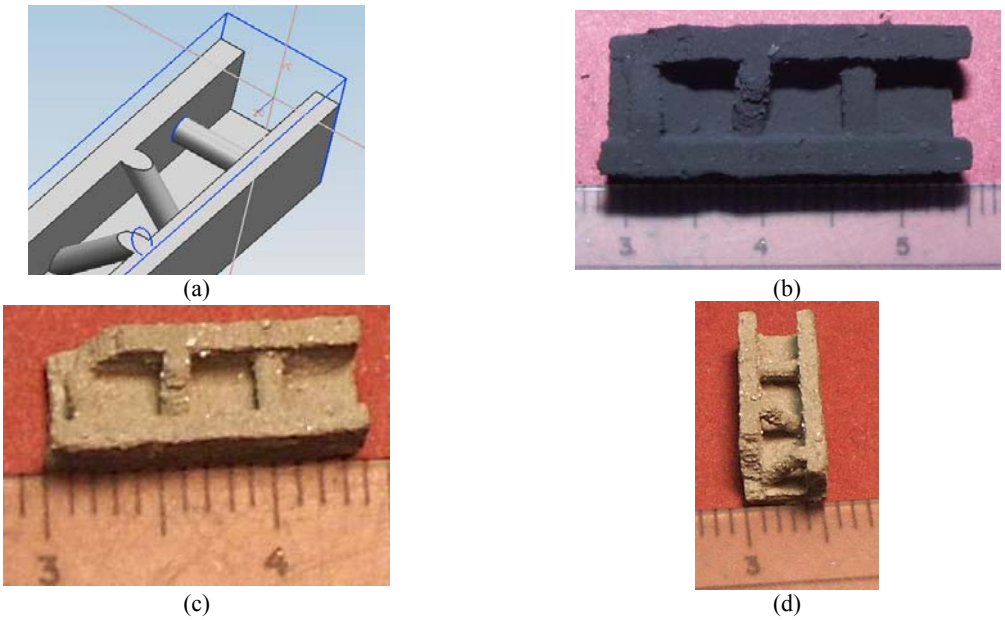

Figure 7.22 – Angled Truss Test; (a) CAD representation, (b) green part, (c) & (d) sintered and reduced part

The second test piece was created to test the process's ability to realize longer trusses at more acute angles. As such, two sets of 3 angled features are featured on the test piece. Specifically, two sets of trusses (one at 2.5 mm and the other at 1.75 mm in

green diameter) at 45, 30, and 20 degree inclines to the build plane. The results from this test are presented in Figure 7.23.

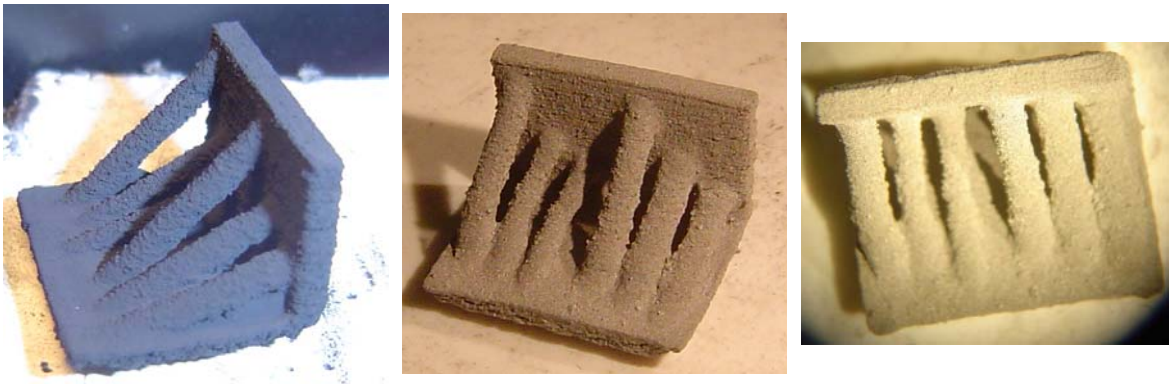

(a) (b) (c)

Figure 7.23 – Angled Strut Test; (a) green part, (B) & (c) sintered and reduced part

As can be seen in the above figure, all trusses of both sets of diameters were able to be processed successfully in the green state. Each truss also survived the reduction and sintering post-process. A small amount of sagging is observed visually; although it is unclear if this is due to the inability of the part to support itself during binder burnout, or if small cracks were imparted on the trusses during green cleaning.

7.3.4 Complex Geometry Test

With the process's ability to realize the geometrical building blocks of parts of designed mesostructure (thin walls, small channels, angled trusses) verified, a series of parts that feature a combination of these features are created in order to verify the process's ability to realize parts with complex geometry.

Trussed Channel

The part shown in Figure 7.24 featured a channel of 5 mm square and 30 mm in length in its green state. Four trusses (2 mm in diameter in green state) span the channel.

In its fired state, the channel is 2.6 mm square and 21 mm in length, with 1.1 mm diameter trusses.

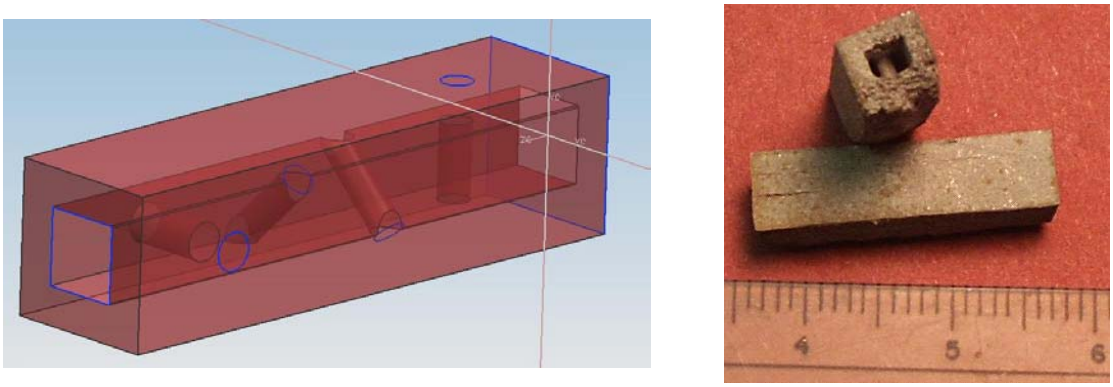

(a) (b)

Figure 7.24 – Trussed Channel Test Sample; (a) CAD representation, (b) sintered and reduced

The unbound powder was easily removed from the sample parts via compressed air. Although this test geometry was successfully created, it should be noted that there exists a limit to the size of channel that can be created with this process due primarily to an inability to remove unbound powder from small and/or closed channels as noted in Section 7.3.2. Through additional tests it was found that channels smaller than 2 mm in diameter (green state) could not consistently be depowdered; variation of success was dependent upon channel length and whether or not the channel was open on both ends

Tetrahedra

The part shown in Figure 7.25 features a series of three linked tetrahedra composed of trusses which are inclined at 70^{o} to the build angle and are 1.1 mm in diameter (2 mm in green state).

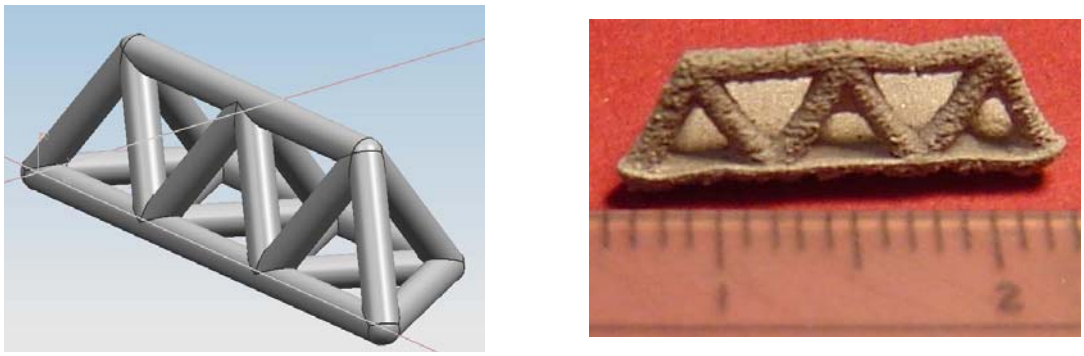

(a) (b)

Figure 7.25 – Tetrahedra Test Sample; (a) CAD representation, (b) sintered and reduced

It is important to observe that the horizontal strut has some sagging in between the right-most pair of tetrahedral (seen in Figure 7.25). This is primarily due to a "tear" that developed in the green part during post-processing. This tear is made worse during sintering as the struts shrink and pull away from each other, thus creating a sagging structure. This problem can be alleviated with a more careful post-processing step, or through further strengthening of the green part.

Trussed Structure

In order to fully test the capabilities of the designed manufacturing process chain, a series of test pieces featuring trussed structures are produced (Figures 7.26 – 7.28).

The first of the three parts (Figure 7.26) is a 20 mm cube composed of 3 mm diameter trusses (green state). As can be seen in Figure 7.26d, the sintered part is 14 mm with 1.9 mm trusses. As can be seen in Figure 7.26b, there is a small "tear" in one of the horizontal trusses of the upper face of the green part (an artifact of clumsy cleaning); after sintering (Figure 7.26c) this truss is further pulled apart and begins to sag (as seen previously in Figure 7.26b). Furthermore, the part was built on a small platform in order to circumvent the aforementioned issues with the initially fabricated layers (curling and

powder ejection), thus ensuring that these difficulties wouldn't interfere with the geometry of interest.

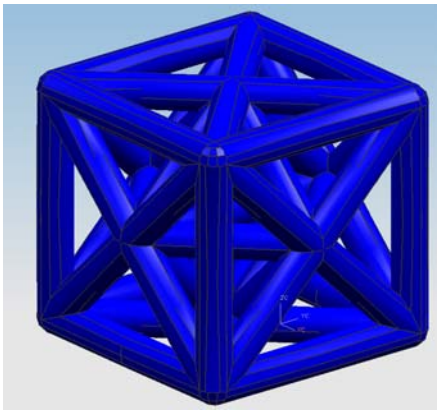

(a)

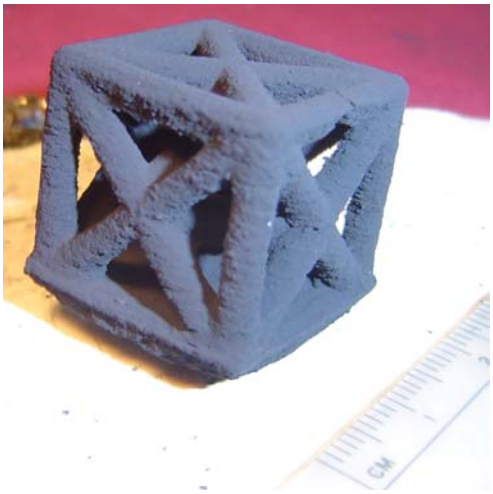

(b)

(c)

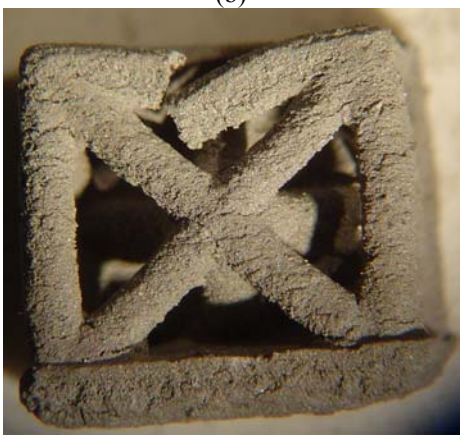

(d)

Figure 7.26 – Large Trussed Cube Test Sample; (a) CAD representation, (b) green part, (c) & (d) sintered and reduced

With the successful realization of a trussed cube with large diameter trusses and large gaps in between the struts, a second trussed geometry (Figure 7.27) is created to investigate if the process is capable of producing a part with smaller trusses (1.75 mm diameter in green state) and smaller strut gaps.

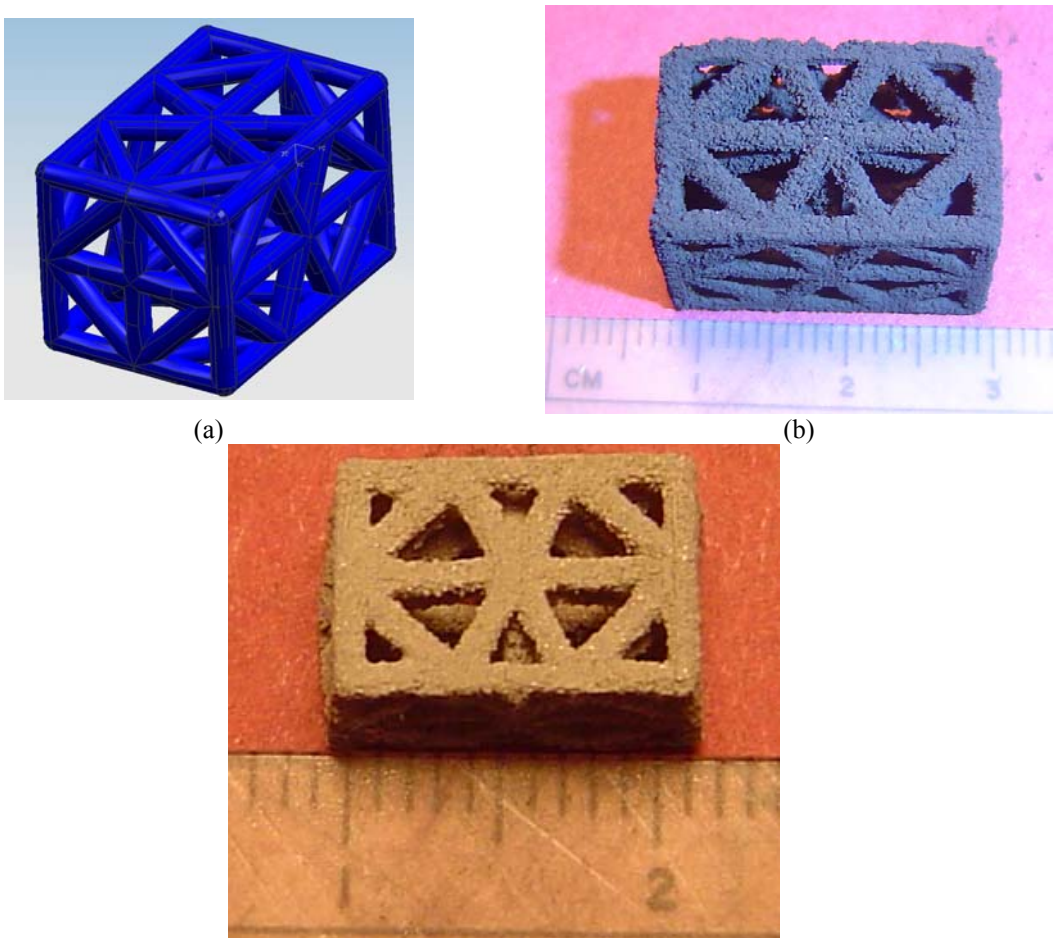

(a) (b)

(c)

Figure 7.27 – Medium Trussed Solid Test Sample; (a) CAD representation, (b) green part, (c) sintered and reduced

As can be seen in Figure 7.27, this part was fabricated successfully. A few of the trusses which lie on the bottom-facing surface are incomplete due to the curling and powder ejection issues mentioned above; the top-surface however, which does not encounter such problems, has a high quality surface finish and feature definition (Figure 7.26c).

With this part successfully created, a larger part is created with the same diameter trusses, but with smaller gaps in between the struts (Figure 7.28). As can be seen in Figure 7.28b, the part is successfully fabricated with the 3DP machine; however (as can be seen in 7.28c), attempting to remove the compacted unbound powder trapped within

the part's voids caused the part to fracture. It is important to note that the bottom-facing surface is the portion of the cube which failed. This is an expected effect from the difficulties associated with powder ejection and curling in the initial layers.

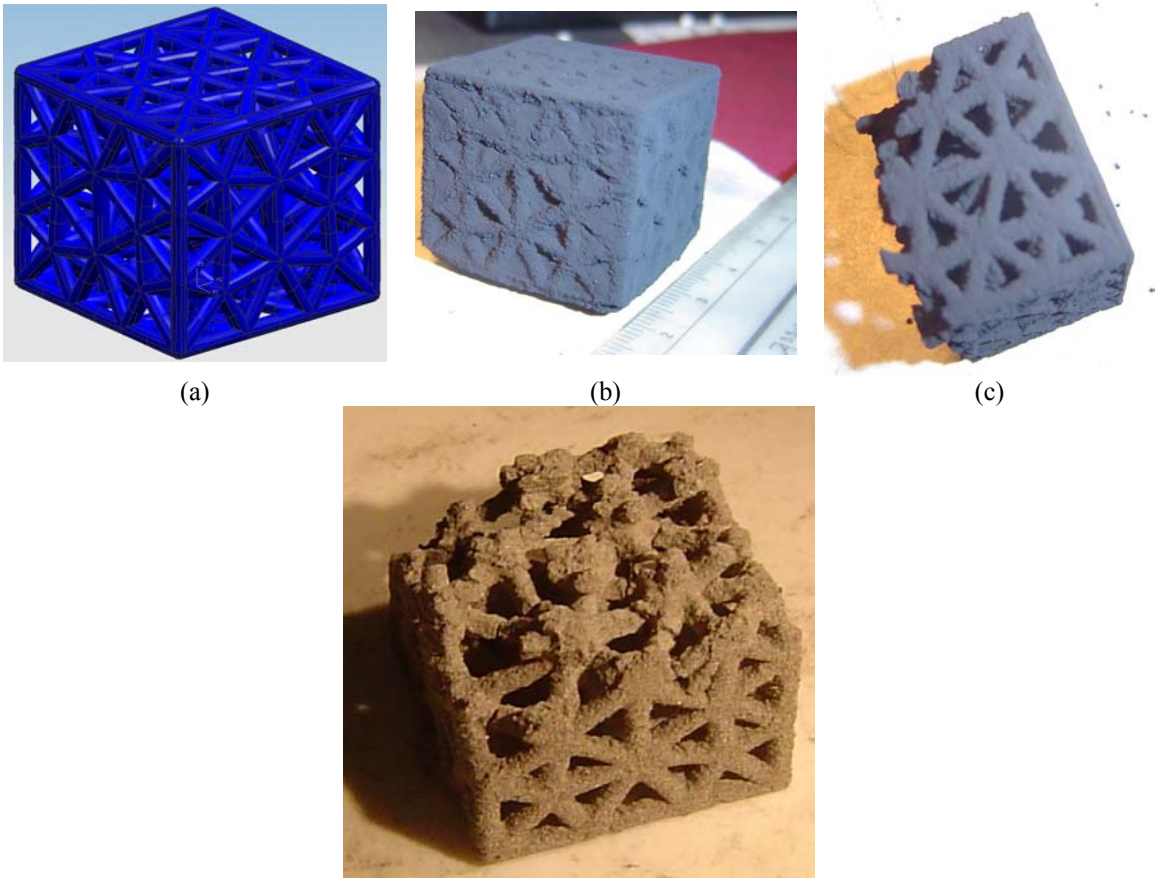

(a) (b) (c)

(d)

Figure 7.28 – Small Trussed Cube Test Sample; (a) CAD representation, (b) & (c) green part, (d) sintered and reduced

Blast Resistant Panel

The final test part represents a blast resistant panel – a structure that is composed of trussed structure sandwiched between two sheets of material (Figure 7.29).

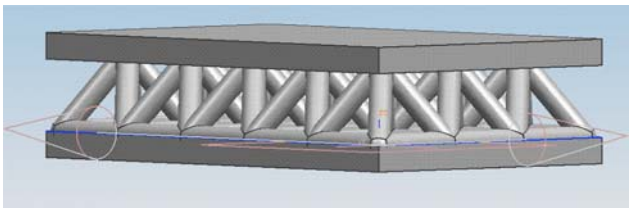

(a)

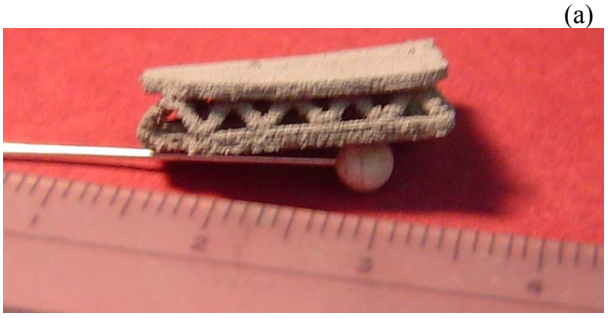

(b)

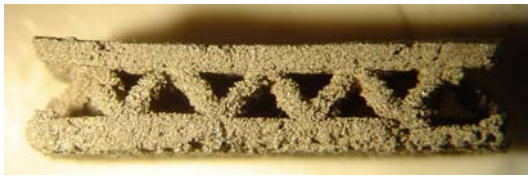

(c)

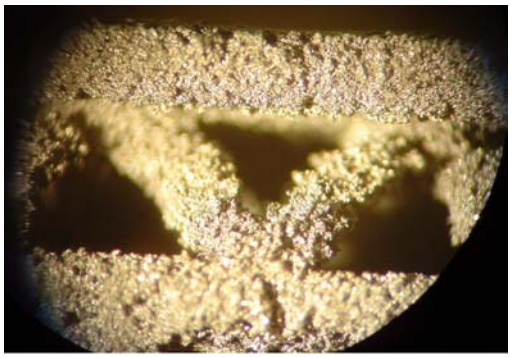

(d)

Figure 7.29 – Blast Resistant Panel Test Sample; (a) CAD representation, (b), (c), and (d) sintered and reduced part

The finished part features trusses with a diameter of 0.86 mm. As can be seen in Figure 7.29c, the only cosmetic flaw in this part is the slight warping of the top surface. This is caused by the curling phenomenon discussed earlier in this chapter. It is important to note that the curling occurs on an upper surface in this part. The upper surface curls because its deposition occurs over dry/unsaturated powder just as seen when initiating a build. Finally, the rough surface typical of all parts created by this process is detailed in Figure 7.29d.

7.4 CRITICAL ANALYSIS OF MANUFACTURING PROCESS

The experimental results are critically analyzed in this section in an effort to verify the primary research hypothesis. The analysis is presented in three separate sub-sections:

(i) weaknesses of the manufacturing process that are due to the specific embodiment used in this research (Section 7.4.1),

(ii) weaknesses of the process that are inherent to the general principal solution (Section 7.4.2), and

(iii) strengths of the process (Section 7.4.3).

The analysis is closed with a comparison of the process's capabilities (as displayed in this research) with the requirements the process was intended to fill (as developed in Section 2.5).

7.4.1 Weaknesses of Specific Embodiment

Observing the parts presented in this chapter, it is evident upon inspection that the manufacturing process has three primary drawbacks:

- poor finished part density,
- poor green part strength,
- and poor surface quality.

While these drawbacks have a significant impact on the quality of the finished parts, it must be noted that the parts created thus far have been fabricated with very little process optimization. These three drawbacks, which all pertain to part quality, can be corrected and/or remedied through further process development. Thus, these weaknesses are characterized as drawbacks which are pertinent to the specific embodiment of the experimental apparatus.

The most significant weakness of the manufacturing process is the inability to fabricate fully dense metal parts. This limitation primarily stems from the inability to achieve sufficiently dense (and close) packing of the metal oxide particles during green part fabrication so as to obtain high density after sintering. However, there are several developmental advancements which could potentially improve finished part density:

- *Increased solvent deposition*: One flaw in this specific embodiment is the inability to increase the amount of solvent that is deposited into the powder bed. As shown in Section 7.2.2, an increase of solvent enhances the deformation of the spray-dried granules, thus bringing the particles closer together, and improving density.
- *Tailored powder & solvent system*: Although complex parts were created with the granule/solvent system chosen, much more research could be done in tailoring the powder/solvent system so as to maximize part quality. Specifically, the solvent's surface tension, droplet size, viscosity, etc. should be tailored to improve the wetting of the chosen ceramic powder. The granule/solvent system should be designed so as to maximize the solvent's spreading and infiltration into the powder bed, and thus ensuring proper overlap (or "stitching") between the printed bands of adjacent primitives and the deposited layers. As discussed in Section 7.2.3, insufficient stitching can lead to porosity between printed bands and layers (such as those found in the parts created by this specific embodiment).

- *Hot isostatic pressing* (HIP): HIPing could be used as a secondary post-processing step in order to increase finished part density; however, this might limit the topologies that can be created by the process.
- *Printing nanoparticle suspension*: Another manner of increasing green part density could be achieved by printing a binder/solvent suspension of ceramic nanoparticles into the powder bed. Once dispersed into the powder bed, the printed nanoparticles would fill the interstitials between the powder bed particles, thus increasing the green part density. Crane and coauthors have displayed improvements in part density and in part creep via submersing green parts in a nanoparticle suspension after printing (Crane et al., 2006).
- *Bimodal powder*: The powder bed packing density can be improved by increasing the size distribution of its particles. Lanzetta and coauthors were able to successfully process a bimodal alumina powder system featuring 20 μm particles with 10 wt% 2.5 μm particles added (Lanzetta and Sachs, 2003). In this embodiment, this can easily be achieved by using the smaller granules that are found on the interior of the spray-drying chamber (known as "chamber wipe down").
- *Improved recoating*: Several different recoating procedures have been proposed in the literature so as to increase the packing density of the powder bed. It is also possible that other recoating embodiments would be able to process finer particles, which would also lead to an improved final part density.

It is important to note that the final two points of the above bulleted list (the use of bimodal powder and the use of a new recoating technique), significantly increase the

density of the powder bed and, unfortunately, create an undesirable side-effect; namely, an increasing the difficulty in removing unbound powder from the green part. Thus, it is important to spend developmental effort in improving the strength of the green part.

First and foremost, the green part can be strengthened by improving its density via the suggestions offered above. Specifically, an improvement in the amount of overlap between primitives via tailoring of the solvent/binder interaction will significantly increase the green part strength (Moon et al., 2002). Furthermore, it would be possible to strengthen the green part by adding a small weight percent of a polymer (e.g., poly-vinyl alcohol, poly-acrylic acid, etc.) into the printed binder/solvent.

In addition to improving the green density and green strength, tailoring the binder/powder system will also improve the part's surface finish. Specifically, surface roughness and delamination effects can be improved by better matching the wetting behavior between the printed and unprinted regions of the powder bed (Grau et al., 1997). Another manner in which the part's surface finish can be improved is through fixating the powder bed surface via misting of a solvent or via the addition of a metal salt, thus minimizing particle ejection during printing (Sachs et al., 1993a). Finally, as seen in (Lanzetta and Sachs, 2003), the use of bimodal powders can improve surface quality as the finer particles rearrange themselves to align on the outer surface of printed lines.

7.4.2 Weaknesses of Principal Solution

While the weakness listed in the previous section can be improved through developmental research, there are some limitations of the principal solution in general that will always prevent the manufacturing process from meeting all of the specified requirements.

- *Density*: It is unlikely that even with an optimized granule/solvent system that fully dense (> 99% relative density) parts will be fabricated by any 3DP process. This is primarily due to its inability to spread fine particles, and specifically particles < 20 μm in diameter. This large particle size cannot be sintered to full density due to the accompanying large interstitial voids. This limitation is further worsened by the use of spray-dried powders which are inherently porous. However, it has been shown (in Table 7.5) that sufficient application of solvent to spray-dried granules might be able to overcome this deficiency as significant deformation of the polymer coating can bring fine particles close enough together so as to enhance their sintering.
- *Surface finish*: Surface finish is an intrinsic limitation of powder-based processing (Ippolito et al., 1995). The inability to process fine particles, and the unintentional wetting of loose granules surrounding the printed region are two sources for poor surface finish in this embodiment. Although the use of bimodal powder and further tailoring of the granule/solvent system will alleviate surface finish deficiencies, the surface finish of finished parts fabricated in a powder bed most likely will never be able to meet stringent requirements. While it is possible to finish (i.e., grind, polish, etc.) the parts created by this process, this is of no benefit when working with cellular materials.
- *Shrinkage*: Large shrinkage is an inherent characteristic of the reduction post-process. Even with an extremely dense green part, sintering and reduction will cause significant shrinkage as the oxygen atoms are removed from the ceramic

material. The use of spray-dried granules also ensures shrinkage, as the polymer coating is removed during firing, thus leaving voids for the material to fill. Finally, it is recommended that further study be directed towards exploring the effects of reduction kinetics on shrinkage of features of variable thicknesses so as to identify any potential geometric limitations which might exist with this working principle.

- *Inhomogeneity*: Another major concern associated with working with a powder bed technology, is the inherent inhomogeneities associated with compacted powders (Tay et al., 2003). Because the powder bed is formed by pushing powder onto a bed via roller recoating, and hence is characterized as loose random packing, it is impossible to have repeatable or predictable microstructure in the finished part. This deficiency is further worsened when shrinkage plays a major role in the finishing process, as it may become impossible to achieve high processing accuracy.
- *Removal of unbound powder*: The powder bed solution principle presents yet another drawback, as it does not provide an ideal manner of creating cellular materials. The presence of unbound powder will preclude a designer from creating parts with internal voids, and, as seen in Section 7.3.4, prevents the creation of fine cells. This deficiency is further worsened by the weakness of the green part which prevents vigorous cleaning efforts. Ironically, green part weakness is primarily due to a key advantage offered by the 3DP process: the small amount of polymer required to fabricate a net shape part.

- *No aluminum or titanium*: Another limitation imposed by the reduction post-processing step is the inability to process aluminum and titanium. These materials play a major role in the aerospace and automotive industries, and can only be introduced to finished parts in a secondary process.
- *Linked parts / joints*: A novel feature of all AM processes is the ability to realize linked and/or jointed assemblies during fabrication. This is achieved in 3DP by removing the unbound powder from the clearances designed into the assembly. Unfortunately, this type of geometry would be very difficult (if not impossible) to achieve given the post-processing procedures that are present in the proposed manufacturing process, as any surfaces touching while in the sintering stage will weld together. This is further worsened by the large amount of shrinkage present in the process, which will require careful fixturing during post-processing so as to ensure that surfaces do not come into contact.
- *Clogged nozzles*: The clogging of the nozzles of the print head is a common problem present in 3DP. As of now, there is no way to know when clogging takes place, and as such, there is no control algorithm for correcting this problem. While this is usually not a major concern while prototyping, it has been illustrated by the results presented in Section 7.2.3 that unbound powder will result in significant porosity in the finished part. An example of a part cross-section (and the associate porosity) created with a clogged nozzle is presented in Figure 7.30. Fabricated with the 2 wt% granule and ZB7 binder system, it is clear when compared to its previously presented counterpart (Figure 7.8) that the clogged nozzle presents significantly poorer results.

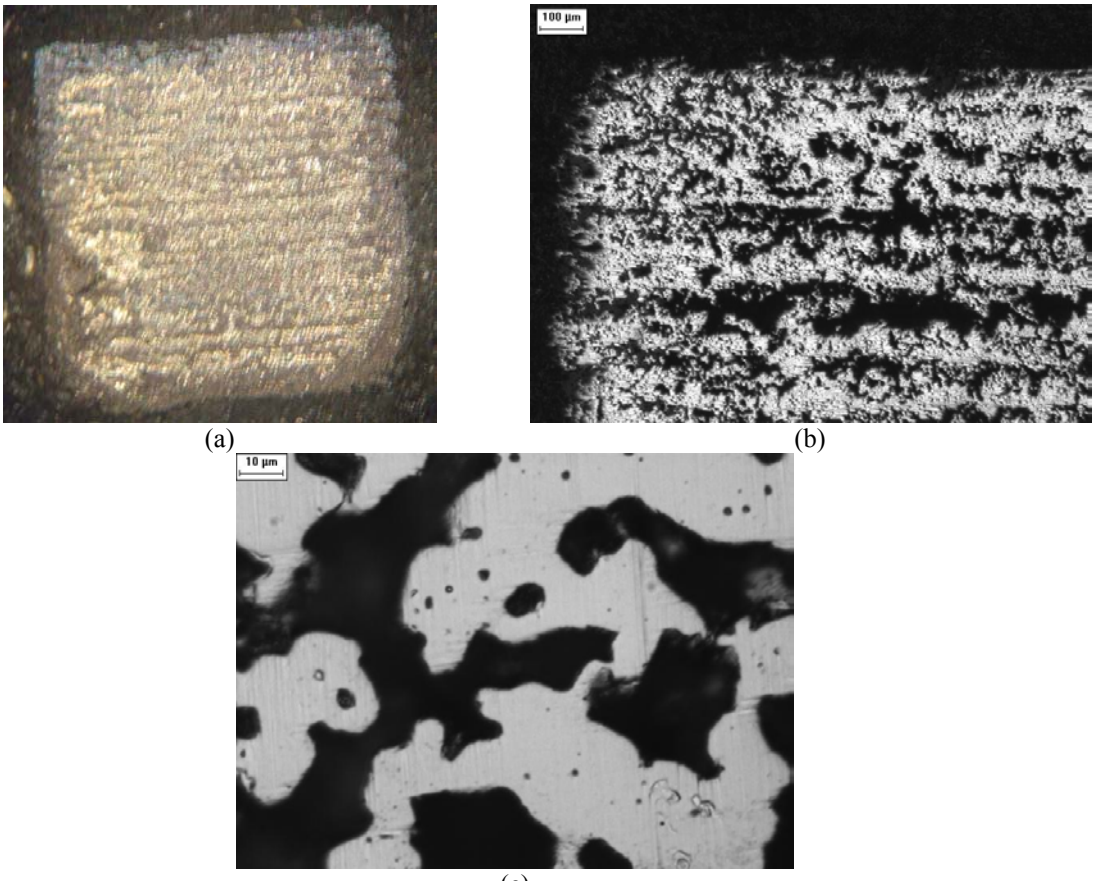

(a) (b)

(c)

Figure 7.30 – X-Y Cross-Section of Part Created with Clogged Nozzle

7.4.3 Strengths of Manufacturing Process

Despite the weaknesses presented in the two previous sections, the manufacturing process embodied thus far has shown significant promise. First and foremost, the combination of 3DP with reduction and sintering has produced metal parts with cellular geometry (as shown in Section 7.3.4) from a metal oxide starting material. Furthermore, features of < 300 μm have successfully been fabricated (Section 7.3.1), as have angled trusses (Section 7.3.3) and small channels (Section 7.3.2). Maybe most importantly, it has been verified that parts created with 3DP (and more generally, with little binder content) are able to survive debinding and sintering (i.e., maintain their shape).

Not only is the designed process able to fabricate parts which meet the geometric requirements established in Chapter 2, the process is able to do so while meeting the production goals as well. Specifically, metal parts of designed mesostructure have been created cost-efficiently by avoiding the use of

- expensive components such as lasers, electron beams,
- expensive materials such as metal powders which are specialized for the process, and
- time consuming fabrication solution principles such as one-dimensional patterning of material and/or energy.

Furthermore, the process can be easily scaled to production levels of capacity as additional print heads and larger build volumes can easily (and cost-efficiently) be added.

Finally, little effort is required in processing new materials with 3DP (Yoo et al., 1993). This is especially true in this specific embodiment; by using a modular combination of PVA spray-dried granules of powders, it is easy to change the core powder without having to re-engineer the granule/solvent system. For example, as shown in Figure 7.31, spray-dried alumina has been processed using the same embodiment presented in Chapter 6. After debinding and sintering (reduction of alumina is not possible), an alumina ceramic part is realized.

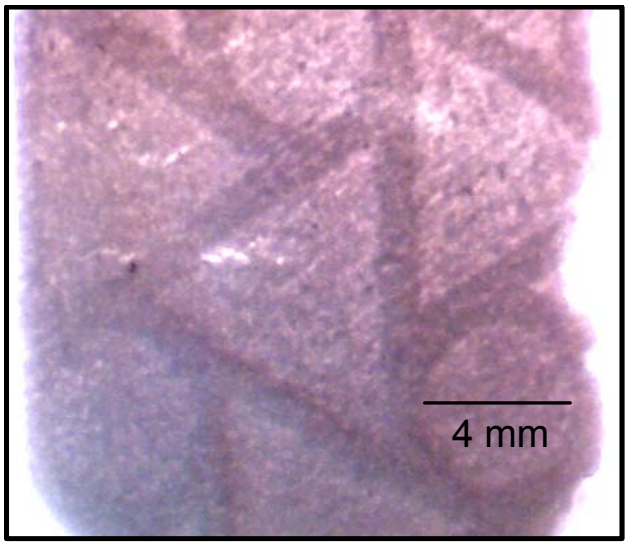

Figure 7.31 – Alumina Chiral Pattern Created via 3DP of Spray-Dried Powder

7.4.4 Comparison Against Requirements List

In a final effort in verifying the initial research hypothesis, the process requirements (originally presented in Table 2.15) are compared with the designed processes capabilities. This comparison is presented in Table 7.7

As can be seen through observing Table 7.7, the majority of the requirements have been met. Most importantly, the geometric requirements have been satisfied. The only requirements that have not been satisfied all pertain to finished part quality. However, as discussed in Section 7.4.1, part quality improvements can be made through further development of the principal solution (aside from the surface finish and relative density requirements, as noted in Section 7.4.2).

Table 7.7 – Requirements List Checklist

D/W	*Requirement*	*Met?*
	Geometry	
D	Able to process any macrostructure geometry	Y
D	Able to process complex geometry: - overhanging features - internal voids - high-aspect ratio structures	 Y Y Y
D	Able to process small cell sizes (0.5 – 2 mm)	1 mm minimum
D	Build small features and wall thicknesses (as small as 200 μm)	300 μm minimum
D	Build trusses from 0.5 mm – 10 mm in diameter	0.8 mm minimum
D	Construct trusses that are inclined at ≥ 35 degrees from the build direction	Y
D	Able to create cross-sections representative of designed mesostructure: - circular depositions with diameter as small as 0.5 mm - 200 μm minimum feature size	 Y 300 μm
	Material	
D	Able to process all transitional metal oxides (excluding alumina and titanium oxide)	Y
D	Process powder particles with diameter ≤ 50 μm	Y
W	Minimize amount of effort required to adapt to a new material	Y
W	Able to process standard working material (i.e., material is not proprietary or require specialized formulation)	spray-dry
	Production	
D	Build envelope is 250 x 250 x 250 mm or larger	Y
D	Deposition rate should be ≥ 10 cm^3/hr	Y
D	Support material must be able to be removed from part with minimal effort (if applicable)	N
	Quality Control	
D	Finished parts have ≥ 95% relative density	N
D	Ceramic green parts have ≥ 40 vol% ceramic solids loading	35-40 %
D	Material properties are comparable to standard	N
D	Material properties of finished part are isotropic	N
D	Minimize surface roughness before finishing (≤ 0.02 mm Ra)	N
D	Maximize accuracy (≥ +/- 0.05 mm)	Y
D	Minimize z-resolution (≤ 0.1 mm)	Y
	Operation	
W	Does not require special operating environment	Y
W	Minimize operator interaction	Y
	Recycling	
W	Minimize environmental impact by minimizing wasted material	Y
W	Reusable wasted material	Y
	Costs	
D	Minimize cost of technology and technology maintenance by avoiding expensive technologies such as lasers and electron beams	Y
D	Minimize cost of material	Y
W	Easily scaled for large applications	Y

7.5 DISSERTATION ROADMAP

In this chapter, parts fabricated using the designed manufacturing process chain are presented as a means of verifying both the primary and secondary research hypotheses. Initial results which verify the preliminary success of the manufacturing process are presented in Section 7.1. The parts are then quantitatively characterized through a series of analyses focused in determining the parts' phase, density, porosity, and shrinkage (Section 7.2). It is in the density analysis that it is verified that the deposition of a solvent into a system of binder-coated particles will result in a higher part density (the secondary research hypothesis). The capability of the process to produce parts of designed mesostructure (the primary research hypothesis) is proven through initial tests focused in fabricating cellular material features (thin walls, angled trusses, and small channels; Sections 7.3.1 – 7.3.3), as well as through the fabrication of parts with complex geometry (Section 7.3.4). Finally, the manufacturing process is critically analyzed in Section 7.4.

As observed in Figure 7.32, the role of Chapter 7 in this dissertation is in verifying the primary and secondary research hypotheses. The role of the Chapter 8 is to present three separate modeling and analysis efforts in order to obtain a better understanding of the designed manufacturing process. Specifically, the creation of a printed primitive in the 3DP process, the failure mode of printed thin trusses, and the cost and throughput of the manufacturing process chain are modeled so as to gain further insight into the research questions posed in this dissertation.

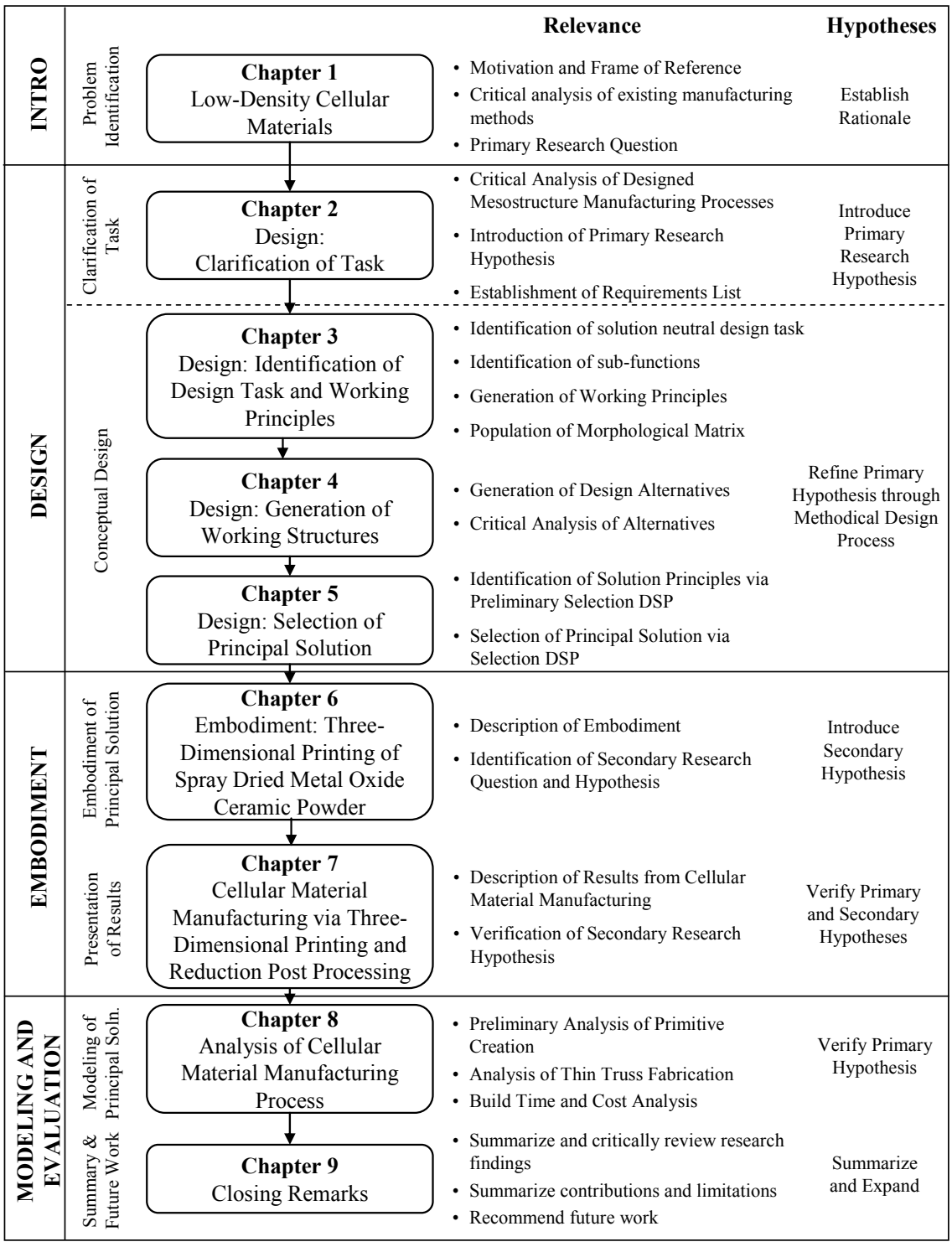

Figure 7.32 – Dissertation Roadmap

CHAPTER 8

PROCESS ANALYSIS AND MODELING

As detailed in Section 7.4, the quality of the parts created by the proposed manufacturing process can be significantly increased through further developmental work dedicated to the improvement of the specific embodiment presented in this work. A foundation for this future developmental effort is established in this chapter through the presentation of models for three separate facets of the manufacturing process.

In Section 8.1, a review and analysis of the existing research efforts in modeling the fundamental physics and kinetics of the formation of individual primitives in 3DP are presented. The understanding gained from these models not only provides further insight into the results presented in Chapter 7, but also provides a basis for improving part quality through optimizing binder/powder interaction.

The fabrication of angled thin trusses, a feature of cellular materials which commonly fails during fabrication via AM processes, is analyzed in Section 8.3. As a result of this analysis, general design rules for realizing trussed geometry are offered so as to improve their rate of successful builds.

Finally, a model of the process's cost and build time is presented in Section 8.4. These models provide a basis on which to compare this process with other manufacturing technologies. They also serve as a means of building confidence in the economic-related claims presented in the dissertation thus far, and of further verifying the primary hypothesis.

8.1 ANALYSIS OF PRIMITIVE CREATION

A review of existing modeling efforts concerning the physics and kinetics of primitive formation is presented in this section in order to provide a foundation for future research towards improving part quality through optimized process planning. In addition, this review provides opportunity for better understanding of the results obtained in Chapter 7. In this subsection, the fundamentals of the physics of powder wetting are first reviewed (Section 8.1.1), as they serve as the foundation for existing models of primitive creation (Section 8.1.2). Models for binder spreading and penetration into the powder bed are presented in Section 8.1.3. A summary is provided in Section 8.1.4 through a listing of generalized relationships between binder and powder parameters and primitive dimensions and geometry.

8.1.1 Fundamentals of Powder Wetting

Analysis of the creation of primitives in 3DP must be based on the physics of wetting. The wetting of a solid by a liquid is a phenomenon of contact angle (Ring, 1996), as shown in Figure 8.1.

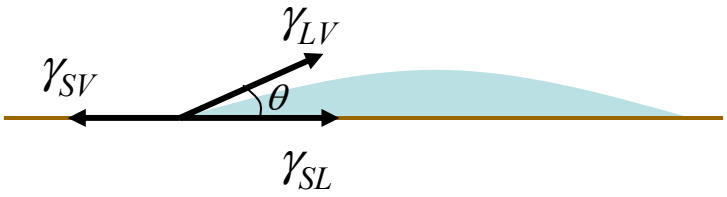

Figure 8.1 – Wetting of a Powder by a Liquid (adapted from (Ring, 1996))

For a droplet of liquid in contact with a solid, the balance of the surface tensions (γ_{ij}) of the solid-vapor (SV), solid-liquid (SL), and liquid-vapor (LV) interfaces dictates the contact angle (θ), as seen in Equation 8.1 (Young's equation).

$$\cos\theta = \frac{\gamma_{SV} - \gamma_{SL}}{\gamma_{LV}} \quad [8.1]$$

The contact angle must approach 0 so that the liquid can spread over the surface easily. Specifically, (spontaneous) wetting will only occur when the work of adhesion, penetration, and spreading (the three fundamental steps of wetting) is negative (as described in a thermodynamic context).

The expressions of work of adhesion (W_A), penetration (W_P), and spreading (W_S) are presented in Equations 8.2 – 8.4.

$$W_A = -(\gamma_{SV} - \gamma_{SL}) - \gamma_{LV} \quad [8.2]$$

$$W_P = -(\gamma_{SV} - \gamma_{SL}) \quad [8.3]$$

$$W_S = -S_{L/S} = -(\gamma_{SV} - \gamma_{SL}) + \gamma_{LV} \quad [8.4]$$

From these expressions it is observed that spontaneous wetting occurs when $\gamma_{SV} > \gamma_{LV}$ and $\gamma_{SL} < \gamma_{SV}$ or when $\gamma_{SV} < \gamma_{LV}$. $S_{L/S}$ (Equation 8.4) is the spreading coefficient; a positive value indicates spontaneous spreading, which occurs when the contact angle is less than 90^o (or when $(\gamma_{SV} - \gamma_{SL}) > \gamma_{LV}$).

Fortunately for the experimental embodiment presented in this work, wetting occurs instantaneously between aqueous suspensions and oxide surfaces. It is important to be aware of the role of surface tension between the liquid, solid, and vapor interfaces, however, as they dictate the rate and amount of penetration and spreading on the powder surface. In the context of creating primitives via 3DP, these rates dictate the size of the primitives that are created.

The rate of penetration of liquid into a bed of agglomerated particles with internal porosity is given by the Washburn equation (Equation 8.5), where l is the infiltration length in time t, k is the permeability of the powder bed (as dictated by the radius of the curvature of the particles' pores), and η is the viscosity of the liquid.

$$\frac{\partial l}{\partial t} = \sqrt{\frac{k\left(\gamma_{SV} - \gamma_{SL}\right)}{4t\eta}} = \sqrt{\frac{k\left(\gamma_{LV}\cos\theta\right)}{4t\eta}} \qquad [8.5]$$

8.1.2 Fundamentals of Primitive Creation

From the fundamental physical principles presented in the previous sub-section, it is clear that the creation of a primitive via 3DP is primarily a function of the surface tension of the binder and the powder bed. Sachs and coauthors confirm this in their observation of the processes undertaken in the formation of a primitive (Sachs et al., 1993a):

- The droplet enters the powder bed and begins to spread until its kinetic energy dissipates and reaches an equilibrium state, at which it begins to penetrate and coat the particles of the powder bed
- Capillary pressure draws binder selectively into the necks between the powder particles
- The liquid attempts to minimize its surface energy by reducing its surface to volume ratio and minimizing the area of the liquid/vapor (LV) interface, thus resulting in a spherically shaped primitive (Moon and coauthors comment that the primitives have a "cap shape" due to the radial penetration of the binder droplet (Moon et al., 2002); this is observed in this research in Figure 6.11)
- The result is the densification of the powder particles as the particles slide over one another in response to the surface tension of the liquid

This desire to minimize surface energy by capillary forces is also responsible for the cylindrical lines that result from droplets that are printed close enough to overlap (Lanzetta and Sachs, 2003).

Although the solvent/granule system featured in this research differs from the binder/powder system traditionally found in 3DP, the primitive formation steps listed above are applicable. In this embodiment, solvent infiltrates the spray-dried granules and deforms their binder coatin; this differs from the manner in which binder coats powder particles in standard 3DP. However, because the desire to minimize surface energy still remains, the same spherical primitive shape is formed.

It is important to note that the creation of a primitive via 3DP does not simply rely on the differences of surface tension; in reality, this interaction is far more complex. Moon and coauthors note that the binder-powder bed interaction is influenced by the microstructure of the powder bed as well as physical properties of the binder and the printing conditions, which in turn, influence the final primitive geometry (Moon et al., 2002). The properties of the binder and powder which affect the geometry of the solid primitive are presented in Table 8.1.

Table 8.1 – Properties of the Binder and Powder which Affect Primitive Creation

Binder properties	**Powder properties**
Surface tension	Shape
Viscosity	Size (and associated pore size)
Molecular weight	Surface roughness
Impact velocity	Internal porosity of particle (or granule)
Volume of dose	Microstructure of powder bed
Binder / Powder interaction (wetting characteristics)	

A specific example is the way in which surface roughness or irregularity can affect the contact angle of wetting, as shown in Equation 8.6.

$$\cos\theta = \frac{(\gamma_{SV} - \gamma_{SL})i}{\gamma_{LV}} \qquad [8.6]$$

The variable *i* is the degree of roughness or irregularity and is measured by the ratio of the actual true area of the surface by its projected area. *i* is equal to 1 for liquids, and is greater than 1 for all solids. From this equation, it is observed that the contact angle is decreased for rough surfaces, thus increasing the amount of dispersion of the liquid.

Another example is how the shape of the powder particle can affect primitive geometry. Sachs and coauthors observe that irregularly-shaped powders bond across their large, flat faces when wetted, while spherical powders are bonded by small amounts of binder at their necks (Sachs et al., 1993a). This results in a more efficient binding of spherical powders, as a single droplet can bind significantly more spherical powder since it readily segregates to the idealized two-particle neck. Faceted particles arrange so that large, flat surfaces face one another, which requires a large amount of binder (and resulting in a smaller primitive size. Furthermore, since spherical particles rearrange much easier than their faceted counterparts, surface tension forces have a much greater influence on them. This observation is applicable in the specific embodiment presented in this research, as the spray-dried granules are spherical.

8.1.3 Binder Spreading and Penetration

As discussed in the previous section, the problem of modeling the formation of a primitive created by 3DP is extremely complex. The existing methods for modeling the primitives' dimensions and kinetics are presented in this section. The kinetics of spreading and penetration directly affect the primitives' dimensions: Holman and coauthors note that since spreading is interrupted by the infiltration of the liquid into the

powder bed, the relative rates of spreading and infiltration determine the diameter of the primitive achieved. Modifying these rates will affect the maximum droplet diameter: a more rapid infiltration will halt spreading more quickly, which will result in a smaller droplet diameter (Holman et al., 2002a). However, it should be noted that these models are not complete due to the complexity of the problem; even experimental studies have led to inconsistent rates of penetration that cannot be accounted for in the existing models (Moon et al., 2002).

Spreading and Primitive Width

Obviously, as discussed above, the width of the printed primitive is a function of contact angle of the binder on the powder surface. Assuming a spherical cap-shaped primitive, Hollman and coauthors model the equilibrium droplet radius, r_e, as:

$$r_e = \left(\frac{3V \sin^3 \theta}{\pi (1 - \cos\theta)^2 (2 + \cos\theta)} \right)^{1/3} \quad [8.7]$$

where θ is the contact angle and V is the droplet volume (Holman et al., 2002a). The droplet volume is directly related to the binder dose, which is identified by Moon and coauthors as an integral part of modeling the primitive width (Moon et al., 2002).

$$\text{Binder dose } (\text{cm}^2) = \frac{\text{flow rate } (\text{cm}^3/\text{s})}{\text{print speed (cm/s)}} \quad [8.8]$$

The binder dose (Equation 8.8) is related to the width of the deposited line by the following:

$$\text{line width} = 2\left(\frac{\text{binder dose}\left(\sin^2 \theta\right)}{\theta - \sin\theta\cos\theta} \right)^{1/2} \quad [8.9]$$

However, as stated in the previous section, the spreading of the binder droplet is not simply a function of the binder's wetting characteristics. Moon and coauthors state that the extent of spreading is governed by the droplet impact velocity, viscosity, and the surface tension of the binder (Moon et al., 2002). Furthermore, Lanzetta and coauthors empirically determine that the spreading of the binder droplet, and thus the width of the primitive, is inversely proportional to the spacing of the binder droplets:

$$\text{line diameter} = \frac{K}{\sqrt{\text{drop spacing}}} \qquad [8.10]$$

where K is a constant that depends on the combination of the binder and powder bed.

The kinetics of droplets spreading on a solid surface is governed by

$$r(t) = c(d + t)^n \qquad [8.11]$$

where c, d, and n are empirically determined constants (Holman et al., 2002a). The value of n is dependent on the temperature, humidity, pH, the presence of impurities, polymers, and surface charges, as well as the roughness and topography of the surface. The limiting factor in spreading kinetics is typically the viscosity of the binder. It is observed that the binder impact size is inversely proportional to the square root of the binder viscosity due to viscous energy dissipation. As the viscosity of the binder increases, there exists more resistance to binder spreading, thus narrowing the width of the primitive (Moon et al., 2002).

Penetration and Primitive Height

Contrary to spreading, Holman and coauthors suggest that the size of the primitive is not dictated by the extent of the infiltrating liquid, but by the location of a boundary surface where the polymer concentration drops below some critical value (Holman et al.,

2002b). Similar to the cure depth (C_d) and depth of penetration (D_p) variables present in stereolithography analysis, this difference occurs because polymer molecules are effectively filtered from the binder solution since they become charged upon contact with the ceramic surface and adsorb to the ceramic surface. This is not necessarily applicable to the embodiment presented in this research, as solvents are being used to activate the polymer in-bed. Thus, deformation occurs wherever granules are wetted.

Similar to spreading, the amount of penetration achieved by the binder is directly related to its kinetics (Holman et al., 2002a), which is governed by the Washburn equation (Equation 8.5). The infiltration rate depends not only on the binder properties such as contact angle, viscosity, and surface tension, but also on powder bed characteristics such as particle size and pore fraction (Moon et al., 2002). Specifically, it is shown in (Moon et al., 2002) that infiltration time is proportional to the square of the infiltration depth. Since the infiltration depth is related to the primitive width, the infiltration time should vary linearly with binder dose.

8.1.4 General Trends

As can be seen through this review of existing 3DP modeling efforts, there does not exist a single, exhaustive model of primitive creation. Not only is the problem complex, but the inhomogeneity of the powder bed prevents quantifiable repeatability or predictability during part fabrication. In an effort to obtain a better view of the process, general trends which have been observed empirically and presented in the literature are summarized below.

- *Primitive cross-section decreases as the specific area of the ceramic powder increases* (Holman et al., 2002b). The surface area available for adsorption will increase the rate at which the binder/solvent is removed from solution.
- *As the affinity of the polymer for the ceramic surface increases, the primitive size decreases* (Holman et al., 2002b). If the binder exhibits no affinity for the ceramic particles, it is able to pass down through the powder bed relatively unaffected by the ceramic surfaces.
- *Line width increases with decreasing binder viscosity and surface tension* (Grau et al., 1997; Moon et al., 2002). Low surface tension binder has a high penetration rate and a high spreading rate, thus reducing the printing resolution as compared to the high surface tension binder. Increased viscosity increases resistance to momentum transfer when the binder drop is spreading.
- *High surface tension binder gives spherical primitives; low surface tension binder gives disc-shaped primitives* (Moon et al., 2002). A binder of low surface tension leads to increased spreading, resulting in primitives which are shallower and wider than those created with high surface tension binder.
- *Line width decreases with increasing surface roughness* (Moon et al., 2002). Compared to a smooth surface, surface roughness promotes spreading of the liquid as dictated in Equation 8.6. However, excess roughness can impede the spreading of the binder on the powder-bed surface.
- *The smaller the pore size of the powder bed, the longer the infiltration time* (Moon et al., 2002).

- *Feature size is primarily dependent on the size of the binder droplets used* (Sachs et al., 1993a). However, dimensional tolerance is primarily dependent on the degree of reproducibility of the droplet spreading characteristics of the binder material.

Although the "create primitive" working principle featured in this embodiment is centered in dissolving the binder coating of spray-dried granules with a solvent (which differs from the traditional 3DP method of coating particles with a binder), all of the general trends listed above remain applicable.

8.2 ANALYSIS OF THE FABRICATION OF THIN TRUSSES VIA LAYERED FABRICATION

One of the specific requirements for the designed manufacturing process is the ability to create trussed mesostructure. This geometrical feature is common of cellular materials (Figure 8.2a; also previously shown in Figures 2.9 and 4.6); its consideration is the primary reason why extrusion-based solution principles were not chosen for this manufacturing process, since the small discrete depositions required to fabricate such mesostructure (Figure 8.2b) are difficult to fabricate via extrusion (Section 4.3.1).

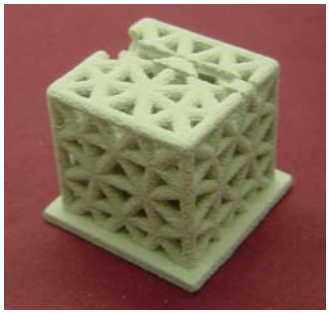

(a)

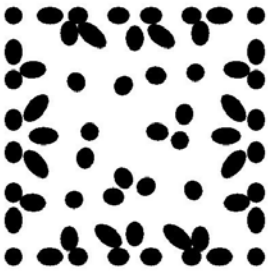

(b)

Figure 8.2 – Cube Composed of Angled Trusses; (a) as-built, (b) x-y cross-section

8.2.1 Problem Overview

This type of geometry can be difficult to realize in any additive manner, since large layer thicknesses can lead to fabricated layers which do not adhere to one another. Illustrated in Section 2.5.1 (specifically, Figure 2.6) and in Figure 8.3 below, a large layer thickness coupled with a small truss diameter can lead to non-overlapping layers, and are thus not able to be produced in a layer-based process.

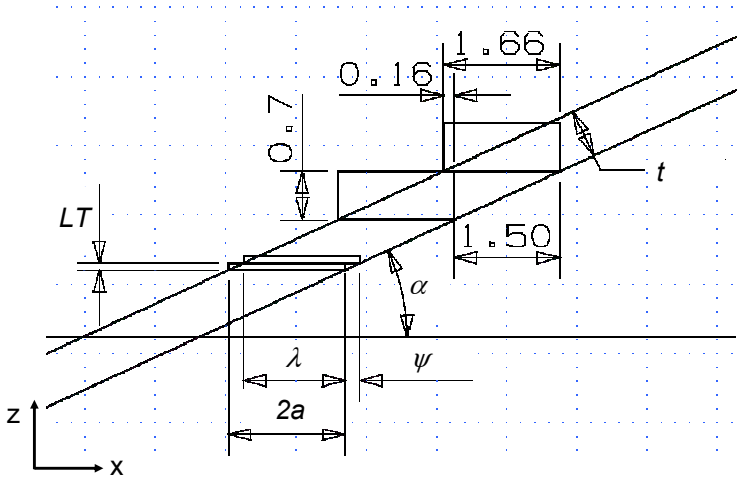

Figure 8.3 – X-Z Cross-Section of Angled Truss Creation via Layered Fabrication

In the above figure, t is the thickness of the truss (0.7 mm in the figure), α is the angle of truss with build plane (25^o in the figure), LT represents the processing layer thickness, the variable γ represents the amount of overlap between two layers, and ψ represents the amount of material overhang between successive layers.

Assuming that the truss inclined with the build plane has a circular cross-section, the layer which must be fabricated is of an elliptical shape (Figure 8.4) wherein the minor radius, b, is the radius of the circular truss, and the major radius, a, is given as:

$$a = \frac{1}{2}\frac{t}{\sin\alpha} \qquad [8.12]$$

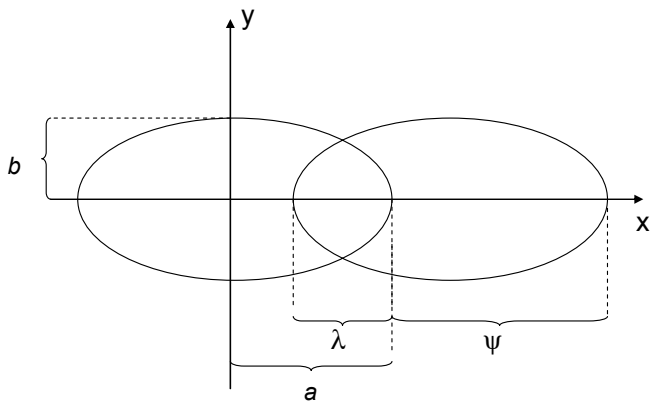

Figure 8.4 – X-Y Cross-Section of Circular Truss Created via Layered Fabrication

The material overhang is calculated as in Equation 8.13. Knowing that the major radius is the sum of the material overhang and the material overlap (Equation 8.14), the material overlap can be calculated as in Equation 8.15.

$$\psi = \frac{LT}{\tan\alpha} \quad [8.13]$$

$$\lambda + \psi = 2a \quad [8.14]$$

$$\lambda = \frac{t}{\sin\alpha} - \frac{LT}{\tan\alpha} \quad [8.15]$$

The calculation of overlap is illustrated for a 1 mm diameter truss at a 45^o angle incident to the build plane built with a 0.1 mm layer thickness in Figure 8.5. This results in an overlap length of 1.3 mm.

In their investigation of creating trusses with the EBM process, Cansizoglu and coauthors corroborated this calculation of material overlap (Cansizoglu et al., 2006). Furthermore, in their analysis, Cansizoglu and coauthors stated that, generally, AM processes are unable to fabricate trusses with angles smaller than roughly 35-40^o with respect to the build plane. This statement is inaccurate, however. Further investigation is needed to identify the limits of layered fabrication of angled trusses.

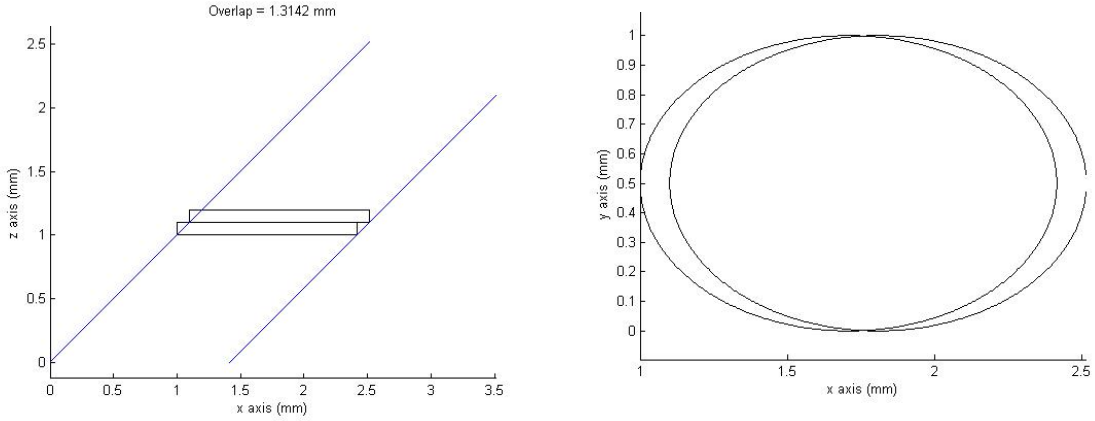

(a) X-Z Cross-Section (b) X-Y Cross-Section

Figure 8.5 – Calculation of Material Overlap Between Layers of an Angled Truss

8.2.2 Length of Layer Overlap

In order to better quantify the troubles associated with poor layer overlap when fabricating angled trusses, the angle at which the overlap (λ) is equal to 0 is presented in Equation 8.16.

$$\alpha_{\lambda=0} = \cos^{-1}\left(\frac{t}{LT}\right) \qquad [8.16]$$

From this it is deduced that there will always be material overlapping between layers (i.e., $\lambda > 0$) at any angle (for all $0 < \alpha < 90$) when the truss diameter, t, is greater than the layer thickness, LT (i.e., $t/LT > 1$). If $t < LT$ (i.e., $t/LT < 1$), sequential layers of the thin truss feature will not overlap for those angles smaller than $\alpha_{\lambda=0}$ as calculated in Equation 8.16, thus preventing the successful fabrication of the truss.

This discussion is illustrated in Figure 8.6. There is no overlap between layers for a truss to layer thickness ratio of 0.8 when the truss is angled to the build plane at all angles less than 36.9 degrees for all values of layer thickness.

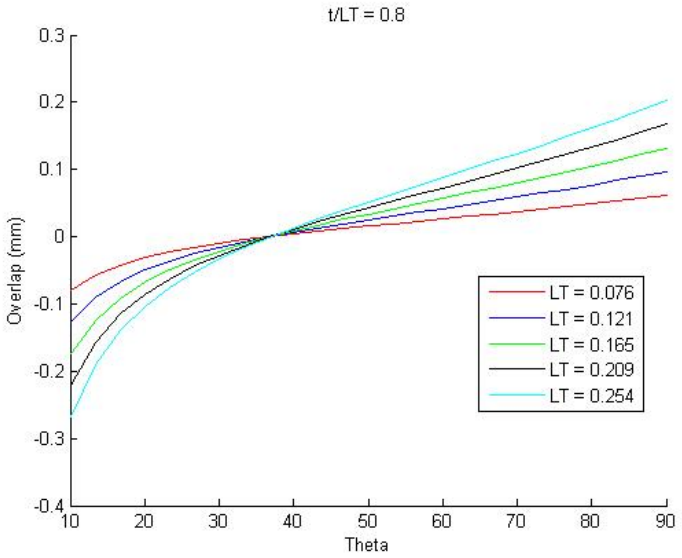

Figure 8.6 - Layer Overlap as a Function of Angle for a Truss Diameter / Layer Thickness Ratio < 1

Figure 8.7 is presented in order to gain insight on the effect that truss diameter, layer thickness, and angle have on layer overlap (λ). As can be seen, layer overlap is plotted as a function of truss angle for various different ratios of *t/LT* (at a constant *LT* = 0.165 mm).

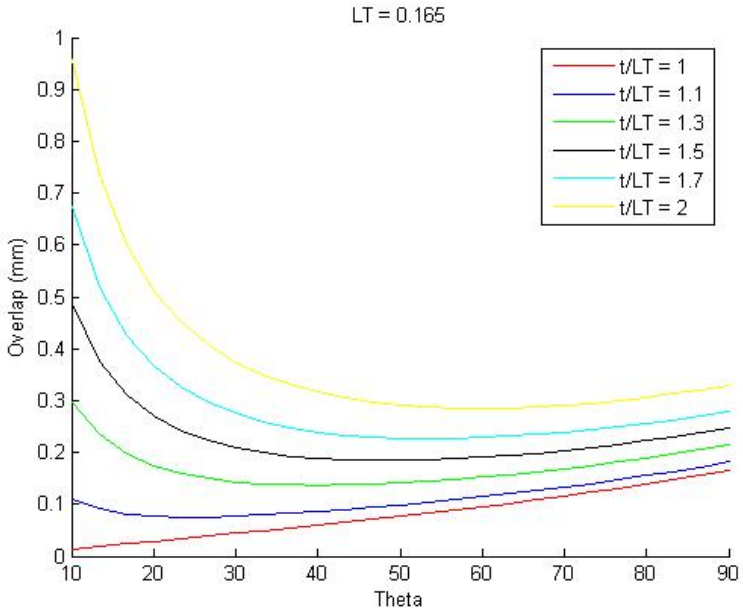

Figure 8.7 – Layer Overlap as a Function of Angle for Ratios of Truss Diameter and Layer Thickness > 1

It is clear that the results presented in Figure 8.7 contradict the claims made by Cansizoglu and co-authors: large values of layer overlap can be found at acute angles. Specifically, there exists an angle, $\alpha_{\lambda,min}$, at which the amount of layer overlap is minimized. This angle is found by taking the first order derivative of Equation 8.15 (Equation 8.17), setting it to zero, and solving for $\alpha_{\lambda,min}$ (Equation 8.18).

$$\frac{\partial \lambda}{\partial \alpha} = \frac{LT - t\cos\alpha}{\sin^2 \alpha} \quad [8.17]$$

$$\alpha_{\lambda,\min} = \cos^{-1}\left(\frac{LT}{t}\right) \quad [8.18]$$

In the example presented in Figure 8.7 (where LT = 0.165 mm) the angle at which the least amount of overlap is observed is 60 degrees for a truss diameter of 0.33 mm (t/LT = 2) and 24.6 degrees for a truss diameter of 0.18 mm (t/LT = 1.1). The results provided by the calculation of Equation 8.18 can serve as a constraint for an engineer designing cellular mesostructure which is to be fabricated in a layer-based manner.

8.2.3. Area of Layer Overlap

The area of overlap between subsequent layers is presented in Equation 8.19. Its derivation, based upon the integration of the ellipse equation, is presented in Appendix D.

$$A_{overlap} = 2ab\left[\sin^{-1}\left(\frac{x}{a}\right) + \left(\frac{x}{a}\right)\left(\sqrt{1-\left(\frac{x}{a}\right)^2}\right)\right]\Bigg|_{a-\lambda/2}^{a} \quad [8.19]$$

A simplified form of Equation 8.19 is presented in Equation 8.20.

$$A_{overlap} = \pi ab - 2ab\left(\sin^{-1}\left(1-\lambda/2a\right) + \left(1-\lambda/2a\right)\left(\sqrt{1-\left(1-\lambda/2a\right)^2}\right)\right) \quad [8.20]$$

The area of overlap is plotted against truss angle in Figure 8.8 with lines of constant *t/LT* (with *LT* = 0.165 mm) as done with overlap length in Figure 8.7. As expected, the area of overlap varies along the angle (for a given *t/LT* ratio) in a similar manner observed for the overlap distance.

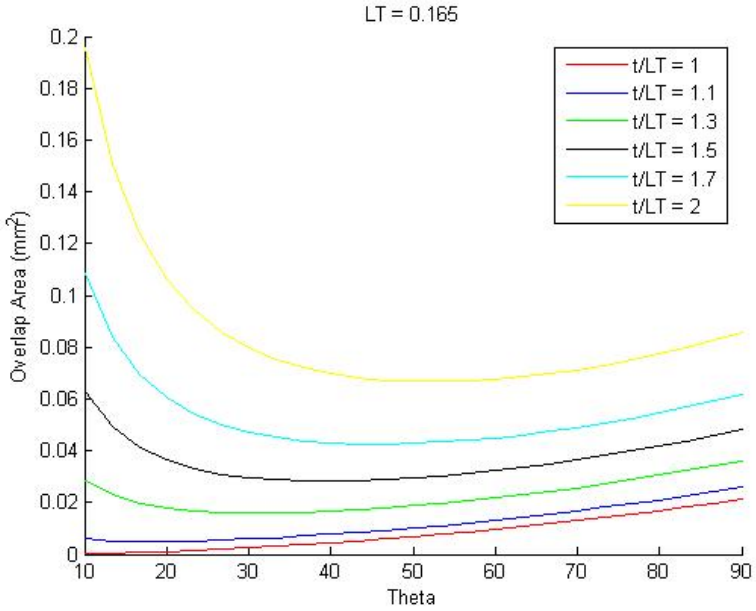

Figure 8.8 – Overlap Area as a Function of Angle for Ratios of Truss Diameter and Layer Thickness > 1

Thus far in the analysis, it is not clear why trusses at acute angles fail to build properly in layer-based processes. Aside from very thin trusses (whose diameter approaches the layer thickness), it would seem as if a smaller angle leads to a larger contact area. In order to fully understand the problem, the amount of material that hangs over the layer overlap is analyzed.

8.2.4 Area of Overhanging Material

As can be observed in Figure 8.3, the area of the ellipse which is cantilevered over the previous layer ($A_{overhang}$) is equal to the difference of the ellipse area (product of π, ellipse minor radius and major radius), and the area of the layer overlap (Equation 8.20).

$$A_{overhang} = \pi ab - A_{overlap} \quad [8.21]$$

Thus, the volume of the overhanging material is simply the product of the overhang area and the layer thickness, as seen in Equation 8.22.

$$V_{overhang} = A_{overhang} LT \quad [8.22]$$

When plotted in a similar fashion as Figures 8.7 and 8.8 (i.e., area of overhang is plotted against truss angle with lines of constant *t/LT* with a constant *LT*), it is observed that as the angle of the truss decreases, the amount of overhanging material significantly increases (as seen in Figure 8.9).

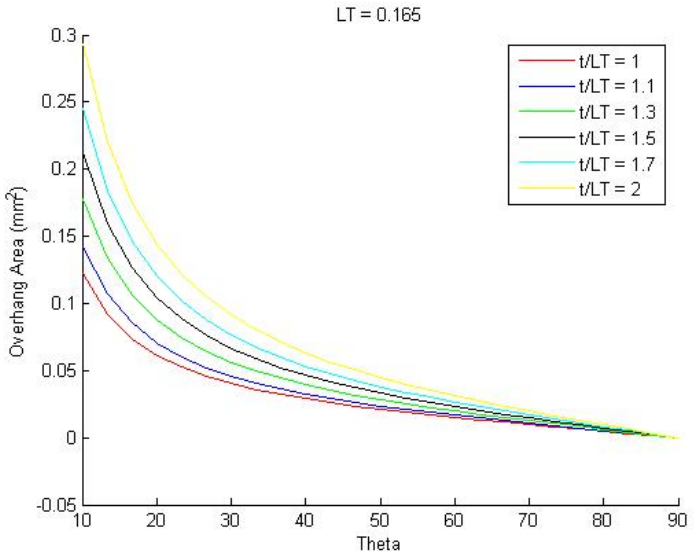

Figure 8.9 – Overhang Area as a Function of Angle for Ratios of Truss Diameter and Layer Thickness > 1

Given this observation, it is likely that the failure of thin, acutely-angled trusses is not due to poor overlapping between layers, but instead due to the stress induced by the accumulation of the mass of overhanging layers.

8.2.5 Failure of Green Truss

Figure 8.10 (modified from Figures 8.3 and 8.4) is presented below in an effort to gain better understanding of the stress induced by the cantilevered stacking of multiple layers encountered when a thin, angled truss is fabricated by a layer-based process.

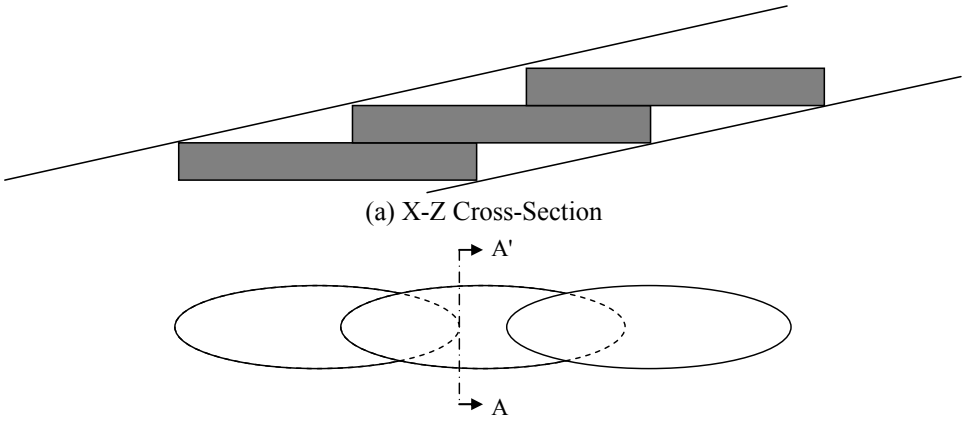

(a) X-Z Cross-Section

(b) X-Y Cross-Section

Figure 8.10 – Non-Cohesive Layers

As can be seen, when the distance between overlapping layers is significant, the entire load of stacked layers is placed upon the area of a single layer of material. This load, F, can be calculated via Equation 8.23 where n is the number of stacked layers, g is the force due to gravity, and the mass of each overhang is denoted by $m_{overhang,i}$. The mass of each overhang is calculated via Equation 8.24, where ρ_{green} is the density of the green part and $V_{overhang}$ is the volume of the overhang as calculated in Equation 8.22.

$$F = \sum_{i}^{n} m_{overhang,i} g \qquad [8.23]$$

$$m_{overhang} = \rho_{green} V_{overhang} \qquad [8.24]$$

The average shear stress on the green part, τ_{green}, is thus:

$$\tau_{green} = \frac{F}{A_{fracture}} \quad [8.25]$$

where $A_{fracture}$ is the minimum cross-sectional area of the portion of the single layer that is unsupported by surrounding layers (i.e., Section A-A in Figure 8.10).

This area is determined first by identifying the width of the fracture surface. This variable is determined by using the ellipse equation (Equation 8.26) wherein the *x*-coordinate of the surface is represented by the difference between the major radius and the overlap length (Equation 8.27).

$$y = \sqrt{b^2\left(1 - \frac{x^2}{a^2}\right)} \quad [8.26]$$

$$y_{fracture} = \sqrt{b^2\left(1 - \frac{(a-\lambda)^2}{a^2}\right)} = \frac{b}{a}\sqrt{\lambda(2a-\lambda)} \quad [8.27]$$

The area of the fracture surface is the product of the layer thickness and the width of fracture surface, as presented in Equation 8.28.

$$A_{fracture} = 2y_{fracture}LT = \frac{2bLT}{a}\sqrt{\lambda(2a-\lambda)} \quad [8.28]$$

Uhland and coauthors propose that the ultimate strength of the green part (σ_{max}) is a function of the packing fraction of the powder particles, ϕ, the volume fraction of the binder relative to the ceramic, v_B, and the strength of the binder, σ_B, as shown in Equation 8.29 (Uhland et al., 2001).

$$\sigma_{\max} = \left(\frac{9\phi}{8\left(1-\sigma_{\max}\right)^{1/2}} \right) \left(v_B\right)^{1/2} \sigma_B \qquad [8.29]$$

In an effort to decrease the likelihood of green part failure, one might want to constrain the design of angled trusses that are to be fabricated by layered-based fabrication to only allow cohesive layers, as illustrated in Figure 8.11.

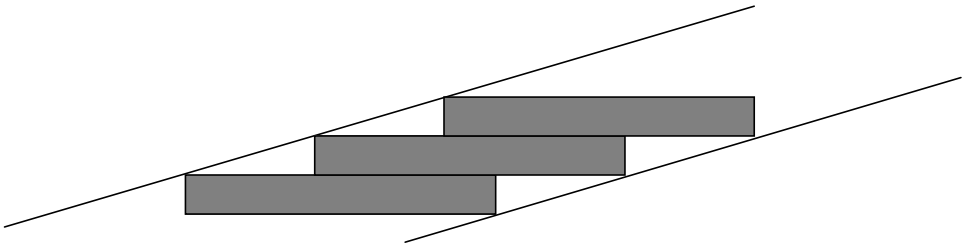

(a) X-Z Cross-Section

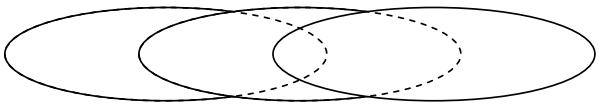

(b) X-Y Cross-Section

Figure 8.11 – Illustration of Cohesive Layers

The cohesion of multiple layers is ensured when the overlap, λ, is greater than or equal to the major radius of the elliptical cross-sections, a. The minimum angle at which cohesion is assured is found by substituting $a = \lambda$ into Equation 8.15 and solving for α. The resulting solution is presented in Equation 8.30.

$$\alpha_{cohesive\_\min} = \cos^{-1}\left(\frac{t}{2LT}\right) \qquad [8.30]$$

From this, it is observed that cohesion is assured for all values of α when the ratio of t to LT is ≥ 2. As the ratio of t to LT decreases, the minimum angle required for cohesion increases, as shown in Figure 8.12.

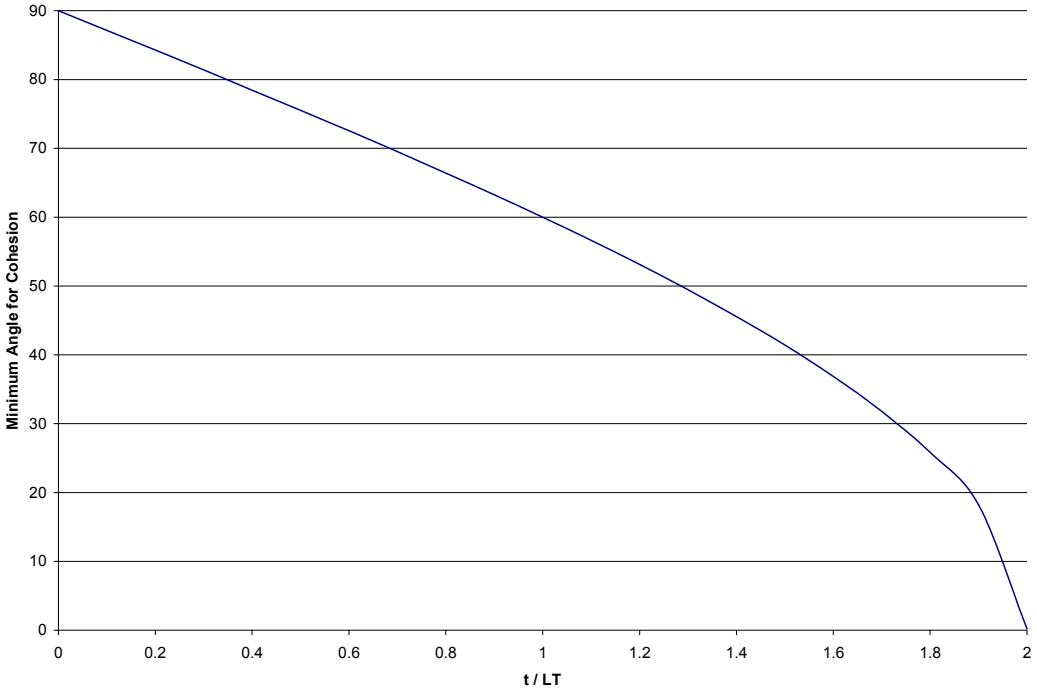

Figure 8.12 - Plot of Minimum Angle for Cohesion for *t/LT* Ratios

8.3 BUILD TIME AND PROCESS COST MODELS

One of the key reasons for the selection of the 3DP principal solution in Chapter 5 is because of its low technology cost and high rate of deposition (Table 5.16). In this section, these attributes are verified through the modeling of the build time (Section 8.3.1) and the process cost (Section 8.3.2). These models are tested and analyzed through the execution of an example problem (Section 8.3.3).

8.3.1 Build Time Model

To place further emphasis on the desire to consider the proposed manufacturing process as capable of operating as a production system, the build time model is centered on the notion of producing batches of parts. These batches are composed of several layers of individual parts. This is easily achievable in powder-based layered manufacturing processes, as unbound powder serves as the support structure (Figure

8.13). It should be noted, however, that stacking layers of parts in the build chamber can result in distorting lower-level parts due to the resultant compressive loads (Lee et al., 1995).

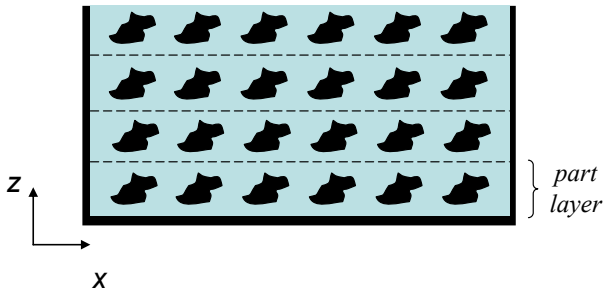

Figure 8.13 – Building "Layers" of Parts

The total time to build a batch of parts, t_{tot}, is given as:

$$t_{tot} = t_{pl}N_{pl} + t_{setup} + t_{clean}N_{pl}N_p + t_{dry} + t_{sinter} \quad [8.34]$$

where:

- t_{pl} - the time to build a layer of several parts, as illustrated in Figure 8.13 (i.e., not a single layer of the build); defined in Equation 8.37.
- N_{pl} - the number of part layers in the build
- t_{setup} - the time to set up the build
- t_{clean} - the time to clean each part of the batch
- N_p - the number of parts in a part layer
- t_{dry} - the drying time of the batch
- t_{sinter} - the sintering time of the batch

The number of part layers in the build, N_{pl}, can be calculated as in Equation 8.35 (assuming that the parts of each layer are of equivalent height).

$$N_{pl} = \frac{d_{bed}}{d_p + 25LT} \quad [8.35]$$

d_{part} is the depth of the part and d_{bed} is the depth of the build bed. The $25LT$ factor is included to account for the 25 layer buffer "between" part layers (illustrated in Figure 8.13).

An advantage that the manufacturing process developed in this research has over other direct-metal AM processes is that the setup time is negligible. Unlike DMLS and EBM, the powder bed does not need to be heated nor does the chamber need to be evacuated. The only setup time is due to loading the feed bed with powder and compacting it with a stamper. Therefore, t_{setup} is typically on the order of 5 minutes for 3DP.

t_{clean} is included into the processing time model since each part of the batch must be cleaned after fabrication and before sintering. This term is highly dependent on the part geometry; bulk parts require little cleaning time, whereas complex geometries and fine features require longer times due to the need to remove unbound powder from overhangs and internal geometry in addition to the additional care needed in handling them. Automation of the cleaning process would reduce this time considerably.

Since t_{clean} is the time to clean a single part, it must be multiplied by the number of parts per layer, N_p, and the number of part layers in the build, N_{pl}. Assuming that the goal is maximize the build capacity of the machine by packing the powder bed with parts, N_p is a function of the build area of the powder bed (the product of the width, w_b, and height, h_b, of the bed), the cross-sectional dimensions of the parts being built (part width, w_p, and part height, h_p), and the amount of spacing placed between parts in a part layer (x_{space} and y_{space}), as shown in Equation 8.36.

$$N_p = \left(\frac{w_b}{w_p + x_{space}} \right) \left(\frac{h_b}{h_p + y_{space}} \right) \quad [8.36]$$

Once the parts are built, post-processing of the parts begins. This includes a secondary drying step (which ensures that the polymer in the green part is fully solidified) and reduction and sintering in a furnace. Both of these processes are able to be batched (i.e., every part built in the printer can be processed together). The drying time, t_{dry}, is typically 0.5 hrs in duration; the sintering time, t_{sinter}, is 25 hours.

The time to build a layer of parts, t_{pl}, is modeled as:

$$t_{pl} = N_l(t_l + t_{recoat}) + t_{prime,tot} \quad [8.37]$$

where:

- t_l - the time required to print a single build layer
- N_l - the number of layers required to build the part
- t_{recoat} - the time required to recoat the build powder bed
- $t_{prime,tot}$ - the total time spent on priming the print cartridge during the build

It should be noted that 3DP has an advantage over other AM processes as it does not require additional time to build support structures due to its use of the powder bed working principle.

The time required to print a single layer of the build, t_l, is calculated as:

$$t_l = \left(\frac{2h_b}{v_{fast}} \right) N_p N_{bands} + \frac{w_b}{v_{slow}} \quad [8.38]$$

where:

- N_{bands} - the number of passes ("bands") required of the printhead to create a part
- v_{fast} - the velocity of the fast axis (i.e., velocity of printhead)

- v_{slow} - the velocity of the slow axis (i.e., velocity of printing gantry)

The distance of printing along the fast axis is simply twice the height of the part, y_b, as the head cycles back and forth along the part height to complete the print. Because it is assumed that the printhead velocity, v_{fast}, is constant whether or not printing is taking place, the time required to print a single band of a part is the quotient of $2h_b$ and v_{fast}. A unique feature of printing-based AM processes is how the specific geometry and features of parts do not influence the total build time; only the overall part dimensions influence build time.

The number of passes of the printhead along the fast axis that are required to build a single layer of a single part, N_{bands}, is calculated as the width of the part, w_p, divided by the width of the printhead assembly, w_{head}, as shown in Equation 8.39.

$$N_{bands} = \frac{w_p}{w_{head}} = \frac{w_p}{N_{heads}\left(N_{nozzle} d_n\right)} \quad [8.39]$$

The width of the printhead assembly is the product of the number of printheads, N_{heads}, the number of nozzles in each printhead, N_{nozzle}, and the diameter of the nozzles is, d_n.

As the printing gantry must traverse the entire width of the build bed, w_b, in order to initiate recoating, the width of the individual parts being built does not have any influence on the build time (assuming that the velocity of the slow axis, v_{slow}, is equivalent when printing or when traversing to a printing spot).

Returning to Equation 8.37, the number of layers required to build a single part is simply the depth of the part, d_p, divided by the layer thickness.

$$N_l = \frac{d_p}{LT} \quad [8.40]$$

The time required for recoating includes the amount of time required to move the gantry across the feed and build powder beds as well as the amount of time taken in raising/lowering the feed/build pistons (which occur simultaneously). Thus t_{recoat} is calculated as:

$$t_{recoat} = \left(\frac{LT}{v_{pist}} \right) + \left(\frac{w_b + w_f}{v_{recoat}} \right) \quad [8.41]$$

where:

- v_{pist} - the velocity of the raising/lowering of the feed/build pistons
- v_{recoat} - the velocity of the printing gantry during recoating
- w_f - the width of the feed bed

Similar to the FDM process, the 3DP process automatically initiates a process to clean its deposition heads at regular intervals. Thus, the total time taken in cleaning, $t_{prime,tot}$, is simply the product of the amount of time it takes to clean the nozzles and prime the print cartridge, t_{prime} (about 10 seconds), and the number of times that cleaning is initiated. It is assumed that cleaning is initiated every 20 layers.

$$t_{prime,tot} = t_{prime} \left(\frac{N_l}{20} \right) \quad [8.42]$$

8.3.2 Process Cost Model

The total annual cost of producing parts using the designed process is modeled using Equation 8.43.

$$C_{tot} = C_{fixed} + C_{batch} \left(\frac{N_{ppy}}{N_{pl} N_p} \right) \quad [8.43]$$

As can be seen, the total annual cost is composed of two separate costs: fixed costs (C_{fixed}, Equation 8.44) and batch costs (C_{batch}, Equation 8.45). Fixed costs are those costs associated with purchasing equipment, and are spread over the number of parts fabricated per year, N_{ppy}. Batch costs are the variable costs associated with processing a single batch of parts; the total annual costs associated with part processing is the product of the cost of each batch and the number of batches processed per year (the number of parts fabricated each year divided by the number of parts created in each batch).

Fixed costs are calculated using Equation 8.44.

$$C_{fixed} = \left(C_{3DP} + C_{maint}\right) N_{3DP} + C_{furnace} + C_{spraydry} \quad [8.44]$$

where:

- C_{3DP} - the cost of purchasing a 3DP machine
- C_{maint} - the cost of maintaining a 3DP machine
- N_{3DP} - the number of 3DP machines purchased
- $C_{furnace}$ - the cost of purchasing a furnace
- $C_{spraydry}$ - the cost of purchasing the spray drying machine

The cost of processing a single batch with the process is calculated using Equation 8.45.

$$C_{batch} = C_{material} N_{pl} N_p + C_{operation} t_{pl} N_{pl} + C_{reduction} \quad [8.45]$$

where:

- $C_{material}$ - the cost of the material used per batch
- $C_{operation}$ - the cost of operating a 3DP machine per hour of use
- $C_{reduction}$ - the cost of reducing a batch of parts (relative to the amount of gas used)

The material costs associated with a single part is calculated using Equation 8.46.

$$C_{material} = V_{part} \rho_{oxide} \left(C_{oxide} + P_{binder} C_{binder}\right) + V_{part} C_{solvent} \quad [8.45]$$

where:

- ρ_{green} - the density of the oxide material
- V_{part} - the volume of the green part, (the product of w_p, h_p, and d_p)
- C_{oxide} - the cost of the oxide powder ($/g)
- P_{binder} - the weight percent of the binder coating of the granules (2 or 4 wt%)
- C_{binder} - the cost of the binder material used to spray-dry particles ($/g)
- $C_{solvent}$ - the cost of the printed solvent ($/cm^3)

The cost per part is calculated with Equation 8.46.

$$C_{part} = \frac{C_{tot}}{N_{ppy}} \qquad [8.46]$$

8.3.3 Example Problem

In an effort to verify and analyze the models formulated, an example problem is presented in this sub-section.

Problem Statement

Consider a manufacturer who uses the designed manufacturing process that is presented in this research. The manufacturer uses the current research embodiment as a production process in which 150,000 parts per year are made. The average product is 25.4 mm cubed, as seen in Table 8.2.

Table 8.2 – Part Dimensions

Variable	Acronym	Value
Part width	w_p	25.4 mm
Part height	h_p	25.4 mm
Part depth	d_p	25.4 mm

The manufacturer is using the 4 wt% granule system to fabricate the green parts as shown in Table 8.3.

Table 8.3 – Material Specifications

Variable	Acronym	Value
oxide density	ρ_{oxide}	5.58 g/cm^3
wt % of binder	P_{binder}	0.04

The manufacturer is using one ZCorp Z402 printer (same as presented in Chapter 6), which has the specifications that are listed in Table 8.4.

Table 8.4 – Z402 Machine Specifications

Variable	Acronym	Value
Number of machines	N_{3DP}	1
Build bed width	w_b	254 mm
Build bed height	h_b	200 mm
Build bed depth	d_b	200 mm
Feed bed width	w_f	190 mm
Number of printheads	N_{heads}	1
Number of nozzles	$N_{nozzles}$	128
Nozzle diameter	d_n	0.07 mm
Velocity of fast axis	v_{fast}	450 mm/s
Velocity of slow axis	v_{slow}	300 mm/s
Velocity of piston	v_{pist}	1 mm/s
Nozzle priming time	t_{prime}	20 s

The build parameters are constant for every build and are presented in Table 8.5.

Table 8.5 – Build Parameters

Variable	Acronym	Value
Layer thickness	LT	0.089 mm
Horizontal part spacing	x_{space}	10 mm
Vertical part spacing	y_{space}	10 mm
Velocity of recoat	v_{recoat}	430 mm/s

The times associated with pre- and post-processing are constant as well, and are presented in Table 8.6.

Table 8.6 – Pre/Post-Processing Times

Variable	Acronym	Value
Machine setup time	t_{setup}	5 min
Cleaning time	t_{clean}	5 min
Drying time	t_{dry}	30 min
Sintering time	t_{sinter}	25 hr

The associated costs of the process employed by the manufacturer are presented in Table 8.7.

Table 8.7 – Cost Information

Variable	Acronym	Value
Machine cost	C_{3DP}	20,000 $
Maintenance cost	C_{maint}	4000 $/year
Furnace cost	$C_{furnace}$	5000 $
Spray-drier cost	$C_{spraydry}$	12000 $
Cost of reduction	$C_{reduction}$	8 $/batch
Cost of operation	$C_{operation}$	3 $/hr
Cost of oxide material	C_{oxide}	0.03 $/g
Cost of binder coating	C_{binder}	0.002 $/g
Cost of solvent	$C_{solvent}$	0 $/cm3

The cost of reduction, $C_{reduction}$, is a fixed cost that corresponds with the cost of purchasing the gas tanks needed for the furnace. Given that tanks of pre-mixed Ar/H_2 generally cost $40, and a conservative estimate that a new tank would be purchased for every five runs (for a large furnace and large quantity of parts), $C_{reduction}$ is estimated to be $8. The cost of operation is stated as $3/hr, which is an estimate of the costs associated with operating the equipment (e.g., electricity and employee costs). Since the 3DP machine is suited for operation in an office environment, its cost of operation is similar to that of a computer or a standard printer.

Results of Example Problem

Given the specifications of the problem as presented in Tables 8.2 – 8.7, the models presented in the previous sub-sections are used to evaluate the key process metrics. These results are presented in Table 8.8. The MATLAB code developed to evaluate the models and obtain these results is presented in Appendix E.

Table 8.8 – Values of Process Metrics

Parameter	Acronym / Equation Number	Value
Time per build layer	t_l	13.8 s
Time per part layer	t_{pl}	1.26 hr
Total build time	$t_{pl}N_{pl}$	9.15 hr
Total process time	t_{tot}	59.19 hr
Fixed cost	C_{fixed}	$41,000
Cost of 1 batch	C_{batch}	$842.68
Total year 1 cost	C_{tot}	$471,690
Cost per part	C_{part}	$3.14

These results can be verified through a rough comparison with existing estimates presented in the literature. Michaels and co-authors state that the vertical build rate for a 32 nozzle printhead is 2.5 cm/hr (Michaels et al., 1992). As can be seen in Table 8.8, this estimate is close to that presented by the model – the time taken to build a part layer (which is 2.54 cm high) is 1.26 hr. The 30 minute difference can be explained by the fact that the model developed in this research is for building several parts on a single part layer, as well as the increased amount of nozzles.

As seen in Table 8.8, the cost per part produced by this process is extremely inexpensive ($3.14). This value is actually probably over-estimated, as it includes the cost of paying for the printing, spray-drying, and sintering equipment in the first year of production. Michaels and co-authors calculated a cost per part of only $0.10 for traditional 3DP (Michaels et al., 1992).

This cost per part could be lowered if the manufacturer were to use a newer model of 3DP machine which has the following specifications different from the earlier model (Table 8.9).

Table 8.9 – Spectrum Z510 Machine Specifications

Variable	Acronym	Value
Build bed height	h_b	356 mm
Number of printheads	N_{heads}	4
Machine cost	C_{3DP}	50,000 $

With multiple, larger heads, the time required to fabricate a layer is only 4 seconds, and the total build time is significantly reduced in (3 hrs). The cost per part is slightly increased in this embodiment ($3.25) due to the increase in machine cost.

Compared to existing direct-metal AM processes, this manufacturing process is very inexpensive and extremely fast. As presented in Chapter 2, these machines are very expensive have high maintenance costs due to the high-tech equipment, have extremely high material costs (on the order of 10x more expensive), and are slow due to their 1D patterning working principle. Finally, it is unlikely that stacks of part layers could be successfully built in these machines due to problems with heat conduction throughout the powder bed, thus limiting the batch sizes of these machines.

The economic advantages presented by this technology are evident when compared directly to that of the EBM technology. A single EBM machine costs $1,000,000 to purchase, and has an annual maintenance fee of $50,000. The improvement in part cost of 3DP is evident when noting that the annual maintenance fee of the EBM process is more than twice that of the purchase price of a 3DP machine. Comparable part costs associated with the EBM process are on the order of hundreds of dollars (~$400).

From this modeling, it is acknowledged that another design requirement is met, and that the primary research hypothesis is further verified.

8.4 DISSERTATION ROADMAP

In this chapter, three separate modeling efforts are presented. A review of the existing models which attempt to characterize the creation of individual primitives is presented in Section 8.1. A model for the process of realizing angled trusses is proposed

in Section 8.2, along with new insight as to why they fail during fabrication. Finally, a build time and cost model for the manufacturing process are presented as a means of further verifying the primary research hypothesis.

As seen in the dissertation roadmap, Figure 8.14, the results of the proposed manufacturing process have been presented, evaluated, analyzed, and modeled in this dissertation. With those tasks completed, the author concludes this phase of the research and offers closing remarks in the final chapter.

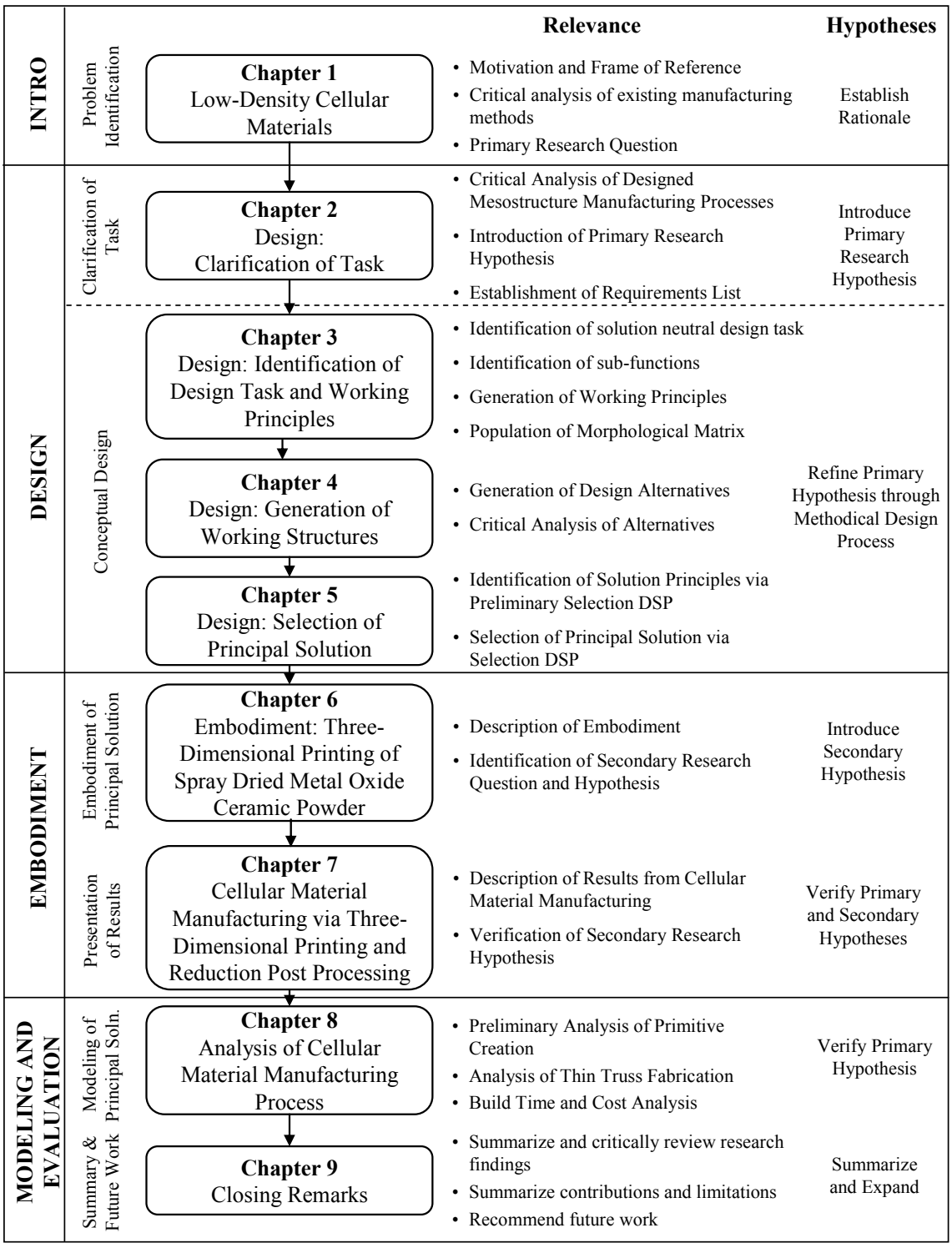

Figure 8.14 – Dissertation Roadmap

CHAPTER IX

CLOSING REMARKS

The driving force underlying this research is the opportunity that exists to improve the design of existing products, and the ability to reap the benefits of cellular materials in new applications. As such, the principal goal in this dissertation is to design, embody, and analyze a manufacturing process that provides a designer with the ability to specify the material type, material composition, void morphology, and mesostructure topology for any conceivable part geometry.

A summary of the research completed in this body of work is presented in Section 9.1. This summary includes a review of the research questions and hypotheses, as well as a synopsis of the research strategy used to verify the hypotheses. Contributions resulting from each of the three phases of this research are highlighted in Section 9.2. A critical analysis of the design and embodiment of the manufacturing process is presented in Section 9.3 along with suggestions for future work. Finally, recommendations and conclusions are offered in Section 9.4.

9.1 RESEARCH SUMMARY

At the onset of this work, an opportunity for improving the amount of design freedom offered to designers and manufacturers of cellular materials was discovered through the completion of a critical evaluation of existing cellular material manufacturing techniques (presented in Section 1.2). Specifically, it is found that existing manufacturing techniques severely constrain a designer's decision space with respect to

the material, mesostructure topology, and/or macrostructure topology of the artifact. As such, the focus in this work is to design, embody, and analyze a manufacturing process that is capable of producing materials of designed mesostructure without constraining a designer's decisions with respect to these crucial parameters.

This stated research goal led to the development of the primary research question (Section 1.3.4):

Primary Research Question:

How to manufacture three-dimensional, low-density cellular metal structures while maintaining designer freedom in the selection of the material and the design of the part mesostructure and macrostructure?

A hypothesis for this research question is formulated (Section 2.4) from a critical analysis of two existing techniques for manufacturing parts of designed mesostructure, direct metal additive manufacturing (AM, Section 2.2) and linear cellular alloy extrusion (LCA, Section 2.3).

Primary Research Hypothesis:

Three-dimensional, low-density cellular metal structures of any macrostructure, mesostructure, or material can be manufactured via layer-based additive manufacturing of metal-oxide ceramic material followed by post-processing in a reducing atmosphere.

This hypothesis reflects the belief that the combination of the best traits (Table 1.2) of AM and the reduction of metal oxide powders (as seen in the LCA manufacturing process) will provide an opportunity to reach the primary research goal. Specifically, the

capability of AM to selectively place material throughout a part alleviates the macrostructure limitations found in the LCA manufacturing process. Conversely, the extensive material selection and excellent material properties found in the metal oxide reduction technique are a perfect complement to the material limitations found in traditional AM processes and the (post-) processing issues found in direct metal AM technologies.

A three-phase research strategy was implemented in order to verify the primary research hypothesis. These phases include the design, embodiment, and evaluation of a manufacturing process for the realization of parts of designed mesostructure (Figure 1.8). The results of these three phases are presented in the body of this work, and are organized so as to establish proof that the primary hypothesis has been verified (as outlined by the dissertation roadmap, seen in Figure 9.1).

9.1.1 Summary of the Design Phase

The first phase of the research involved the design of a manufacturing process for the realization of parts with designed mesostructure. In order to avoid an ad hoc developmental approach to the research goal, a rigorous, systematic design method was implemented. Specifically, the method posed by Pahl & Beitz (as outlined in Appendix A) is used as a framework for maintaining solution neutrality and guiding design decisions. The design followed three phases: clarification of task (Chapter 2), conceptual design (Chapters 3 and 4), and the selection of the principal solution (Chapter 5).

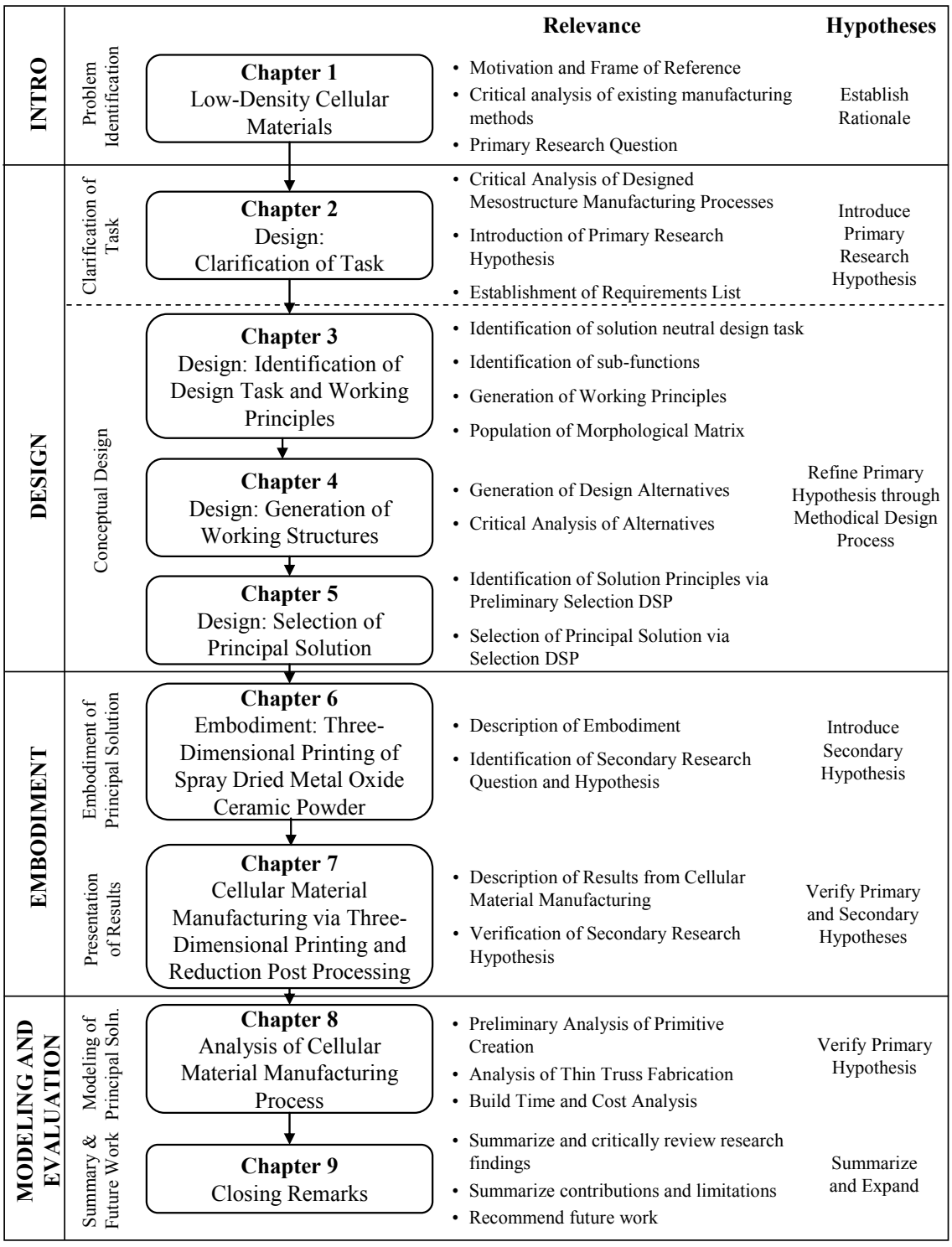

Figure 9.1 – Dissertation Roadmap

The result of the clarification of task phase is a list of design requirements for an AM process dedicated to the realization of cellular materials. This list was systematically composed through a review of the needs specific to the process proposed by the primary research hypothesis (Section 2.5.5). This list of requirements provides a concrete means on which the verification of the research hypothesis can be measured.

The conceptual design effort is presented in this dissertation in two chapters. Chapter 3 is focused in the identification of the design task and the proposal of working principles. The design task is elucidated through the identification of the key design requirements. These key requirements are identified through a systematic progression of a series of abstraction exercises (Section 3.1). From these key requirements, the essential tasks of the to-be-designed process are abstracted, resulting in the identification and organization of the process's core functions (Section 3.2). Finally, working principles were ideated through a comprehensive review existing AM technologies dedicated to the fabrication of ceramic green parts and grouped together using a morphological matrix (Figure 3.6).

The second portion of the conceptual design process (presented in Chapter 4) is centered in the generation, and critical analysis, of working structures that are generated through the combination of the working principles. As a result of this systematic approach to conceptual design, thirteen different design alternatives were generated.

The final stage of the design process, the selection of the principal solution, is presented in Chapter 5. This phase of the design process is centered in the identification of the manufacturing process that is the most likely to satisfy the design requirements

according to their relative importance as judged by the author. This phase consisted of two separate selection exercises:

(i) A preliminary selection exercise is first implemented to identify those design alternatives that are "most-likely-to-succeed" as based upon the soft engineering data available to the author. This exercise consists of a systematic comparison of each design alternative through the establishment of several datum and an evaluation of the resulting apparent preferences towards certain design alternatives. The result of this exercise was the identification of five design concepts worthy of further investigation.

(ii) With five solution principles identified, a selection decision was then implemented to identify the principal solution. Following the rigorous procedure as outlined by the selection compromise Decision Support Problem framework, the five principles are evaluated using hard engineering data, technical specifications, and scales which quantify qualitative data.

As a result of these systematic selection exercises, three-dimensional printing (3DP) was chosen as the principal solution. The primary research hypothesis was then updated to reflect this important design decision.

Updated Primary Research Hypothesis:

Three-dimensional, low-density cellular metal structures of any macrostructure, mesostructure, or material can be manufactured via three-dimensional printing of metal-oxide ceramic powder followed by post-processing in a reducing atmosphere.

9.1.2 Summary of the Embodiment Phase

The embodiment phase of this research, presented in Chapters 6 and 7, is focused in the verification of the primary research hypothesis. In Chapter 6, the working principles of 3DP are further explored in an effort to identify needs for augmentation of the existing 3DP embodiment. From this systematic exploration of the working principles for each sub-function of 3DP, a secondary research question and accompanying research hypothesis are posed. Specifically, a hypothesis for improving the density of the green parts which result from the 3DP process is developed through exploring different alternatives in the "store material" and "create primitive" sub-functions (Sections 6.1.1 and 6.1.3

Secondary Research Question:

How can the density of metal parts created by the thermal-chemical conversion of ceramic green parts fabricated by three-dimensional printing be improved?

Secondary Research Hypothesis:

The density of metal parts which result from the thermal-chemical conversion of ceramic green parts can be improved by creating primitives via printing a solvent into a bed of binder-coated powder particles.

Chapter 6 closes with a description of the specific embodiment of the 3DP solution principle that is used for the verification of the research hypotheses. This includes a full description of the machine (Section 6.2.1), the materials (Section 6.2.2), and the post-processing procedure (Section 6.2.3).

The second portion of the embodiment phase, presented in Chapter 7, is focused in the description of the experiments used to verify the research hypotheses and the report of their results. The characteristics of the parts realized by the designed manufacturing process are reported in Section 7.2. Specifically, the parts' phase, density, porosity, and shrinkage are analyzed. The secondary research hypothesis is verified through this analysis, as those components created via the deformation of binder-coated granules exhibited a greater density than those created by other means (detailed in Section 7.2.2).

The primary research hypothesis is verified through the successful creation of parts which have features common of cellular materials (Section 7.3). Specifically, thin walls ($\leq$ 300 μm), narrow channels (1 mm square and 5 mm long), and thin angled trusses (1 mm at 20^{o}) are successfully created. The primary hypothesis is further verified through the successful creation of a series of complex geometries with designed mesostructure (Section 7.3.4).

A critical analysis of the results obtained by the designed manufacturing process is presented in Section 7.4. In a final effort to verify the primary research hypothesis, the process's capabilities are compared against the design requirements that were originally generated in the initial phase of design. This comparison (originally presented as Table 7.7) is shown in Table 9.1.

9.1.3 Summary of the Modeling & Evaluation Phase

The final phase of the research presented in this dissertation is centered in analyzing and modeling aspects of the designed process so as to gain a better understanding. Three different aspects of the process are analyzed and/or modeled:

(i) In Section 8.1, a review of the existing models for the fundamental physics and kinetics of individual primitive formation in 3DP is presented. This analysis provides additional insight into the results obtained in the embodiment research phase.

(ii) As an important classification of mesostructure found in cellular materials, the layer-based fabrication of thin trusses is analyzed in Section 8.2. Through this analysis, a rough model of the estimation of fabrication failure is presented. Several design rules for the fabrication of thin trusses are also extracted from this analysis.

(iii) A model for the estimation of process build time and cost is developed in order to verify claims of the process's economic viability as a production machine. From these models it is estimated that the process is able to fabricate metal parts of designed mesostructure for ~$4 / part. The models' estimation accuracy are verified through a comparison with results found in the literature.

The first two modeling efforts provide a foundation for future research. Process improvements will arise through a thorough understanding of the fundamental physics of primitive formation and truss failure during fabrication. The results of the cost and throughput model not only provide a basis for comparing the designed AM process against existing direct-metal AM processes, but it also provides insight into the feasibility of it as a production-scale manufacturing process.

Table 9.1 – Requirements List Checklist

D/W	*Requirement*	*Met?*
	Geometry	
D	Able to process any macrostructure geometry	Y
D	Able to process complex geometry: - overhanging features - internal voids - high-aspect ratio structures	 Y Y Y
D	Able to process small cell sizes (0.5 – 2 mm)	1 mm minimum
D	Build small features and wall thicknesses (as small as 200 μm)	300 μm minimum
D	Build trusses from 0.5 mm – 10 mm in diameter	0.8 mm minimum
D	Construct trusses that are inclined at ≥ 35 degrees from the build direction	Y
D	Able to create cross-sections representative of designed mesostructure: - circular depositions with diameter as small as 0.5 mm - 200 μm minimum feature size	 Y 300 μm
	Material	
D	Able to process all transitional metal oxides (excluding alumina and titanium oxide)	Y
D	Process powder particles with diameter ≤ 50 μm	Y
W	Minimize amount of effort required to adapt to a new material	Y
W	Able to process standard working material (i.e., material is not proprietary or require specialized formulation)	spray-dry
	Production	
D	Build envelope is 250 x 250 x 250 mm or larger	Y
D	Deposition rate should be ≥ 10 cm^3/hr	Y
D	Support material must be able to be removed from part with minimal effort (if applicable)	N
	Quality Control	
D	Finished parts have ≥ 95% relative density	N
D	Ceramic green parts have ≥ 40 vol% ceramic solids loading	35-40 %
D	Material properties are comparable to standard	N
D	Material properties of finished part are isotropic	N
D	Minimize surface roughness before finishing (≤ 0.02 mm Ra)	N
D	Maximize accuracy (≥ +/- 0.05 mm)	Y
D	Minimize z-resolution (≤ 0.1 mm)	Y
	Operation	
W	Does not require special operating environment	Y
W	Minimize operator interaction	Y
	Recycling	
W	Minimize environmental impact by minimizing wasted material	Y
W	Reusable wasted material	Y
	Costs	
D	Minimize cost of technology and technology maintenance by avoiding expensive technologies such as lasers and electron beams	Y
D	Minimize cost of material	Y
W	Easily scaled for large applications	Y

9.2 SUMMARY OF CONTRIBUTIONS

Contributions to the design, additive manufacturing, and materials communities can be identified in each phase of the research completed in this dissertation.

9.2.1 Design Phase Contributions

A high-level contribution of this work is the documentation of a systematic design process of an additive manufacturing technology. While past development of AM processes was typically due to the discovery of a specific embodiment "pattern material" and/or "pattern energy" sub-functions (thus, a "technology push"); the design endeavor presented in this body of work is unique in that it is driven by the specific requirements of manufacturing cellular materials (thus, an "application pull"). In this context, there exists value in the archival of this process, as the learning points presented within can be of benefit to future design attempts. Specific contributions which resulted directly from the design phase are as follows:

- *New classification of cellular materials.* As a result of the critical analysis of the existing cellular manufacturing techniques, a new classification of manufacturing processes is developed (Section 1.3.1). Specifically, the "parts of designed mesostructure" classification is added to the existing classifications, "Stochastic" and "Ordered." This additional classification places emphasis on the desire for designer freedom in the manufacture of cellular materials and distinguishes those processes that offer designer freedom in the specification of material composition, mesostructure topology, and macrostructure geometry.

- *Critical analysis of direct-metal AM processes.* In the clarification of task phase of the design portion of this research, a critical review and analysis of existing direct-metal AM processes is offered in the context of their capability in realizing cellular materials (Section 2.2 and Appendix B). This documentation of design rationale is of relevance to the design and AM communities, and has been published and presented at an international conference (Williams et al., 2005a).
- *Critical analysis of ceramic AM processes.* The generation of design alternatives in the conceptual design phase of this research resulted in a critical review and evaluation of existing ceramic AM processes in the context of their capability of realizing cellular materials (Chapters 4 and 5). This is of relevance to the AM community, and has been published and presented at the annual Solid Freeform Fabrication Symposium (Williams et al., 2005b).
- *Functional classification of AM technologies.* By following a systematic series of abstraction exercises, a functional classification of AM technologies is offered (Chapter 3). This provides a new way to classify AM technologies, and is of benefit as a user can classify all existing AM technologies. This classification can be reused by designers for future AM process-design efforts.
- *Critical analysis of AM processes at a functional level*. A secondary result of progressing through a systematic selection exercise was a critical analysis of existing AM processes at their functional levels (Section 5.1.6). This is of relevance to the design and AM communities as this analysis provides insight into the current limitations of existing technologies (Williams and Rosen, 2007).

9.2.2 Embodiment Phase Contributions

The primary contribution of this research is the embodiment of a layer-based additive manufacturing process for the realization of metal parts with designed mesostructure. The process features the three-dimensional printing of spray-dried metal oxide ceramic powders followed by a post-production process wherein the green part is sintered and reduced in a hydrogen/argon atmosphere, thus chemically converting the part to metal (Chapter 6). The process has been shown to successfully create parts with designed mesostructure (Chapter 7). It is capable of creating walls as thin as 300 μm and channels as small as 0.92 mm in diameter. Angled trusses that are 1 mm in diameter have also been successfully fabricated.

From these results, Table 1.2 (a summary of the design freedom offered by cellular material manufacturing technologies) is updated to include the process embodied in this research, as shown Table 9.2.

Table 9.2 – Summary of Design Freedom Offered by Cellular Material Manufacturing Technologies

		Processes	*Repeatable*	*Material Freedom*	*Mesostructure Freedom*	*Macrostructure Freedom*
Stochastic	Metal Foams	Hydro / Alcam / Combal		✓		
		Alporas				
		Gasar / Lotus				
		Alulight / Foaminal				✓
		Formgrip				✓
		Metal Sponges		✓		✓
		Hollow Sphere foams	✓			
Ordered		Honeycombs (via crimping & stamping)	✓	✓		
		Lattice Block Materials	✓			
Designed		Linear Cellular Alloys	✓	✓	✓	
		Additive Manufacturing	✓		✓	✓
		Metal Oxide 3DP + Reduction	✓	✓	✓	✓

9.2.3 Modeling & Evaluation Phase Contributions

Additional contributions resulted from the process analysis and modeling efforts presented in Chapter 8. A new understanding of the failure mode of thin trusses when fabricated via layered manufacturing is offered in Section 8.2. In addition, generalized design rules are presented to assist designers in the creation of trussed material.

Finally, a model of the process's cost and throughput is offered in Section 8.3. This model is of use to the AM community, as it is generalized for the application to any 3DP process.

9.3 CRITICAL ANALYSIS & FUTURE WORK

In this section, the design and embodiment phases of this research effort are critically analyzed. Suggestions for future work are offered as a means of addressing these limitations.

9.3.1 Critical Analysis of Design Phase

At the most fundamental level, the design phase of this research is considered successful since following the progression of design steps resulted in a manufacturing process which satisfies the large majority of the design requirements (as seen in Table 9.1). The use of a systematic design process ensured solution neutrality, abstraction of requirements to identify the crux of the design task, and the consideration of the designer's preferences. However, like all problems of design, there is a possibility that a better solution exists, and might have been identified had more complete information been available.

One manner in which more information could have been obtained is through further embodiment of the solution principles identified at the end of preliminary selection (following Section 5.1). Through further experimentation, more "hard engineering data" could have been gathered, and thus added more credibility to the rankings of the various selection attributes for each alternative. Specifically, there are several alternatives that are evaluated with an interval scale that could have been ranked via a ratio scale through additional engineering (e.g., surface finish and deposition rate). This criticism of the design phase of this research is made even more valid when considering that the five solution principles evaluated in the selection phase (Section 5.2) share very similar merit function values. Obviously, any additional information would contribute in better distinguishing between the alternatives. Ideally, it would be best to further the embodiment of each of the alternatives to an equal level of detail in order to achieve the most meaningful result from the selection DSP.

The primary critique of the design phase of this research is the discontinuation of the implementation of the systematic design process for the embodiment of the principal solution. As outlined by Pahl & Beitz (Appendix A), the design process closes with an Embodiment Design phase and a Detailed Design phase once the principal solution is selected (at the closure of the Conceptual Design phase). The Embodiment Design phase consists of the ideation, arrangement, and selection of specific embodiments for each solution principle. Various combinations of each principle's embodiment are combined to check for compatibility via the generation of a morphological matrix (as done in conceptual design, Section 3.4). A systematic selection process is then used to identify

the set of embodiments that will best satisfy the design requirements (as done in conceptual design, Chapter 5).

Proving the feasibility of the manufacturing process (i.e., verification of the primary and secondary hypotheses) was the crux of the research task of this dissertation – thus the embodiment effort was focused in adapting a current embodiment to the design requirements as best as possible. Furthermore, a lack of prior experience and detailed knowledge of the 3DP process (and its adaptation to fabricating ceramic metal oxide parts) made such a high-quality, in-depth systematic embodiment design process challenging, which resulted in only a limited embodiment design process.

A systematic embodiment design process would involve repeated experimentation with many different granule sizes, shapes, and binder compositions, as well as with various solvents in order to determine the embodiment which provides the best primitive creation. The various inkjet deposition technologies would also need to be investigated. Finally, various recoating techniques should be explored so as to determine which provides the highest green part density. Assuming the current embodiments of the functions regarding translation of the printing and powder piston stages do not change, the next series of embodiment design decisions are summarized in Table 9.3.

Finally, it is noted that the author does not claim that the manufacturing process designed in this research is the only and/or "best" solution to the stated design goal. While the completion of the selection process in this research suggests that the 3DP principal solution more completely satisfies the design requirements, this selection is dictated by the author's preferences for the relative importances for each selection criterion. A different designer, maybe with more intimate knowledge of the various AM

processes, might come to a different conclusion. Fundamentally, any design decision made is only as "good" as the information on which it is based. Ideally, a designer would have an infinite amount of time and resources in order to explore an infinite amount of concepts and to iterate through the design process as many times necessary so as to make fully informed decisions. As this is not feasible (especially in the context of completing a dissertation), the design presented in this work is as good as the information supplied by the literature.

Table 9.3 – Potential Decisions to be Featured in the Systematic Completion of Embodiment Design

Function	Decision	Potential Principles
Store material	Shape / size granules	Spherical, multi-faceted particles, etc.; various sizes
Create granules (bind particles)	Selection of binder coating and its content	PVA, PMMA, etc.; 2wt%, 4wt%, etc.
Create primitives (deform granules)	Selection of deposited solvent	Water, alcohol, acetone, various mixtures, etc.
Create droplet	Selection of droplet actuation technology	Bubble jet, thermal jet, acoustic, etc.
Process droplet	Selection of print head technology	Continuous, drop-on-demand inkjetting
Recoat powder bed	Selection of recoating mechanism	Roller, doctor blade, w/ or w/o vibration, counter-rolling, tapping, etc.
Convert green part to metal	Selection of post-process cycle (i.e., burnout, reduction, and sintering hold times, ramps, and temperatures	Various sintering cycles

9.3.2 Critical Analysis of Embodiment

A critical analysis of the designed manufacturing process is offered in Section 7.4. This analysis is presented in two separate categories: weaknesses of the process due to the specific embodiment, and weaknesses of the process due to the general 3DP principal solution itself.

Weaknesses of the process due to the embodiment specific for this research include (as seen in Section 7.4.1)

- poor finished part density
- poor surface quality, and
- poor green part strength.

As illustrated in Figure 9.2, these weaknesses are primarily due to poor powder bed packing density, an inability to spread fine particles, and insufficient solvent deposition. These causes are further aggravated by limited control and understanding of process variables and physics (e.g., binder/powder interaction, binder/printhead compatibility, process planning, etc.).

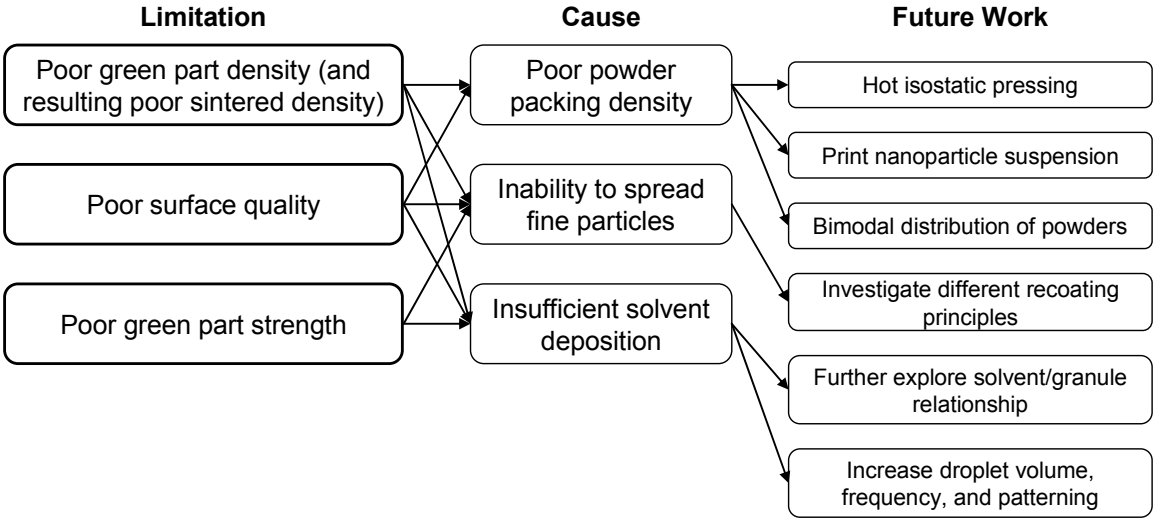

Figure 9.2 – Limitations of Embodiment and Suggestions for Future Work

Weaknesses of the process due to the 3DP principal solution are as follows (as seen in Section 7.4.2):

- The inability to process fine particles will always preclude the ability to achieve ~99% relative density in the finished part.
- The implementation of the powder bed working principle will inherently lead to a poor surface finish.

- The large amount of shrinkage due to the reduction process can lead to dimensional inaccuracy.
- The random packing of particles found in the powder bed can lead to green part inhomogeneity, which will result in part curling, warping, and anisotropic material properties.
- The use of a powder bed significantly increases the difficulty in cleaning parts of designed mesostructure due to the potential for trapped unbound material within the designed voids.
- The reliance on the reduction post-process to realize metal parts prevents the process from being able to fabricate aluminum and titanium as their oxidized counterparts cannot be reduced.
- Some complex geometries which can be processed with traditional AM technologies cannot be fabricated using this process due to the inability to remove unbound powder from internal voids, large shrinkages during post-processing, and the welding of contacting surfaces during sintering. Examples include joints, single-part assemblies, and powder-filled cells.
- A final limitation with the printing patterning working principle is the potential for (frequent) clogging of the material printheads. Nozzle clogging has shown to lead to significantly reduced finished part relative density.

The finished parts' porosity (Section 7.2.3), and accompanying poor density, are significant limitations. Ideally the parts would have < 5% open porosity, as any amount more than this constraint almost eliminates the materials from any engineering application. Porous parts fail early in fatigue situations, and thus are only useful for static

loading conditions. Furthermore, the manner in which the porosity is aligned in the finished parts severely hampers their mechanical properties. Furthermore, the surface roughness of finished parts may preclude the realization of fine features and small channels.

Should future development fail to address these limitations, the parts resulting from this process might still be useful in those engineering structures which have static loads. Coupled with the rough surface, this process could be used to fabricate tailored structural heat exchangers. The creation of customized metal filters is another potential application of the parts that can be created from this process.

9.3.3 Future Work

Suggestions for future work towards improving the manufacturing process are separated into two categories according to their scope.

Short-Term Suggestions for Future Work

Short-term suggestions for future work are related to improving the current embodiment of the designed manufacturing process (originally presented in Section 7.4.1, and illustrated in Figure 9.3). Most of these suggestions would best be fulfilled through the continuation of a systematic embodiment design process (as presented in Table 9.3).

- *Increased solvent deposition*: One flaw in this specific embodiment is the inability to increase the amount of solvent that is deposited into the powder bed. As shown in Section 7.2.2, an increase of solvent enhances the deformation of the spray-dried granules, thus bringing the particles closer together, and improving density.

- *Tailored powder & solvent system*: Although complex parts were created with the granule/solvent system chosen, much more research could be done in tailoring the powder/solvent system so as to maximize part quality. Specifically, the solvent's surface tension, droplet size, viscosity, etc. should be tailored to improve the wetting of the chosen ceramic powder. The granule/solvent system should be designed so as to maximize the solvent's spreading and infiltration into the powder bed, and thus ensuring proper overlap (or "stitching") between the printed bands of adjacent primitives and the deposited layers. As discussed in Section 7.2.3, insufficient stitching can lead to porosity between printed bands and layers (such as those found in the parts created by this specific embodiment).
- *Hot isostatic pressing* (HIP): HIPing could be used as a secondary post-processing step in order to increase finished part density; however, this might limit the topologies that can be created by the process. Infiltration with a secondary material phase is another manner in which density can be increased.
- *Printing nanoparticle suspension*: Another manner of increasing green part density could be achieved by printing a binder/solvent suspension of ceramic nanoparticles into the powder bed. Once dispersed into the powder bed, the printed nanoparticles would fill the interstitials between the powder bed particles, thus increasing the green part density. Crane and coauthors have displayed improvements in part density and in part creep via submersing green parts in a nanoparticle suspension after printing (Crane et al., 2006).

- *Bimodal powder*: The powder bed packing density can be improved by increasing the size distribution of its particles. Lanzetta and coauthors were able to successfully process a bimodal alumina powder system featuring 20 μm particles with 10 wt% 2.5 μm particles added (Lanzetta and Sachs, 2003). In this embodiment, this can easily be achieved by using the smaller granules that are found on the interior of the spray-drying chamber (known as "chamber wipe down").
- *Improved recoating*: Several different recoating procedures have been proposed in the literature so as to increase the packing density of the powder bed. It is also possible that other recoating embodiments would be able to process finer particles, which would also lead to an improved final part density.
- *Analysis of finished part strength*: As is typical of other AM processes, build orientation and powder bed location could have significant impact on the strength of the finished parts. Additional testing is needed to verify the presence of these effects for this manufacturing process.

Long-Term Suggestions for Future Work

Looking towards long-term achievement of the research goal, one can identify several suggestions for improvement that are related to the principal solution of the designed manufacturing process.

At the most basic level, the ideal manufacturing process for designers and manufacturers alike is a technology which can quickly create parts through the placement of (any) material at the atomic level. Since this is not immediately achievable, researchers of AM have continually scaled this concept up in size until it can be realized.

Basically, in order to achieve the design goals as stated in this research, one needs the ability to place and affix small material voxels in order to create custom geometry on the meso-scale.

As such, it is suggested that the hot-melt inkjet printing solution principle be further explored to identify its potential in satisfying the design requirements. Its ability to deposit single voxels of materials in an economic manner is very promising. Furthermore, its ability to deposit multiple materials is very appealing, as a sacrificial support material, which could be automatically removed through pyrolysis, would greatly enhance the ease of use of the overall process. Its one limitation, the inability to print droplets with a high content of ceramic particles (and thus fabricate dense green parts), might be able to be alleviated through future progress in the realm of inkjet printing. One example of such progress can be found in current research centered in the development of ultrasonic micro-nozzles, which have shown promise in jetting viscous materials (Meacham et al., 2004; Meacham et al., 2005).

Another solution principle that might be applicable to this specific application in the future is the use of micro-pipettes to selectively deposit individual powder particles through the application of specialized ultrasonic waveforms. Should a manner of creating three-dimensional primitives with this technology arise, it would be an ideal candidate for the creation of cellular materials with a meaningful engineering material.

Finally, the quality of the process's finished parts could be greatly enhanced through the development of a process planning structure that is founded upon detailed modeling of the primitive creation process in 3DP. Furthermore, models relating changes

in geometry (both physics and kinetics) with reduction process parameters would significantly enhance the quality of the final parts.

9.4 REMARKS AND RECOMMENDATIONS

The primary contribution of this work is the establishment of a manufacturing process chain which is capable of producing metallic parts of designed mesostructure that offer a designer the freedom to specify part material, mesostructure, and macrostructure. Furthermore, these metallic parts of complex, customized, cellular geometry have been realized at a cost up to 100 times less than comparable AM technologies

As those on this dissertation's reading committee have pointed out, however, there is more to a manufacturing process than simply its cost. If poor part quality renders the finished parts useless, then the manufacturing cost is of no concern since the process itself would be worthless. Evans argues that the capability to fabricate microstructure and shape concurrently may justify (additive) manufacturing processes with extreme costs and poor throughput (Evans, 2001). However, it is my opinion that the extreme savings in cost offered by this manufacturing process (as illustrated in Section 8.3) justifies further investment and exploration.

As mentioned in Section 9.3.1, information is the most valuable resource in any design task. It is hypothesized that further accumulation of additional information will lead to a more informed decision. Further experimentation with the various alternatives would lead to more quantitative attribute rankings, and thus instill additional confidence in the decision. Despite this, given the experiences and knowledge that I have gained

through this research, it is unlikely that the design decisions presented herein would significantly change with additional information.

Since the major criticism of the current embodiment is the resulting poor final part density, it is fitting that it was chosen as the most important (and thus heavily weighted) attribute in the selection process. Thus, it is appropriate that, despite having similar merit function values (Section 5.2.4), 3DP was selected over IJP-W primarily because of its larger green part density (Table 9.4).

Table 9.4 – Comparison of Green and Finished Densities for Various Ceramic AM Technologies

Alternative	Green density	Finished relative density	Reference
3DP	35-55	65-92 %	(Michaels et al., 1992; Cima et al., 1995)
S-3DP	65	95 %	(Kernan et al., 2003)
SLS	-	50 %	(Klocke and Ader, 2003)
FDC	55	97 %	(Vaidyanathan et al., 2000)
IJP-W	35	80 %	(Ainsley et al., 2002)
IJP-A	65	98 %, "almost full"	(Teng et al., 1997), (Zhao et al., 2002a)
SLA	53	90.5 %	(Hinczewski et al., 1998a)

Although other ceramic AM processes might offer higher part densities than 3DP, other aspects of their solution principle prevent them from being appropriate choices for a process dedicated to the fabrication of parts of designed mesostructure (as discussed in Chapter 5).

Although I am confident in my selection of 3DP, I still recommend further exploration of the IJP-W process. It is clear that the 3DP process needs further development in order to achieve the higher finished densities as seen in the literature. It is likely that further development of the IJP-W process might one day increase the density of its finished parts. In fact, the IJP-W process has the most to gain from further development, as its ability to selectively deposit multiple materials (including sacrificial support material) makes it better suited for fabricating parts of designed mesostructure than the powder bed-based 3DP process.

Of the many future work suggestions offered in Section 9.3.3, I hypothesize that printing a nanoparticle suspension into the powder bed is the best candidate for increasing part density, and thus significantly improve the quality of the finished parts. If verified, this hypothesis would provide new knowledge to the AM community (as it has not been done before) with very little effort. Furthermore, minor additional effort in the proper selection of the solvent would enhance part quality tremendously. Finally, it is my recommendation that an investment in a 3DP test-rig is made so the printing process parameters can be tailored to the solvent/granule working principle.

Another recommendation is to explore the use of this process to fabricate copper parts. To my knowledge, no one has processed copper materials in an AM context. Furthermore, the current material property limitations prominent in the parts created by this process might limit it to structural heat-exchanger applications; thus, the ability to create copper parts would be extremely valuable.

Finally, to close this dissertation, I offer a general recommendation to continue to place importance on research collaboration. It is the collaboration between Georgia Tech's Systems Realization Laboratory, the Rapid Prototyping and Manufacturing Institute, and the Lightweight Structures Group that made this research possible. Further collaboration is needed with several other engineering disciplines in order to improve this process as well as those processes on which it relies. Perhaps a new powder processing technique will be developed which creates a shape of granule which has a higher packing density. Or, perhaps a new way of inkjet printing will be developed that allows for the creation of small, precise, repeatable droplets of a viscous, powder-filled suspension. Collaboration provides an opportunity for the discovery of new applications (and their

associated requirements) which will benefit from the inclusion of a customized metallic part of designed mesostructure. Collaboration is the key to furthering the relevance of the Mechanical Engineering discipline, for it is at the boundaries of disciplines where opportunities for creating new knowledge exist.

APPENDIX A

THE PAHL AND BEITZ SYSTEMATIC DESIGN METHODOLOGY

The Pahl and Beitz systematic design methodology, developed by Gerhard Pahl and Wolfgang Beitz, approach is divided into four main phases: Planning and Clarification of Task, Conceptual Design, Embodiment Design, and Detail Design. These phases are presented graphically in the flowchart shown in Figure A.1, and detailed below.

Planning and Clarification of Task

The first phase, Planning and Clarifying the Task, begins with a designer identifying and analyzing the market for a potential product. From this analysis, product ideas are generated and a product proposal is developed. The task is then clarified by collecting information about the requirements and specific constraints on the future product. This phase ends with the articulation of a Requirements List based on the identified requirements and constraints.

Conceptual Design

In Conceptual Design, a designer uses the requirements developed in the Planning and Clarification of Task phase as a foundation for concept development. A designer first abstracts the requirements to identify a solution neutral problem statement, then establishes a function structure for the future product based on the essential problem identified. A designer then searches for functional solutions (working principles) for the identified functions and sub-functions. Next, working structures (preliminary concepts) are developed by combining suitable working principles. These working structures are then firmed up into solution variants and a designer evaluates these variants against

technical and economic criteria. The Conceptual Design phase ends with the specification of a principal solution.

Embodiment Design

During this phase, a designer develops a preliminary physical layout for the concept selected at the closure of the Conceptual Design phase. In most cases, several layouts are developed. These layouts are evaluated based on concrete technical and economic criteria and the best layout is selected. This preliminary layout is then refined into a definitive layout by identifying and eliminating it shortcomings.

Detail Design

During Detail Design, a designer finalizes the arrangement, forms, dimensions, and surface properties of the product. This phase also includes material specification, cost estimation, and the development of all production documents needed.

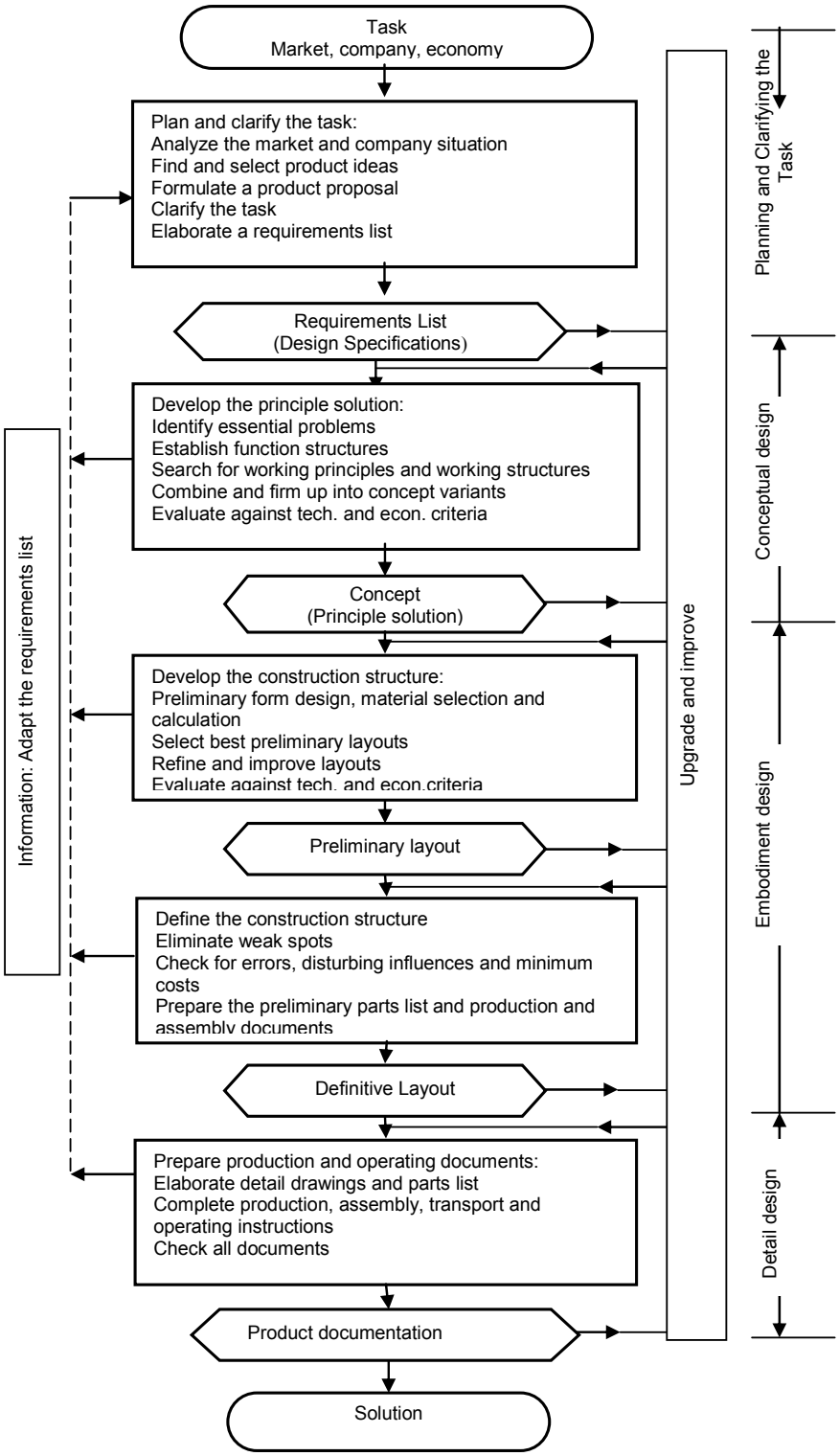

Figure A.1 – Flowchart of Pahl and Beitz Systematic Design Method (Pahl and Beitz, 1996)

APPENDIX B

PRELIMINARY SELECTION OF DIRECT METAL ADDITIVE MANUFACTURING TECHNOLOGIES

In an effort to systematically evaluate the ability of the direct metal AM technologies to produce parts of designed mesostructure (as dictated by the requirements outlined in Section 2.1), a methodical preliminary selection process was implemented. Proposed by Mistree and coauthors, the Preliminary Selection Decision Support Problem (DSP) is a technique for making selections in a complex, multi-faceted design environment (Mistree et al., 1994). The Preliminary Selection DSP provides a designer a framework in which the most-likely-to-succeed concepts can be identified through the systematic comparison of alternatives based upon "soft" (i.e., predominately qualitative) engineering data. The technologies being evaluated are described in detail in Sections 2.2.2 – 2.2.6. Although a great deal of quantitative engineering data is presented for each alternative, there is not enough to proceed with a full engineering selection process.

To begin the preliminary selection process, selection criteria must be developed around the requirements listed. As such, each concept will be evaluated by the criteria outlined in Table B.1.

The selection criteria listed in Table B.1 represent criteria that are specific to manufacturing parts of all classes (low cost, high throughput, multiple materials, good material properties), as well as criteria that are specific to manufacturing parts of designed mesostructure (extremely small features, excellent surface finish, and complex geometries).

Table B.1 – Preliminary Selection Criteria

Category / Criteria	*Description*
Economics	
Technology Cost	The cost of purchasing the technology. Prefer low cost.
Additional Costs	The cost of the equipment necessary for post-processing as well as the cost for maintaining the technology. Prefer low cost.
Time	
Deposition Rate	The amount of volume deposited per unit time. Prefer high rate (> 10 cm^3/hr)
Cycle Time	The total amount of time to create a part – focus on post-processing. Prefer low cycle time.
Performance	
Minimum Feature Size	The smallest feature able to be produced by technology. Prefer small size; wall thicknesses 50-300 μm.
Complex Geometry	The ability of the technology to create complex geometry. Preference goes to those technologies that can produce overhangs and small channels that are typical of cellular materials.
Surface Finish	Quality of surface able to be produced by machine. Prefer small surface roughness < 0.02 mm Ra.
Materials	
Material Properties	Quality of materials produced by technology. Preference goes to those technologies that are capable of producing materials that are close to standard values.
Material Selection	The number of metallic materials able to be processed by the technology. Prefer technologies that can process multiple materials.

The Preliminary Selection DSP technique involves a series of comparisons between each working principle alternative and a chosen datum in the context of the different selection criteria. The concepts are evaluated against the datum and are judged to be inferior (-1), equal (0), or superior (+1). Since the comparisons are based upon soft engineering data, this three-point scale is appropriate; at this point in the design process a designer can only identify that one concept is preferred over another, but cannot quantitatively identify by how much the concept is preferred. It is noted that value assessments are subjective and experience-based; however, this is not a shortcoming - evaluation procedures are meant to enhance an engineer's decision-making ability.

The scores are then summed and normalized within each category. Ranks are assigned based on the summed score of all the normalized scores of each criterion. A sample comparison matrix, wherein SLM is the chosen datum, is given in Table B.2.

While this was chosen as the initial datum, the multiple iterations of the DSP process make it an insignificant choice.

Table B.2 – Comparison Matrix for Selective Laser Melting Datum

	SLS	DMLS	LENS	UOC	EBM	MJS	SLM	3DP
ECONOMICS								
Technology Cost	0	0	-1	0	-1	1	0	1
Additional Costs	-1	-1	0	0	0	-1	0	0
Score	-1	-1	-1	0	-1	0	0	1
Normalized Score	0.00	0.00	0.00	0.50	0.00	0.50	0.50	1.00
TIME								
Deposition rate	1	1	1	1	1	1	0	1
Cycle time	-1	-1	0	0	1	-1	0	0
Score	0	0	1	1	2	0	0	1
Normalized Score	0.00	0.00	0.50	0.50	1.00	0.00	0.00	0.50
PERFORMANCE								
min. feature size	-1	-1	-1	-1	-1	-1	0	0
complex geometry	0	0	-1	-1	0	-1	0	0
surface finish	-1	-1	-1	0	-1	0	0	-1
Score	-2	-2	-3	-2	-2	-2	0	-1
Normalized Score	0.33	0.33	0.00	0.33	0.33	0.33	1.00	0.67
MATERIALS								
mat. Properties	-1	-1	0	-1	1	-1	0	-1
material selection	-1	-1	0	-1	-1	0	0	0
Score	-2	-2	0	-2	0	-1	0	-1
Normalized Score	0.00	0.00	1.00	0.00	1.00	0.50	1.00	0.50
OVERALL SCORE								
Sum of Scores	0.33	0.33	1.50	1.33	2.33	1.33	2.50	2.67
Rank	7	7	4	5	3	5	2	1

An important aspect of performing preliminary selection is the recording of the viewpoints that guide each scoring. One interesting point to be noted is that the "Technology Cost" criterion is not solely based on the machine cost listed in Tables 2.2 – 2.6. Since different companies have different pricing and marketing strategies, the machine costs cannot be assumed to be the actual technology cost. Furthermore, different machines have different build envelopes, which also skew the pricing strategies. For this metric, scores are based on the assumption that laser-based machines are often more expensive than those technologies that use alternative methods of deposition. Of course, this same logic affects the cost of annual maintenance in the "Additional Costs" criterion. Finally, it is important to note that many of the scores are based on the

incomplete data collected through the rigorous literature review presented in Section 2.2. AM companies do not fully disclose machine performance specifications; since those specifications that are disclosed are usually done so through a sales brochure, scoring must often be based on an educated engineering guess.

Multiple weighting schemes are employed in the Preliminary Selection DSP technique to address the interaction of the selection criteria. The weighting schema for each scenario in this selection exercise is presented in Table B.3.

Table B.3 – Weighting Scheme Scenarios

Criteria	*One*	*Two*	*Three*	*Four*
Economics	0.2	0.1	0.15	0.35
Time	0.2	0.1	0.2	0.35
Geometry	0.3	0.4	0.4	0.15
Materials	0.3	0.4	0.25	0.15

The first three scenarios represent increasing amount of importance placed on the technology's ability to create the geometry common in cellular materials out of multiple materials. The fourth scenario represents a case wherein importance is placed on the speed and cost of the process.

Normalized scores for each concept are computed by multiplying the normalized score of each concept's attribute category (Table B.2) by the weighting values (Table B.3). The summed score serves as the merit function for each generalized concept. The results from the SLM datum are graphically shown in Figure B.1.

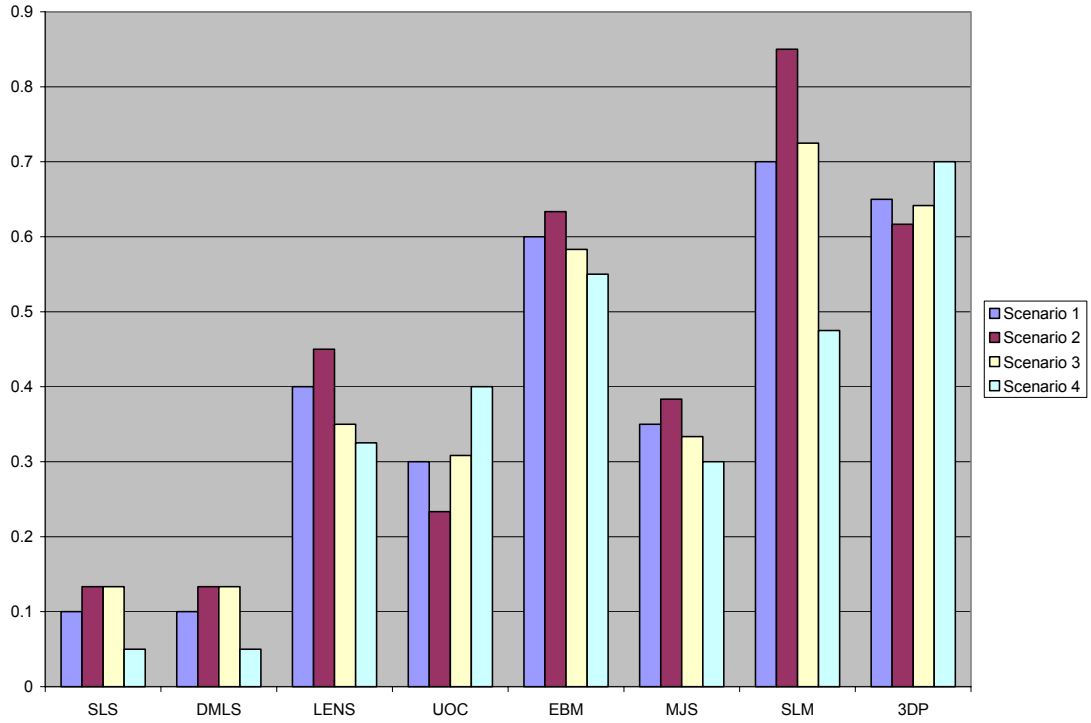

Figure B.1 – Evaluated Merit Functions for the SLM Datum

From the merit function values, a ranking for each of the alternatives is completed. The results of the ranking for the SLM datum are shown in Table B.4. The results shown in Figure B.2 and Table B.4 indicate that SLM is the most likely to succeed technology for all scenarios when it is set as the datum.

Table B.4 – Ranking of Concepts for the SLM Datum

	Scenario Number			
Alternative	One	Two	Three	Four
SLS	7	7	7	7
DMLS	7	7	7	7
LENS	4	4	4	5
UOC	6	6	6	4
EBM	3	2	3	2
MJS	5	5	5	6
SLM	1	1	1	3
3DP	2	3	2	1

This step is repeated in a similar manner using multiple datums for all weighting scenarios in order to dispel any prejudice. Once the comparison process is repeated for multiple datums, the average overall merit function for each of the alternatives for all weighting scenarios is calculated. These results are shown in Table B.5. Rank ordering these values results in a list of most likely to succeed technologies, as presented in Table B.6.

Table B.5 – Overall Merit Function for Preliminary Selection

	Scenario Number			
Alternative	One	Two	Three	Four
SLS	0.301	0.351	0.343	0.227
DMLS	0.320	0.376	0.354	0.237
LENS	0.400	0.457	0.367	0.315
UOC	0.351	0.227	0.345	0.536
EBM	0.587	0.616	0.559	0.543
MJS	0.491	0.516	0.472	0.454
SLM	0.756	0.878	0.775	0.572
3DP	0.817	0.797	0.812	0.846
	Overall Merit Function			

Table B.6 – Overall Rankings for the Most Likely to Succeed Concepts

	Scenario Number			
Alternative	One	Two	Three	Four
SLS	8	7	8	8
DMLS	7	6	6	7
LENS	5	5	5	6
UOC	6	8	7	4
EBM	3	3	3	3
MJS	4	4	4	5
SLM	2	1	2	2
3DP	1	2	1	1
	Rank			

From the rankings it is observed that Selective Laser Melting (SLM) and Three-Dimensional Printing (3DP) are the most likely to succeed technologies. These technologies were consistently preferred because of their ability to create complex geometries with multiple materials and with good material properties. 3DP was often

preferred over SLM because of its high deposition rate and its ability to be economically scaled.

Technologies such as SLS and DMLS were often scored low because of their poor selection of materials, poor material properties (due to the necessary infiltration), and poor surface finish. UOC was often scored low despite of its high deposition rate, because of its ability to only process aluminum, its anisotropic material properties, and inability to create complex geometry.

The most important learning point taken away from this preliminary selection exercise is the uncovering of the limitations of existing metal AM technologies. Materials of designed mesostructure are a unique class of geometry that require a manufacturing process that can selectively deposit a wide variety of materials with good surface finish, material properties, resolution, and shape complexity. From this investigation of metal AM technologies it is observed that no current technology is capable of satisfying all of the requirements listed in Section 2.1. Even those technologies identified as most likely to succeed are not completely sufficient for the creation of materials of designed mesostructure.

APPENDIX C

PRELIMINARY SELECTION COMPARISON FOR VARIOUS DATUMS

In Section 5.1, the preliminary selection DSP technique is used to those concepts which will most likely satisfy the requirements defined at the beginning of the design task. The Preliminary Selection DSP technique involves a series of comparisons between each working structure alternative and a chosen datum in the context of the different selection criteria. The concepts are evaluated against the datum as inferior (-1), equal (0), or superior (+1) (based upon the criteria preference listed in Table 5.2). The scores are then summed and normalized within each category, utilizing the relative importance for each criterion presented in Table C.1 (Table 5.3).

Table C.1 – Scenarios for the Relative Importance of Specific Criteria

		Scenario	
Generalized Criteria	***Specific Criteria***	**A**	**B**
Economics	TECHCOST	0.5	0.4
	DEPRATE	0.5	0.6
Performance	MINFEAT	0.3	0.35
	COMPGEO	0.3	0.5
	SURFIN	0.3	0.15
Materials	GREENLOD	0.5	0.35
	MATSEL	0.5	0.65

This systematic comparison procedure is repeated for multiple datums in order to dispel any prejudice. In this appendix, a listing of the results from the full gamut of comparisons is presented. For each datum, a comparison matrix and the resulting rankings of each concept for the individual scenarios is presented.

Multiple weighting schemes are employed in the Preliminary Selection DSP to address the interaction of the generalized selection criteria and their relative importance. The weighting schemas for each scenario are presented in Table C.2 (Table 5.5).

Table C.2 – Scenarios for the Relative Importance of Generalized Criteria

	Scenario Number				
Generalized Criteria	**1**	**2**	**3**	**4**	**5**
Economics	0.33	0.2	0.2	0.6	0.2
Performance	0.33	0.2	0.6	0.2	0.4
Materials	0.33	0.6	0.2	0.2	0.4

The first scenario represents an equal preference weighting for the three generalized criteria. Scenarios 2-4 represent a large weighting placed on each individual generalized criteria. Finally, Scenario 5 represents an accurate portrayal of the preferences expressed in the design task. Specifically, it is of utmost importance to design a process that is able to fabricate cellular green parts; the economics of the process are slightly less important.

Normalized scores for each concept are computed by multiplying the normalized score of each concept's attribute category (Tables C.3, C.5, C.7, C.9) by the weighting values (Table C.2). The summed score serves as the merit function for each generalized concept. The results for all scenarios from the LS datum are graphically shown in Figures C.1 – C.5.

Each alternative is ranked from the merit function values for each scenario. Ranking results for the LS datum are shown in Tables C.4, C.6, C.8, and C.10.

IJP-W Datum

Table C.3– Comparison Matrix for IJP-W Datum

	LS	SL	HSS	MSL	FDC	LOM	EP	3DP	S-3DP	UV-3DP	IJP-A	IJP-W	IJP-UV
ECONOMICS													
TECHCOST	-1	-1	-1	-1	0	-1	0	0	0	-1	0	0	-1
DEPRATE	-1	-1	0	-1	-1	1	0	-1	-1	-1	-1	0	0
Score A	-1.00	-1.00	-0.50	-1.00	-0.50	0.00	0.00	-0.50	-0.50	-1.00	-0.50	0.00	-0.50
Score B	-1.00	-1.00	-0.40	-1.00	-0.60	0.20	0.00	-0.60	-0.60	-1.00	-0.60	0.00	-0.40
Normalized Score A	0.00	0.00	0.50	0.00	0.50	1.00	1.00	0.50	0.50	0.00	0.50	1.00	0.50
Normalized Score B	0.00	0.00	0.50	0.00	0.33	1.00	0.83	0.33	0.33	0.00	0.33	0.83	0.50
PERFORMANCE													
MINFEAT	-1	-1	0	1	-1	-1	-1	0	0	0	1	0	0
COMPGEO	-1	-1	-1	-1	0	-1	0	-1	-1	-1	-1	0	0
SURFIN	-1	0	-1	0	-1	-1	-1	-1	0	0	1	0	0
Score A	-0.99	-0.66	-0.66	0.00	-0.66	-0.99	-0.66	-0.66	-0.33	-0.33	0.33	0.00	0.00
Score B	-1.00	-0.85	-0.65	-0.15	-0.50	-1.00	-0.50	-0.65	-0.50	-0.50	0.00	0.00	0.00
Normalized Score A	0.00	0.25	0.25	0.75	0.25	0.00	0.25	0.25	0.50	0.50	1.00	0.75	0.75
Normalized Score B	0.00	0.15	0.35	0.85	0.50	0.00	0.50	0.35	0.50	0.50	1.00	1.00	1.00
MATERIALS													
GREENLOD	1	1	1	0	1	1	1	1	1	1	1	0	0
MATSEL	0	-1	0	-1	0	0	-1	0	0	-1	0	0	-1
Score A	0.50	0.00	0.50	-0.50	0.50	0.50	0.00	0.50	0.50	0.00	0.50	0.00	-0.50
Score B	0.35	-0.30	0.35	-0.65	0.35	0.35	-0.30	0.35	0.35	-0.30	0.35	0.00	-0.65
Normalized Score A	1.00	0.50	1.00	0.00	1.00	1.00	0.50	1.00	1.00	0.50	1.00	0.50	0.00
Normalized Score B	1.00	0.35	1.00	0.00	1.00	1.00	0.35	1.00	1.00	0.35	1.00	0.65	0.00
OVERALL SCORE - Scenario 1													
Sum of Scores, A	0.33	0.25	0.58	0.25	0.58	0.67	0.58	0.58	0.67	0.33	0.83	0.75	0.42
Rank, A	10	12	5	12	5	3	5	5	3	10	1	2	9
Sum of Scores, B	0.33	0.17	0.62	0.28	0.61	0.67	0.56	0.56	0.61	0.28	0.78	0.83	0.50
Rank, B	10	13	4	11	5	3	7	8	5	11	2	1	9

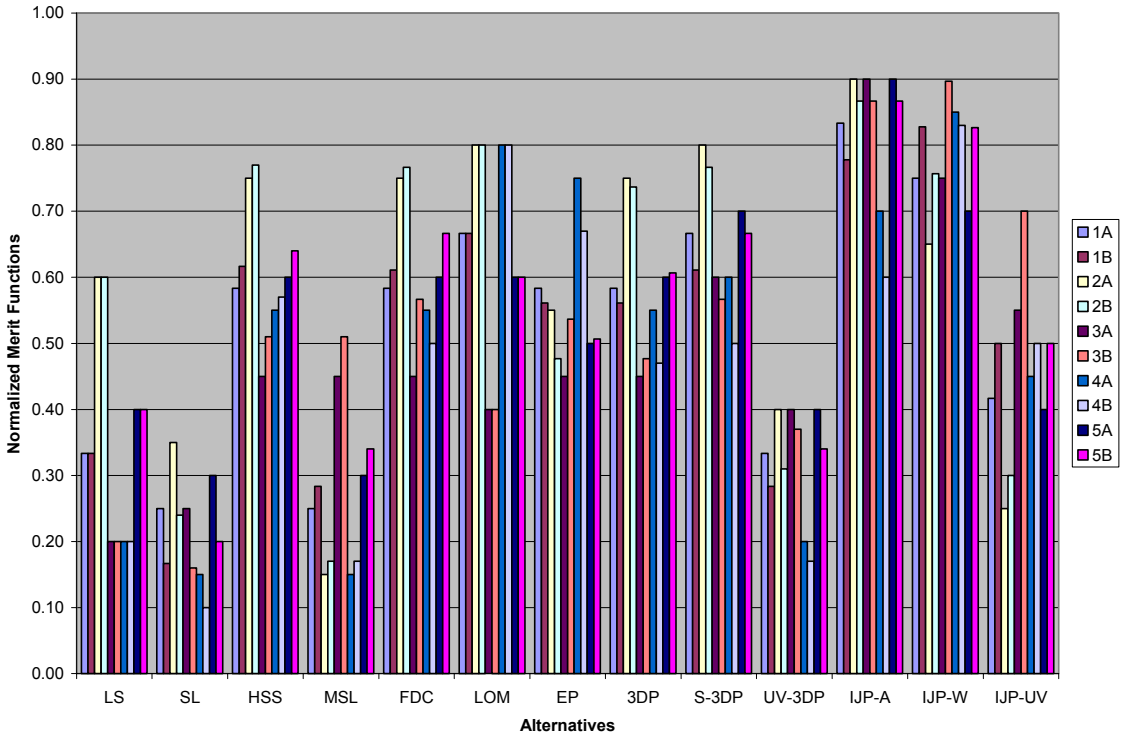

Figure C.1– Graphical Representation of Evaluated Merit Functions for IJP-W Datum

Table C.4 – Ranking of Evaluated Merit Functions for each Scenario of the IJP-W Datum

	Scenario Number									
Alternative	1A	1B	2A	2B	3A	3B	4A	4B	5A	5B
LS	10	10	8	8	13	12	10	10	9	10
SL	12	13	11	12	12	13	13	13	13	13
HSS	5	4	4	3	5	7	6	5	5	5
MSL	12	11	13	13	5	7	12	11	12	11
FDC	5	5	4	4	5	4	6	6	5	3
LOM	3	3	2	2	10	10	2	2	4	7
EP	5	7	9	9	5	6	3	3	8	8
3DP	5	8	4	7	5	9	6	9	5	6
S-3DP	3	5	3	4	3	4	5	6	2	3
UV-3DP	11	11	10	10	11	11	11	12	11	12
IJP-A	1	2	1	1	1	2	4	4	1	1
IJP-W	2	1	7	6	2	1	1	1	2	2
IJP-UV	9	9	12	11	4	3	9	6	9	9

3DP Datum

Table C.5– Comparison Matrix for 3DP Datum

	LS	SL	HSS	MSL	FDC	LOM	EP	3DP	S-3DP	UV-3DP	IJP-A	IJP-W	IJP-UV
ECONOMICS													
TECHCOST	-1	-1	-1	-1	0	-1	0	0	0	-1	0	0	-1
DEPRATE	-1	-1	1	0	-1	1	1	0	-1	-1	-1	1	1
Score A	-1.00	-1.00	0.00	-0.50	-0.50	0.00	0.50	0.00	-0.50	-1.00	-0.50	0.50	0.00
Score B	-1.00	-1.00	0.20	-0.40	-0.60	0.20	0.60	0.00	-0.60	-1.00	-0.60	0.60	0.20
Normalized Score A	0.00	0.00	0.67	0.33	0.33	0.67	1.00	0.67	0.33	0.00	0.33	1.00	0.67
Normalized Score B	0.00	0.00	0.75	0.38	0.25	0.75	1.00	0.63	0.25	0.00	0.25	1.00	0.75
PERFORMANCE													
MINFEAT	-1	-1	0	1	-1	-1	-1	0	0	0	1	0	0
COMPGEO	0	-1	0	-1	1	-1	1	0	-1	0	-1	1	1
SURFIN	0	1	0	1	-1	-1	0	0	1	0	1	1	1
Score A	-0.33	-0.33	0.00	0.33	-0.33	-0.99	0.00	0.00	0.00	0.00	0.33	0.66	0.66
Score B	-0.35	-0.70	0.00	0.00	0.00	-1.00	0.15	0.00	-0.35	0.00	0.00	0.65	0.65
Normalized Score A	0.40	0.40	0.60	0.80	0.40	0.00	0.60	0.60	0.60	0.60	0.80	1.00	1.00
Normalized Score B	0.39	0.18	0.61	0.61	0.61	0.00	0.70	0.61	0.39	0.61	0.61	1.00	1.00
MATERIALS													
GREENLOD	0	0	0	-1	-1	1	0	0	1	0	1	-1	-1
MATSEL	0	-1	0	-1	0	0	-1	0	0	-1	0	0	-1
Score A	0.00	-0.50	0.00	-1.00	-0.50	0.50	-0.50	0.00	0.50	-0.50	0.50	-0.50	-1.00
Score B	0.00	-0.65	0.00	-1.00	-0.35	0.35	-0.65	0.00	0.35	-0.65	0.35	-0.35	-1.00
Normalized Score A	0.67	0.33	0.67	0.00	0.33	1.00	0.33	0.67	1.00	0.33	1.00	0.33	0.00
Normalized Score B	0.74	0.26	0.74	0.00	0.48	1.00	0.26	0.74	1.00	0.26	1.00	0.48	0.00
OVERALL SCORE - Scenario 1													
Sum of Scores, A	0.36	0.24	0.64	0.38	0.36	0.56	0.64	0.64	0.64	0.31	0.71	0.78	0.56
Rank, A	10	13	5	9	10	7	3	5	3	12	2	1	7
Sum of Scores, B	0.38	0.15	0.70	0.33	0.45	0.58	0.65	0.66	0.55	0.29	0.62	0.83	0.58
Rank, B	10	13	2	11	9	6	4	3	8	12	5	1	6

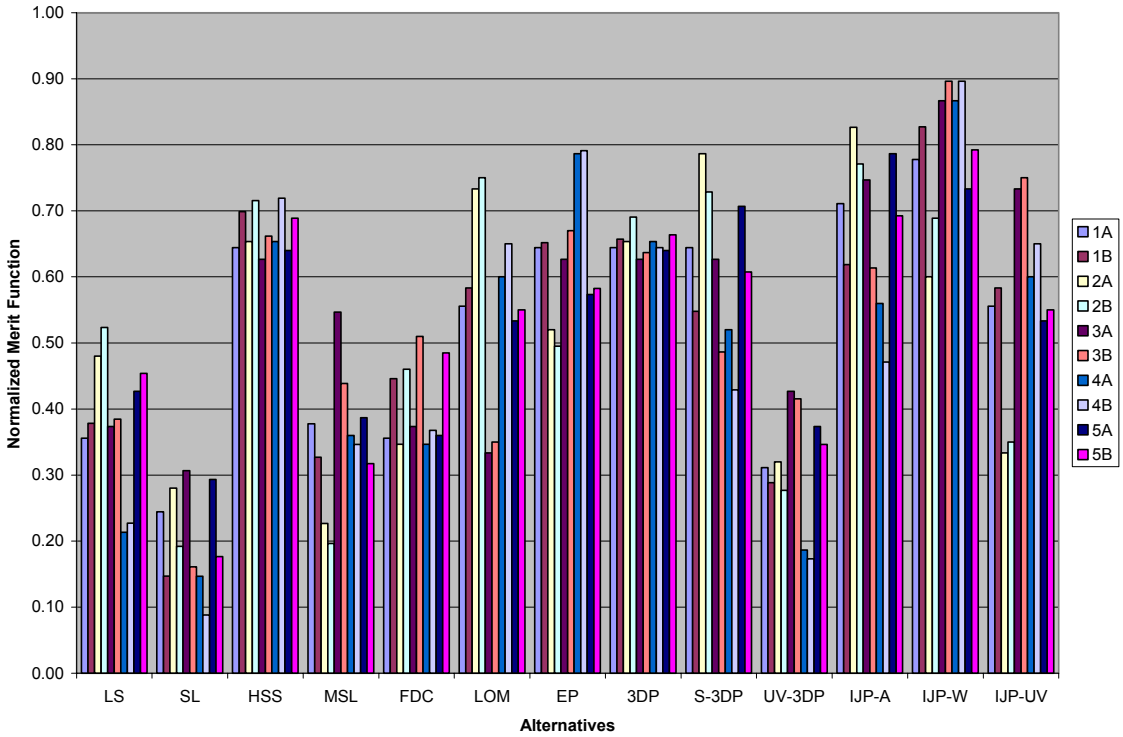

Figure C.2– Graphical Representation of Evaluated Merit Functions for 3DP Datum

Table C.6 – Ranking of Evaluated Merit Functions for each Scenario of the 3DP Datum

	Scenario Number									
Alternative	1A	1B	2A	2B	3A	3B	4A	4B	5A	5B
LS	10	10	8	7	10	11	11	11	9	10
SL	13	13	12	13	13	13	13	13	13	13
HSS	5	2	4	4	6	4	3	3	4	3
MSL	9	11	13	12	8	9	9	10	10	12
FDC	10	9	9	9	10	7	10	9	12	9
LOM	7	6	3	2	12	12	5	4	7	7
EP	3	4	7	8	4	3	2	2	6	6
3DP	5	3	4	5	6	5	3	6	4	4
S-3DP	3	8	2	3	4	8	8	8	3	5
UV-3DP	12	12	11	11	9	10	12	12	11	11
IJP-A	2	5	1	1	2	6	7	7	1	2
IJP-W	1	1	6	6	1	1	1	1	2	1
IJP-UV	7	6	10	10	3	2	5	4	7	7

HSS Datum

Table C.7– Comparison Matrix for HSS Datum

	LS	SL	HSS	MSL	FDC	LOM	EP	3DP	S-3DP	UV-3DP	IJP-A	IJP-W	IJP-UV
ECONOMICS													
TECHCOST	-1	-1	0	0	1	-1	1	1	1	0	1	1	0
DEPRATE	-1	-1	0	-1	-1	1	0	-1	-1	-1	-1	0	0
Score A	-1.00	-1.00	0.00	-0.50	0.00	0.00	0.50	0.00	0.00	-0.50	0.00	0.50	0.00
Score B	-1.00	-1.00	0.00	-0.60	-0.20	0.20	0.40	-0.20	-0.20	-0.60	-0.20	0.40	0.00
Normalized Score A	0.00	0.00	0.67	0.33	0.67	0.67	1.00	0.67	0.67	0.33	0.67	1.00	0.67
Normalized Score B	0.00	0.00	0.71	0.29	0.57	0.86	1.00	0.57	0.57	0.29	0.57	1.00	0.71
PERFORMANCE													
MINFEAT	-1	-1	0	1	-1	-1	-1	0	0	0	1	0	0
COMPGEO	0	-1	0	-1	1	-1	1	0	-1	0	-1	1	1
SURFIN	0	1	0	1	-1	-1	0	0	1	0	1	1	1
Score A	-0.33	-0.33	0.00	0.33	-0.33	-0.99	0.00	0.00	0.00	0.00	0.33	0.66	0.66
Score B	-0.35	-0.70	0.00	0.00	0.00	-1.00	0.15	0.00	-0.35	0.00	0.00	0.65	0.65
Normalized Score A	0.40	0.40	0.60	0.80	0.40	0.00	0.60	0.60	0.60	0.60	0.80	1.00	1.00
Normalized Score B	0.39	0.18	0.61	0.61	0.61	0.00	0.70	0.61	0.39	0.61	0.61	1.00	1.00
MATERIALS													
GREENLOD	0	0	0	-1	-1	1	0	0	1	0	1	-1	-1
MATSEL	0	-1	0	-1	0	0	-1	0	0	-1	0	0	-1
Score A	0.00	-0.50	0.00	-1.00	-0.50	0.50	-0.50	0.00	0.50	-0.50	0.50	-0.50	-1.00
Score B	0.00	-0.65	0.00	-1.00	-0.35	0.35	-0.65	0.00	0.35	-0.65	0.35	-0.35	-1.00
Normalized Score A	0.67	0.33	0.67	0.00	0.33	1.00	0.33	0.67	1.00	0.33	1.00	0.33	0.00
Normalized Score B	0.74	0.26	0.74	0.00	0.48	1.00	0.26	0.74	1.00	0.26	1.00	0.48	0.00
OVERALL SCORE - Scenario 1													
Sum of Scores, A	0.36	0.24	0.64	0.38	0.47	0.56	0.64	0.64	0.76	0.42	0.82	0.78	0.56
Rank, A	12	13	5	11	9	7	4	5	3	10	1	2	7
Sum of Scores, B	0.38	0.15	0.69	0.30	0.55	0.62	0.65	0.64	0.66	0.38	0.73	0.83	0.57
Rank, B	11	13	3	12	9	7	5	6	4	10	2	1	8

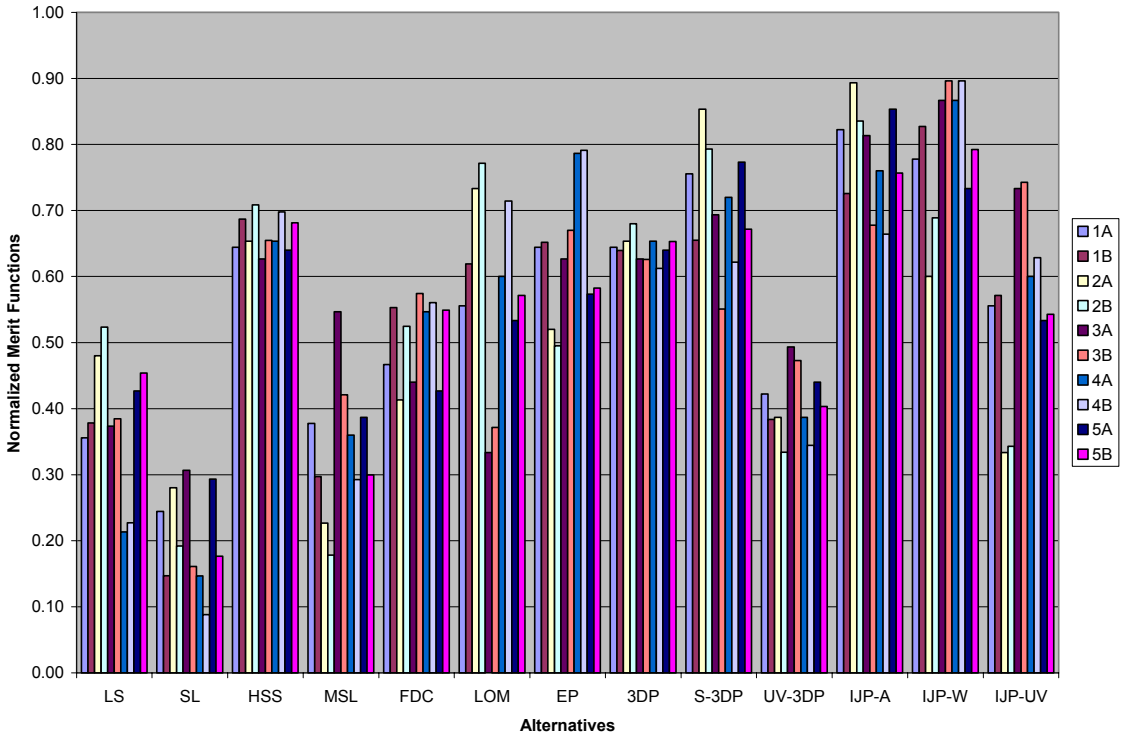

Figure C.3– Graphical Representation of Evaluated Merit Functions for HSS Datum

Table C.8 – Ranking of Evaluated Merit Functions for each Scenario of the HSS Datum

	Scenario Number									
Alternative	1A	1B	2A	2B	3A	3B	4A	4B	5A	5B
LS	12	11	8	8	11	11	12	12	10	10
SL	13	13	12	12	13	13	13	13	13	13
HSS	5	3	4	4	6	5	5	4	4	3
MSL	11	12	13	13	8	10	11	11	12	12
FDC	9	9	9	7	10	7	9	9	10	8
LOM	7	7	3	3	12	12	7	3	7	7
EP	4	5	7	9	5	4	2	2	6	6
3DP	5	6	4	6	6	6	5	8	4	5
S-3DP	3	4	2	2	4	8	4	7	2	4
UV-3DP	10	10	10	11	9	9	10	10	9	11
IJP-A	1	2	1	1	2	3	3	5	1	2
IJP-W	2	1	6	5	1	1	1	1	3	1
IJP-UV	7	8	11	10	3	2	7	6	7	9

S-3DP Datum

Table C.9– Comparison Matrix for S-3DP Datum

	LS	**SL**	**HSS**	**MSL**	**FDC**	**LOM**	**EP**	**3DP**	**S-3DP**	**UV-3DP**	**IJP-A**	**IJP-W**	**IJP-UV**
ECONOMICS													
TECHCOST	-1	-1	-1	-1	0	-1	0	0	0	-1	0	0	-1
DEPRATE	-1	-1	1	1	-1	1	1	1	0	1	-1	1	1
Score A	-1.00	-1.00	0.00	0.00	-0.50	0.00	0.50	0.50	0.00	0.00	-0.50	0.50	0.00
Score B	-1.00	-1.00	0.20	0.20	-0.60	0.20	0.60	0.60	0.00	0.20	-0.60	0.60	0.20
Normalized Score A	0.00	0.00	0.67	0.67	0.33	0.67	1.00	1.00	0.67	0.67	0.33	1.00	0.67
Normalized Score B	0.00	0.00	0.75	0.75	0.25	0.75	1.00	1.00	0.63	0.75	0.25	1.00	0.75
PERFORMANCE													
MINFEAT	-1	-1	0	1	-1	-1	-1	0	0	0	1	0	0
COMPGEO	1	0	1	0	1	-1	1	1	0	1	1	1	1
SURFIN	1	0	-1	1	-1	-1	-1	-1	0	-1	1	-1	-1
Score A	0.33	-0.33	0.00	0.66	-0.33	-0.99	-0.33	0.00	0.00	0.00	0.99	0.00	0.00
Score B	0.30	-0.35	0.35	0.50	0.00	-1.00	0.00	0.35	0.00	0.35	1.00	0.35	0.35
Normalized Score A	0.67	0.33	0.50	0.83	0.33	0.00	0.33	0.50	0.50	0.50	1.00	0.50	0.50
Normalized Score B	0.65	0.33	0.68	0.75	0.50	0.00	0.50	0.68	0.50	0.68	1.00	0.68	0.68
MATERIALS													
GREENLOD	-1	-1	-1	-1	-1	-1	-1	-1	0	-1	0	-1	-1
MATSEL	0	-1	0	-1	0	0	0	0	0	-1	0	0	-1
Score A	-0.50	-1.00	-0.50	-1.00	-0.50	-0.50	-0.50	-0.50	0.00	-1.00	0.00	-0.50	-1.00
Score B	-0.35	-1.00	-0.35	-1.00	-0.35	-0.35	-0.35	-0.35	0.00	-1.00	0.00	-0.35	-1.00
Normalized Score A	0.50	0.00	0.50	0.00	0.50	0.50	0.50	0.50	1.00	0.00	1.00	0.50	0.00
Normalized Score B	0.65	0.00	0.65	0.00	0.65	0.65	0.65	0.65	1.00	0.00	1.00	0.65	0.00
OVERALL SCORE - Scenario 1													
Sum of Scores, A	0.39	0.11	0.56	0.50	0.39	0.39	0.61	0.67	0.72	0.39	0.78	0.67	0.39
Rank, A	8	13	6	7	9	9	5	3	2	9	1	3	9
Sum of Scores, B	0.43	0.11	0.69	0.50	0.47	0.47	0.72	0.78	0.71	0.48	0.75	0.78	0.48
Rank, B	12	13	6	7	10	10	4	1	5	8	3	1	8

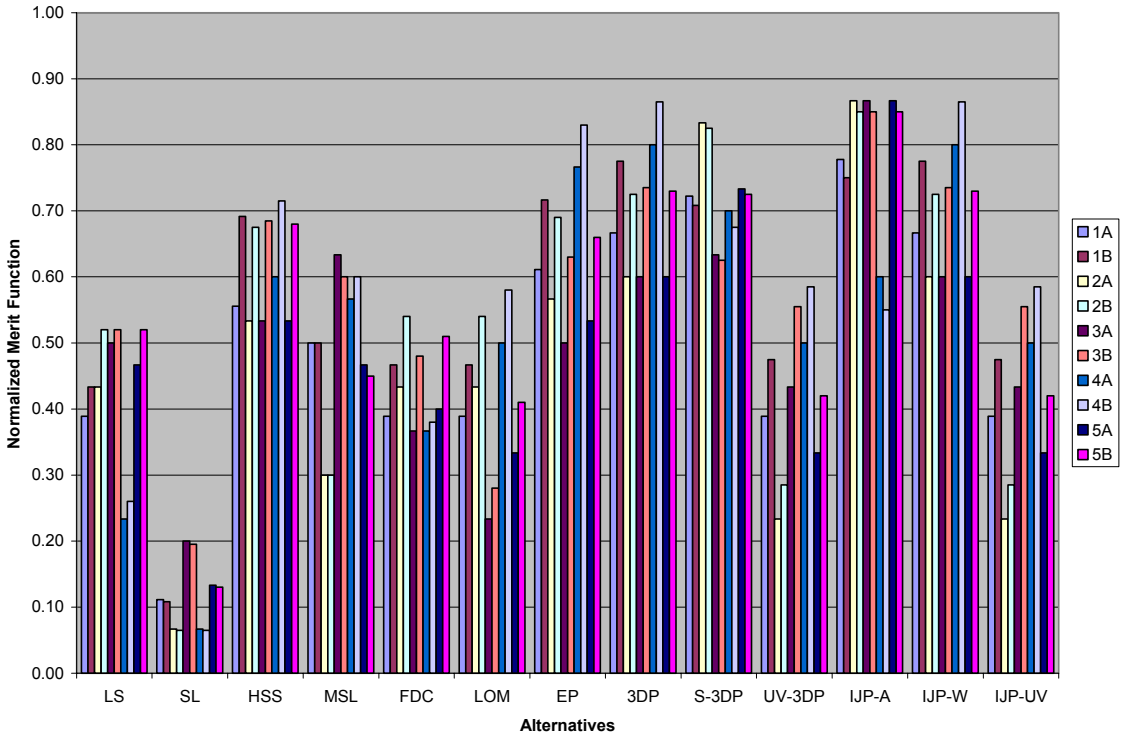

Figure C.4– Graphical Representation of Evaluated Merit Functions for S-3DP

Table C.10 – Ranking of Evaluated Merit Functions for each Scenario of the S-3DP Datum

	Scenario Number									
Alternative	1A	1B	2A	2B	3A	3B	4A	4B	5A	5B
LS	8	12	7	9	7	10	12	12	7	7
SL	13	13	13	13	13	13	13	13	13	13
HSS	6	6	6	6	6	4	6	4	5	5
MSL	7	7	10	10	2	7	7	6	8	9
FDC	9	10	7	7	11	11	11	11	9	8
LOM	9	10	7	7	12	12	8	9	10	12
EP	5	4	5	5	7	5	3	3	5	6
3DP	3	1	3	3	4	2	1	1	3	2
S-3DP	2	5	2	2	2	6	4	5	2	4
UV-3DP	9	8	11	11	9	8	8	7	10	10
IJP-A	1	3	1	1	1	1	5	10	1	1
IJP-W	3	1	3	3	4	2	1	1	3	2
IJP-UV	9	8	11	11	9	8	8	7	10	10

APPENDIX D

DERIVATION OF AREA OF ELLIPITCAL CROSS-SECTION OVERLAP FOR ANGLED TRUSSES

In this appendix an equation is derived in for the determination of the area of the overlap that exists between stacked elliptical cross-sectioned layers when fabricating thin, angled trusses by a layered fabrication process (as illustrated in Figure D.1, and discussed in Section 8.2).

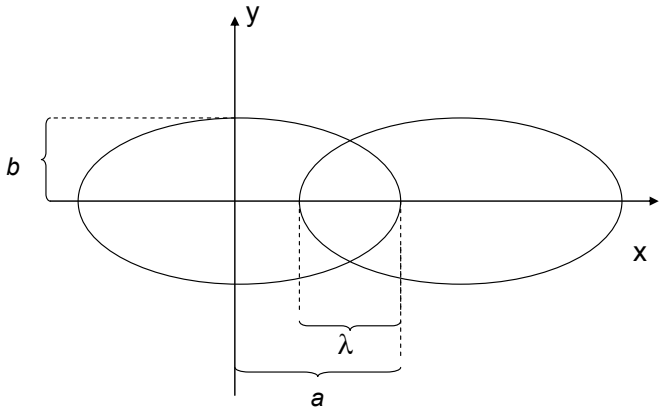

Figure D.1 – Illustration of Overlapping Ellipses

The equation for an ellipse is given as:

$$\frac{x^2}{a^2}+\frac{y^2}{b^2}=1 \qquad [D.1]$$

where *a* is major radius and *b* is minor radius of ellipse as seen in Figure D.1. Restating Equation D.1 as a function of *y*:

$$y=\sqrt{b^2\left(1-\frac{x^2}{a^2}\right)} \qquad [D.2]$$

This simplifies to:

$$y = \frac{b}{a}\sqrt{a^2 - x^2} \qquad [D.3]$$

The point at which the two ellipses intersect occurs at

$$x = a - \lambda/2 \qquad [D.4]$$

and from Equation D.3, at

$$y = \frac{b}{a}\sqrt{a\lambda - \frac{\lambda^2}{4}} \qquad [D.5]$$

The area underneath one of the four curves which represent the area of ellipse overlap is obtained by integrating Equation D.3 from the points of ellipse intersection:

$$Area = \int_{a-\lambda/2}^{a} \frac{b}{a}\left(\sqrt{a^2 - x^2}\right)dx \qquad [D.6]$$

This is further simplified:

$$Area = b\int_{a-\lambda/2}^{a} \sqrt{1 - \left(\frac{x}{a}\right)^2}\,dx \qquad [D.7]$$

Substitution is required to solve this integral. Specifically, substitute:

$$\sin u = \frac{x}{a} \qquad [D.8]$$

Since $x = a\sin u$,

$$dx = a\cos u du u \qquad [D.9]$$

Substituting Equations D.8 and D.9 into D.7, the area underneath one of the four intersecting curves is expressed as:

$$Area = b\int \sqrt{1-\sin^2 u}\,(a\cos u)\,du \qquad [D.10]$$

$\cos^2 u = 1-\sin^2 u$ is substituted into Equation D.10 to simplify, as shown in Equation D.11.

$$Area = ab\int \cos^2 u du \qquad [D.11]$$

Since $\cos^2 u = \frac{1}{2}(1+\cos 2u)$, Equation D.11 is rewritten as:

$$Area = \frac{1}{2}ab\int (1+\cos 2u)\,du \qquad [D.12]$$

Integrating Equation D.12 results in:

$$Area = \frac{1}{2}ab\left(u+\frac{1}{2}\sin 2u + C\right) \qquad [D.13]$$

Substituting, $\cos u = \sqrt{1-\sin^2 u}$ into Equation D.13, it is simplified to:

$$Area = \frac{1}{2}ab\left[u+\sin u\left(\sqrt{1-\sin^2 u}\right)+C\right] \qquad [D.14]$$

Reverting the earlier substitution of Equation D.8, $u = \sin^{-1}\left(\frac{x}{a}\right)$ is substituted into Equation D.14.

$$Area = \frac{1}{2}ab\left[\sin^{-1}\left(\frac{x}{a}\right)+\sin\left(\sin^{-1}\left(\frac{x}{a}\right)\right)\sqrt{1-\sin^2\left(\sin^{-1}\left(\frac{x}{a}\right)\right)}\right]\Bigg|_{a-\lambda/2}^{a} \qquad [D.15]$$

Equation D.15 represents the area underneath one of the four curves which define the area of overlap. Thus, the total area of overlap is defined by Equation D.16.:

$$Area = 2ab\left[\sin^{-1}\left(\frac{x}{a}\right)+\left(\frac{x}{a}\right)\left(\sqrt{1-\left(\frac{x}{a}\right)^2}\right)\right]\Bigg|_{a-\lambda/2}^{a} \qquad [D.16]$$

APPENDIX E

BUILD TIME AND COST MODEL MATLAB CODE

This Matlab code is developed in order to quickly evaluate the build time and cost models that are presented in Section 8.3. The definition of the variables is presented Tables 8.2 – 8.7.

```
%--- BUILD AND COST MODEL FOR 3DP ----%


%part specs (mm)
xp = 25.4;
yp = 25.4;
zp = 25.4;

%material specs
dens = 5.58; %g/cm3
Pbinder = 0.04; %2wt% binder

%machine specs (mm & mm/s)
wb = 254;
hb = 200;
db = 200;
wf = 190;
Nheads = 1;
Nnozzles = 128; %newer models have 304
dn = 0.07;
vfast = 450;
vslow = 300;
vpist = 1;
tprime = 20;
N3dp = 1;

%build parameters (mm & mm/s)
LT = 0.089;
xspace = 10;
yspace = 10;
%xspace = 224; %setting for 1 part
%yspace = 174; %setting for 1 part
vrecoat = 430;

%Pre/Post-processing times (hours)
tdry = 0.5;
tsinter = 25;
tclean = 5/60;
tsetup = 5/60;
```

```
%fixed costs
C3dp = 200000;
Cmaint = 4000;
Cfurnace = 5000;
Cspraydry = 12000;
Creduction = 8;
Coperation = 3; %$/hr

%variable costs
Coxide = 0.03; %$/g
Cbinder = 0.002;%$/g
Csolvent = 0;%$/cm3

%# of parts per part layer
%Np = wb*hb / ((xp + xspace) + (yp + yspace))
Npx = wb / (xp + xspace);
Npy = hb / (yp + yspace);
Np = Npx * Npy
%# of part layers
Npl = db / (zp + 25*LT)

Nppy = 150000;% Parts produced per year

%---TIME MODEL---
% time per build layer (seconds)
Nbands = xp / (Nheads*Nnozzles*dn);
tl = (2*yp / vfast) * Np * Nbands + (wb / vslow) %s
Nl = zp / LT;
%time to recoat
trecoat = (LT / vpist) + ((wb + wf)/vrecoat); %s
%time to prime cartridge
tprimetot = tprime * (Nl/20); %s

%time per part layer
tpl = (tl*Nl + trecoat*Nl + tprimetot)/3600 %hr

%total build time
tpltot = tpl*Npl %total operating time (hr)

%total batch time
ttot = (tpl*Npl) + tsetup + tclean*Npl*Np + tdry + tsinter %hrs


%---COST MODEL---
Cfixed = N3dp*(C3dp + Cmaint) + Cfurnace + Cspraydry
Cmaterial = (xp*yp*zp/10^3)*dens*(Coxide + (Pbinder*Cbinder)) + (xp*yp*zp/10^3)*Csolvent
Cbatch = (Cmaterial*Npl*Np) + (Coperation*tpltot) + Creduction
Ctot = (Cfixed) + (Cbatch*(Nppy/(Np*Npl)))
Cpart = Ctot / Nppy
```

REFERENCES

3D Systems, 2004, "Laser Sintering Materials - Datasheets", http://www.3dsystems.com/products/solidimaging/lasersintering/datasheets.asp.

3D Systems, 2007, "3D Modeling & Desktop Prototyping with V-Flash by 3D Systems", http://www.modelin3d.com/.

Abe, F., E. Costa Santos, Y. Kitamura and M. Shiomi, 2003, "Influence of Forming Conditions on the Titanium Model in Rapid Prototyping with the Selective Laser Melting Process," *Proceedings of the I MECH E Journal of Mechanical Engineering Science,* Vol. 217, No. 1, pp. 119-126.

Abe, F., K. Osakada, M. Shiomi, K. Uematsu and M. Matsumoto, 2001, "The Manufacturing of Hard Tools from Metallic Powders by Selective Laser Melting," *Journal of Materials Processing Technology,* Vol. 111, pp. 210-213.

Agarwala, M., D. Bourell, J. Beaman, H. Marcus and J. Barlow, 1995, "Direct Selective Laser Sintering of Metals," *Rapid Prototyping Journal,* Vol. 1, No. 1, pp. 26-36.

Agarwala, M. K., V. R. Jamalabad, N. A. Langrana, A. Safari, P. J. Whalen and S. C. Danforth, 1996, "Structural Quality of Parts Processed by Fused Deposition," *Rapid Prototyping Journal,* Vol. 2, No. 4, pp. 4-19.

Ainsley, C., N. Reis and B. Derby, 2002, "Freeform Fabrication by Controlled Droplet Deposition of Powder Filled Melts," *Journal of Materials Science,* Vol. 37, pp. 3155-3161.

Aljdelsztajn, L., B. Jodoin, G. E. Kim and J. M. Schoenung, 2005, "Cold Spray Deposition of Nanocrystalline Aluminum Alloys," *Metallurgial and Materials Transactions,* Vol. 36A, No. 3, pp. 657-666.

Arcam, 2004, "ARCAM AB: CAD to Metal", http://www.arcam.com/technology/index.asp.

Ashby, M. F., A. G. Evans, N. A. Fleck, L. J. Gibson, J. W. Hutchinson and H. N. G. Wadley, 2000, *Metal Foams: A Design Guide*, Butterworth-Heinemann, Woburn, MA.

Badrinarayan, B. and J. W. Barlow, 1991, "Manufacture of Injection Molds using SLS," *Solid Freeform Fabrication Symposium*, Austin, TX, pp. 245-250.

Bandyopadhyay, A., R. Atisivan and S. Bose, 1999, "Novel Ceramics and Metal-Ceramic Composites via Fused Deposition Process," *Solid Freeform Fabrication Symposium*, Austin, TX., pp. 361-368.

Banhart, J., 2000, "Manufacturing Routes for Metallic Foams," *The Member Journal of the Minerals, Metals & Materials Society,* Vol. 52, No. 12, pp. 22-27.

Banhart, J. and D. Weaire, 2002, "On the Road Again: Metal Foams Find Favor," *Physics Today,* July, pp. 37-42.

Beaman, J. J., J. W. Barlow, D. L. Bourell, R. H. Crawford, H. L. Marcus and K. P. McAlea, 1997, *Solid Freeform Fabrication: A New Direction in Manufacturing* Kluwer Academic Publishers, Boston, Mass.

Bender, B. A., R. J. Rayne and T. L. Jessen, 2001, "Laminated Object Manufacturing of Functional Ceramics," *Ceramic Engineering and Science Proceedings*, pp. 127-134.

Bertsch, A., S. Jiguet and P. Renaud, 2004, "Microfabrication of Ceramic Components by Microstereolithography," *Journal of Micromechanics and Microengineering,* Vol. 14, pp. 197-203.

Blazdell, P. F., J. R. G. Evans, M. J. Edirisinghe, P. Shaw and M. J. Binstead, 1995, "The Computer Aided Manufacture of Ceramics Using Multilayer Jet Printing," *Journal of Materials Science Letters,* 14, pp. 1562-1565.

Bourell, D., H. Marcus, J. Barlow, J. Beaman and C. R. Deckard, 1995, "Multiple Material Systems for Selective Beam Sintering," 5,382,308, Board of Regeants, The University of Texas System, United States.

Brady, G. A., T. M. Chu and J. W. Halloran, 1996, "Curing Behavior of Ceramic Resin for Stereolithography," *Solid Freeform Fabrication Symposium*, Austin, TX., pp. 403-405.

Brady, G. A. and J. W. Halloran, 1998, "Differential Photo-Calorimetry of Photopolymerizable Ceramic Suspensions," *Journal of Materials Science,* Vol. 33, pp. 4551-4560.

Brooks, W., C. Sutcliffe, W. Cantwell, P. Fox, J. Todd and R. Mines, 2005, "Rapid Design and Manufacture of Ultralight Cellular Materials," *16th Solid Freeform Fabrication Symposium*, Austin, TX., pp. 231-241.

Calvert, P., 2001, "Inkjet Printing for Materials and Devices," *Chemistry of Materials,* Vol. 13, pp. 3299-3305.

CAM-LEM, Inc., 2004, "CAM-LEM Technologies", www.camlem.com/camlemtech.html.

Cansizoglu, O., D. Cormier, O. Harrysson, H. West and T. Mahale, 2006, "An Evaluation of Non-Stochastic Lattice Structures Fabricateed Via Electron Beam Melting," *Solid Freeform Fabrication*, Austin, TX., pp. 209-2119.

Carreno-Morelli, E., S. Martinerie and J.-E. Bidaux, 2007, "Three-Dimensional Printing of Shape Memory Alloys," *Materials Science Forum,* Vols. 534-536, pp. 477-480.

Carrion, A., 1997, "Technology Forecast on Ink-Jet Head Technology Applications in Rapid Prototyping," *Rapid Prototyping Journal,* Vol. 3, No. 3, pp. 99-115.

Carter, W. T. and M. G. Jones, 1993, "Direct Laser Sintering of Metals," *Solid Freeform Fabrication Symposium*, Austin, TX., pp. 51-59.

Celanese Chemicals, 2007, "Celvol 203", http://info.chemvip.com/index/products_index/celvol/celvol-celvol-203.htm.

Chartier, T., R. Penarroya, C. Pagnoux and J. F. Baumard, 1997, "Tape Casting Using UV Curable Binders," *Journal of the European Ceramic Society,* Vol. 17, pp. 765-771.

Chi, X., H. Yang, S. Yang and J. R. G. Evans, 2006, "Direct Extrusion Freeforming of Ceramic Pastes," *Solid Freeform Fabrication Symposium*, Austin, TX, pp. 304-315.

Chiras, S., D. R. Mumm, A. G. Evans, N. Wicks, J. W. Hutchinson, K. Dharmasena, H. N. G. Wadley and S. Fichter, 2002, "The Structural Performance of Near-Optimized Truss Core Panels," *International Journal of Solids and Structures,* Vol. 39, pp. 4093-4115.

Church, B. C., B. M. Dempsey, J. L. Clark, T. H. Sanders Jr. and J. K. Cochran Jr., 2001, "Copper Alloys from Oxide Reduction for High Conductivity Applications," *Proceedings of IMECE 2001, International Mechanical Engineering Congress and Exposition*, New York.

Cima, M. J., A. Lauder, S. Khanuja and E. Sachs, 1992, "Microstructural Elements of Components Derived from 3D Printing," *Solid Freeform Fabrication Symposium*, Austin, TX., pp. 220-227.

Cima, M. J., J. Yoo, S. Khanuja, M. Rynerson, D. Nammour, B. Giritlioglu, J. Grau and E. M. Sachs, 1995, "Structural Ceramic Components by 3D Printing," *Solid Freeform Fabrication Symposium*, Austin, TX, pp. 479-488.

Clarinval, A., R. Carrus and T. Dormal, 2003, "Development of Material for Optoform Process," *1st International Conference on Advanced Research in Virtual and Rapid Prototyping (VRAP)*, Leiria, Portugal, pp. 279-282.

Clarinval, A., R. Carrus and T. Dormal, 2007, "Fabrication of Stainless Steel and Ceramic Parts with the Optoform Process," *Advanced Research in Virtual and Rapid Prototyping*, Leiria, Portugal, pp. 415-418.

Cochran, J. K., K. J. Lee, D. McDowell, T. H. Sanders, B. Church, J. Clark, B. Dempsey, K. Hurysz, T. McCoy, J. Nadler, R. Oh, W. Seay and B. Shapiro, 2000, "Low Density Monolithic Metal Honeycombs by Thermal Chemical Processing," *Fourth Conference on Aerospace Materials, Processes, and Environmental Technology*, Huntsville, AL.

Cochran, J. K., K. J. Lee, D. L. McDowell and T. H. Sanders, 2002, "Multifunctional Metallic Honeycombs by Thermal Chemical Processing," *Processing and Properties of Lightweight Cellular Metals and Structures (TMS)*, pp. 127-136.

Cochran, J. K., K. J. Lee and T. H. Sanders, 2003, "Metallic Articles Formed by Reduction of Nonmetallic Articles and Method of Producing Metallic Articles," US 6,582,651 B1, Georgia Tech Research Corporation, USA.

Cormier, D., O. Harrysson and H. West, 2004a, "Characterization of H13 Steel Produced via Electron Beam Melting," *Rapid Prototyping Journal,* Vol. 10, No. 1, pp. 35-41.

Cormier, D., H. West, O. Harrysson and K. Knowlson, 2004b, "Characterization of Thin Walled Ti-6Al-4V Components Produced via Electron Beam Welding," *Solid Freeform Fabrication Symposium*, Austin, TX.

Crane, N. B., J. Wilkes, E. Sachs and S. M. Allen, 2006, "Improving Accuracy of Powder-Based SFF Processes by Metal Deposition from a Nanoparticle Dispersion," *Rapid Prototyping Journal,* Vol. 12, No. 5, pp. 266-274.

Crocker, J. E., S. Lianchao, H. Ansquer, L. L. Shaw and H. L. Marcus, 1999, "Processing and Characterization of SALDVI Ceramic Structures," *Solid Freeform Fabrication Symposium*, Austin, TX., pp. 495-501.

Das, A., G. Madras, N. Dasgupta and A. M. Umarji, 2003, "Binder Removal Studies in Ceramic Thick Shapes Made by Laminated Object Manufacturing," *Journal of the European Ceramic Society,* Vol. 23, pp. 1013-1017.

de Gans, B., P. C. Duineveld and U. S. Schubert, 2004, "Inket Printing of Polymers: State of the Art and Future Developments," *Advanced Materials,* 16, 3, pp. 203-213.

Deckard, L. and T. D. Claar, 1993, "Fabrication of Ceramic and Metal Matrix Composites from Selective Laser Sintered Ceramic Preforms," *Solid Freeform Fabrication Symposium*, Austin, TX., pp. 215-222.

Derby, B. and N. Reis, 2003a, "Inket Printing of Highly Loaded Particulate Suspensions," *Materials Research Society Bulletin,* Vol. 28, No. 11, pp. 815-818.

Derby, B. and N. Reis, 2003b, "Inkjet Printing of Highly Loaded Particulate Suspensions," *Materials Research Society Bulletin*, November, pp. 815-818.

Desktop Factory, Inc., 2007, "Desktop Factory: 3D Printers", http://www.desktopfactory.com/.

Doreau, F., C. Chaput and T. Chartier, 2000, "Stereolithography for Manufacturing Ceramic Parts," *Advanced Engineering Materials,* Vol. 2, No. 8, pp. 493-496.

EOS GmbH, 2004, "EOS Products EOSINT M", http://www.eos-gmbh.de/0/020300_prod_eosm.htm.

Evans, A. G., J. W. Hutchinson, N. A. Fleck, M. F. Ashby and H. N. G. Wadley, 2001, "The Topological Design of Multifunctional Cellular Materials," *2nd International Conference on Cellular Metals and Metal Foaming Technology (MetFoam 2001)*, Bremen, Germany.

Evans, J. R. G., 2001, "Direct Ink Jet Printing of Ceramics: Experiment in Teleology," *British Ceramic Transactions,* Vol. 100, No. 3, pp. 124-128.

Evans, R. S., D. L. Bourell, J. Beaman and M. I. Campbell, 2005, "Rapid Manufacturing of Silicon Carbide Composites," *Rapid Prototyping Journal,* Vol. 11, No. 1, pp. 37-40.

ExHone, 2007, "The ExOne Company", http://www.exone.com/.

Extrude Hone Corporation, 2004, "Extrude Hone ProMetal - Rapid Production", http://http://www.prometal-rt.com/.

Fedorov, A. G. and F. L. Degertekin, 2005, "Electrospray Systems and Methods," US 2005/0054208 A1, United States.

Feenstra, F., B. Holmer, H. Pohl, G. Tromans, N. Moos and B. Mieritz, 2003, "RP, RT, RM Trends and Developments/Research Survey," *4th National Conference of Rapid & Virtual Prototyping and Applications*, Buckinghamshire, UK, pp. 95-138.

Fockele & Schwarze, 2004, "F&S Products: SLM", http://www.fockeleundschwarze.de/english/fsproductsfs-rea.html.

Fu, Q., O. Jongprateep, A. Abbott and F. Dogan, 2006, "Freeze-Spray Processing of Layered Ceramic Composites," *Solid Freeform Fabrication Symposium*, Austin, TX., pp. 339-348.

Geving, B., A. Kataria, C. Moore, I. Ebert-Uphoff, T. R. Kurfess and D. W. Rosen, 2000, "Conceptual Design of a Generalized Stereolithography Machine," *Japan-USA Symposium on Flexbile Automation*, Ann Arbor, MI.

Gibson, L. J. and M. F. Ashby, 1997, *Cellular Solids: Structures and Properties*, Cambridge University Press, Cambridge, UK.

Grau, J., J. Moon, S. Uhland, M. J. Cima and E. Sachs, 1997, "High Green Density Ceramic Components Fabricated by the Slurry-Based 3DP Process," *Solid Freeform Fabrication Symposium*, Austin, TX., pp. 371-378.

Greul, M., F. Petzoldt, M. Greulich and J. Wunder, 1997, "Rapid Prototyping Moves on Metal Powders," *Metal Powder Report,* Vol. 52, No. 10, pp. 24-27.

Greul, M., T. Pintat and M. Greulich, 1996, "Rapid Prototyping of Functional Metallic and Ceramic Parts Using the Multiphase Jet Solidification (MJS) Process," *Advances in Powder Metallurgy and Particulate Materials*, Washington, D.C., pp. 7.281-7.287.

Greulich, M., 1997, "Rapid Prototyping and Fabrication of Tools and Metal Parts by Laser Sintering of Metal Powders," *Materials Technology,* Vol. 12, No. 5, pp. 155-157.

Greulich, M., M. Greul and T. Pintat, 1995, "Fast, Functional Prototypes via Multiphase Jet Solidification," *Rapid Prototyping Journal,* Vol. 1, No. 1, pp. 20-25.

Grida, I. and J. R. G. Evans, 2003, "Extrusion Freeforming of Ceramics through Fine Nozzles," *Journal of European Ceramic Society,* Vol. 23, pp. 629-635.

Griffin, C. and Dautenbach, 1995, "Solid Freeform Fabrication of Functional Ceramic Components Using a Laminated Object Manufacturing Technique," *Solid Freeform Fabrication Symposium*, Austin, TX., pp. 25-30.

Griffith, M. and J. W. Halloran, 1994a, "Ultraviolet Curing of Highly Loaded Ceramic Suspensions for Stereolithography of Ceramics," *Solid Freeform Fabrication Symposium*, Austin, TX, pp. 396-403.

Griffith, M., D. M. Keicher, C. Atwood, J. Romero, J. Smugeresky, L. Harwell and D. Greene, 1996, "Free Form Fabrication of Metallic Components Using Laser Engineered Net Shaping (LENS)," *Solid Freeform Fabrication Symposium*, Austin, TX.

Griffith, M. L. and J. W. Halloran, 1994b, "Ultraviolet Curable Ceramic Suspensions for Stereolithography of Ceramics," *Manufacturing Science and Engineering, ASME, Production Engineering Division,* Vol. 68, No. 2, pp. 529-534.

Griffith, M. L. and J. W. Halloran, 1995, "Stereolithography of Ceramics," *Proceedings of the Sixth International Conference on Rapid Prototyping*, Dayton, OH, pp. 25-29.

Griffith, M. L. and J. W. Halloran, 1996, "Freeform Fabrication of Ceramics via Stereolithography," *Journal of the American Ceramic Society,* Vol. 79, No. 10, pp. 2601-2608.

Griffith, M. L. and J. W. Halloran, 1997, "Scattering of Ultraviolet Radiation in Turbid Suspensions," *Journal of Applied Physics,* Vol. 81, No. 6, pp. 2538-2546.

Halloran, J. W., 1999, "Freeform Fabrication of Ceramics," *British Ceramic Transactions,* Vol. 98, pp. 299-303.

Hattiangadi, A. and A. Bandyopadhyay, 1999, "Processing, Characterization and Modeling of Non-Random Porous Ceramic Structures," *Solid Freeform Fabrication Symposium*, Austin, TX, pp. 319-326.

Hayes, A. M., A. Wang, B. M. Dempsey and D. L. McDowell, 2001, "Mechanics of Linear Cellular Alloys," *IMECE: International Mechanical Engineering Congress and Exposition*, New York, NY.

Hedges, M. and D. M. Keicher, 2002, "Laser Engineered Net Shaping - Technology and Applications," *3rd National Conference on Rapid Prototyping, Rapid Tooling, and Rapid Manufacturing*, Buckinghamshire, UK, pp. 17-23.

Himmer, T., T. Nakagawa and H. Noguchi, 1997, "Stereolithography of Ceramics," *Solid Freeform Fabrication Symposium*, Austin, TX., pp. 363-369.

Hinczewski, C., S. Corbel and T. Chartier, 1998a, "Ceramic Suspensions Suitable for Stereolithography," *Journal of the European Ceramic Society,* Vol. 18, pp. 583-590.

Hinczewski, C., S. Corbel and T. Chartier, 1998b, "Stereolithography for the Fabrication of Ceramic Three-Dimensional Parts," *Rapid Prototyping Journal,* Vol. 4, No. 3, pp. 104-111.

Holman, R. K., M. J. Cima, S. Uhland and E. Sachs, 2002a, "Spreading and Infiltration of Inkjet-Printed Polymer Solution Droplets on a Porous Substrate," *Journal of Colloid and Interface Science,* 249, pp. 432-440.

Holman, R. K., S. Uhland, M. J. Cima and E. Sachs, 2002b, "Surface Adsorption Effects in the Inkjet Printing of Aqueous Polymer Solution on a Porous Oxide Ceramic Substrate," *Journal of Colloid and Interface Science,* 247, pp. 266-274.

Hopkinson, N. and P. Erasenthiran, 2004, "High Speed Sintering - Early Research into a New Rapid Manufacturing Process," *Solid Freeform Fabrication Symposium*, Austin, TX., pp. 312-320.

Hopkinson, N. and P. Erasenthiran, 2006, "Method and Apparatus for Combining Particulate Material," WO/2005/011959, United Kingdom.

Huang, T., M. S. Mason, G. E. Hilmas and M. C. Leu, 2006, "Freeze-form Extrusion Fabrication of Ceramic Parts," *International Journal of Virtual and Physical Prototyping,* Vol. 1, No. 2, pp. 93-100.

Ippolito, R., L. P. Jilano and A. Gatto, 1995, "Benchmarking of Rapid Prototyping Techniques in Terms of Dimensional Accuracy and Surface Finish," *CIRP Annals,* Vol. 44, No. 1, pp. 157-160.

Jafari, M. A., W. Han, F. Mohammadi, A. Safari, S. C. Danforth and N. A. Langrana, 2000, "A Novel System for Fused Deposition of Advanced Multiple Ceramics," *Rapid Prototyping Journal,* Vol. 6, No. 3, pp. 161-174.

Jamcorp Inc., 2004, "Jonathon Aerospace Materials website", www.jamcorp.com.

Jandin, G., J.-M. Bertin, L. Dembinski and C. Coddet, 2005, "Manufacture of Stainless Steel Parts by Selective Laser Melting Process," *2nd International Conference on Advanced Research in Virtual and Rapid Prototyping*, Leiria, Portugal, pp. 431-434.

Jang, J. H., S. Wang, S. M. Pilgrim and W. A. Schulze, 2000, "Preparation and Characterization of Barium Titanate Suspensions for Stereolithography," *Journal of the American Ceramic Society,* Vol. 83, No. 7, pp. 1804-1806.

Jardini, A. L., R. Maciel, M. A. Scarparo, S. R. Andrade and L. F. Moura, 2003, "The Development in Infrared Stereolithography Using Thermosensitive Polmers," *International Conference on Advanced Research in Virtual and Rapid Prototyping*, Leiria, Portugal, pp. 273-277.

Johnson, R. W., J.-H. Park, W. J. Lackey and D. W. Rosen, 2003, "Advances in Laser Chemical Vapor Depostion of Metals and Ceramics," *International Conference on Advanced Research in Virtual and Rapid Prototyping*, Leiria, Portugal.

Karlsen, R. and J. Reitan, 2003, "Metal Printing - Development of a New Rapid Manufacturing Process for Metal and Ceramic Objects," *International Conference on Advanced Research in Virtual and Rapid Prototyping*, Leiria, Portugal, pp. 569-589.

Keicher, D. M., 1998, "Beyond Rapid Prototyping to Direct Fabrication: Forming Metallic Hardware Directly from a CAD Solid Model," *Materials Technology,* Vol. 13, No. 1, pp. 5-7.

Kernan, B. D., E. M. Sachs, M. A. Oliveira and M. J. Cima, 2003, "Three Dimensional Printing of Tungsten Carbide-Cobalt Using a Cobalt Oxide Precursor," *Solid Freeform Fabrication Symposium*, Austin, TX., pp. 616-631.

Khiang, M. W., J. Y. H. Fuh and L. Lu, 2001, "Direct Metal Laser Sintering for Rapid Tooling: Processing and Characterization of EOS Parts," *Journal of Materials Processing Technology,* Vol. 113.

Khoshnevis, B., S. Bukkapatnam, H. Kwon and J. Saito, 2001, "Experimental Investigation of Contour Crafting Using Ceramic Materials," *Rapid Prototyping Journal,* Vol. 7, No. 1, pp. 32-41.

Kim, S.-J. and D. E. McKean, 1998, "Aqueous TiO2 Suspension Preparation and Novel Application of Ink-Jet Printing Technique for Ceramics Patterning," *Journal of Materials Science Letters,* Vol. 17, pp. 141-144.

King, B. H., S. Morissette, H. Denham, J. Cesarno and D. B. Dimos, 1998, "Influence of Rheology on Deposition Behavior of Ceramic Pastes in Direct Fabrication Systems," *Solid Freeform Fabrication Symposium*, Austin, TX., pp. 391-398.

Klocke, F. and C. Ader, 2003, "Direct Laser Sintering of Ceramics," *Solid Freeform Fabrication Symposium*, Austin, TX., pp. 447-455.

Klosterman, D. A., R. P. Chartoff, N. R. Osborne, G. A. Graves, A. Lightman, G. Han, A. Bezeredi and S. Rodrigues, 1999, "Development of a Curved Layer LOM Process for Monolithic Ceramics and Ceramic Matrix Composites," *Rapid Prototyping Journal,* Vol. 5, No. 2, pp. 61-71.

Klosterman, D. A., R. P. Chartoff, N. R. Osborne, G. A. Graves, A. Lightman, G. Han, A. Bezeredi, S. Rodrigues, S. Pak, G. Kalmanovich, L. Dodin and S. Tu, 1998, "Curved Layer LOM of Ceramics and Composites," *Solid Freeform Fabrication Symposium*, Austin, TX., pp. 671-679.

Kruth, J. P., L. Froyen, J. Van Vaerenbergh, P. Mercelis, M. Rombouts and B. Lauwers, 2004a, "Selective Laser Melting of Iron-Based Powder," *Journal of Materials Processing Technology,* Vol. 149, Iss. 1-3, pp. 616-622.

Kruth, J. P., P. Mercelis, L. Froyen and M. Rombouts, 2004b, "Binding Mechanisms in Selective Laser Sintering and Selective Laser Melting," *Solid Freeform Fabrication Symposium*, Austin, TX., pp. 44-59.

Kruth, J. P., P. Mercelis, J. Van Vaerenbergh and T. Craeghs, 2007, "Feedback Control of Selective Laser Melting," *Advanced Research in Virtual and Rapid Prototyping*, Leiria, Portugal, pp. 521-527.

Kruth, J. P., P. Mercelis, J. VanVaerenbergh, L. Froyen and M. MRombouts, 2003, "Advances in Selective Laser Sintering," *International Conference on Advanced Research in Virtual and Rapid Prototyping*, pp. 59-69.

Laeng, J., J. G. Stewart and F. W. Liou, 2000, "Laser Metal Forming Processes for Rapid Prototyping - A Review," *International Journal of Production Research,* Vol. 38, No. 16, pp. 3973-3996.

Lanzetta, M. and E. Sachs, 2003, "Improved Surface Finish in 3D Printing Using Bimodal Powder Distribution," *Rapid Prototyping Journal,* Vol. 9, No. 3, pp. 157-166.

Lee, S.-J. J., E. Sachs and M. J. Cima, 1995, "Layer Position Accuracy in Powder-Based Rapid Prototyping," *Rapid Prototyping Journal,* Vol. 1, No. 4, pp. 24-37.

Lenk, R., 2000, "Rapid Prototyping of Ceramic Components," *Advanced Engineering Materials,* Vol. 2, Iss. 1-2, pp. 40-47.

Lewis, J. A., 2000, "Colloidal Processing of Ceramics," *Journal of the American Ceramic Society,* Vol. 83, No. 10, pp. 2341-2359.

Li, Q. and J. A. Lewis, 2003, "Nanoparticle Inks for Directed Assembly of Three-Dimensional Periodic Structures," *Advanced Materials,* Vol. 15, No. 19, pp. 1639-1643.

Li, X., H. Choi and Y. Yang, 2002, "Micro Rapid Prototyping System for Micro Components," *Thin Solid Films,* Vol. 420-421, pp. 515-523.

Lim, T. J., B. Smith and D. L. McDowell, 2002, "Behavior of a Random Hollow Sphere Metal Foam," *Acta Materialia,* Vol. 50, pp. 2867-2879.

Limaye, A. and D. W. Rosen, 2006, "Process Planning for Mask Projection Stereolithography," *Rapid Prototyping Journal,* Vol. 12, No. 5.

Liu, Z., N. Suppakarn and J. D. Cawley, 1999, "Coated Feedstock for Fabrication of Ceramic Parts by CAM-LEM," *Solid Freeform Fabrication Symposium*, Austin, TX., pp. 393-401.

Liu, Z. E., T. C. Ko, J. Best, J. D. Cawley and A. H. Heuer, 1997, "CAM-LEM Processing: Materials Flexibility," *Solid Freeform Fabrication Symposium*, Austin, TX, pp. 379-382.

Lu, X., S. Yang, L. Chen and J. R. G. Evans,2006. "Dry Powder Microfeeding System for Solid Freeform Fabrication," Austin, TX.**:** pp. 636-643.

Mazumder, J., A. Schifferer and J. Choi, 1999, "Direct Materials Deposition: Designed Macro and Microstructure," *Materials Research Innovations,* Vol. 3, No. 3, pp. 118-131.

McNulty, T. F., F. Mohammadi, A. Bandyopadhyay, D. J. Shanefield, S. C. Danforth and A. Safari, 1998, "Development of a Binder Formulation for Fused Deposition of Ceramics," *Rapid Prototyping Journal,* Vol. 4, No. 4, pp. 144-150.

Meacham, J. M., C. Ejimofor, S. Kumar, F. L. Degertekin and A. G. Fedorov, 2004, "Micromachined Ultrasonic Droplet Generator Based on a Liquid Horn Structure," *Review of Scientific Instruments,* Vol. 75, No. 5, pp. 1347-1352.

Meacham, J. M., M. J. Varady, F. L. Degertekin and A. G. Fedorov, 2005, "Droplet Formation and Ejection from a Micromachined Ultrasonic Droplet Generator: Visualization and Scaling," *Physics of Fluids,* Vol. 17, No. 1, pp. 1-8.

Mercelis, P. and J. P. Kruth, 2006, "Residual Stresses in Selective Laser Sintering and Selective Laser Melting," *Rapid Prototyping Journal,* Vol. 12, No. 5, pp. 254-265.

Merz, R., F. B. Prinz, K. Ramaswami, M. Terk and L. E. Weiss, 1994, "Shape Deposition Manufacturing," *Solid Freeform Fabrication Symposium*, Austin, TX.

Michaels, S., E. M. Sachs and M. J. Cima, 1992, "Metal Parts Generation by Three Dimensional Printing," *Solid Freeform Fabrication Symposium*, Austin, TX., pp. 244 - 250.

Mining & Chemical Products Ltd., 2004, "MCP Realizer - SLM Technology", http://www.mcp-group.co.uk/rpt/rpttslm.html.

Mistree, F. M., K. Lewis and L. Stonis, 1994, "Selection in the Conceptual Design of Aircraft," *AIAA/NASA/USAF/ISSMO Symposium on Multidisciplinary Analysis and Optimization*, Panama City, Florida, Paper No. AIAA-94-4382-CP.

Moon, J., J. Grau and M. J. Cima, 2000, "Slurry Chemistry Control to Produce Easily Redispersible Ceramic Powder Compacts," *Journal of the American Ceramic Society,* Vol. 83, No. 10, pp. 2401-2408.

Moon, J., J. Grau, V. Knezevic, M. J. Cima and E. M. Sachs, 2002, "Ink-Jet Printing of Binders for Ceramic Components," *Journal of the American Ceramic Society,* Vol. 85, No. 4, pp. 755-762.

Morissette, S. L., J. A. Lewis, J. Cesarno, D. B. Dimos and T. Baer, 2000, "Solid Freeform Fabrication of Aqueous Alumina-Poly(vinyl alcohol) Gelcasting Suspensions," *Journal of the American Ceramic Society,* Vol. 83, No. 10, pp. 2409-2416.

Morse, T., 1979, *Handbook of Organic Additives for Use in Ceramic Body Formulation*, Montana Energy and MHD Research and Development Institute, Butte, MT.

Mott, M., J. H. Song and J. R. G. Evans, 1999, "Microengineering of Ceramics by Direct Ink-Jet Printing," *Journal of the American Ceramic Society,* Vol. 82, No. 7, pp. 1653-1658.

Moussa, K. M., K. J. Newell, C. Hinczewski and C. H. Zenuk, 2003, "Metallic Filled Pastes," US 6,630,009, 3D Systems, Inc., United States.

Nakagawa, T., 1985, "Laser Cut Sheet Laminated Forming Dies: Diffusion Bonding," *Proceedings of the 25th International MTDR Conference*, pp. 505-510.

Objet Geometries Ltd., 2005, "PolyJet Technology Description", http://www.2objet.com/Tech/Index.html.

Optomec, 2004, "Optomec - Laser Engineered Net Shaping", http://www.optomec.com/html/lens.htm.

Orme, M., Q. Liu and R. Smith, 2000, "Molten Aluminum Micro-Droplet Formation and Deposition for Advanced Manufacturing Applications," *Aluminum Transactions Journal,* Vol. 3, No. 1, pp. 95-103.

Pahl, G. and W. Beitz, 1996, *Engineering Design: A Systematic Approach*, Springer-Verlag, London.

Percin, G. and B. T. Khuri-Yakub, 2003, "Piezoelectric Droplet for Ink-Jet Printing of Fluids and Solid Particles," *Review of Scientific Instruments,* Vo. 74, No. 2, pp. 1120-1127.

Pham, D. T., S. S. Dimov, C. Ji and R. S. Gault, 2003, "Layer Manufacturing Processes: Technology Advances and Research Challenges," *1st International Conference on Advanced Research in Virtual and Rapid Prototyping*, Leiria, Portugal, pp. 107-113.

Phenix Systems, 2005, "Phenix Systems Products", http://www.phenix-systems.com/home_en.php.

Rahaman, M. N., 2003, *Ceramic Processing and Sintering*, M. Dekker, New York.

Reed, J. S., 1995, *Principles of Ceramics Processing*, John Wiley & Sons, Inc., New York.

Rehme, O., C. Emmelmann and D. Schwarze, 2007, "Selective Laser Melting of Lattice Structures in Solid Shells," *Advanced Research in Virtual and Rapid Prototyping*, Leiria, Portugal, pp. 529-535.

Reis, N., C. Ainsley and B. Derby, 2005, "Viscosity and Acoustic Behavior of Ceramic Suspensions Optimized for Phase-Change Ink-Jet Printing," *Journal of the American Ceramic Society,* Vol. 88, No. 4, pp. 802-808.

Rice, C. S., P. F. Mendez and S. B. Brown, 2000, "Metal Solid Freeform Fabrication Using Semi-Solid Slurries," *The Member Journal of the Minerals, Metals & Materials Society,* Vol. 52, No. 12.

Ring, T. A., 1996, *Fundamentals of Ceramic Powder Processing and Synthesis*, Academic Press, San Diego, CA.

Robinson, C. J., C. Zhang, G. D. Janaki Ram, E. J. Siggard, B. Stucker and L. Li, 2007, "Maximum Height to Width Ratio of Freestanding Structures Built Using Ultrasonic Consolidation," *Solid Freeform Fabrication Symposium*, Austin, TX., pp. 502-516.

Sachs, E., M. J. Cima, J. Cornie, D. Brancazio, J. Bredt, A. Curodeau, T. Fan, S. Khanuja, A. Lauder, J. Lee and S. Michaels, 1993a, "Three-Dimensional Printing: The Physics and Implications of Additive Manufacturing," *CIRP Annals,* Vol. 42, No. 1, pp. 257-260.

Sachs, E., M. J. Cima, P. Williams, D. Brancazio and J. Cornie, 1992, "Three Dimensional Printing: Rapid Tooling and Prototypes Directly from a CAD Model," *Journal of Engineering for Industry,* Vol. 114, pp. 481-488.

Sachs, E. M., 2000, "Powder Dispensing Apparatus Using Vibration," 6,036,777, Massachusetts Institute of Technology, United States.

Sachs, E. M., J. S. Haggerty, M. J. Cima and P. A. Williams, 1993b, "Three-Dimensional Printing Techniques," 5,204,055, Massachusetts Institute of Technology, United States.

Sagi, O. and A. Libermann, 2007, "Expanding Applications and Opportunities with Polyjet Rapid Prototyping Technology," *Advanced Research in Virtual and Rapid Prototyping*, Leiria, Portugal, pp. 569-573.

Sanders, W. S. and L. J. Gibson, 2003, "Mechanics of Hollow Sphere Foams," *Materials Science and Engineering,* Vol. A347, pp.70-85.

Seepersad, C. C., J. K. Allen, D. McDowell and F. M. Mistree, 2006, "Robust Design of Cellular Materials with Topological and Dimensional Imperfections," *Journal of Mechanical Design,* Vol. 128, No. 6, pp. 1285-1297.

Seepersad, C. C., R. S. Kumar, J. K. Allen, F. M. Mistree and D. L. McDowell, 2004, "Multifunctional Design of Prismatic Cellular Materials," *Journal of Computer-Aided Materials Design,* Vol. 11, No 2, pp. 163-181.

Seerden, K. A. M., N. Reis, J. R. G. Evans, P. S. Grant, J. W. Halloran and B. Derby, 2001, "Ink-Jet Printing of Wax-Based Alumina Suspensions," *Journal of the American Ceramic Society,* Vol. 84, No. 11, pp. 2514-2520.

Sewell, N. T., M. Felstead, M. R. Sloan and M. A. Jenkins, 2007, "A Study of the Degradation of Duraform PA Due to Cyclic Processing," *Advanced Research in Virtual and Rapid Prototyping*, Leiria, Portugal, pp. 299-303.

Sirringhaus, H. and T. Shimoda, 2003, "Inkjet Printing of Functional Materials," *Materials Research Society Bulletin: Inket Printing of Functional Materials,* Vol. 28, No. 11, pp. 802-806.

Slade, C. E. and J. R. G. Evans, 1998, "Freeforming Ceramics Using a Thermal Jet Printer," *Journal of Materials Science Letters,* Vol. 17, pp. 1669-1671.

Smay, J. E., J. Cesarno and J. A. Lewis, 2002a, "Colloidal Inks for Directed Assembly of 3-D Periodic Structures," *Langmuir,* Vol. 18, pp. 5429-5437.

Smay, J. E., G. M. Gratson, R. F. Shepherd, J. Cesarno and J. A. Lewis, 2002b, "Directed Colloidal Assembly of 3D Periodic Structures," *Advanced Materials,* Vol. 14, No. 18, pp. 1279-1283.

Solidica, Inc., 2004, "Solidica: Direct to Metal Aluminum Tooling for Advanced Manufacturing", www.solidica.com/technology.html.

Solidscape, 2006, "Solidscape: Products", http://www.solid-scape.com/products.html.

Song, J. H., M. J. Edirisinghe and J. R. G. Evans, 1999, "Formulation and Multilayer Jet Printing of Ceramic Inks," *Journal of the American Ceramic Society,* Vol. 82, No. 12, pp. 3374-3380.

Stratasys, February 2007, 2007, "The Added Convenience of WaterWorks", http://www.stratasys.com/systems_misc.aspx?id=132.

Subramanian, P. K. and H. L. Marcus, 1995, "Selective Laser Sintering of Alumina Using Aluminium Binder," *Material and Manufacturing Processes,* Vol. 10, No. 4, pp. 689-706.

Suh, N. P., 1990, *The Principles of Design*, Oxford University Press, New York.

Sun, C. and X. Zhang, 2002, "The Influences of the Material Properties on Ceramic Micro-Stereolithography," *Sensors and Actuators,* Vol. 101, pp. 364-370.

Sypeck, D. J. and H. N. G. Wadley, 2002, "Cellular Metal Truss Core Sandwich Structures," *Advanced Engineering Materials,* Vol. 4, No. 10, pp. 759-764.

Tang, H., 2002, "Direct Laser Fusing to Form Ceramic Parts," *Rapid Prototyping Journal,* Vol. 8, No. 5, pp. 284-289.

Tay, B. Y., J. R. G. Evans and M. J. Edirisinghe, 2003, "Solid Freeform Fabrication of Ceramics," *International Materials Reviews,* Vol. 48, No. 6, pp. 341-370.

Teng, W. D., M. J. Edirisinghe and J. R. G. Evans, 1997, "Optimization of Dispersion and Viscosity of a Ceramic Jet Printing Ink," *Journal of the American Ceramic Society,* Vol. 80, No. 2, pp. 486-494.

Thomas, H. R., N. Hopkinson and P. Erasenthiran, 2007, "High Speed Sintering - Continuing Research into a New Rapid Manufacturing Process," *Solid Freeform Fabrication Symposium*, Austin, TX., pp. 682-691.

Thompson, S. C., H. Muchnick, H. Choi, D. McDowell, J. K. Allen and F. M. Mistree, 2006, "Robust Materials Design of Blast Resistant Panels," *AIAA/ISSMO Multidisciplinary Analysis and Optimization Conference*, Portsmouth, VA, AIAA 2006-7005.

Thornell, G., L. Klintberg, T. Laurell, J. Nilsson and S. Johansson, 1999, "Desktop Microfabrication - Intial Experiments with a Piezoceramic," *Journal of Micromechanics and Microengineering,* Vol. 9, pp. 434-437.

Tolochko, N. K., T. Laoui, Y. V. Khlopkov, S. E. Mozzharov, V. I. Titov and M. B. Ignatiev, 2000, "Absorptance of Powder Materials Suitable for Laser Sintering," *Rapid Prototyping Journal,* Vol. 6, No. 3, pp. 155-160.

Uhland, S., R. K. Holman, S. Morissette, M. J. Cima and E. M. Sachs, 2001, "Strength of Green Ceramics with Low Binder Content," *Journal of the American Ceramic Society,* Vol. 84, No. 12, pp. 2809-2818.

Utela, B., R. L. Anderson and H. Kuhn, 2006, "Advanced Ceramic Materials and Three-Dimensional Printing (3DP)," *17th Solid Freeform Fabrication Symposium*, Austin, TX, pp. 290-303, pp. 290-303.

Vaidyanathan, R., J. L. Lombardi, J. Walish, S. Kasichainula, P. Calvert and K. Cooper, 1999, "Extrusion Freeform Fabrication of Functional Ceramic Prototypes," *Solid Freeform Fabrication Symposium*, Austin, TX, pp. 327-334.

Vaidyanathan, R., J. Walish, J. L. Lombardi, S. Kasichainula, O. Calvert and K. C. Cooper, 2000, "The Extrusion Freeforming of Functional Ceramic Prototypes," *Journal of Materials Science,* Vol. 52, No. 12, pp. 34-37.

Vaucher, S., D. Paraschivescu, C. Andre and O. Beffort, 2002, "Selective Laser Sintering of Aluminum-Silicon Carbide Metal Matrix Composites," *Werkstoffwoche 2002 (Materials Week)*, ICM-Mun.

Wadley, H. N. G., 2002, "Cellular Metals Manufacturing," *Advanced Engineering Materials,* Vol. 4, No. 10, pp. 726-733.

Wadley, H. N. G., N. A. Fleck and A. Evans, 2003, "Fabrication and Structural Performance of Periodic Cellular Metal Sandwich Structures," *Composites Science and Technology,* Vol. 63, pp. 2331-2343.

Wang, H. and D. W. Rosen, 2002a, "Computer-Aided Design Methods for Additive Fabrication of Truss Structures," *International Conference on Manufacturing Automation*, Hong Kong.

Wang, H. and D. W. Rosen, 2002b, "Parametric Modeling Method for Truss Structures," *ASME Computers and Information in Engineering Conference*, Montreal, CA, DETC2002/CIE-34466.

Wang, H. V., S. R. Johnston and D. W. Rosen, 2006, "Design of a Graded Cellular Structure for an Acetabular Hip Replacement Component," *17th Solid Freeform Fabrication Symposium*, Austin, TX, pp. 111-123.

Wang, T. and B. Derby, 2005, "Ink-Jet Printing and Sintering of PZT," *Journal of the American Ceramic Society,* Vol. 88, No. 8, pp. 2053-2058.

Wang, T., B. Derby, R. C. Patel and L. Messe, 2007, "A Novel Combination of Materials for Rapid Manufacturing of 3-Dimensional Objects by Ink-Jet Printing," *Advanced Research in Virtual and Rapid Manufacturing*, Leiria, Portugal, pp. 575-579.

Watson, J. K., K. M. B. Taminger, R. A. Hafley and D. D. Peterson, 2002, "Development of a Prototype Electron Beam Freeform Fabrication System," *13th Solid Freeform Fabrication Symposium*, Austin, TX, pp. 458-465.

Weerasinghe, V. M. and W. M. Steen, 1983, "Laser Cladding by Powder Injection," *Proceedings of the 1st International Conference on Lasers in Manufacturing*, Brighton, UK, pp. 125-132.

White, D. and D. E. E. Carmein, 2002, "Ultrasonic Object Consolidation System and Method," 6,463,349, Solidica, Inc., United States.

Williams, C. B., F. Mistree and D. W. Rosen, 2005a, "Investigation of Solid Freeform Fabrication Processes for the Manufacture of Parts with Designed Mesostructure," *ASME IDETC Design for Manufacturing and the Life Cycle Conference*, Long Beach, California, DETC2005/DFMLC-84832.

Williams, C. B., F. Mistree and D. W. Rosen, 2005b, "Towards the Design of a Layer-Based Additive Manufacturing Process for the Realization of Metal Parts of Designed Mesostructure," *16th Solid Freeform Fabrication Symposium*, Austin, TX, pp. 217-230.

Williams, C. B. and D. W. Rosen, 2007, "Manufacturing Cellular Materials via Three-Dimensional Printing of Spray-Dried Metal Oxide Ceramic Powder," *3rd*

International Conference on Advanced Research in Virtual and Rapid Prototyping, Leiria, Portugal.

Windle, J. and B. Derby, 1999, "Ink Jet Printing of PZT Aqueous Ceramic Suspensions," *Journal of Materials Science Letters,* Vol. 18, pp. 87-90.

Wohlers, T., 2001, *Wohlers Report 2001: Rapid Prototyping, Tooling & Manufacturing State of the Industry Annual Worldwide Progress Report*, Wohlers Associates, Inc., Fort Collins, Colorado.

Wohlers, T., 2004, *Wohlers Report 2004: Rapid Prototyping, Tooling & Manufacturing State of the Industry Annual Worldwide Progress Report*, Wohlers Associates, Inc., Fort Collins, Colorado.

Wohlers, T., 2006, *Wohlers Report 2006: Rapid Prototyping, Tooling & Manufacturing State of the Industry Annual Worldwide Progress Report*, Wohlers Associates, Inc., Fort Collins, Colorado.

Wright, M. J. and J. R. G. Evans, 1999, "Ceramic Deposition Using an Electromagnetic Jet Printer Station," *Journal of Materials Science Letters,* Vol. 18, pp. 99-101.

Xiang, Q. F., J. R. G. Evans, M. J. Edirisinghe and P. F. Blazdell, 1997, "Solid Freeforming of Ceramics Using a Drop-on-demand Jet Printer," *Proceedings of the I MECH E Part B Journal of Engineering Manufacture,* Vol. 211, No. 3, pp. 211-214.

Yang, S. and J. R. G. Evans, 2004, "Acoustic Control of Powder Dispensing in Open Tubes," *Powder Technology,* Vol. 139, pp. 55-60.

Yoo, J., M. J. Cima, S. Khanuja and E. M. Sachs, 1993, "Structural Ceramic Components by 3D Printing," *Solid Freeform Fabrication Symposium*, Austin, TX., pp. 40-50.

Z Corporation, November 5, 2007, "3D Printers", http://www.zcorp.com/Products/3D-Printers/spage.aspx.

ZCorporation, 1996, *Z402 3D Printer Manual*.

Zhang, X., X. N. Jiang and C. Sun, 1999, "Micro-stereolithography of Polymeric and Ceramic Microstructures," *Sensors and Actuators,* Vol. 77, pp. 146-156.

Zhao, X., J. R. G. Evans and M. J. Edirisinghe, 2002a, "Direct Ink-Jet Printing of Vertical Walls," *Journal of the American Ceramic Society,* Vol. 85, No. 8, pp. 2113-2115.

Zhao, X., J. R. G. Evans and M. J. Edirisinghe, 2002b, "Ink-Jet Printing of Ceramic Pillar Arrays," *Journal of Materials Science,* 37, pp. 1987-1992.

Zhao, X., J. R. G. Evans, M. J. Edirisinghe and J. H. Song, 2001, "Ceramic Freeforming Using an Advanced Multinozzle Ink-Jet Printer," *Journal of Materials Synthesis and Processing,* Vol. 9, No. 6, pp. 319-327.

Zimbeck, W., M. Pope and R. W. Rice, 1996, "Microstructures and Strengths of Metals and Ceramics Made by Photopolymer-based Rapid Prototyping," *Solid Freeform Fabrication Symposium*, Austin, TX., pp. 411-418.

Zwicky, F., 1967, "The Morphological Approach to Discovery, Invention, Research and Construction," *New Methods of Thought and Procedure*, (*F. Zwicky and A. G. Wilson, eds.*), Springer-Verlag, New York, pp. pp. 273-297.

VITA

Christopher Bryant Williams received his doctorate in Mechanical Engineering (ME) from the Georgia Institute of Technology in the spring semester of 2008. He was a National Science Foundation (NSF) IGERT Graduate Research Fellow specializing in systems design and computer-aided engineering.

Previously, he earned his master's degree, also in ME from Georgia Tech, in 2003. During that time, he was a Georgia Tech President's Fellow. He received his bachelor's degree in ME from the University of Florida in 2000, graduating with high honors. During that time he was a University Scholars Program Research Fellow.

His research interests are focused in the issues surrounding both the design and manufacture of customized products. His most recent areas of research activity include: additive manufacturing, metal and ceramic based solid freeform fabrication technologies, low-density cellular materials, engineering design methodologies, and decision and computer support for designing engineering systems.

Williams's research experience and interests are characterized by collaboration with multiple engineering disciplines. During his doctoral research, in which he designed and developed an additive manufacturing technology that creates cellular materials with metal oxide powder, Williams worked in conjunction with researchers in Georgia Tech's Department of Materials Science and Engineering to develop to a post-processing technique that chemically converts the parts to metal via sintering in a reducing atmosphere. In the research completed for his Master's degree, Williams worked with researchers from Georgia Tech's School of Industrial Systems and Engineering to apply a

product platform design methodology to the scheduling of workstation capacity in the presence of non-uniform demand. In addition, Williams worked alongside business and law school students in Georgia Tech's NSF IGERT-funded Technological Innovation: Generating Economic Results (TI:GER) program to develop commercialization strategies for additive manufacturing technologies and a novel heart valve design.

As a researcher with a passion for excellence in education, Williams' also has research interests in the integration of design techniques into engineering education, as well as in the analysis and development of strategies for active learning in the classroom.

Among his additional honors, Williams was named one of the University of Florida's Outstanding Graduating Students in 2000, and he received an Honorable Mention in the 2000 and 2001 NSF Graduate Research Fellowship awards.

While attending the University of Florida, he served as the vice president of Pi Tau Sigma and as the program director for the American Society of Mechanical Engineers (ASME). In addition to these organizations, he is also a member of the American Society for Engineering Education (ASEE), Pi Tau Sigma, Tau Beta Pi, and Golden Key National Honor Society.

Christopher Williams is currently an Assistant Professor at the Virginia Polytechnic Institute and State University (Virginia Tech) with a dual appointment in the Mechanical Engineering and Engineering Education departments.